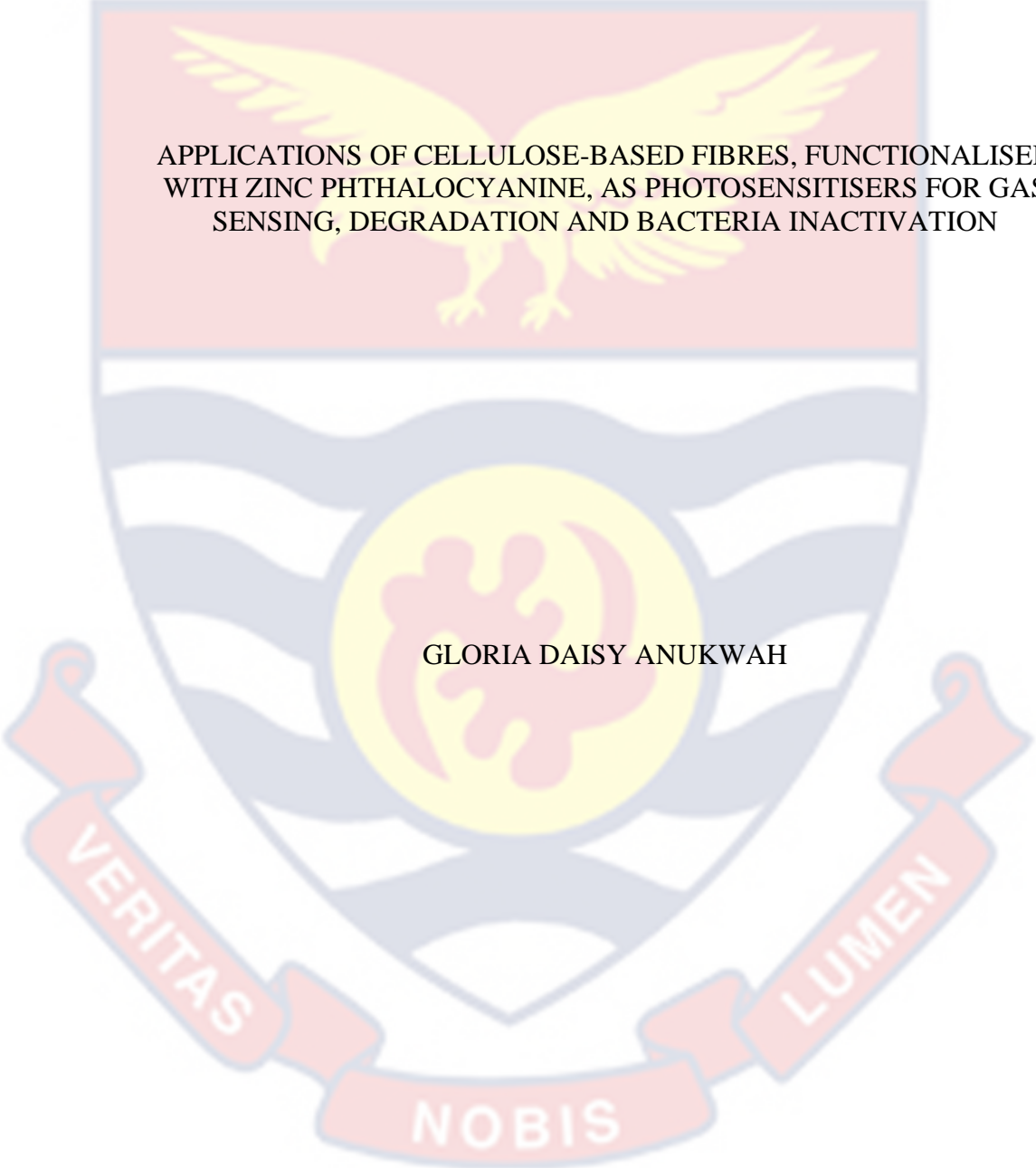UNIVERSITY OF CAPE COAST

APPLICATIONS OF CELLULOSE-BASED FIBRES, FUNCTIONALISED WITH ZINC PHTHALOCYANINE, AS PHOTOSENSITISERS FOR GAS SENSING, DEGRADATION AND BACTERIA INACTIVATION

GLORIA DAISY ANUKWAH

2023

©2023

Gloria Daisy Anukwah

University of Cape Coast

UNIVERSITY OF CAPE COAST

APPLICATIONS OF CELLULOSE-BASED FIBRES, FUNCTIONALISED WITH ZINC PHTHALOCYANINE AS PHOTOSENSITISERS FOR GAS SENSING, DEGRADATION AND BACTERIA INACTIVATION

BY

GLORIA DAISY ANUKWAH

Thesis submitted to the Department of Chemistry of the School of Physical Sciences, College of Agriculture and Natural Sciences, University of Cape Coast, in partial fulfilment of the requirements for the award of Doctor of Philosophy degree in Chemistry

JULY 2023

DECLARATION

Candidate's Declaration

I hereby declare that this thesis is the result of my own original research and that no part of it has been presented for another degree in this University or elsewhere.

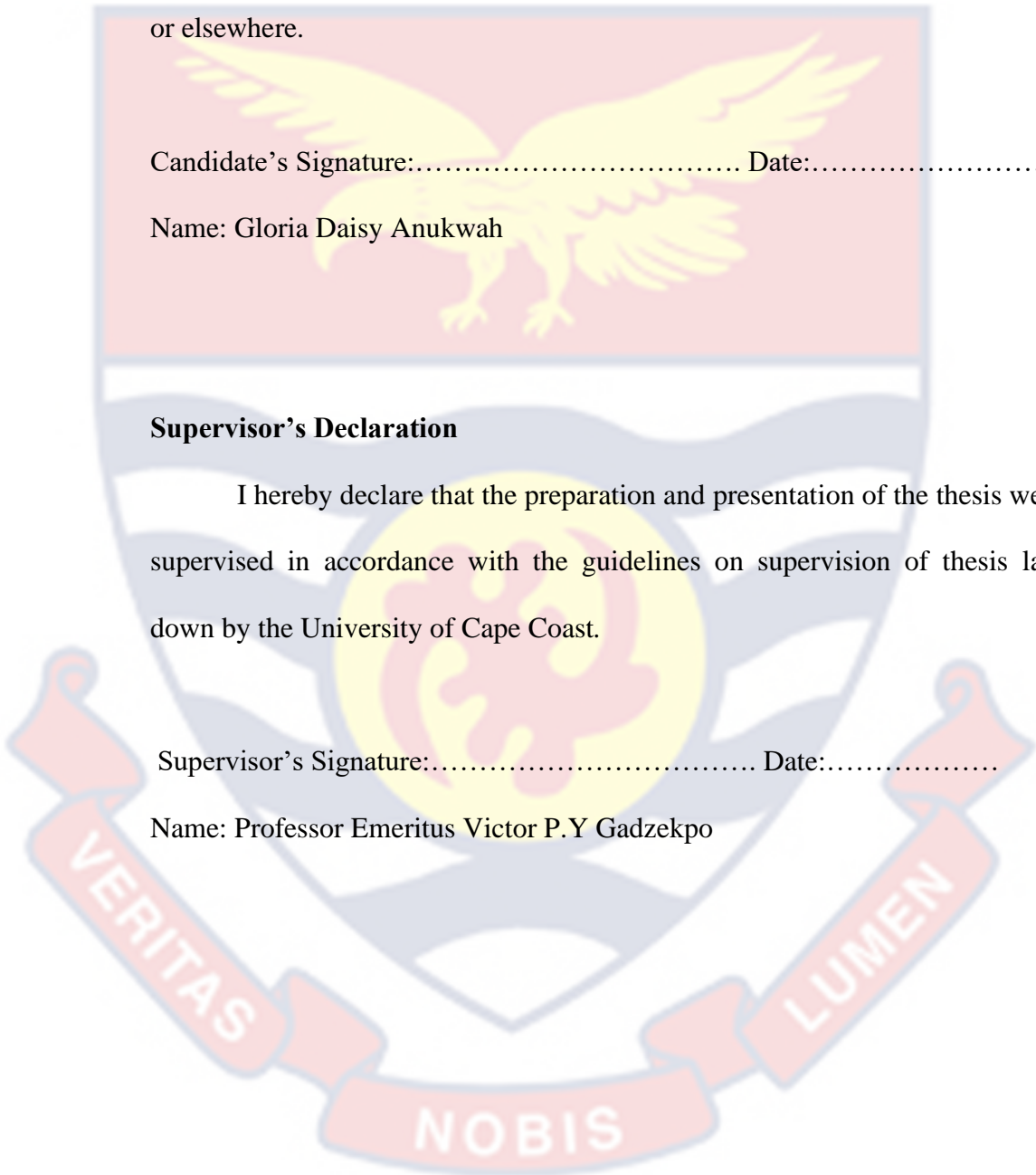Candidate's Signature:…………………………. Date:…………………….

Name: Gloria Daisy Anukwah

Supervisor's Declaration

I hereby declare that the preparation and presentation of the thesis were supervised in accordance with the guidelines on supervision of thesis laid down by the University of Cape Coast.

Supervisor's Signature:…………………………. Date:………………

Name: Professor Emeritus Victor P.Y Gadzekpo

ii

ABSTRACT

Zinc phthalocyanine complex was synthesised and incorporated into natural cellulose-based fibres extracted, from oil palm mesocarp fibres and pineapple leaves wastes, with the view of producing ZnPc-functionalised fibres, to compensate for its' aggregation challenge in most solutions and for easy recovery from reaction solutions, easy disposal after use and for repeated use. The ZnPc-functionalised fibres were characterised by different spectroscopic, thermal and microscopic methods. The results suggested that, the free zinc phthalocyanine dye was indeed embedded and well dispersed within the cellulose-based fibres. The physico-chemical properties of the functionalised cellulose-based fibres were also assessed and found to exhibit the same fluorescence behaviour, that is characteristic of zinc phthalocyanine in solution. This makes them promising for qualitative detection of gases by fluorescence quenching. The photoactivity and singlet oxygen production effects of zinc phthalocyanine were also preserved within the fibre matrices, making them promising photosensitisers for photo-oxidation and photodynamic applications. When applied for optical detection of nitrogen dioxide gas, photodegradation of crystal violet dye and invitro photodynamic antibacterial susceptibility tests, they showed promise for qualitative detection of nitrogen dioxide gas by fluorescence quenching, for the conversion of an organic pollutant, crystal violet in aqueous solutions and as a topical antibacterial agent against methicillin/multidrug-resistant strains, Staphylococcus aureus (MRSA) and Pseudomonas aeruginosa under day/sunlight and redlight radiations.

iii

KEY WORDS

Antibacterial photodynamic therapy (APDT)

Functionalised cellulose-based fibres

Photodegradation

Photosensitiser

Singlet oxygen

Zinc Phthalocyanine

iv

ACKNOWLEDGMENTS

I owe it to Jesus Christ my Lord and Saviour who granted me the grace, divine strength, wisdom and the opportunity for this research. I am most grateful to my mentor and principal supervisor Professor Emeritus Victor P.Y. Gadzekpo, for his fatherly warmth, constructive suggestions, counsel, tutoring and for not giving up on me, but stood by me throughout this research to accomplish this feat together. To Professor Ruphino Zugle, for providing an initial copy of a publication regarding the work.

Much thanks go to Professor Nicholas Dayie, of the Department of Microbiology, University of Ghana, Korle-Bu Campus, for the opportunity to work in their microbiology laboratory for the first trials of the antibacterial activity tests and for providing the bacteria standards for the work; to Daniel Edem Azumah (PhD), Head of Laboratory Dept and Mr Francis Kobina Arthur, Head, Microbiology Unit of the Cape Coast Teaching Hospital, for the opportunity to use their laboratory to complete the antibacterial tests. To Professor Benjamin Anderson, Head of the Department of Laser and Fibre Optic Centre (LAFOC), for the opportunity to use their lab. for the fluorescence analysis and to Mr Andrew Huzortey, for the immense assistance throughout the analysis; to Dr Jerome A. Kpan, for assisting with the purchases of some of the chemicals directly from Sigma-Aldrich, Germany; Dr Andrews Quashie of CSIR, Accra; Dr Rachel Mills, Biomedical; Prosper Dordunu of Fisheries and Aquatic Science; Mr Maclight for his unflinching support, and all staffs of the Department of Chemistry.

Finally, to my wonderful husband, In-laws and family, I say 'ayeekoo' for your unflinching support, prayers and counsel.

DEDICATION

To my mentor, Professor Emeritus V P.Y. Gadzepko; my husband, Dr

Miyittah-Kporgbe and son, Edudzi

TABLE OF CONTENTS

viii

xi

LIST OF TABLES

xiii

LIST OF FIGURES

xv

xvii

xviii

xxii

LIST OF ABBREVIATIONS

B-OPMF	Bleached Oil Palm Mesocarp Fibre
B-PLF	Bleached Pineapple Leave Fibre
CNC	Crystalline nano-cellulose
CoPc	Cobalt phthalocyanine
CS	Chitosan
DMF	N,N-Dimethylformamide
DMSO-$_{d6}$	Deuterated Dimethyl sulphoxide
DMSO	Dimethyl Sulphoxide
DPBF	1,3-Diphenylisobenzofuran
DCP	2,4-Dichlorophenol
DSC	Differential Scanning Calorimetry
FT-IR	Fourier-Transform Infrared
GB	Gauze Bandage
GW	Glass wool
IC	Internal Conversion
ISC	Intersystem Crossing
LCAO	Linear Combination of Atomic Orbitals
LED	Light-Emitting Diode
LUMO	Lowest Unoccupied Molecular Orbital
MCM-41	Mesoporous molecular sieves
MHA	Müeller-Hinton Agar
MO	Methyl Orange
MRSA	Methicillin Resistant *Staphylococcus aureus*
MWCNTs	Multi-walled carbon nanotubes

xxiii

NiPcS	Nickel phthalocyanine
NH_2-KIT-6	Mesoporous KIT-6
OPMF	Oil Palm Mesocarp Fibre
Pc	Phthalocyanine
PDT	Photodynamic Therapy
P-GB	Plain Gauze Bandage
PLF	Pineapple Leave Fibre
Ps	Photosensitiser
PS	Polystyrene
PUR	Polyurethane
PXRD	Powder X-Ray Diffraction
RB	Reactive blue
ROS	Reactive Oxygen Species
r.p.m	Rounds per minutes
S_0	Singlet ground state
S_1	Second excited singlet state
SEM	Scanning Electron Microscope
T_1	First excited triplet state
TAZnPc	Tetra Amino Zinc Phthalocyanine
TBZnPc	Tetra (4-terbutyl) Zinc phthalocyanine
TMS	Tetramethyl-silane
TNZnPc	Tetra nitro Zinc Phthalocyanine
Ur-OPMF	Unrefined Oil Palm Mesocarp Fibre
Ur-PLF	Unrefined Pineapple Leave Fibre
UV-Vis	Ultraviolet Visible

xxiv

XRD	X-ray Diffraction
ZnMCPPc	Zinc Carboxy Phenoxy Phthalocyanine
ZnTCPPc	Zinc (4-Carboxy Phenoxy) Phthalocyanine
ZnTIPAPc	Zinc (4-Isophthalic Acid) Phthalocyanine
ZnTNPc	Zinc Tetranitro Phthalocyanine
ZnPc	Zinc Phthalocyanine
ZnPc-GB	Zinc Phthalocyanine-Gauze Bandage
ZnPc-OPMF	Zinc Phthalocyanine-Oil Palm Mesocarp fibre
ZnPc-PLF	Zinc Phthalocyanine-Pineapple Leave Fibre
ZnPcPy	Zinc Phthalocyanine Tetra Pyridine
ZnPcS	Zinc Phthalocyanine tetra-Suphoxy tetrasodium Salt
ZnPcTs	Zinc Phthalocyanine Tetra-suphoxy complex

LIST OF CHEMICAL SYMBOLS

C	Carbon
Cu	Copper
H	Hydrogen
Mg	Magnesium
μM	Micromolar
mM	Millimolar
N	Nitrogen
O	Oxygen
Wt %	Weight percentage
Zn	Zinc
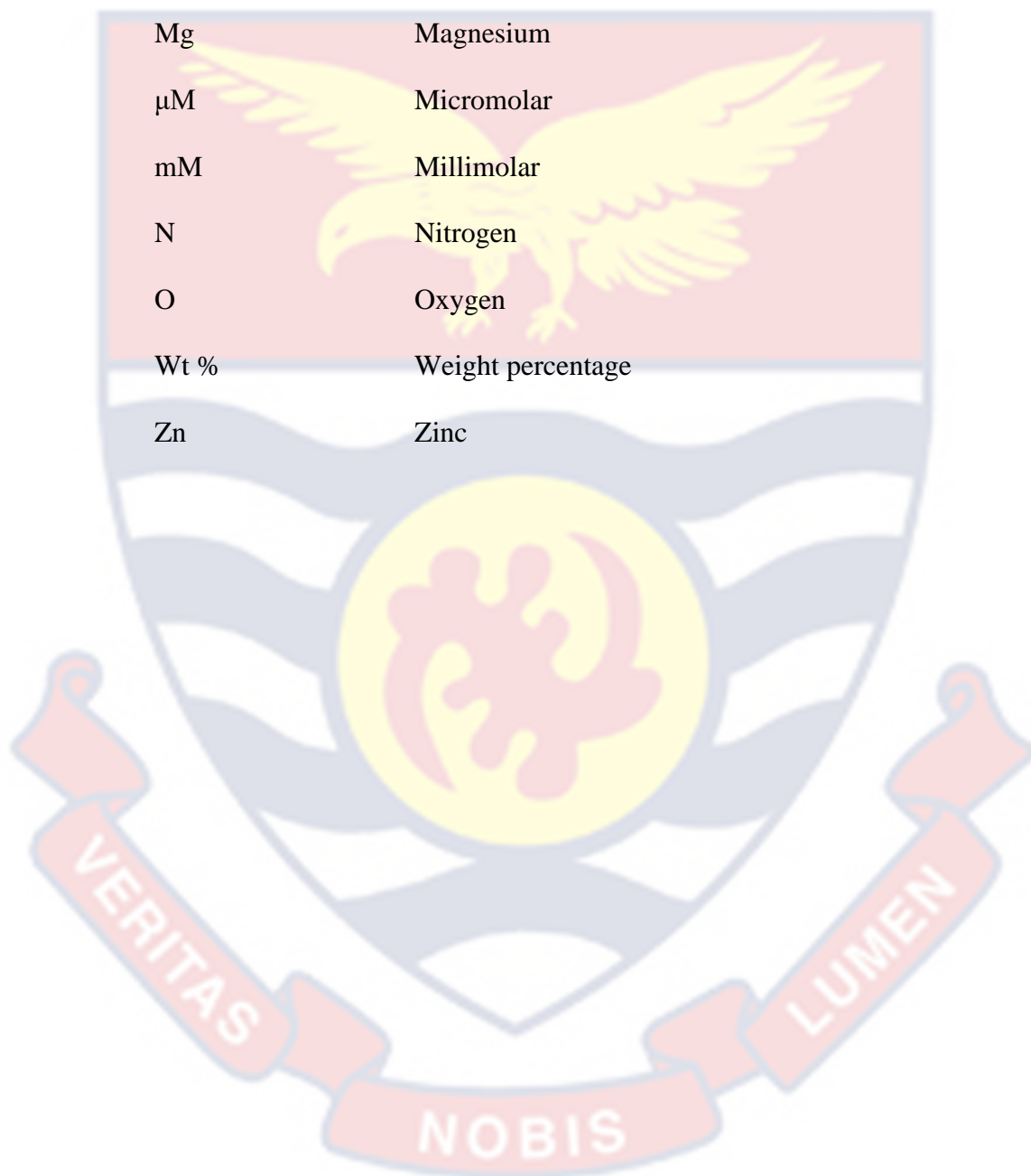
CHAPTER ONE

INTRODUCTION

Phthalocyanines (Pcs) are aromatic heterocycles. They have planar conjugation systems with 18 π-electrons and 4 iso-indole subunits linked, by meso nitrogen atoms. They show two distinct bands in the UV-Vis absorption spectrum, the strong Q band around 600-800 nm and the weak Soret (B) band around 300-400 nm. They can exist as metal-free species or can be metalated by co-ordinating the four inner ring nitrogens with most transition and main group metals (McKeown, 1998) and their photochemical properties are strongly influenced by the type of central metal ion coordinated in their macromolecule. For example, ions with a closed and diamagnetic shell, such as Zn^{2+}, play an important role in metal-phthalocyanine complexes because, of their high ability to generate singlet oxygen, which is essential for effective photodynamic therapy (Goundena *et al.*, 2020), photocatalysis, water and blood disinfection, gas sensing, etc. (Claessens *et al.*, 2008; Doppagne *et al.*, 2018; Imada *et al.*, 2016).

Phthalocyanines are hydrophobic and insoluble in physiological solvents (Chen *et al.*, 2010), aqueous solvents, and some organic solvents (Ghani *et al.*, 2012). They tend to form aggregates (Kobak *et al.*, 2015), that absorb light and suppress the activity of these solvents for singlet oxygen production. Therefore, their immobilisation on appropriate solid supports, capable of exhibiting their photosensitising properties as in solution, will help solve the aggregation, recovery, reusability and disposal problems, often encountered in applications such as photocatalysis and photodynamic therapy (PDT) in which, mainly aqueous solutions are used.

1

Background to the Study

Metal-phthalocyanine complexes are widely used in numerous applications and various research fields, including antimicrobial photodynamic therapy (APDT), photodynamic therapy (PDT), chemosensors, and catalysis (Managa *et al.*, 2014; Sorokin, 2013. Woehrle *et al.*, 2004). When phthalocyanines are used in photocatalysis, reactive oxygen species (ROS) like singlet oxygen are frequently produced. In particular, metal-phthalocyanines containing a strong diamagnetic metal core, show extreme singlet oxygen producing ability (Shinohara *et al.*, 2006). The metal content of the phthalocyanine core has been shown to have a significant effect on the efficacy of photodynamic therapy (PDT). Out of all the phthalocyanines that contain metal cores like Zn, Cu, and Mg, Zinc has demonstrated the greatest efficacy in APDT applications. (Jori *et al.,* 2006). Therefore, this study focuses on the use of Zinc as the central metal.

Recent studies have shown that zinc phthalocyanines can be functionalised as potent photosensitisers against Gram-positive and Gram-negative bacteria (Chen *et al.*, 2014; Güzel *et al.*, 2017; İşci *et al.*, 2016; Liu *et al.*, 2018; Mantareva *et al.*, 2007; Minnock *et al.*, 1996; Wang *et al.*, 2017). Additionally, the antibacterial effects of zinc phthalocyanine have been tested in in-vivo animal models for clinical studies (Schieweck *et al.*, 1994; Vecchio *et al.*, 2013). Chen *et al.*, (2014) reported the use of the zinc phthalocyanine derivative zinc pentalysine-β-carbonyl phthalocyanine (ZnPc-(Lys)$_5$) in APDT, promising antibacterial effects on bacterially infected skin, and increased healing rates after treatment with APDT in animal models. Their study showed that phthalocyanine-based photosensitisers have specific

2

affinities for bacterial cells. They showed more efficient bacterial cell uptake and improved antimicrobial efficacy in-vitro, as well as a significant increase in the healing rate of *S. aureus*-infected excisional wounds in mice. However, these photosensitisers are mainly applied orally, intravenously (Ferreira *et al.*, 2007) and/or topically in the form of solutions (Wang *et al.*, 2017). Therefore, it is not possible to selectively kill bacteria by this method (Chen *et al.*, 2006) and it is difficult to remove excess photosensitisers from the body or blood after photodynamic therapy (PDT). Immobilisation of these photosensitisers on appropriate carriers can selectively kill bacteria and facilitate their removal and disposal after PDT without damaging the human tissue.

The use of metal-phthalocyanine complexes as multipurpose catalysts in various reactions have also been widely investigated (Li *et al.*, 2020; Liu & McCrory, 2019; Makarov *et al.*, 2020), especially in the field of bio-based catalysis (Ren *et al.*, 2019; Sorokin, 2013; Wu *et al.*, 2019), considering their structural relations to naturally occurring metal-porphyrin complexes. Their attractiveness as catalysts stems from their ease of preparation and their chemical and thermal stability (Chen *et al.*, 2017; Sorokin, 2013). The catalytic performance of metal-phthalocyanines is strongly influenced by aggregation when dispersed directly in solution (Iliev *et al.*, 1999; Kluson *et al.*, 2008). Therefore, immobilisation of the active catalysts on suitable supports is highly recommended to ensure high catalyst stability, easy recovery and reuse for further oxidation, product purification, and reduction of inert aggregates (Nyokong & Ahsen, 2012). By recovering and reusing the immobilised photosensitiser, the photo-oxidation process can be applied in a

3

real wastewater treatment system, thereby avoiding disposal and subsequent contamination of the wastewater.

Many materials of natural and synthetic sources have been used for catalysts immobilisation, including porous materials (Shimomura et al., 2008), nanotubes (Chao *et al.*, 2013; Kong *et al.*, 2009), nanoparticles, inorganic materials (Moses Phiri *et al.*, 2019; Rahman *et al.*, 2010) and biopolymers, by physical adsorption, ion separation, or covalent bonding (Abbasi *et al.*, 2016; Pakapongpan & Poo-Arporn, 2017) and others (Ding *et al.*, 2015; Jiang *et al.*, 2017). These properties suggest that immobilised catalysts represent a greener and more sustainable alternative to homogeneous catalyst systems (Chu, 2021; Morshed, 2021).

Several factors are considered when choosing the right support including, the ability to readily introduce anchor functions, degree of functionalisation, ability to participate in reactions, stability under reaction conditions, and environmental availability (Sorokin, 2013). Fibres, especially those based on natural cellulose, are very fine and have a large surface area per volume. They also contain sufficient amounts of reactive and hydrophilic functional groups to support metal-phthalocyanines (Kadish *et al.*, 2012). These supports/carriers provide a strong and long-lasting antimicrobial effect on penetration into the biological environment. This is a unique advantage over other antimicrobial materials, as bacteria need to come into direct contact with the surface of these supports (Hassan *et al.*, 2020). This makes them a useful alternative in situations such as water filtration, bacterial filtration, and wound dressings (Rashki *et al.*, 2021).

Statements of the Problem

Bacteria resistance to antibiotics lowers their ability to effectively treat infected wounds. This can lead to complications such as delayed wound healing, sepsis, and ultimately death (Vazquez, 2006). *Staphylococcus aureus* and *Pseudomonas aeruginosa* infections commonly occur in open wounds and are among the most common nosocomial infections (Benvindo *et al.*, 2008). *Staphylococcus aureus* is a Gram-positive bacterium, known to be highly virulent and develop resistance to antibiotics (Bumah *et al.*, 2015; Santos *et al.*, 2002). *Pseudomonas aeruginosa*, on the other hand, is a Gram-negative bacterium and also highly resistant to antibiotics (Neves *et al.*, 2011; de Sousa *et al.*, 2015). These bacteria can enter open wounds and use them as entry points for more dangerous invasive infections (Chambers & DeLeo, 2009). Fighting them with antibacterial photodynamic therapy (APDT) is the last resort, to prevent them from developing resistance and complicating conditions.

However, most photosensitisers available in clinical applications, e.g. CGP55847, Photosens, Pc 4, Photofrin®, methylene blue, etc. (Ackroyd *et al.*, 2001; Dolmans *et al.*, 2003; Ferreira *et al.*, 2007; Mody, 2000; Ochsner, 1996; Sharman *et al.*, 1999; Wainwright & Crossley, 2002), are in injectable forms. After intravenous injection into peri wound tissue and irradiation (that is, after PDT), removal of residual photosensitisers from the blood or body is challenging (i.e., slow clearance rate from blood or body). It can be excreted in the urine however, it takes a long time, even years, for it to be cleared from the body. In addition, photosensitisers remain in the body for a long time after PDT, which can lead to photosensitive skin after prolonged exposure to light.

5

Therefore, since the photosensitiser can still be effective even if it doesn't physically touch the cell or penetrate the bacterium (Dahl, *et al.*, 1987), targeting bacteria by immobilisation (i.e., supported photosensitiser) can help with the above problems:

1. By removal of the excess immobilised photosensitiser from the wound after antibacterial photodynamic therapy (APDT),

2. By eliminating the damage to the host's healthy tissues, as only the singlet oxygen produced, on the wound surface upon light exposure with the immobilised photosensitiser, causes the cytotoxic effects.

Dyes/pigments emitted from various sources such as the textile industry are highly coloured and affect the environment, especially aquatic life, even in small amounts. These effluents prevent sunlight from penetrating, which impacts aquatic plants' ability to photosynthesise. Organic dyes have been removed from effluents, through variety of physicochemical processes, including precipitation, coagulation, (Daneshvar, 2003) adsorption onto activated carbon etc. But, these processes just transfer the dye to another phase, that require further treatments (Slokar & MareChal, 1998). Among various refining processes, heterogeneous photocatalysis, an advanced oxidation process (AOP), is highly efficient in the complete decolourisation and mineralisation of organic pollutants through the initiation of reactive oxygen species (ROS), without generating unwanted by-products). It is an efficient and cost-effective method for removing stable organic compounds, including dye molecules. It is also environmentally friendly as the catalyst can be removed and reused, reducing the cost of the remediation process (Abdul *et al.*, 2016). Therefore, cellulose-based fibres functionalised with zinc

6

phthalocyanine can be used, under photocatalysis to remove crystal violet (a model organic dye) from water because of its great stability, easy recovery from reaction products, recycling for further oxidations, and reduction of inactive aggregates usually, associated with the free metal-phthalocyanines in aqueous solutions.

Toxic and combustible gas detection is an increasing challenge in both local and manufacturing settings. The common detectors of gases are mostly the semiconductor metal oxide detectors (Varghese & Grimes, 2003), which detect changes in electrical conductivity. But they consume a lot of energy and are sensitive to moisture, making them unattractive as gas or fire detectors (Zugle, 2012). Phthalocyanine applications in gas sensing mostly utilise thin films that exploit the semiconductor properties of phthalocyanines (Dogo *et al.*, 1992; Hsieh *et al.*, 1998; Krier *et al.*, 1993; Mortesson *et al.*, 1990; Wright *et al.*, 1993; Sun *et al.*, 2018; Zhu *et al.*, 2020). Few utilise the fluorescence properties of phthalocyanines in nanostructured matrices (Fernández-Sánchez, 2006), polystyrene polymers (Sanchez *et al.*, 2001), and electro-spun synthetic polymer fibres (Zugle & Nyokong, 2012). Therefore, the use of zinc phthalocyanine-functionalised natural cellulose-based fibres for qualitative fluorescence sensing of nitrogen dioxide gas is reported in this study for the first time.

As far as the authors are aware, very little or no research has been done regarding the immobilization of ZnPc, using green and sustainable natural cellulose-based fibres (from oil palm mesocarp fibres and pineapple leaves), as supports for gas detection, photodegradation of organic pigments in aqueous media and antibacterial photodynamic therapy.

7

Below (Figure 1) is an illustration of the immobilisation and the photosensitisation processes that have been developed in this study.
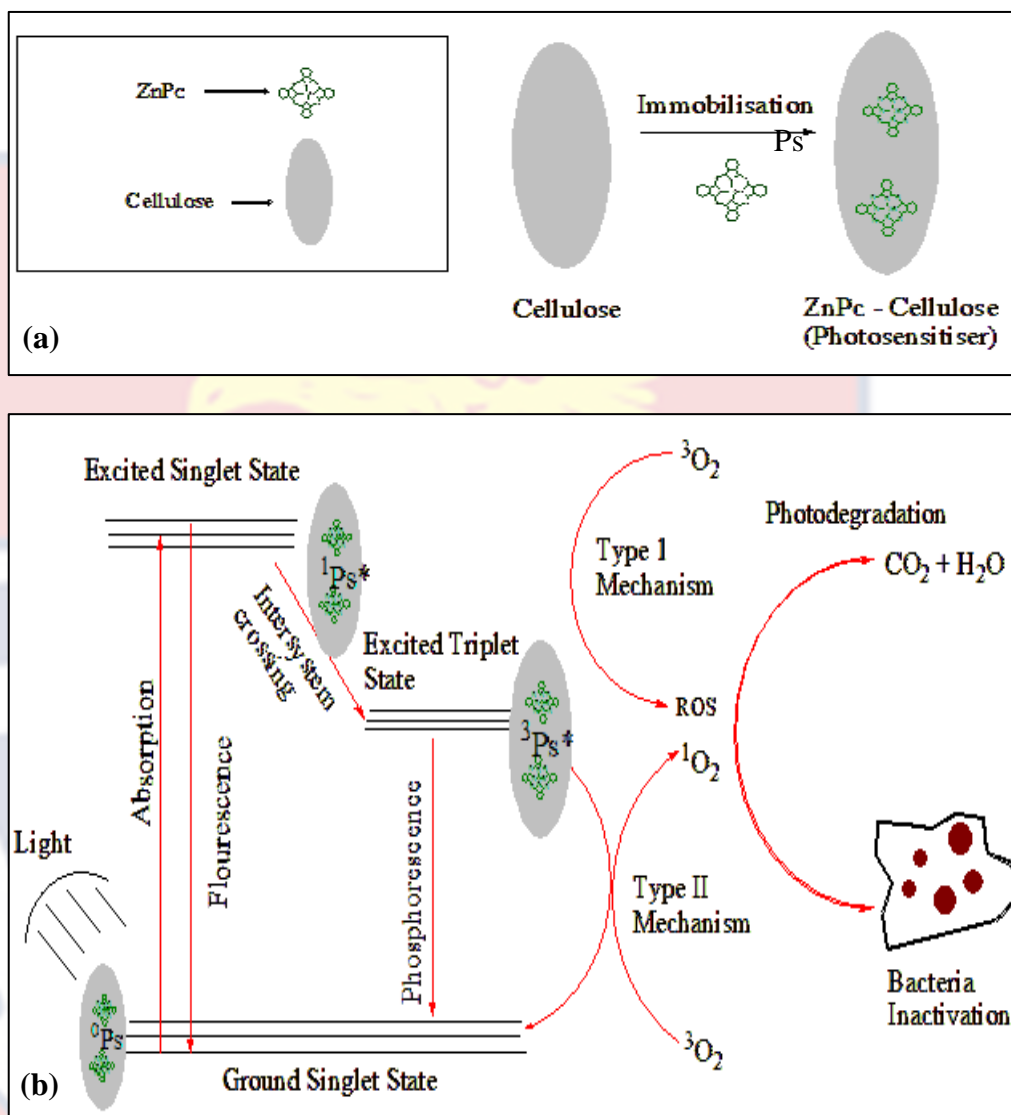
Figure 1: Illustration of the (a) immobilisation process and the (b) mechanism of photosensitisation, leading to remediation of organic pollutants and bacteria inactivation.

Briefly, zinc phthalocyanine is immobilised on porous cellulose-based fibres. The functionalised fibres (Ps) in a photocatalytic system, absorb light and become exited (^{1}Ps*), then either emit the light through fluorescence (for gas detection) or moves to the triplet exited state (^{3}Ps*) through intersystem crossing, reacts with oxygen to produce reactive oxygen species (especially, $^1O_2$) for photodegradation and photodynamic bacteria inactivation.

8

Purpose of the Study

The study's main goal is to investigate the concept of microwave synthesis, cellulose extraction, purification and catalyst immobilisation methods, to produce eco-friendly functionalised cellulose-based fibres that may find use in household, commercial and medical settings. Furthermore, the hypothesis of whether the immobilised catalysts are suitable for nitrogen dioxide sensing, or are able to degrade organic dyes in aqueous media and/or would be suitable for photodynamic inactivation of bacteria, is being tested in the thesis.

Research Objectives

The general objective is to produce zinc phthalocyanine-functionalised cellulosed-based fibres, that can serve as photosensitisers for gas sensing, photodegradation and photodynamic inactivation of bacteria.

Specific objectives

The subsequent specific objectives would be pursued to help achieve the general objective:

1. Synthesis and characterisation of non-substituted zinc phthalocyanine.

2. Extraction of natural cellulose-based fibres (from oil palm mesocarp fibres and fresh pineapple leaves wastes), to be used as support materials using gauze bandage as a reference cellulose.

3. Immobilisation of the synthesised zinc phthalocyanine on the cellulose-based fibre supports and characterisation by spectroscopy (FT-IR, Fluorescence), microscopy (SEM-EDS) and TGA-DSC,

4. Evaluate the photoactivity of the zinc phthalocyanine in the functionalised cellulose-based fibres.

9

5. Evaluate the impact of the zinc phthalocyanine-functionalised cellulosed-based fibres as gas detection fibre support on nitrogen dioxide gas.

6. Evaluate the impact of the zinc phthalocyanine-functionalised cellulosed-based fibres as catalyst supports for photodegradation of organic dyes in aqueous media

7. Evaluate the impact of the zinc phthalocyanine-functionalised cellulosed-based fibres on photodynamic bacteria inactivation in aid of wound healing.

Research Questions and Hypotheses

The ensuing research questions and hypotheses would be set to help accomplish the research objectives:

Research questions

1. Was unsubstituted zinc phthalocyanine synthesised?

2. Is the quality of the extracted cellulose-based fibres, from the oil palm mesocarp fibres and pineapple leaves wastes, comparable to that of the reference gauze bandage?

3. Were the cellulose-based fibres, successfully functionalised with zinc phthalocyanine?

4. Are the zinc phthalocyanine-functionalised cellulosed-based fibres able to exhibit and maintain the photophysical and photochemical properties of the free zinc phthalocyanine?

5. Are the functionalised cellulose-based fibres suitable for fluorescence sensing of nitrogen dioxide gas in the environment?

10

6. Are the functionalised cellulose-based fibres able to photodegrade organic dyes in aqueous media?

7. Are the functionalised cellulose-based fibres suitable for photodynamic bacteria inactivation?

Hypotheses

1. Unsubstituted zinc phthalocyanine was synthesised

2. The quality of the extracted cellulose-based fibres, from the oil palm mesocarp fibres and pineapple leaves wastes, is comparable to that of the reference gauze bandage.

3. The cellulose-based fibres were functionalised with zinc phthalocyanine

4. The cellulose-based fibres, functionalised with zinc phthalocyanine exhibited photoactivity and fluorescence properties of the free Zinc phthalocyanine in solution.

5. The functionalised cellulose-based fibres can be used for fluorescence sensing of nitrogen dioxide gas in the environment

6. The functionalised cellulose-based fibres can degrade organic dyes in aqueous media with sunlight/daylight and LED redlight irradiations.

7. The functionalised cellulose-based fibres can inactivate bacteria with daylight and LED redlight irradiations.

Significance of the Study

This study will significantly contribute to the design of a simple but inexpensive eco-friendly functional cellulose-based fibres, that can be applied as nitrogen dioxide gas sensors, photocatalysts and photodynamic antibacterial dressings. The advantage of this type of application is easy handling, easy

11

disposal after use and repeated usage. What is interesting about these photodynamic and photodegradation processes is that, they can utilise both daylight/sunlight and LED redlight radiations. Therefore, regular daylight can be used in place of LED redlight as a cost-effective alternative.

Delimitations

1. Cellulose-based fibres were extracted from oil palm mesocarp fibres and pineapple leaves.

2. Bacteria samples are reference and clinical resistant isolates including, Methicillin Resistant Staphylococcus aureus (MRSA) 3646 - a resistant phenotype, Methicillin Resistant *Staphylococcus aureus* (MRSA) ATCC 43300, *Staphylococcus aureus* ATCC 25923, *Pseudomonas aeruginosa* and *Pseudomonas aeruginosa* ATCC 27312.

3. Research evaluation and conclusions are laboratory-based experimental data and their respective analyses.

Limitations

Certain influences and conditions could not be controlled in this study, which limited the methodology and consequently the findings. These limitations are:

1. The difficulty in conducting experiments smoothly and efficiently because, the equipment and devices used, were distributed in laboratories all over the country.

2. The exact concentrations of the zinc phthalocyanine dispersed in/on the functionalised fibres could not be quantified due to the nature of the fibres.

Organisation of the Study

The study has different sections, including an introduction and literature review on phthalocyanines, their preparations and physicochemical properties, photodynamic therapy, catalysts and methods of immobilisation, and applications of metal-phthalocyanine functionalised porous supports.

It is also involved in the laboratory microwave synthesis, extraction, characterisation and immobilisation of zinc phthalocyanine on cellulose-based fibres and the subsequent application of these functional fibres in gas sensing, photocatalysis and in-vitro photodynamic antimicrobial inactivation processes.

Finally, a thesis is presented in which the final results are reported and discussed and some recommendations are given.

13
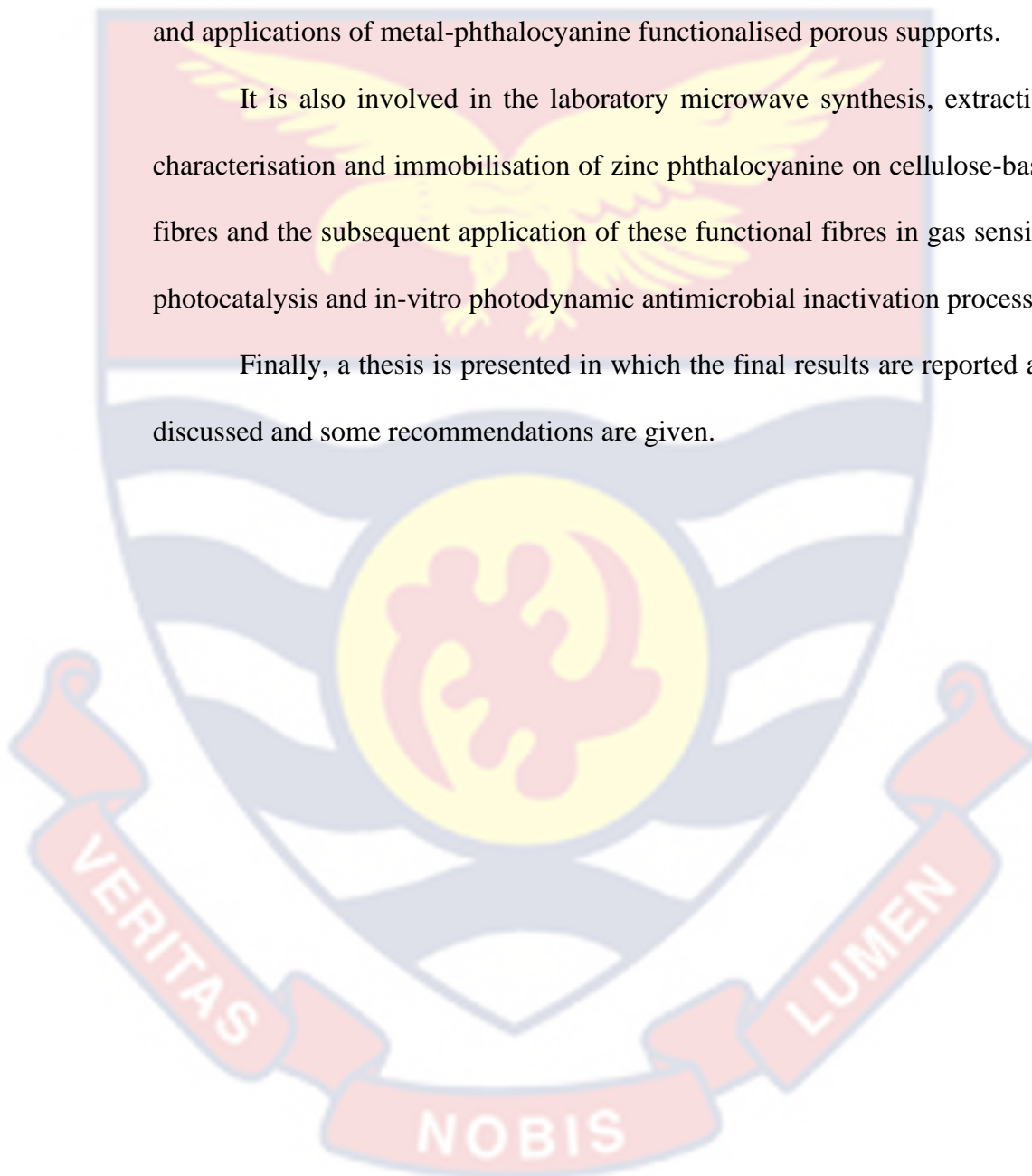
CHAPTER TWO

LITERATURE REVIEW

Introduction

This chapter provides background and common synthetic routes to phthalocyanines. It also describes how other researchers synthesised metal-phthalocyanines through various precursors using microwave synthesis, which achieves higher production yields and faster reactions, as compared with conventional synthesis and the physicochemical properties of phthalocyanines.

It also reviews the background of photodynamic therapy (PDT); metal-phthalocyanine-based antimicrobial photodynamic therapy (APDT), with lists of the various phthalocyanine-antimicrobial agents currently on the market; catalyst immobilisation techniques on fibrous supports; phthalocyanine-immobilised polymer supports, along with research examples of cellulose-based metal-phthalocyanine immobilised supports.

The chapter ends with an overview of the various applications of immobilised phthalocyanines in nitrogen dioxide gas sensing, photodegradation of organic pollutants, and antimicrobial photodynamic therapy (APDT).

Background on Phthalocyanines

Phthalocyanines are macrocyclic organic molecules that resemble naturally occurring porphyrin ring systems. Four iso-indole sub-units connected by aza nitrogen atoms make up the phthalocyanine molecule, which also has an aromatic inner nucleus with 18 electrons that delocalizes to four benzo units around it (Figure 2). The phthalocyanine molecule is more thermally and oxidatively stable when the four aza nitrogen atoms are present.

14

When the π-conjugation is extended, the phthalocyanine rings aggregate and become insoluble in water and other organic solvents (Sobbi, Wohrle & Schlettwein, 1993; Stillman *et al.*, 1989).

There are non-metal species (Figure 2b) or metalated with most transition and main group metals, through coordination of the four inner ring nitrogen atoms (Figure 2b). Most metal ions do not induce significant macrocyclic strain, whilst some ions like Pb^{2+}, the core of the phthalocyanine ring is not big enough to integrate the metal ion, causing the coating of the surface of the ring by the metal (McKeown, 1998). In monovalent alkaline earth metals, core is filled with two ions that protrude from the plane of the phthalocyanine ring. The solubility in polar organic solvents is increased by this protrusion, which breaks down the intermolecular forces between the phthalocyanine rings. (Ziolo & Extine, 1981; Ziolo, Günther & Troup, 1981). In general, metal-free phthalocyanines belong to the D_{2h} symmetry point group, while their counterparts, metal-phthalocyanines, belong to the D_{4h} symmetry point group (Stillman & Thomson, 1974) (Figure 2, a-b).

(a) Metal-free (D_{2h}) **(b)** Metalated (D_{4h})
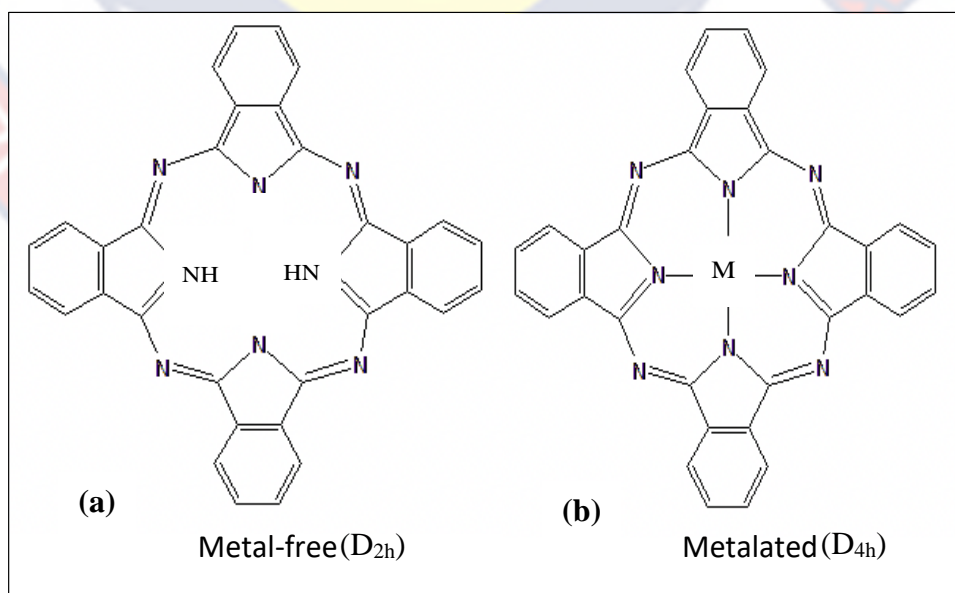
Figure 2: Metal-free and metalated phthalocyanine structures

Braun & Tcherniac (1907), produced the first phthalocyanine when they tried to prepare ortho-cyanobenzamides from phthalimide and acetic acid. Treatment of the ortho-cyanobenzamides at elevated temperatures, formed a blue-black insoluble solid that was later named phthalocyanines. Linstead and associates developed the structure of phthalocyanines and the synthesis of some of their metal derivatives (Byme, Linstead & Lowe, 1934; Dent & Linstead, 1934a,b; Linstead, 1934; Linstead & Lowe, 1934a,b). From the Greek words naphtha, which means "rock oil," and cyanine, which means "dark blue," Linstead and his colleagues came up with the term phthalocyanine. Robertson subsequently used the X-ray diffraction technique to confirm the proposed structure (Robertson, 1935).

Common synthetic routes for phthalocyanines

Phthalocyanines are generally synthesised by cyclotetramerization of precursors (phthalonitrile, phthalimide, phthalic acid, phthalic anhydride) in the presence of metal salts and catalysts, or later insertion of metals into the phthalocyanine ring at high temperatures, for metal-phthalocyanines. In the absence of metal salts, the metal-free counterparts are formed (Kadish *et al.*, 1999; Louati *et al.*, 1985). After the reaction, impurities and unreacted substances are removed by successive washings with some acids and bases and subsequent extraction with solvents. Most organic solvents, acids, and bases can dissolve metal-phthalocyanines, which can then be purified using chromatography, recrystallisation, and extraction (Alzeer, Roth & Luedtke, 2009; Lokesh, Uma & Achar, 2009).

Figure 3, shows the various precursors for synthesising metal-phthalocyanines.

16
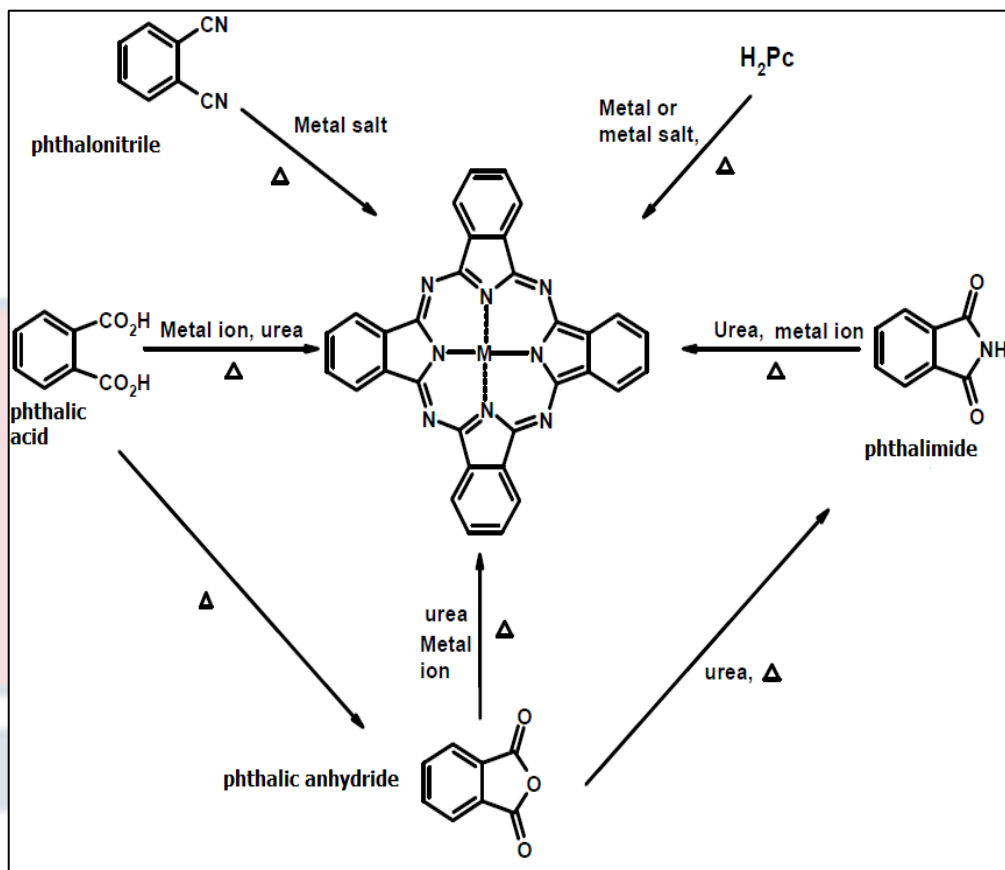
Figure 3: Metal-phthalocyanines synthetic route from different precursors
(Agboola, 2007; Kahya, 2012).

Microwave synthesis of phthalocyanines

Conventional methods for synthesising phthalocyanines were time-consuming and required high-temperature boiling solvents, which resulted in low yields, due to the decomposition of reactants and the formation of by-products. Consequently, a practical high-power microwave technique was developed. Microwave radiation as a substitute to the conventional heating in the production of phthalocyanines and associated counterparts has gained significant interest in latest years (Dumoulin, 2011). All conventional reactions involving heating are now possible with this technology. The main advantage is prompt heating, without any interference with the reaction container and reduction of the prolong reaction times to minutes, thereby

17

restricting the development of by-products which, usually occur under conventional heating. Irradiation with microwave, improves yields and significantly purifies reaction products (Dumoulin, 2011).

Microwaving, utilises the capacity of some chemicals (liquid or solid) to convert electromagnetic energy into heat. Heating is caused by dielectric losses, which contrasts with the conduction and convection processes observed in conventional heating. Some reactions which hitherto, were not possible with the conventional heating are now possible with microwaves (Önal, Dumoulin & Hirel; 2009).

Microwave synthesis of phthalocyanines and its' counterparts are subdivided into: (i) reactions with solvents and (ii) solvent-free reactions. Reactions with solvents are uncommon, due to safety hazards when using domestic or modified domestic ovens. Especially in such systems, reaction temperature and pressure cannot be controlled due to uncontrolled microwave heating. Therefore, focus is now shifted to solvent-free reactions, that are safely carried out in open containers (Dumoulin, 2011).

Solvent-free synthesis of phthalocyanines are performed from phthalic anhydride, phthalic acid, phthalimide or phthalonitrile precursors. Addition of ammonium molybdate always increases reaction yields, regardless of which precursor was used, except when phthalimide is used. (Chauhan *et al.*, 2003). Phthalonitrile ensures a clean reaction and gives a pure phthalocyanine at the end of the reaction. However, this is not the case for other precursors, since an additional source of nitrogen can trigger side reactions and form by-products. Phthalic anhydride is most commonly used because it is cheap (Kahya, 2012).

Many examples of phthalocyanines (Cavaleiro, Tomé & Neves, 2010) and their counterparts, have been synthesised with microwaves, such as macrocycle formation, their metal insertion, or functionalisation. Here are some examples:

The first synthesis of metal-phthalocyanines using microwave irradiation was performed by Shaabani in 1998. A homemade microwave oven operating at a power of 900 W, without temperature control was used. Yields ranged from 81% to 86%, depending on the metal. Various metal-containing Cu, Co, Ni, and Fe phthalocyanines were obtained in the absence of a solvent. A mixture of $C_8H_4O_3$, $CO(NH_2)_2$, $CuCl_2$ and $(NH_4)_6Mo_7O_{24}$, was irradiated for six minutes. The product was washed successively with NaOH, H_2O, HCl, H_2O, recrystallised from H_2SO_4 and then extracted with methanol and methylene to give pure metal-phthalocyanine (Shaabani, 1998).

Shaabani *et al.* (2003), synthesised tetranitro-phthalocyanine complexes of Nickel, Copper, Cobalt, Manganese, Iron, and Palladium in the absence of a solvent and under reflux. 3-Nitrophthalic anhydride, urea, metal chlorides, and ammonium heptamolybdate were microwaved on high power for 1 minute and then on medium power for another 1 minute. The product was then treated with 1M HCl, 1M NaOH and washed with water till neutral pH. The solid was then recrystallised from methanol. Under reflux, initial materials were immersed in nitrobenzene in a round bottom flask with a condenser and irradiated for 5 minutes in a high-power microwave oven. The product was then processed as before and confirmed by elemental, UV-visible and IR analysis.

19

Khaya *et al.* (2019), synthesised zinc phthalocyanine using $CO(NH_2)_2$ (184 mmol), $C_8H_4O_3$ (36 mmol), $ZnCl_2$ (15 mmol) as precursors and $(NH_4)_6Mo_7O_{24}$, (0.13 mmol) as catalyst. After wetting the mixture with 5 mL distilled water in a flask, the mixture was heated for 3 min at 600 W in a microwave. Hot water treatment (200 mL – 70°C) was the first step in the purification process, followed by successive washing steps (200 mL – 40°C), 1 M NaOH (200 mL – 20°C), hot water (200 mL – 70°C), and ethanol (100 mL – 20°C), before filtering. UV-VIS and Fourier-transform infrared (FTIR) spectroscopies were used to verify the purity of the zinc phthalocyanine

Shaabani *et al.* (2007), synthesised both the free- and metalated-phthalocyanine. For the free-phthalocyanines, $C_6H_4(CN)_2$ was used as the precursor, $[(CH_3)_3Si]_2NH$ and $(NH4)_2SO_4$ as catalysts and DMF as solvent for irradiation. The crude solis was then washed with methanol, then dissolved in H_2SO_4 and recrystalised in water. After which it was extracted with methanol. For the metal-phthalocyanines, various precursors such as phthalonitriles, phthalimides and phthalic anhydride were use with hexamethyldisilazane and p-toluenesulfonic acid as catalysts. The product was washed with cold H_2O and $(CH_3)_2CO$ and dried. It was then precipitated from distilled water after being dissolved in H_2SO_4. Analysis using FTIR and UV-Vis spectroscopy verified the different yielded free- and metal-phthalocyanines.

Villemin *et al.* (2001) synthesised various metal-phthalocyanines (Mg, Zn, Cd, Cu, Ni, Pd, Pt, Co, Fe, Ru, Rh, Ti, Cr, Mn, V, Mo, UO_2, Eu) using the microwave method. The metal-phthalocyanines were synthesised from hydrous metal salts and phthalonitriles in a commercial microwave oven. Following water, acetone, and dichloromethane washes, the products were

20

dried under vacuum. Acetonitrile extraction was used to achieve purification, which was then dried at 110 °C. The same experiment was performed using phthalic anhydride and urea to synthesise metal-phthalocyanine chlorides of Fe, Co and Cu. The products were washed with 1M HCl, 1M NaOH and H_2O. Purification was done as before, and UV-Vis and FTIR spectroscopies confirmed the production of metal-phthalocyanines.

Lokesh *et al.* (2009), synthesised platinum tetranitro-phthalocyanine using microwave irradiation. Nitro-phthalonitrile was mixed with platinum (IV) chloride and irradiated at 540 W for the first 2 min, then at increased power (720 W) for 3 min. The product was washed with water and ethanol and extracted with acetone.

Ogunsipe & Opeolu (2020), synthesised aluminium phthalocyanine chloride by grinding a mixture of phthalonitrile (10 mmol, 1.28 g) and aluminium chloride hexahydrate (2.5 mmol, 0.604 g) and subjecting the mixture to microwave irradiation for 10 min. The solid was washed successively with water (15ml), acetone (15ml) and dichloromethane (15ml) and then air dried. It was then extracted by Soxhlet extraction with acetonitrile for 8 hours. After drying at 110 °C, FTIR and UV-VIS spectroscopy were used to analyse the pure phthalocyanine.

In this study, a slightly modified microwave method by Kahya *et al.*, 2019; Shaabani *et al.*, 2007 and Villemin *et al.*, 2001, was used to synthesised the unsubstituted zinc phthalocyanine dye.

The main problem facing these researchers is the aggregation behaviour of metal-phthalocyanines in solution due to large ring-molecular interactions. This restricts their usage in various applications, introducing

various substituents on the macrocycles (Durmuş & Nyokong, 2007) or attaching them to suitable solid supports, can help solve this problem.

In this study, an unsubstituted zinc phthalocyanine dye is incorporated into natural cellulose-based fibre supports. The porous nature, hydrophilicity and large surface area of these fibrous supports provide a suitable environment for dispersing the phthalocyanine throughout the fibrous matrices for use in solution-based applications, where the free zinc phthalocyanine is insoluble.

Spectral properties of phthalocyanines

The electron absorption spectra of the free- and metalated-phthalocyanines have been extensively reviewed in the gaseous, solution and solid states (Hush & Woolsey, 1971; Renge, 1993; Stillman *et al.*, 1989). The basic model often used to describe the source of the distinctive peaks of phthalocyanines is the four-orbit Gutermann model (Gouterman *et al.*, 1963). This model describes a $\pi \rightarrow \pi^*$ transition occurring from the highest occupied molecular orbital (HOMO) to the lowest unoccupied molecular orbital (LUMO) and leading to the Q and B (Soret) bands of the UV-Vis spectrum. The Q band corresponds to electronic transitions from a_{1u} orbitals to e_g orbitals, and the B bands arise from electronic transitions from a_{2u} orbitals to e_g orbitals (Figure 4). Metal-phthalocyanines have degenerate e_g orbitals and a single Q band. The insertion of metal into the central phthalocyanines cavity leads to the formation of a more symmetric (D_{4h}) thermodynamically stable delocalized dianion (Claessens *et al.*, 2008). Metal-free phthalocyanines (H_2Pc) have non-degenerate orbitals (x and y), low symmetry (D_{2h}), and split x- and y-polarised Q-band (Q1 & Q2) components (Mack & Kobayashi, 2011).

22
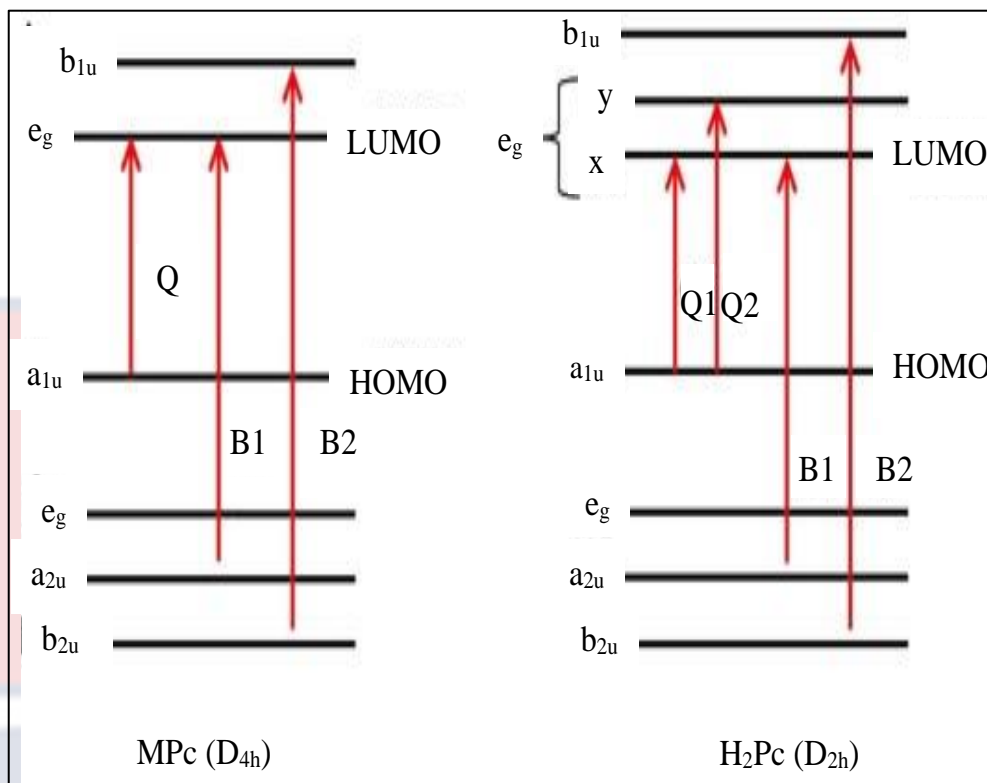
Figure 4: Gouterman's four-orbital model showing electronic transitions and the origin of the two major absorption bands (Q & B) [Gounden *et al.*, 2020; Gouterman *et al.*, 1963].

The electronic spectrum of phthalocyanines is divided into two distinctive peak regions resulting from π-π^* transitions due to the delocalised 18 π electron structure. The spectrum usually, consists of a strong near-infrared band called the Q band which, is defined by a higher molar absorbance than the other band in the spectrum and affects the colour of the entire phthalocyanine molecule (Lever, 1965; Stillman & Thomson, 1974). Q band occurs during conversion from HOMO (a_{1u}) to LUMO (e_g) and so on. As previously mentioned, the highly symmetric metal-phthalocyanine Q band D_{4h}, is single. However, for the metal-free phthalocyanines, Q-band splitting (Q1 & Q2) occurs due to the lower symmetry D_{2h} (Figure 5). Splitting in the Q band occurs, when the symmetry of metal-phthalocyanine is reduced by the insertion of larger metals. The fluorescence spectrum of phthalocyanines

23

includes a B band in the ultraviolet region. Additional bands are shown depending on the solvent in which the spectrum is recorded; N, L, and C can be observed.
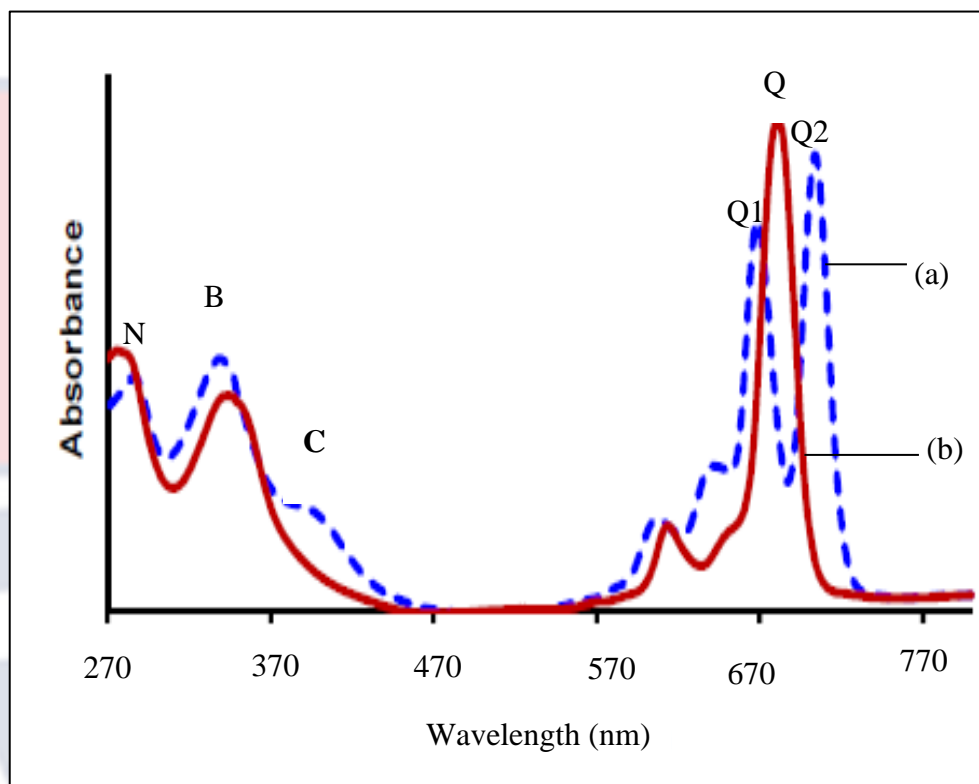
Figure 5: Electronic absorption spectra of (a) metal-free and (b) metalated phthalocyanines with Q, B transition bands (Sönmez, 2014).

Absorption spectra of zinc phthalocyanine

Zinc phthalocyanine (or Zinc tetrabenzo-[5,10,15,20]-tetraaza-porphyrin) exhibits a strong Q-band around 670 nm and broader B-band around 300 nm in the absorption spectrum (Gouterman, Wagnière & Snyder, 1963) (Figure 6).

24
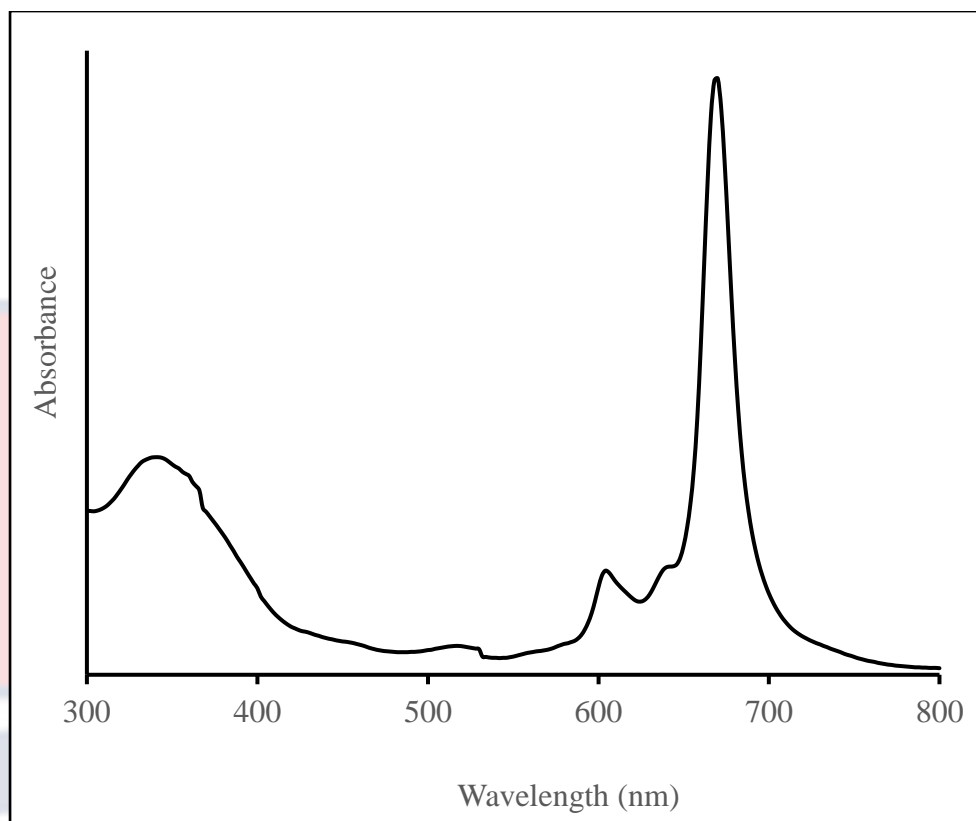
Figure 6: Typical absorption spectrum of zinc phthalocyanine in DMF
          solution.

Fluorescence spectra of zinc phthalocyanine

Luminescence is when molecules in the excited states emit light. It is divided into fluorescence and phosphorescence, depending on the nature of the excited state. In fluorescence, light emission occurs from the singlet excited state to the ground state whereas, phosphorescence emission occurs from the triplet excited states. Unlike fluorescence, the transition to the ground state is prohibited and the associated emission leads to longer lifetimes (Lakowicz, 2006).

Fluorescence generally occurs in aromatic molecules with conjugated pi-electrons. The emission spectrum varies with the chemical makeup of the molecule and the solvent employed to dissolve it (Lakowicz, 2006; Kahya,

25

2012). Below are some examples of studies done on the effect of solvents and substituents on the fluorescence properties of zinc phthalocyanines.

Oguncipe *et al.* (2003), studied the effect of solvents on the fluorescence properties of zinc phthalocyanine derivatives, pyrodino zinc phthalocyanine, zinc octaphenoxy-phthalocyanine, and zinc octaestrone-phthalocyanine. Their fluorescence spectra were recorded in dimethyl sulfoxide, tetrahydrofuran, dimethylformamide etc. and the findings demonstrated that the quantum yield and other photochemical characteristics of zinc phthalocyanine and its derivatives, as well as their fluorescence, depend on the type of solvent used.

Kimura *et al.* (1997), studied dendritic zinc phthalocyanines, zinc phthalocyanine was the central dendrimer. Polyetheramide was a functional group that mitigates the tendency of zinc phthalocyanine to aggregate. In addition to studying the production effect on aggregation, they also studied changes in the fluorescence properties of dendrimer phthalocyanines. They argued that molecules in the aggregated state do not exhibit fluorescence, but that fluorescence properties become apparent as aggregation decreases.

Kaya *et al.* (2019), synthesised zinc phthalocyanine (ZnPc), tetra nitro zinc phthalocyanine (TNZnPc) and tetra amino zinc phthalocyanine (TAZnPc and studied their fluorescence in DMF. In their study, the ZnPc pigment showed two emission peaks when excited at 340 nm: a larger peak at 680 nm and a smaller peak at 740 nm. In contrast to the TAZnPc pigment, which was excited at 400 nm and had emission peaks at 465 and 800 nm, the TNZnPc pigment had emission peaks at 460 and 685 nm. There was no fluorescence with DMF alone. There was a clear distinction in their

26

emission spectra: for ZnPc, the fluorescence intensity decreased with concentration, but for TNZnPc and TAZnPc, it increased. With rising concentrations, the peaks of ZnPc, TNZnPc, and TAZnPc also slightly moved to the right.

Photo-physicochemical processes

Phthalocyanines can absorb suitable wavelengths of visible light which, trigger interesting physical processes such as fluorescence, and can also influence chemical changes in compounds such as organic substrates (Shen, Yuan & Xu 1989; Tau & Nyokong, 2007).

The foundation of the photo-physicochemical processes is interpreted by Jablonski diagram (Figure 7). When the molecule is illuminated with light (hv) during absorption, the electron gains energy and transitions from the ground state (S_0) to the first excited state (S_1) or higher excited states (S_2) and (S_3). Vibrational relaxation occurs by colliding with the molecules of solvent and the excited S_2 molecule returns to the original vibrational level of S_1, from which several possibilities are possible: fluorescence (F), phosphorescence (P), or exotherm. Fluorescence is a radiative process that occurs when molecules excited by S_1 lose energy and return directly to the ground state. The time interval of the $S_1 \rightarrow S_0$ transition leading to fluorescence (F) is very short (10^{-8} to 10^{-5} s). Phosphorescence (P) is preceded by the non-radiative processes, internal conversion (IC) and intersystem crossing (ISC). The decay of phosphorescence is comparable to fluorescence, except for electron spin transitions to the 'forbidden' triplet state (T_1) rather than the lowest excited singlet state. This transition is called an intersystem crossover. The drop from the electronic level T_1 occurs at lower energies compared to fluorescence.

27

When this transition occurs in tissues, the participating molecules transfer energy to the ground state of the oxygen molecule (in triplet state), generating singlet oxygen as one of the reactive oxygen species (ROS) that can initiate tissue oxidation. The concept of photodynamic therapy (PDT) is based on this property (Nakai *et al.*, 2003; Jablonski, 1935).
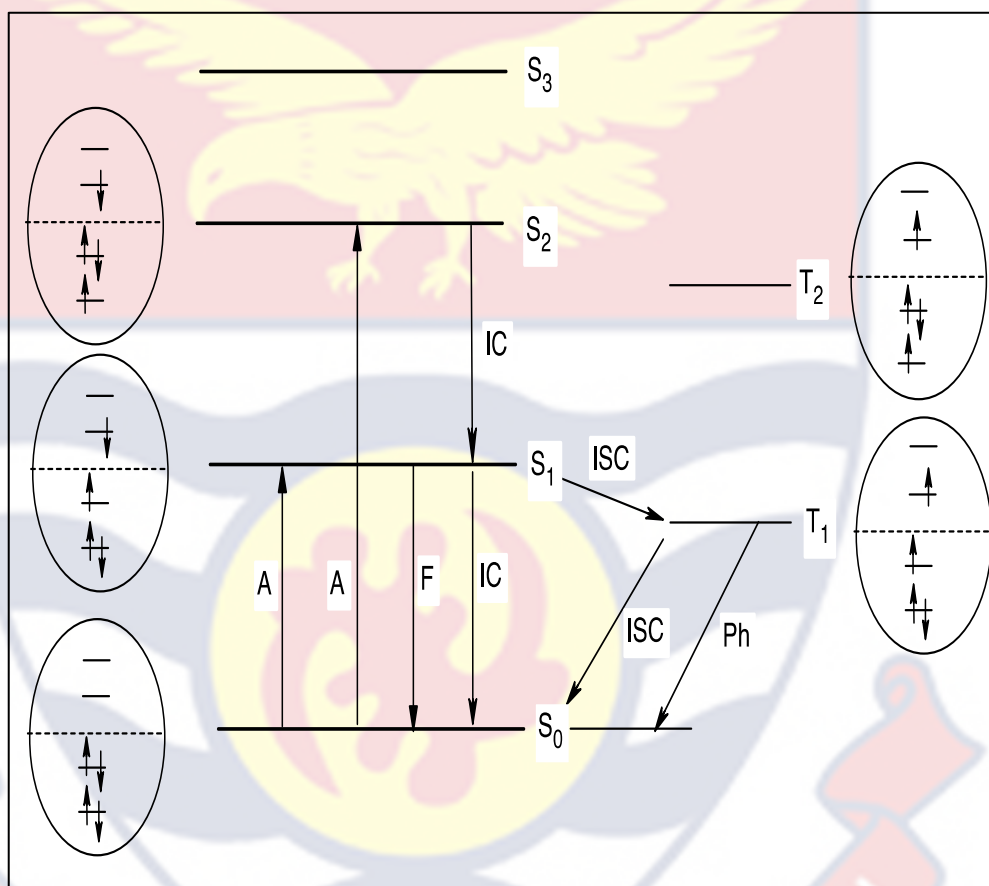
Figure 7: Illustration of photo-physicochemical processes by Jablonski diagram (Jablonski, 1935; Hesse *et al.*, 1997).

Phthalocyanines with big diamagnetic metals are famous for promoting inter-system transition from $S_1 \rightarrow T_1$, thereby producing $^1O_2$. Singlet oxygen ($^1O_2$) is involved in a number of photooxidation processes (Kaestner *et al.*, 2003) and is also used for photochemical metabolism of various analytes (Agboola, Ozoemena & Nyokong, 2006; Tau & Nyokong, 2007). Most of the phthalocyanine applications, such as photodynamic therapy (Kaestner *et al.*,

28

2003) and homogeneous catalysis (Tau & Nyokong, 2007), are usually performed in solution. However, in some applications, solid state use may be preferred, for example in read/write CDs (Gu *et al.*, 1995) or immobilised support systems, which give better advantages such as easier recovery, reuse and disposal after use. In this study, unsubstituted zinc phthalocyanine is immobilised on cellulose-based fibres and used for gas sensing and photocatalysis.

Background on Photodynamic Therapy (PDT)

Photodynamic therapy (PDT) was chanced upon over 100 years ago by Oskar Raab and Hermann von Tappiner, when they sighted the presence of Paramecium sp. which, was stained with acridine orange, have died due to exposure to bright light (Raab, 1900). They concluded that this photodynamic effect could have medical applications. Afterwards, another dye called eosin was used to apply the photodynamic theory to dermatology (Roberts & Cairnduff, 1995). In 1912, Friedrich Meyer Betz published the results of experiments he had performed on himself by injecting mixtures of porphyrin oligomers, showing that erythematous reactions occurred only in light-irradiated tissues, proving that photodynamic effects depend on light and photosensitisation (Meyer-Betz, 1913; Roberts & Cairnduff, 1995). In the 1970s and 1980s, protocols developed by Dougherty and his group used a photosensitiser called a hematoporphyrin derivative (HPD, later named Photofrin®, similar to the one Meyer injected himself with. Hematoporphyrin derivatives (HPDs) have shown great potential for the treatment of tumours, leading to the FDA's approval of PDT as a treatment for head and neck cancer (Dougherty, 1992; Dougherty *et al.*, 1978). Oseroff and co-workers then

29

proposed a strategy to target intracellular organelles rather than tumour vasculature (Modica-Napolitano *et al.*, 1990). Later, intracellular photosensitisers were tested clinically and found to be potentially more effective. Since then, PDT has established itself as a tool to treat a variety of tumours and has become the primary tool used to treat age-related macular degeneration (Denis & Hamblin, 2011). Photodynamic therapy (PDT) uses harmless visible light in combination with light-sensitive dyes (called photosensitisers) and oxygen present in and around cells to kill diseased cells.

Antimicrobial photodynamic therapy (APDT)

The idea of photodynamic cell death was quickly expanded to include the treatment of infections (i.e., its photo-antimicrobial activity (Wainwright, 1998; 2009). An effective non-invasive technique for treating infections is called antimicrobial photodynamic therapy (APDT). The type, concentration, charge, and microbial class of the photosensitiser all affect how effective antimicrobial photodynamic therapy is against different microorganisms. The structural makeup, permeability, and capacity to bind foreign molecules vary amongst microbial cell walls (Huang *et al.*, 2012). Due to the special structure of the cell envelope, Gram-positive pathogens are much more sensitive to anionic and neutral photosensitisers, due to the thick and porous peptidoglycan layer on their outer surface. Gram-negative bacteria are less prone to uptake exogenous compounds thanks to the additional outer membrane and the permeability barrier conferred by the lipopolysaccharide. In some cases, negatively charged or neutral photosensitisers are more effective than high concentrations of cationic photosensitisers (Mejlholm & Dalgaard, 2015; Tomé *et al.*, 2004). Also, there are reports that photosensitisers do not

even need to penetrate or affect cells to be effective. According to some authors, generation of sufficient amounts of singlet oxygen near the bacterial outer membrane can damage vital structures (Dahl *et al.*, 1987). Therefore, antimicrobial photodynamic therapy (APDT) may be successful without direct contact between photosensitisers and bacteria.

The primary APDT treatment is therefore, believed to be a Type II mechanism, through singlet oxygen as the main reactive specie, responsible for cell destruction (Dhami & Philips, 1996; Ryter & Tyrrell, 1998). Despite numerous studies on the effects of photodynamic therapy on various microbes, the development of resistance has not been reported (Mayhew *et al.*, 2001; O'Riordan, Akilov & Hasan, 2005). This important phenomenon does not appear to be confined to microorganisms, and studies have shown that, except in rare circumstances (Hornung *et al.*, 1998), cancer cells also do not develop resistance to photodynamic therapy (Davies & Davies, 2010; Laptev *et al.*, 2006). In this regard, it remains unclear, why photodynamic therapy (PDT) differs from other cytotoxic strategies such as antibiotics and anticancer chemotherapy, where the development of multidrug resistance after repeated exposure to free drug is the norm (Minnock *et al.*, 2000; Tan *et al.*, 2010).

Mechanism action of photodynamic therapy (PDT)

Photodynamic therapy (PDT) requires the simultaneous use of a chromogenic molecule called a photosensitiser (Ps), oxygen and light. Upon illumination, the photosensitiser transitions from the ground state (^{0}Ps) to the singlet excited state (^{1}Ps*). In this state, ^{1}Ps* returns to the ground state and transitions to the triplet excited state (^{3}Ps*) by short-lived fluorescence emission or intersystem crossing. The short-lived triplet excited state Ps (^{3}Ps*)

31

can return to the ground state either by phosphorescence emission (with a half-life of ~1 s) or by two different mechanisms. In a Type I mechanism, $^3Ps^*$ donates electrons to a reducing substrate (lipid component of the cell membrane) to form the short-lived radical Ps ($^3Ps^-$). This radical Ps ($^3Ps^-$) readily reacts with oxygen to produce a cascade of reactive oxygen species (ROS) such as superoxide anions (O_2^-), hydrogen peroxide (H_2O_2), or hydroxyl radicals (OH^*). In contrast, in the Type II mechanism, $^3Ps^*$ reacts directly with ground-state molecular oxygen. The oxygen molecule is originally in the triplet ($^3O_2$) state. Both triplet species react and self-annihilate, and through energy transfer the oxygen molecule in the triplet ground state forms a singlet oxygen reactive species ($^1O_2^*$). Both mechanisms involve oxygen, but Type I relies on intimate contact with the substrate and Type II relies on the availability of molecular oxygen in the medium (Figure 8).
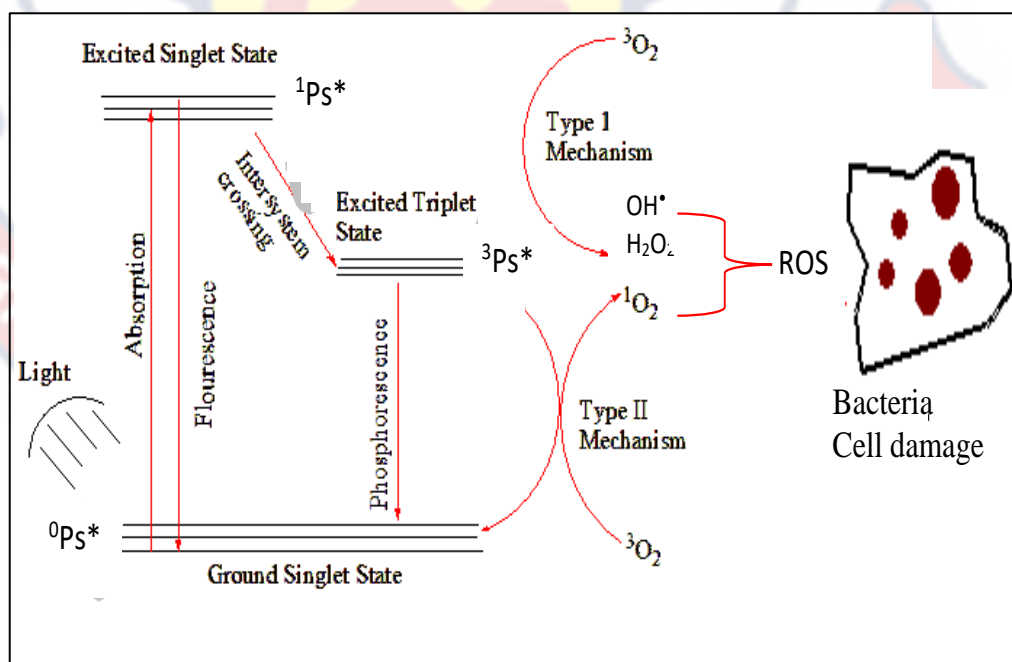
Figure 8: Photochemical mechanism routes of photodynamic bacteria cell destruction.

32

Because the Type II response is mediated by singlet oxygen species, it is believed to be the main route of microbial cell inhibition (De Rosa & Bentley, 2000; Konpka & Goslinski, 2007). But, it is hard to differentiate between both mechanisms. Contributions by both mechanisms indicate that, the damage is dependent on the oxygen partial pressure and the photosensitiser amount (Konopka & Goslinski, 2007).

The appearance of large amounts of radically oxidising and non-radically oxidising species on microorganisms is extremely destructive for two main reasons. One is the lack of effective microbial defence against these species and multiple targets. Although cells are equipped with several natural defence mechanisms against reactive species, the magnitude of the redox imbalance caused by PDT is several orders of magnitude greater than the level or protection provided by intracellular enzymatic and molecular antioxidants. Furthermore, bacteria can protect themselves from superoxide radicals and hydrogen peroxide, whereas hydroxyl radicals and singlet oxygen cannot be deactivated naturally. An important advantage of PDT is therefore the lack of microbial resistance (Wainwright, 1998; 2004).

Studies have indicated that, photosensitiser and light do not affect bacteria or normal tissue when used separately. Only the combination of both affects the bacteria in APDT (Burns *et al.*, 1993; Williams *et al.*, 2003, 2004).

Light sources

According to the British Dermatology Group and the American Society of Photodynamic Therapy Board, no standardised guidelines exist for "optimal irradiance wavelength, and total dose characteristics of PDT" (Goldberg, 2008; Nakano *et al.*, 2009). However, a basic requirement for a

PDT light source is to match the activation spectrum (maximum absorption band) of the photosensitiser and produce sufficient light intensity at this wavelength (Wilson & Patterson 2008). Currently, PDT mainly uses helium-neon lasers (633 nm), gallium aluminium arsenide diode lasers (630-690, 830 or 906 nm), and argon lasers (488-514 nm) as light sources at specific wavelengths (630-800 nm). The wavelengths of these sources range from visible light to the blue of argon lasers, or the red of helium-neon and gallium aluminium arsenide lasers, to the infrared of some diode lasers (Klotz *et al.*, 1999). Common light sources include mercury lamps (for UV systems), fluorescent lamps, and Xe arc lamps (for visible light systems).

Recently, light-emitting diodes (LEDs) have attracted interest due to advantages such as short warm-up time, no hazardous material disposal, long life, compatibility, narrow emission spectrum (Kuipers, 2014; Kuipers *et al.*, 2015), and low cost. Light emitting diodes (LEDs) have recently been used in PDT to illuminate particularly surfaces of tissues that are easy targets (Gursoy *et al.*, 2013; Juzeniene & Moan 2007). Attempts have also been made to use LEDs as light sources for the photo-oxidation process (Carra *et al.*, 2015; Kuipers *et al.*, 2015; Verma & Sillanpää, 2015). Both daylight/sunlight and LED redlight sources are used in this study.

Zinc phthalocyanines as antimicrobial agents

Phthalocyanines are primarily used in antimicrobial photodynamic therapy because of their high fluorescence and singlet oxygen quantum yield. Metals at the centre of phthalocyanines have been shown to have a significant impact on the efficacy of antimicrobial photodynamic therapy. Closed-shell diamagnetic metal-phthalocyanines are more suitable for PDT due to higher

34

yields and longer lifetimes of triplet states (Zn^{2+}, Al^{3+}, Ga^{3+}, etc.) than their paramagnetic counterparts (Brasseur, 2003). Among phthalocyanines that contain Zn, Cu, and Mg, in their core, Zn has shown the greatest efficacy for antibacterial photodynamic therapy applications (Jori *et al.*, 2006). Zinc phthalocyanine has attracted attention as a photosensitiser due to its strong absorption in the near-infrared region, excellent singlet oxygen generation efficiency, high photostability, low dark toxicity and rapid clearance. Zinc phthalocyanine properties such as water or lipid solubility and ionisation constant (De Filippis, Dei, Fantetti, & Roncucci, 2000) are also important for photoinactivation on cells. Recent studies have shown that zinc phthalocyanines can be functionalised as potent photosensitisers against Gram-positive and Gram-negative bacteria (Lui *et al.*, 2018; Mantareva *et al.*, 2007; Tşci *et al.*, 2016; Wang *et al.*, 2017). Free zinc phthalocyanine has been shown not to affect Gram-negative bacteria (Bertolini *et al.*, 1990), but when combined with membrane-disrupting agents such as ethylenediaminetetra-acetic acid (EDTA) and calcium chloride, delivery to (internal) cells is guaranteed (Giuliani *et al.*, 2010; Scalise & Durantini, 2005; Soncin *et al.*, 2002). In contrast, zinc phthalocyanines show affinity for Gram-positive bacteria, where they are involved in binding to membrane proteins of the cytoplasmic membrane (Bertolini *et al.*, 1990; Spesia & Durantini, 2013). The antibacterial effects of zinc phthalocyanine have also been tested in in-vivo animal models for clinical studies (Schieweck *et al.*, 1994; Vecchio *et al.*, 2013). The list of metal-phthalocyanine drugs currently in clinical trials include the sulfonated aluminium derivative Photosens, a liposomal formulation of the zinc phthalocyanine CGP55847, and a silicon complex

called PC-4 (Figure 9). The general tendency of metal-phthalocyanines to aggregate in solution, leading to reduced bioavailability and photochemical activity, can be overcome (or minimised) by using appropriate chemical modifications (e.g. Photosens), pharmaceutical formulations (e.g. liposomal formulations of the Zinc phthalocyanine, CGP55847) (Rak *et al.*, 2019) or by incorporation and functionalisation on solid supports.

Figure 8 shows the structures of some metal-phthalocyanines currently used in antimicrobial photodynamic therapy.
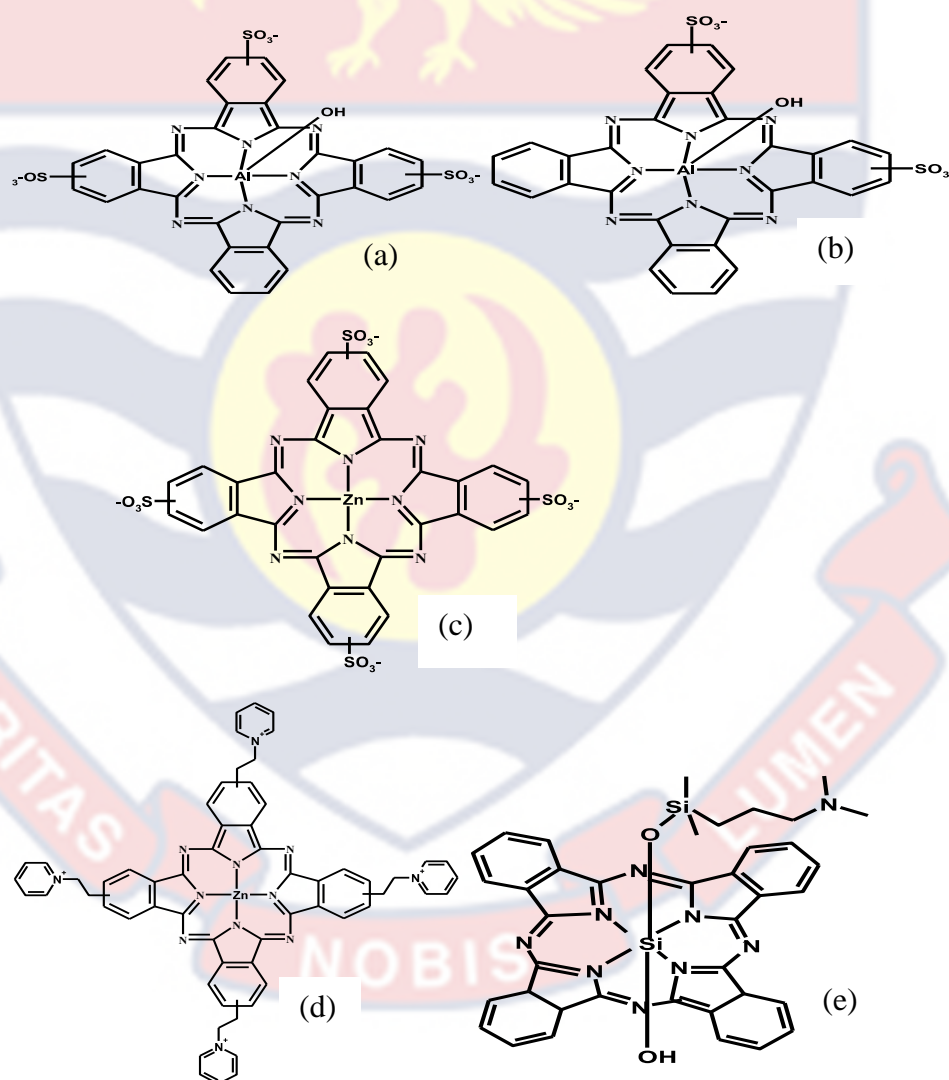
Figure 9: Metal-phthalocyanines used in antimicrobial photodynamic therapy
(a) Photosens, (b) AlPcS$_2$, (c) zinc phthalocyanine tetra sulphonate,
(d) zinc phthalocyanine tretrapyridium and (e) PC-4 (Howe &
Zhang, 1998; Sharman *et al.*, 1999).

Most of these drugs (Figure 9) are available as injectables. After intravenous injection into peri-wound tissue and irradiation (that is, after PDT), removal of residual photosensitisers from the blood/body is problematic (slow clearance rate from blood/body). It is excreted in the urine, but it may take some time before it is completely cleared from the body. In addition, photosensitisers remain in the body for a long time after PDT, which can lead to photosensitive skin after prolonged exposure to light. In this study, an antimicrobial agent (zinc phthalocyanine) is incorporated into a cellulosic carrier to facilitate removal and disposal after APDT.

Catalysts and Catalyst Systems

A catalyst is a compound that is added to a reaction to speed it up. It is neither produced nor consumed in the reaction (Wisniak, 2010).

The two main catalytic systems are the homogeneous and heterogeneous systems. In homogeneous catalysis, the catalyst is in the same phase (gas or liquid) as the reactants, whereas in heterogeneous catalysis, the catalyst is in a different phase than the reactants. Heterogeneous catalysis most often involves the use of solid catalysts in liquid reaction mixtures (Copéret *et al.*, 2003). Homogeneous catalysis mostly occur in liquids, whiles heterogeneous catalysis can occur in liquids or gases (Bhaduri & Mukesh, 2014).

Support materials for catalysts immobilisation

In order to make it easier to recover and recycle the catalyst and avoid any possibility of catalyst contamination of the finished product, a thorough investigation has been conducted into the immobilisation of multiple solid supports in catalyst systems (Ding *et al.*, 2015; Piermatti, Abu-Reziq &

37

Vaccaro, 2020). They include, ceramic materials (Zdarta *et al.*, 2018), mesoporous materials (Zhang *et al.*, 2018) nanoparticles (Fan *et al.*, 2015) carbon nanotubes (Kumar *et al.*, 2019), graphene and graphene oxide (Zhang *et al.*, 2010), electro-spun materials (nanofibrous mat), polymeric membranes (cellulose, chitosan, polyurethane etc.), hybrid and composite materials (Esquivel-Peña *et al.*, 2019).

Catalyst immobilisation methods

Catalyst immobilisation is "physically confining or placing the catalyst in a defined area that maintains catalytic activity and allows repeated and continuous use" (Homaei *et al.*, 2013; Klibanov, 1979). By immobilising the catalyst on a solid matrix, the soluble catalyst remains in the solid phase in the reaction solution, allowing easy separation (by squeezing, filtration, centrifugation, magnetic separation, etc.), recovery and recycling of the catalyst, and rapid isolation of the desired reaction product (Abate *et al.*, 2015; Bartók, 2015; Ferré *et al.*, 2015; Molnár & Papp, 2017; Tian *et al.*, 2015; Veerakumar *et al.*, 2017; Zhong *et al*., 2017). Furthermore, insoluble catalysts can be well dispersed in the reaction medium by immobilisation to avoid unwanted agglomeration (Levin *et al.*, 2015; Li *et al.*, 2017; Paul *et al.*, 2015; Sudakar *et al.*, 2016).

The four common catalyst immobilisation methods are physisorption, covalent bonding, cross-linking and entrapment. These are applied in two separate procedures; the dipping procedure, where the catalyst and support are immersed in solution to form a complex and the printing procedure, where the catalyst and solvent are mixed to produce the ink. Immersion allows relatively

higher catalyst loadings than printing because, all parts of the fibrous material in solution, are exposed at once (Morshed, 2021).

In physisorption immobilisation of catalysts, catalysts are bound to the surface of the support matrix by weak forces such as van der Waals forces, electrostatic forces, hydrophobic interactions and hydrogen bonding (Bone *et al.*, 2018). Physisorption is mostly chosen due to the simplicity of preparing the heterogenized catalysts. Simple procedures can be used to immobilise catalysts onto supports without prior functionalisation of the catalyst or solid support (Bannwarth, 2004). The advantages of physisorption methods for immobilising catalysts include ease and high yields of catalyst, with negligible impact on properties of the immobilised catalysts. A physisorption method was used to immobilise the Zinc phthalocyanine dye on the plain cellulose supports in this study.

In covalent bonding, both catalyst and support materials generally have functional groups that can interact to form covalent bonds. Functionalisation and surface modification of the catalyst are therefore unavoidable in some cases (End & Schöning, 2004; Kirschning, 2004).

Crosslinking is an irreversible process that forms crosslinks between catalyst molecules on the support through covalent bonding (Gao *et al.*, 2014).

Immobilisation by entrapment (encapsulation), entraps the catalyst within a network of support matrices that allow the passage of substrates and products while keeping the catalyst in place (Thangaraj & Solomon, 2019; Zhao *et al.*, 2006).

Cellulose Supports

Cellulose materials are becoming increasingly important in various industries. Cellulose, an important structural component of green plants, is the most abundant organic polymer in nature. It is considered an almost inexhaustible source of raw materials as the demand for renewable and biocompatible products continues to increase (Klemm *et al.*, 2005). Cellulose is formed by linking repeating building blocks of D-glucose and possesses many remarkable properties such as hydrophilicity, biodegradability, chirality and versatile semi-crystalline fibre morphology. Cellulose, in the form of wood, cotton, and other plant fibres, is widely used as an energy source, building material, and clothing (Grishkewich *et al.*, 2017). Cellulose has been used as a chemical raw material in various industries for over a century, because it is cheap, very strong and has versatile chemical modification capabilities. It has been used as a material for nanoparticles due to its excellent chemical and physical durability, biocompatibility, and chirality (Li *et al.*, 2017; Van Rie & Thielemans, 2017; Wu *et al.*, 2016b), as proteins (Kauffmann *et al.*, 2000; Zhang & Rojas, 2017), as antibodies and anticancer agents (Anaya-Plaza et al., 2017; Raghuwanshi *et al.*, 2017). In this study, cellulose was extracted and purified from oil palm mesocarp fibres and pineapple leaves, as a carrier for the immobilisation process.

Phthalocyanine Immobilised Polymer Supports

Polymer composite technology opens up the prospect of fabricating materials from phthalocyanines supported on polymer matrices (Konovalova *et al.*, 2001; Stilman, 1991). Phthalocyanines that are physically supported are bound by sorption forces and are incorporated into polymer matrices during

40

polymer synthesis, thin films formation, fibres and composites (Nikolaeva *et al.*, 2006). Among the biopolymers, polysaccharides (such as cellulose) and proteins are most commonly used (Zugle, 2012). For example, Alam *et al.* (2020) recently prepared highly fluorescent cellulose nanocrystals (CNCs) by attaching carboxylated zinc phthalocyanine to two different types of cellulose nanocrystals. Lbova & Vasil'ev (2008) suggested that, porous phthalocyanine-immobilised polymer supports could be used as catalysts in industrial petroleum and water treatment for sulphur removal. Such porosity is observed in cellulose, a biopolymer. The incorporation of phthalocyanines into cellulose fibres while retaining the properties of the phthalocyanines in the fibres have been reported. These functionalised fibres are favourable for various applications. Table 1 gives some examples of cellulosic supports functionalised with metal-phthalocyanines.

Table 1: Examples of Cellulose-Based Supports, Functionalised with Metal-Phthalocyanines

Phthalocyanine	Cellulose Type	References
Zinc phthalocyanines	Glass wool	Sindelo *et al.*, 2022
Zinc phthalocyanines	Cellulose paper	Grammatikova *et al.*, 2019
Cobalt (II) tetraamino Phthalocyanine	Bacterial cellulose	Teng, *et al.*, 2018
Cobalt (II) tetraamino Phthalocyanine	Bacterial cellulose	Chen & Teng, 2017
Cobalt (II) tetraamino Phthalocyanine	Cellulose acetate nanofiber mats	Chen, Huang & Xu, 2012
Cobalt (II) tetraamino Phthalocyanine	Cellulose acetate nanofiber mats	Chen, Huang & Xu, 2011

Source: Compiled by author

Applications of Immobilised Phthalocyanines

Phthalocyanines absorb light mostly in the visible part of the electromagnetic spectrum, making them more accessible as sensitisers, than the ultraviolet part required for other sensitisers (Silva *et al.*, 2004; Suri *et*

41

al.,1993). Due to their high thermal and chemical stability, phthalocyanines can be used as liquid-phase or gas-phase oxidants in a variety of catalytic reactions (García-Sánchez *et al.*, 2013). In order to enhance their physicochemical strength, they first need to be immobilised on suitable supports (García-Sánchez *et al.*, 2013). Incorporation of phthalocyanines into polymer supports in chemical sensors for instance, can be used as functional molecules to detect toxic gases in the environment (Sanchez *et al.*, 2001). It has been reported that, cobalt phthalocyanine-functionalised polystyrenes are very sensitive to NO_2 and also react with chloroform and perchlorethylene (Tsuiki & Maeda, 1996). Furthermore, zinc phthalocyanines-immobilised glass wool have been reported to exhibit photocatalytic activity towards methyl orange (Sindelo *et al.*, 2022). Below are some examples of studies on the various applications of immobilised phthalocyanines in nitrogen dioxide gas detection, photodegradation of organic pollutants and antimicrobial photodynamic therapy (APDT).

Immobilised phthalocyanines in nitrogen dioxide gas sensing

Metal-phthalocyanine sensitivity and response to gases have been shown to depend on the chemical properties of the phthalocyanine complex and (if present) its peripheral substituents, the nature of the central metal ion, as well as on the thin layer morphology (Kratochvılova, *et al.*, 2008; Šebera *et al.*, 2009). The strong 18 π-electronic structure of phthalocyanines boost interactions with water and gases, through reversible and irreversible chemical reactions (Claessens *et al.*, 2008; Öztürk *et al.*, 2009), resulting in detectable physical changes (Duruk *et al.*, 2015*;* Kumawat *et al.*, 2015), in fluorescence conductivity, and mass density. Phthalocyanines are sensitive to gases and are

42

oxidised or reduced by molecules with redox activity such as hydrogen sulphide (H_2S), nitrogen dioxide (NO_2) etc. etc (Jha *et al.*, 2014; Kumar *et al.*, 2017; Liu *et al.*, 2019; Wu *et al.*, 2016a). Since phthalocyanine was proposed as the active layer for $NO_{2(g)}$ detection, many researchers have studied the sensitivity of copper phthalocyanine under various conditions. Cadmium, cobalt, aluminium (Chakane et al., 2003; Maleysson et al., 1994) and lanthanide phthalocyanines (De Saja & Rodriguez-Mendez, 2005) are also studied as NO_2 gas sensors.

Phthalocyanines, generally have low solubility in common solvents, so it is essential to use a suitable solid carrier system in which the phthalocyanines are well dispersed. Therefore, the following gas-permeable supports, have been proposed for the development of phthalocyanine-based sensors for $NO_{2(g)}$ detection: tin-modified mesoporous silica (Yuliarto *et al.*, 2004), tin dioxide (Ling & Leach, 2004), gas-permeable liquid-core waveguides (Dasgupta *et al.*, 1998), and porous silicon (Chakane *et al.*, 2003). Nonetheless, metal-phthalocyanines that have been immobilised on cellulose-based fibres for the detection of gases, especially $NO_{2\ (g)}$, have not been well studied, despite the many advantages of its use. Cellulose fibres are generally porous and permeable to gas molecules. Furthermore, they have a high surface area to volume ratio and relatively large pores, making the entire cellulose surface fully accessible to the substrate (Li & Xia 2004). Table 2 shows examples of metal-phthalocyanine immobilised supports for NO_2 gas detection.

43

Table 2: Metal-Phthalocyanine-Immobilised Supports for NO₂ Gas Sensing

Phthalocyanines	Supports	Analyte	References
Zinc phthalocyanine	ultrathin films	NO$_2$	Zhu *et al.*, 2020
Copper phthalocyanine	thin films	NO$_2$	Liu *et al.*, 2019
Fluoroalkoxy-substituted phthalocyanine	thin films	NO$_2$	Sun *et al.*, 2018
Zinc phthalocyanine	electrospun nano-fabrics	NO$_2$	Zugle & Nyokong, 2012
Iron phthalocyanine complex	nanostructure matrix	NO$_2$	Fernández-Sánchez, 2006
Cobalt phthalocyanine	polystyrene polymer	NO$_2$	Sanchez *et al.*, 2001
Lead phthalocyanine	thin films	NO$_2$	Hsieh *et al.*, 1998
Zinc phthalocyanine	thin films	NO$_2$	Inagaki *et al.*, 1996
Copper phthalocyanine	thin films	NO$_2$	Dogo *et al.*, 1992
Tetrasulphonated Copper phthalocyanine	thin films	NO$_2$	Mortesson *et al.*, 1990

Source: Compiled by author

As shown in Table 2, the applications of phthalocyanines have been limited to thin films by taking advantage of their semiconducting properties (Dogo *et al.*, 1992; Hsieh *et al.*, 1998; Inagaki *et al.*, 1996; Liu *et al.*, 2019; Mortesson *et al.*, 1990; Sun *et al.*, 2018; Zhu *et al.*, 2020). Few studies involving the exploitation of the fluorometric properties of phthalocyanines on polystyrene polymers (Sanchez *et al.*, 2001), nanostructured matrices (Fernández-Sánchez, 2006), and electrospun synthetic polymer nanofabrics (Zugle & Nyokong, 2012) have been reported. This study employs the use of zinc phthalocyanine immobilised natural cellulose fibres for fluorometric NO$_{2(g)}$ sensing for the first time.

Immobilised phthalocyanines in photodegradation of organic pollutants

Metal-phthalocyanine photosensitisers can strongly absorb visible light or sunlight and therefore, have attracted interest for visible light photocatalytic degradation of toxic organic pollutants (Tao *et al.*, 2002, 2003) which, leads to

the production of less harmful photoproducts (Agboola *et al.*, 2006), and most often complete mineralisation. Photosensitised degradation of organic pollutants in aqueous media with metal-phthalocyanine sensitisers mostly occur by the well-known Type II mechanism, which involves the generation of the highly oxidative singlet oxygen, responsible for the destruction of organic pollutants. Type I mechanism, which involves superoxide radicals, may also take part in the reaction but most often does not occur (Agboola *et al.*, 2006). Yet these homogeneous metal-phthalocyanine catalysts are hardly recovered at the end of reaction for reuse (Gaigneaux *et al.*, 1996; Pasiuk-Bronikowska *et al.*, 1998) and suffer from limited lifetime activity due to the formation of inactive aggregates in solutions and bridged μ-oxo dimers which, significantly affect their catalytic activities (Kobayashi, 2002; Pergrale & Sorokin, 2000). Enhancing the stability and the dispersion of metal-phthalocyanines in solutions is therefore, essential to full exploitation of their photocatalytic activity. Immobilisation to solid supports, particularly porous supports, can stabilise crystals against oxidation while reducing aggregation by ordering the crystal packing and localising the internal space (Luo *et al.*, 2004; Tao *et al.*, 2003). The molecules are dispersed there, have good photocatalytic activity, and can therefore, be isolated from the reaction product and reused. Table 3 gives examples of some immobilised porous metal-phthalocyanines and their application in photolysis processes.

Table 3: Lists of Porous Metal-Phthalocyanine-Immobilised Photocatalysts and their Application in Photodegradation Processes

Catalyst	Application	Irradiation Source	Irradiation Time (min)	References
GW-ZnMCPPc, GW-ZnTCPPc, GW- ZnTIPAPc	Degradation of MO	Modulight 690 nm laser	720 min	Sindole *et al.*, 2022
NiPcS-NH$_2$-KIT-6	Degradation of DCP	Visible	150	Mousali & Zanjanchi, 2020
ZnTNPc–MWCNTs	Degradation of RB	Visible	120	Wang *et al.*, 2016
CoPc/MCM-41	Degradation of MO	Visible	120	Wang *et al.*, 2015

Source: Compiled by author

**GW-ZnMCPPc: glass wool-Zinc (carboxy phenoxy) phthalocyanines; GW-ZnTCPPc: glass wool-Zinc (4-carboxy phenoxy) phthalocyanines; GW-ZnTIPAPc: glass wool-Zinc (4-isophthalic acid) phthalocyanines; CoPc/MCM-41: cobalt phthalocyanine/mesoporous molecular sieves; ZnTNPc-MWCNTs: Zinc Tetranitro Phthalocyanine multi-walled carbon nanotubes.

Phthalocyanine-immobilised cellulose have the potential to reduce various accumulation conditions and increase the effective surface area of the catalysts by allowing recovery and reuse, but are uncommon, as shown in Table 3. In this study, Zinc phthalocyanine immobilised on natural cellulose fibres was used for the degradation of a model organic pollutant, crystal violet dye, in aqueous media, using sunlight and red LED light sources.

Immobilised phthalocyanines in antibacterial photodynamic therapy

Photodynamic therapy (PDT) is based on the systemic or topical administration of non-toxic drugs or dyes called photosensitisers (Ps) to diseased patients. After some time, the lesion is irradiated with visible light (usually far-red light), which in the presence of oxygen causes the formation of cytotoxic species and consequent cell death and tissue destruction. It is a

46

safe treatment with no known cumulative toxicity (Castano, Demidova & Hamblin, 2004; Fonda-Pascual *et al.*, 2016). Phthalocyanines have attracted considerable interest over the years as photosensitisers in antimicrobial photodynamic therapy. Photosensitisers are chromogenic compounds that can transfer energy from absorbed visible light to surrounding biological organic molecules or dissolved oxygen (Macdonald & Dougherty, 2001). They are used in the free form for most antimicrobial applications. However, photosensitisers encapsulated in liposomes, combined with antibiotics, and immobilised on solid supports have been reported to be active (Cahan *et al.*, 2010; Nakonechny *et al.*, 2013; Nisnevitch *et al.*, 2010; Nisnevitch *et al.*, 2013). The latter application was first proposed in the 1970s (Blossey *et al.*, 1973; Nilsson & Kearns, 1974) and quickly showed several advantages over the use of the free photosensitisers. These include easy removal after processing, reusability and continued use, improved resistance to photobleaching, and the ability to use solvents in which the free photosensitiser is insoluble (Nakonechny *et al.*, 2013; Paczkowski & Neckers, 1985; Schaap *et al.*, 1975). Chen *et al.*, (2011) also showed that the polycationic lysine moiety used as a carrier for Zinc phthalocyanine is active against Gram (+) and Gram (-) bacteria both in vitro and in vivo.

The recent development of antimicrobial hydrogels has received a great deal of attention. The ability of hydrogels as excellent wound dressings and drug reservoirs, to deliver sustained drug delivery and achieve high local drug concentrations is well documented (Leung *et al.*, 2020). Table 4 shows a list of some metal phthalocyanine immobilised carriers and their applications in antimicrobial photodynamic therapy (APDT).

Table 4: Lists of Metal-Phthalocyanine-Immobilised Supports and their Applications in Antimicrobial Photodynamic Therapies (APDTs)

Ps	Support	Light type	Target Organism	Light Dose	Irrad. Period	Ref.
ZnPcPy	Cellulose paper	Fluorescent lamp	*S. aureus, E. coli and C. albicans*	270 Lux	30 and 60 min	Grammatikova *et al.*, 2019
ZnPcPy	Cellulose paper	LED lamp	*S. aureus, E. coli and C. albicans*	4000 Lux	30 and 60 min	Grammatikova *et al.*, 2019
ZnPc	Electro-spun PS fibers	300 W lamp + 600 nm glass + water filters	*S. aureus*	-	90 min	Masilela *et al.*, 2013
ZnPc	Electro-spun PUR fibres	150 W cold white light	*E. coli*	-	30 min	Mosinger *et al.*, 2009
TBZnPc ZnPcTS	silicate matrix	Bonnett-Pell lamp 660 nm max.	*E. coli*	0.60 mW cm^{-2}	120 min	Artarsky *et al.*, 2006
ZnPcS	CS membrane	500 W halogen lamp	*E. coli*	-	90 min	Bonnett *et al.*, 2006

Source: Compiled by author

***CS: Chitosan; Irrad: irradiation; Ps: Photosensitiser; PS: Polystyrene; PUR: Polyurethane; TBZnPc: Tetra (4-terbutyl) Zinc phthalocyanine; ZnPcPy: Zinc phthalocyanine tetra pyridine; ZnPcS: Zinc phthalocyanine tetra-suphoxy tetrasodium salt; ZnPcTS: Zinc phthalocyanine tetra-suphoxy complex. (Spagnul, Turner & Boyle; 2015).

As shown in Table 4, aside the cellulose paper which, is natural-based (Grammatikova *et al.*, 2019), the rest of the researchers used synthetic polymer-immobilised metal-phthalocyanines for antimicrobial photodynamic applications.

Natural cellulose is the material chosen for this study because, it is abundant in natural resources. They are inexpensive, biodegradable, exhibit high porosity, water permeability and flexibility, good mechanical properties, chemical resistance, and high stability in most organic solvents, including a

very high surface fraction for interaction with cells (Jonoobi *et al.*, 2010; Kalia *et al.*, 2011; Moohan *et al.*, 2020; Zeng *et al.*, 2021). The ability to accommodate different molecules to optimise their properties for a particular application, and the ability to modify their structure and function, make them attractive for antimicrobial applications (Grammatikova *et al.*, 2019; Huang *et al.*, 2003).

Furthermore, unlike polysiloxane and polyurethane matrices, the cellulose-based fibres do not block the interaction between the photosensitiser (zinc phthalocyanine in this case) triplet state and oxygen molecules. This is because their porous structure generally promotes the formation of reactive oxygen species, especially singlet oxygen, which is the main cytotoxic agent in antibacterial processes (Filatov *et al.*, 2016).

Efficient immobilisation of photosensitisers on solid supports and the resulting stability help reduce costs through efficient recovery, recycling, and easy removal after processing.

Chapter Summary

A review on the background and common synthetic routes to phthalocyanines; how other researchers used various precursors to synthesise metal-phthalocyanines through the microwave method; the background of photodynamic therapy (PDT); metal-phthalocyanine-based antimicrobial photodynamic therapy (APDT); catalyst immobilisation techniques on fibrous supports; phthalocyanine-immobilised polymer supports and the various applications of immobilised phthalocyanines in nitrogen dioxide gas sensing, photodegradation of organic pollutants, and antimicrobial photodynamic therapy (APDT) was reported.

49

CHAPTER THREE

MATERIALS AND METHODS

Introduction

This chapter presents the materials and methods used in the synthesis, preparation, extraction, and purification of zinc phthalocyanine and cellulose fibre supports. It also includes the various tools used in product characterisation and analysis, including the exact quantities used in each experiment and finally, the methods used in their application as photosensitisers to inactivate bacteria and degrade an organic dye with both daylight and LED redlight irradiations.

Reagents and Chemicals

Deuterated dimethyl sulfoxide (DMSO-$_{d6}$) and 1,3-diphenyl isobenzofuran (DPBF 97%) were purchased from Sigma Aldrich, Germany; Acetonitrile (HPLC grade) and Sulphuric acid (95-98%) from Merck KGaA, 64271 Darmstadt, Germany; absolute Ethanol (100%), Methanol (100%), Hydrogen peroxide (30%), Hydrochloric acid (37%), Nitric acid, Sodium azide (100.2%), Sodium hydroxide (99%) and Metallic Copper from VWR (BHD Prolabo®) Chemicals, Belgium; N,N-dimethylformamide (DMF) >99% - HPLC grade, urea (> 98%) and Sodium iodide (extra pure) from Daejung Chemicals & Metals Co., Ltd, Korea; Zinc(II) chloride (98%), from Park Science Ltd-Northampton, UK; Ammonium hepta-molybdate tetrahydrate (99.3-101.8%), from Oxford Lab Fine Chem LLP, India; Phthalic anhydride (99%) from Nice Chemicals (P) Ltd, Manimala Road, Edappally, Kochi-682024, Kerala, India.

50

Bacterial Isolates and Culture Media

Clinical isolates and strains from the American Type Culture Collection (ATCC), including methicillin-resistant Staphylococcus aureus (MRSA) 3646 - a resistant phenotype; Methicillin-resistant Staphylococcus aureus (MRSA) ATCC 43300; Staphylococcus aureus ATCC 25923 - facultative anaerobic gram-positive bacteria, leading cause of surgical site infections and multidrug resistance; Pseudomonas aeruginosa and Pseudomonas aeruginosa ATCC 27312 - Gram-negative aerobic isolated from infected wounds, were obtained from the Department of Microbiology, Noguchi Memorial Medical Research Institute, University of Ghana, Legon. Culture media, including Müeller Hinton agar, nutrient agar, mannitol salt agar and gentamicin antimicrobial susceptibility test discs were obtained from Oxoid Ltd, UK. All the chemicals and reagents were used without further treatment.

Instrument

The lists of instruments used in the research are:

1. Bruker FT-NMR Avance 500 spectrometer. Manufactured by Bruker Corperation, Ettlingen, Germany, situated at the Central Laboratory Complex, Kwame Nkrumah University of Science and Technology, Kumasi.

2. JENWAY 7315 Spectrophotometer and T70 UV/VIS Spectrophotometer. Manufactured by the PG Instruments Ltd., the United Kingdom, situated at the Fisheries Department and the Chemistry Department respectively, University of Cape Coast, Cape Coast.

51

3. Fluorescence emission spectra were obtained on a Raman Spectroscopic System set-up, designed and developed in Ghana, at the Laser and Fibre Optics Centre (LAFOC), University of Cape Coast, Cape Coast. The setup components include a 445nm diode laser source, a high pass absorptive edge filter and a CCD-based detector system. Auxiliary components include an optical fibre cable, bifurcated optical fibre probe, fibre port, focusing lens, quartz cuvette and a microscope objective lens.

4. Alpha Platinum ATR FTIR spectrophotometer. Manufactured by the Bruker Corporation, Germany and situated at the Central Laboratory Complex, Kwame Nkrumah University of Science and Technology, Kumasi.

5. PANalytical Empyrean series 2 Powder X-ray Diffractometer. Manufactured by the Malvern Panalytical Spectris Group Company, the Netherlands, situated at the Department of Physics, University of Ghana, Legon, Accra.

6. Simultaneous Thermal Gravimetric Analyzer - Differential scanning calorimetry SDT Q600 V20.9 Build 20. Manufactured by TA Instruments, New Castle, DE, United States of America and situated at the Materials and Engineering Sciences Department, University of Ghana, Legon, Accra.

7. Phenom ProX desktop Scanning Electron Microscope. Manufactured by Thermo Scientific, Eindhoven-the Netherlands and situated at the Department of Earth Science, University of Ghana, Legon.

52

8. Ecocell convection Oven 55. Manufactured by MMM Medcenter Einrichtungen GmbH, Germany, situated at the Department of Chemistry respectively, University of Cape Coast, Cape Coast.

9. Customised LED Lamp. Manufactured by Perfect LED Limited, ShenZhen, GuangDong, China.

10. Center 531 LED Light meter. Manufactured by Center Technology Corp., Taiwan.

11. Dry Oven/Incubator. Manufactured by Bioline International, Germany, situated at the Microbiology laboratory, Cape Coast Teaching Hospital, Cape Coast.

12. Matachana Steriliser/Autoclave. Manufactured by the Matachana Group, Germany, situated at the Microbiology laboratory, Cape Coast Teaching Hospital, Cape Coast.

13. ESCO Class II Biosafety Cabinet. Manufactured by Esco Lifesciences Group, Singapore, situated at the Department of Biomedical Sciences, University of Cape Coast, Cape Coast.

14. Samsung Microwave Oven, model Q ME732K. Manufactured by the Samsung Group, Malaysia.

15. Laboratory Centrifuge, VWR Mega Star 600. Manufactured by VWR Group, Germany. Situated at the Department of Chemistry, University of Cape Coast, Cape Coast.

16. Ultrapure (type 1) Water Purification System. Manufactured by Merck, France. Situated at the Department of Chemistry, University of Cape Coast, Cape Coast.

53

Microwave Synthesis of Zinc Phthalocyanine

Phthalic anhydride (2.6658 g, 18 mmol) was weighed into a mortar and pulverised for 10 min, then Urea (5.5256 g, 92 mmol) was added and pulverised for another 10 min. Then, zinc chloride (1.0224 g, 7.5 mmol) and ammonium hepta-molybdate tetrahydrate catalyst (0.0803 g, 0.065 mmol) were added to the contents in the mortar and pulverised into a smooth paste. The ratio of urea-to-zinc chloride in the mixture was approximately 5:1. The mixture was transferred into a reaction flask (250 ml thick-walled Pyrex Erlenmeyer flask) and 5 mL of distilled water was added to the mixture. The flask was placed on top of a silica gel bath, that acts as an insulator, and then placed in a microwave oven with an output power of 600 W, for the reaction to take place. The total reaction time was between 3 and 4 minutes, divided into four 30-second intervals and two 60-second intervals, with 5-second pauses in between, to prevent the mixture from boiling over. The resultant product was a dark greenish-purple crude Zinc phthalocyanine.

To remove the unreacted raw materials, the crude zinc phthalocyanine was then washed in several millilitres of deionised water (70 ^{o}C), filtered at the pump, then dissolved in 100 mL 6 M HCl solution at 40 ^{o}C, filtered at the pump and then neutralized with 100 mL 1 M NaOH solution, filtered at the pump, washed with several millilitres of distilled water (70 ^{o}C) till neutral pH, followed by 50 mL methanol and dried in the oven at 110 °C. Purification continued by Soxhlet extraction of the dried solid using Acetonitrile as the solvent, till a clear solvent was obtained. The dried solid was then recrystalised by dissolving in 70 % H_2SO_4 solution and poured into distilled water to precipitate. The precipitates were washed with distilled water till pH

54

7 (neutral) and filtered at the pump. The resultant pure zinc phthalocyanine dye was dried in the oven at 110 °C and stored in a dark bottle for further analysis method (Shaabani, 1998; Shaabani *et al.*, 2007; Kahya *et al.*, 2019; Villemin *et al.*, 2001). The schematic presentation of the synthetic process is shown in figure 10.
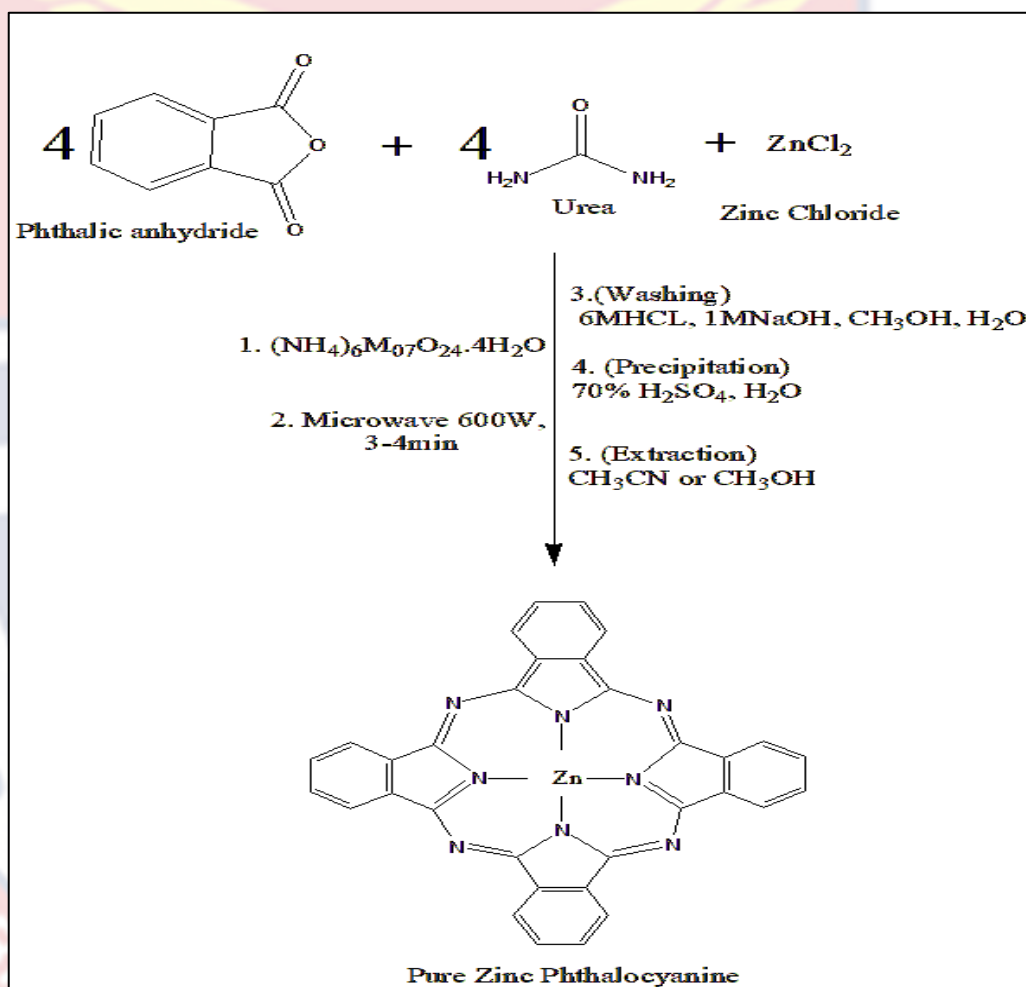
Figure 10: Synthetic routes for the unsubstituted zinc phthalocyanine Dye.

Preparation and Extraction of Cellulose from Oil Palm Mesocarp Fibre

Cellulose from the fibres was extracted according to a modified method (Khenblouche *et al.,* 2019). The unrefined oil palm mesocarp fibres (Ur-OPMF) were obtained after palm oil was extracted from the pulp at a local palm oil manufacturing company. The fibres were sent to the laboratory,

55

washed with tap water and boiled in tap water at 100 °C for 3 hours, to remove excessive wax and other impurities. Then, dried in the oven at 85 °C to a constant weight. The dried unrefined fibres were then heated in ethanol (absolute) at 70 °C for 1.5 hours, to further remove oils, waxes and impurities that were insoluble in the hot water but soluble in the ethanol. This process was repeated twice. The fibre-to-solvent ratio was 1:30 (w/v). The dewaxed fibres were then dried in the oven at 85 °C to a constant weight. The dried dewaxed fibres were then boiled in 1 M NaOH solution at 90 °C for 30 mins with periodic stirring, to remove lignin and hemicellulose for refined cellulose (the longer the processing time, the softer or dissolved the resultant fibre). This process was repeated two more times with a fibre-to-solvent ratio of 1:30 (w/v). The refined cellulose fibres were then filtered from the NaOH solution and washed with deionised water till neutral pH (pH 7). Then, bleached by immersion in hot 5% (v/v) H_2O_2 at pH 11.5 (pH 11.5, was achieved by the addition of 1 M NaOH) at 90 °C for 45 mins, to remove the remaining lignin and whiten the fibres. The process was repeated five more times due to the fibrous nature of the palm fibres, with periodic stirring. The fibre-to-solvent ratio was 1:40 (w/v). The bleached cellulose oil palm mesocarp fibres (B-OPMF) were then filtered from the H_2O_2 solution, washed with deionised water till neutral pH (pH 7) and dried in the oven at 85 °C to a constant weight. Then, stored in labelled air-tight containers for further analysis.

Preparation and Extraction of Cellulose from Pineapple Leaves

The extraction process of the unrefined pineapple leaf fibres (Ur-PLF) differs slightly from that of the unrefined oil palm mesocarp fibres (Ur-OPMF). The pineapple leaf fibres were manually extracted from fresh green

56

pineapple leaves (Smooth cayenne species.), by using the edge of a ceramic plate to scrub off the green extractable waxy substance from the surface of the leaves, on an improvised marble table top, to expose the long tiny threadlike strips. This process removed most of the lignin content in the fibres exposing more of the α-cellulose. The fibres were then washed severally with tap water at ambient temperature, boiled in tap water at 100 °C for 3 hours and then dried in the oven at 85 °C to a constant weight. The dried fibres were then heated in ethanol (absolute) at 70 °C for 1.5 hours to further remove oils, waxes and impurities that were insoluble in the hot water but soluble in the ethanol. This process was repeated twice. The fibre-to-solvent ratio was 1:30 (w/v). The dewaxed fibres were then dried in the oven at 85 °C to a constant weight. The dried dewaxed fibres were then boiled in 1M NaOH at 90 °C for 10 mins, with periodic stirring to remove lignin and hemicellulose for refined cellulose (the longer the processing time, the softer or dissolved the resultant fibre). The fibre-to-solvent ratio was 1:30 (w/v). The refined cellulose fibres were then filtered from the NaOH solution and washed with deionized water till neutral pH (pH 7). Then bleached by immersion in hot 5% (v/v) H_2O_2 at pH 11.5 (pH 11.5, was achieved by the addition of 1 M NaOH) at 90 °C for 15 mins, to remove the remaining lignin and whiten the fibres. The process was repeated two times with a solvent-to-fibre ratio of 1:40 (w/v). The bleached cellulose pineapple leaf fibres (B-PLF) were then filtered from the H_2O_2 solution, washed with deionised water till neutral pH (pH 7) and dried in the oven at 85 °C to a constant weight. They were then stored in labelled air-tight containers for further analysis.

Preparation of the Gauze Bandage

The reference plain gauze bandage (P-GB) was only boiled in deionised water at 100 °C for 3 hours (since, it is an already refined/bleached material). It was dried in the oven at 85 °C to a constant weight and then stored in labelled air-tight containers for further analysis.

Immobilisation of Zinc Phthalocyanine on the Cellulose-Based Fibres

About 0.058 g zinc phthalocyanine dye was dissolved in 2 mL DMF to make a stock solution of 50 mM from which, serial dilutions of various concentrations ranging from 0.35 mM to 50 mM were prepared. The bleached cellulose-based fibre supports (B-OPMF and B-PLF) and the reference fibre (P-GB), were then dispersed in the various zinc phthalocyanine solutions at ambient temperature overnight. The resultant immobilised or functionalised cellulose-based fibres (ZnPc-GB, ZnPc-OPMF and ZnPc-PLF), were then dried in the oven at 110 °C to a constant weight and stored in dark labelled air-tight containers for further analysis.

UV Lamp Images of the Functionalised Cellulose-Based Fibres

The refined cellulose-based and functionalised cellulose-based fibre supports were viewed under the UV lamp to ascertain physically, whether the zinc phthalocyanine dye was successfully immobilised.

Nuclear Magnetic Resonance (NMR) Spectroscopy

About 10 mg of the zinc phthalocyanine dye was weighed and dissolved in ~450μL of DMSO-d6 in a sample vial. The sample was vortexed and filtered into the NMR tube. The prepared sample was tightly capped and the tube was wiped clean with isopropyl alcohol. The tube containing the sample was inserted into the spinner and the depth of the solution was

58

determined to be ~5mm in length. The sample (with the spinner) was then injected into the NMR spectrometer for ^{1}H (proton) experiments.

UV-Visible Spectroscopy

Serial dilutions ranging from 55.5 μM to 0.26 μM concentrations were made from a stock solution of 0.35 mM concentration, by dissolving 0.001g zinc phthalocyanine in 5mL DMF solvent and their absorbances recorded.

Fluorescence Spectroscopy

Fluorescence emission spectra of the synthesised zinc phthalocyanine and functionalised cellulose-based fibres were obtained on a designed and developed Raman spectroscopic system set-up. An amount of the dye was dissolved in a volume of DMF solvent and the emission spectra in a quat supra-cell cuvette was recorded. To further evaluate the effect of the concentration of zinc phthalocyanine solution and that of the functionalised fibres on the fluorescence emission, serial dilutions ranging from 320 μM to 8.5 μM concentrations were made from a stock solution of 3.5 mM concentration, prepared by dissolving 0.01g of the zinc phthalocyanine dye in 5 mL DMF solvent and their emission spectra were recorded. For the functionalised cellulose-based fibre supports, 50 mg of 0.35 mM, 0.87 mM, 3.5 mM, 35 mM and 43 mM concentrations respectively of each of the ZnPc-GB (the reference), ZnPc-OPMF and ZnPc-PLF was, put in a mini beaker and their emissions spectra were recorded.

FT-IR Spectroscopy

A few milligrams of the zinc phthalocyanine dye, the unrefined dried fibres, the refined fibres (P-GB, B-OPMF & B-PLF) and functionalised fibres (ZnPc-GB, ZnPc-OPMF and ZnPc-PLF) respectively, were then placed

directly on the crystal plate to coat the entire surface and then a little pressure was applied to the samples to ensure maximum contact. Then, each sample was scanned 24 times to generate a simple spectrum using software called OPUS.

PXRD Spectrometry

One gram of zinc phthalocyanine dye was mixed thoroughly with a spatula. A flat surface was used to push the powder down and pack it into the recess. This ensured that the particles were tightly packed, randomly oriented, and produced samples with smooth and flat surfaces before analysis

Thermal Gravimetric Analyzer-Differential Scanning Calorimetry (TGA-DSC)

Approximately 1-2 mg (Table 5) of the zinc phthalocyanine dye, the bleached cellulose-based fibres and the functionalised fibres were put in a crucible and placed in the instrument's sample holder for analysis under nitrogen gas conditions. Measurements were done at 20 °C/min to 800 °C. Data was then generated with the TA universal analysis software. The exact amounts that were for the analysis are presented in Table 5.

Table 5: Masses of Samples used in the TGA-DSC Analysis

Sample	Mass (mg)
Zinc phthalocyanine (ZnPc)	1.8710
Plain gauze bandage (P-GB)	1.2890
Bleached oil palm mesocarp fibre (B-OPMF)	1.9570
Bleached pineapple leaf fibre (B-PLF)	2.8380
Zinc phthalocyanine-gauze bandage (ZnPc-GB)	1.4280
Zinc phthalocyanine-oil palm mesocarp fibre (ZnPc-OPMF)	0.9460
Zinc phthalocyanine- pineapple leaf fibre (ZnPc-PLF)	1.0820

Source: Laboratory Analysis (2016-2021)

SEM-EDS

The zinc phthalocyanine dye, bleached fibres (P-GB, B-OPMF & B-PLF) and the functionalised fibres (ZnPc-GB, ZnPc-OPMF & ZnPc-PLF) respectively, were cut and trimmed to fit the specimen stage and then mounted unto an aluminium stub with a pelco double sided carbon adhesive. An ultra-thin coating of gold was sputtered on the cellulose-based fibres due to poor or no conductivity. Optical images were then captured at the lowest magnification of 20x. Backscattered images were captured at different magnifications (minimum to maximum) using an image intensity and high-resolution voltage mode of 10 kV and a backscatter detector until best image focusing ends.

Also, using the Phenom ProSuite software (element identification), EDS point analysis at 15 Kv, duration of 30 seconds and map analysis at 15 Kv, duration of 4 minutes 26 seconds were used for the elemental identification, distribution and concentration respectively.

Photo-Measurements

Singlet oxygen generation and quenching studies, antibacterial photodynamic therapy and photodegradation measurements were done using a customised LED lamp with a 670 ± 5 nm emission spectrum, as the redlight source and the light intensities were measured with the centre 531 light meter.

Photostability Studies of the Zinc Phthalocyanine Solution

Zinc phthalocyanine solution (about 35 µM) was irradiated with an LED redlight (670 ± 5 nm) at 2500-3000 lx (lm/m^2) intensity at ambient temperature and the absorbance was recorded at 30 min time intervals over 90 min period. The difference in absorbance at the Q-band was evaluated and the

61

photostability factor was then calculated and expressed as a percentage (Rocha *et al.*, 2015).

% Photostability Factor $= \frac{I_t}{I_0} \times 100$ ………………………………… Eqn. 1

Where I_t is the Q-band absorbance intensity at a given irradiation time and I_0 is the absorbance intensity before irradiation.

Singlet Oxygen Production Measurements

For the daylight irradiation, a mixture containing 1.5 mL of 55 μM DPBF and 1.5 mL of 9.9 μM zinc phthalocyanine solutions each in DMF in a ratio of 1:1, was exposed to daylight at intensity ranging 850-950 lx (lm/m^2), at ambient temperature. The absorbance of DPBF at 416 nm was then recorded at different irradiation times, using the UV-vis spectrophotometer. For the LED redlight irradiation, a mixture containing 1.5 mL of 66 μM DPBF and 1.5 mL of 9.9 μM zinc phthalocyanine solutions each in DMF in a ratio of 1:1, was exposed to LED redlight (670 ± 5 nm) at intensity ranging 900-920 lx (lm/m^2), at ambient temperature. The absorbance of DPBF at 418 nm was then recorded with the UV-vis spectrophotometer.

The iodometric technique was employed for the functionalised fibres (ZnPc-GB, ZnPc-OPMF and ZnPc-PLF), since they are intended for use in aqueous media. The experiment was performed in the dark. Fifty milligram of 35 mM each of ZnPc-GB (the reference fibre), ZnPc-OPMF and ZnPc-PLF were put in 10 mL beakers and 6 mL of 0.1M NaI solution was added. The beakers containing the samples were then left in the dark for about 30 mins - 1 hr, to allow the fibres to soak in the solution and then irradiated with both LED redlight (670 ± 5 nm) and daylight respectively. Daylight and LED redlight intensities ranged from 2500-5000 lx (lm/m^2) and 2000-2500 lx

62

(lm/m^2) respectively. Portions of the irradiated solution were removed and the absorbances, recorded at 2 min time intervals with the UV-vis spectrophotometer.

Singlet Oxygen Quenching Test

Fifty milligram of 35 mM each of ZnPc-GB, ZnPc-OPMF and ZnPc-PLF were put in 10 mL beakers and 3 mL each of freshly prepared solutions of 0.1 M NaI and 0.1 M NaN$_3$ in a 1:1 ratio was added. The beakers were left in the dark for about 30 mins - 1 hr, to allow the fibres to soak in the solution and then irradiated with LED redlight (670 ± 5 nm) and daylight respectively. Daylight and LED redlight intensities ranged from 850-950 lx (lm/m^2) and 900-920 lx (lm/m^2) respectively. Portions of the irradiated solution were removed and their absorbances recorded at 2 min time intervals with the UV-vis spectrophotometer.

Leaching Studies

The functionalised cellulose fibre supports were immersed in water, saline solution and methanol separately for 24 hours to ascertain, whether the zinc phthalocyanine will leach out of the fibre supports into the solutions. The absorbance of the solutions was then recorded with the UV-vis spectrophotometer.

Fluorometric Detection of Nitrogen Dioxide Gas

Nitrogen dioxide (NO$_2$) gas was produced by reacting copper dust with dilute nitric acid.

$$Cu_{(s)} + 4HNO_{3(l)} \leftrightharpoons 2NO_{2(g)} + Cu\,(NO_3)_{2\,+}\, 2H_2O_{(l)} \dots\dots\dots\dots\dots\dots... \text{Eqn. 2}$$
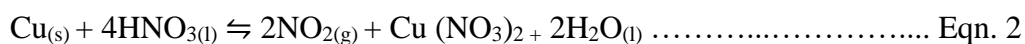
The NO$_2$ gas produced in the test tube was then siphoned into 5 mL syringes for the quenching test. zinc phthalocyanine solution (in DMF) was analysed by

63

first measuring the emission. Then the NO_2 gas (about 5 mL) was bubbled into the solution, one syringe at a time, and the emissions at the Q band were recorded after every 2 minutes of exposure to the NO_2 gas, until the green solution in the cuvette turned brown.

The same procedure was carried out on the functionalized cellulose-based fibres. About 50 mg of each fibre was put in a 10 mL beaker and their emissions were recorded without the $NO_{2(g)}$. After which, $NO_{2(g)}$ (about 3 mL) was sprayed onto the surface of the fibres and the emission spectra were recorded every 2 minutes after spraying. The process was repeated until the fibres turned brownish in colour and the peaks at the Q band disappeared. Yet, the actual quantity of NO_2 gas in every 5 mL or 3 mL syringes respectively, could not be determined because of their gaseous nature.

Heterogeneous Photodegradation of Crystal Violet Dye

Photodegradation experiments were done in reactors (beakers), placed on magnetic stirrers. Sunlight/daylight and LED redlight intensities were measured with a centre 531 LED light meter. Catalyst loads of 200 mg each of ZnPc-GB (the reference), ZnPc-OPMF and ZnPc-PLF (25-50 mM) were immersed in 50 mL aqueous solutions of crystal violet (30-60 mgL^{-1}) in 150 mL beakers. The beakers containing the samples were then left in the dark for 30 min-1 hr to allow the fibres to soak in the solution (Morshed *et al.,* 2020; Sindole *et al.,*2022). The beakers were then put on the magnetic stirrer for continuous stirring at 250 r.p.m and then exposed to both LED redlight (670 ± 5 nm) and sunlight/daylight respectively. Daylight/sunlight and redlight intensities ranged from 12000-50000 lx (lm/m^2) and 8000-10000 lx (lm/m^2) respectively. For the sunlight/daylight irradiations, the reactors were

64

positioned on a corridor in the opening for the desired light intensity, whilst the reactors for the LED redlight (670 ± 5 nm) irradiations, were sandwiched between two LED lamps in a dark room. Distances between the reactors and the LED lamps were measured and varied for the desired redlight intensities. Portions of the irradiated solutions were removed from the reaction mixtures at regular time intervals, centrifuged for 5 min at a speed of 4000 r.p.m and the residual concentrations of the contaminant were detected with the UV-vis spectrophotometer. The percentage degradation of the crystal violet contaminant was calculated by using formula (3):

$$\text{Degradation \%} = \frac{(C_0 - C_t)}{C_0} \times 100 \quad \text{……….…………..……………….. Eqn. 3}$$

where C_0 = initial CV concentration (mg/L) and C_t = CV concentration at time 't' (mg/L).

Photocatalysts recyclability studies

A three-cycled experiment was carried out for the degradation of Crystal Violet (50 mgL^{-1}), under the same experimental conditions above. The functionalised fibres, ZnPc-GB, ZnPc-OPMF and ZnPc-PLF (35 mM) were removed from the solution by squeezing, washed, oven-dried at 110 °C to a consistent weight, after every cycle and reused for the next cycle.

Antibacterial Photodynamic Activity of the Functionalised Fibres

Washing and sterilization

Glassware and forceps were washed autoclaved at 121 °C for 15 min and dried. All media were sterilized by autoclaving at 121°C for 15 minutes prior to use. The inoculation loop and needle were heated to red hot with a spirit lamp flame and air cooled before and after use. The surface of the ESCO

Class II biosafety cabinet were sprayed with 70% ethanol before and after use and wiped with a clean, soft cloth soaked in ethanol.

Preparation of Culture Media

The various culture media i.e. mannitol salt agar, Müeller-Hinton agar, nutrient agar etc were prepared a day before the susceptibility test as below.

Mannitol salt agar media

Dehydrated Mannitol Salt Agar (MSA) powder (22.2 g) was suspended in 200 mL of distilled water. The mixture was placed on a magnetic stirrer hot plate into, which a magnetic stirrer bar was inserted to ensure uniform mixing. The media was boiled until a clear medium was obtained. It was then autoclaved for 15 minutes at 121°C. This was used to perform the identification or the confirmation test on the Staphylococcus aureus species obtained, before using them for the APDT. A positive test will give a yellow colour change on the pink Mannitol Salt agar plate, after 18-24 hrs incubation.

Müeller-hinton agar media

Müeller-Hinton Agar (MHA) powder (38.0 g) was suspended in 1.0 L of distilled water. The mixture was placed on a magnetic stirrer hot plate into, which a magnetic stirrer bar was inserted to ensure uniform mixing. The media was boiled until a clear medium was obtained. It was then autoclaved for 15 minutes at 121°C.

Nutrient agar media

The Nutrient agar was used to culture the test bacteria a day before the APDT. The dehydrated Nutrient agar powder (14.0 g) was suspended in 500 mL of distilled water and placed on a magnetic stirrer hot plate for uniform mixing.

The media was brought to a boil until a clear media was obtained and then autoclaved for 15 minutes at 121°C.

Invitro Antibacterial Photodynamic Activity Test by the Disc Diffusion and Zone Inhibitory Methods

Müeller-Hinton agar plates were used for the disc diffusion and zone inhibition analysis using ISO 20645 *(BS EN ISO 20645, 2004;* Orhan *et al.,* 2009; Pinho *et al.,* 2011*)* and a Kirby-Bauer disc diffusion method (Bauer *et al.,* 1966; CLSI 2021) with slight modification, as the standard protocols to evaluate the susceptibility or resistance of isolates to the functionalised cellulose fibres. The functionalised cellulose-based fibres (ZnPc-GB, ZnPc-OPMF and ZnPc-PLF), with known concentrations of zinc phthalocyanine, were cut into circular discs (10 mm) and autoclaving for 15 mins at 121°C before the susceptibility test. The bacterial suspensions of test isolates were then prepared using normal saline and adjusted to the 0.5 McFarland turbidity standard, approximately $1\text{-}2{\times}10^8$ CFU/ml. The suspensions were subsequently used to inoculate (streak) sterile Müeller-Hinton agar plates to provide bacterial lawns with confluent growth. The functionalised fibre discs were then placed on their surfaces and left in the dark at 36°C for 60 mins. They were then treated with LED redlight (670 $\pm$ 5 nm) and natural daylight radiations, at intensities ranging between 2000-2500 lx (lm/m^2) and 400-1500 lx (lm/m^2) respectively, for 30 min at ambient temperature and then incubated at 36°C for 16-18 hr (*S. aureus*) *and* 24-48 hr (*P. aeruginosa*). For normal daylight (not directly in the sun) treatment, the MHA plates containing the bacteria strains were left near an open window for 30 minutes whilst treatment with the redlight involved placing the 670nm LED lamps, opposite each with

67

the bacteria samples in-between, at a distance to give the desired intensity. After incubation, the diameters of zones of inhibition (clear zones) were measured and recorded.

Control conditions

The bacteria strains were independently given, light-only and photosensitiser-only treatment doses as control treatments. For light-only treatment, the bacteria strains on the MHA plates, were irradiated with high doses of both daylight and LED redlight (670 ± 5 nm) sources at intensities ranging between 2000-3500 lx (lm/m^2) and 4500-5000 lx (lm/m^2) respectively, for 30 min at ambient temperature before, they were incubated in the dark for 18-24 hrs. Whilst for the photosensitiser-only treatment, the bacteria strains on the MHA plates containing the functionalised fibre discs and 10 µg gentamicin discs, were wrapped with aluminium foils and incubated in the dark for 18-24 hrs.

Chapter Summary

The various protocols and instumentations used in the synthesis and characterisation of the zinc phthalocyanine; extraction of the natural cellulose from oil palm mesocarp fibres and fresh pineapple leaves; immobilisation of the zinc phthalocyanine on the bleached cellulose-based fibres and their various instrumentations, including those for the photophysical, photochemical, optical detection of the NO_2 gas, photodegradation of crystal violet dye (a model organic dyes) in water and antibacterial photodynamic processes were specified in this chapter.

68

CHAPTER FOUR

RESULTS AND DISCUSSION

Introduction

The synthesis of Zinc phthalocyanine (ZnPc) dye was achieved through a solvent-free microwave method, followed by extraction and bleaching of unrefined oil palm mesocarp and pineapple leaf fibres. The dye was then immobilized on refined cellulose-based fibres to create functionalised cellulose-based fibres. These fibres were then studied for photodynamic and photodegradation applications, including nitrogen dioxide gas detection, crystal violet dye degradation, and bacteria inactivation. The results and insights from the analyses are therefore, presented in this chapter.

Microwave Synthesis of Zinc Phthalocyanine

The unsubstituted zinc phthalocyanine complex was obtained by the cyclotetramerization reaction of Phthalic anhydride and Urea in a 5:1 molar ratio with zinc chloride, using ammonium heptamolybdate tetrahydrate as a reaction catalyst. The resulting zinc phthalocyanine dye was crystalline in the solid state (Figure 11a) and greenish in DMF and DMSO solvents (Figure 11b).
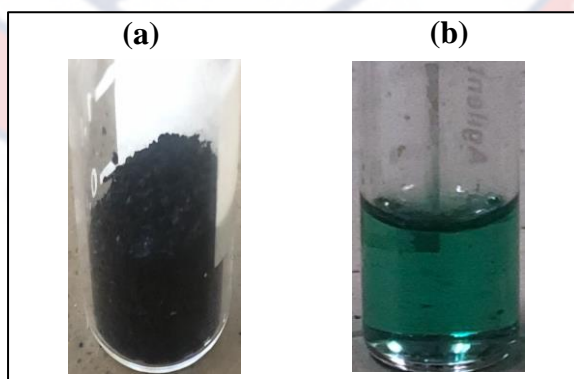
Figure 11: Images of the synthesised zinc phthalocyanine (a) dye and (b) in DMF solution.

Nuclear Magnetic Resonance Analysis of Synthesised Zinc

Phthalocyanine

The proton nuclear magnetic resonance (^{1}H-NMR) spectra of phthalocyanines are known to exhibit large diamagnetic ring current effects due to the macrocyclic 18-π system (Barthel & Hanack, 2000; Haisch *et al.*, 1997; Law *et al.*, 1997). Therefore, signals from aromatic protons of phthalocyanines are shown in the lower panel. Planar phthalocyanines exhibit strong shifts of aromatic and central ring protons at various concentrations and temperatures due to aggregation phenomena (Terekhov *et al.*, 1996). The ^{1}H-NMR spectrum is presented in Figure 12.
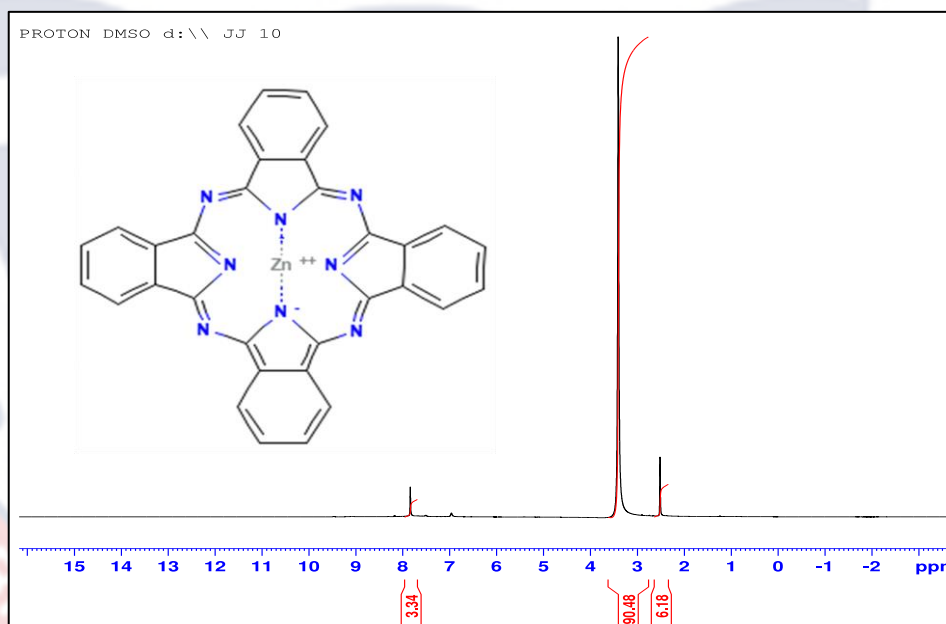
Figure 12: The ^{1}H NMR spectrum of the synthesised zinc phthalocyanine dye

The ^{1}H NMR spectrum of the zinc phthalocyanine showed a single proton signal around 7.84 ppm in the aromatic region (Figure 12), originating from protons on the benzene rings of the four N-bridged isoindole units forming the phthalocyanine ring system (Alam *et al.*, 2020). With all the

symmetry going on in the compound, the aryl protons are expected to be in the same chemical environment hence, yielded one signal.

UV-Visible Spectroscopy of Synthesised Zinc Phthalocyanine in Solution

Ground-state electronic spectra are particularly useful for identifying the structure of phthalocyanines. In general, the UV-Vis spectra of phthalocyanines show typical electronic spectra with two strong absorption bands known as Q-band and B-band. The strong Q-band in the far-red region around 600–750 nm, which accounts for its intense colour, is due to π-π^* transitions from the highest occupied molecular orbital (HOMO) to the lowest unoccupied molecular orbital (LUMO) of the phthalocyanine ring, while the B-band, a set of less intense but higher-energy transitions, is in the blue region of the electromagnetic spectrum around 350 nm (Baumann *et al.*, 1996; Hacıvelioglu *et al.*, 2008; He *et al.*, 2008; Stillman *et al.*, 1989). The absorption spectrum is presented in Figure 13.
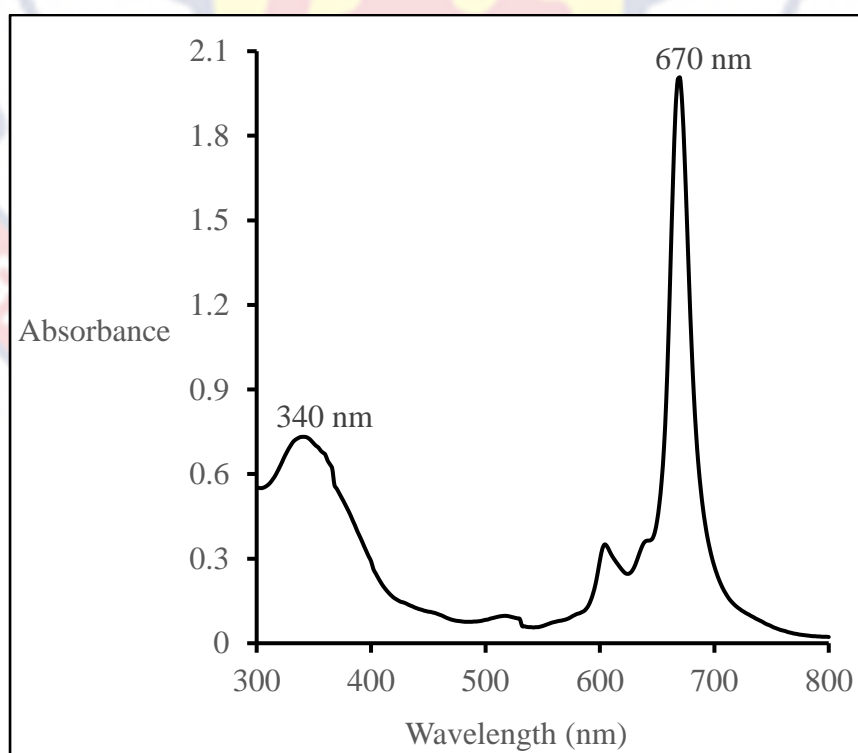
Figure 13: Absorption spectrum of Zinc phthalocyanine in DMF

71

The synthesised zinc phthalocyanine dye in N,N-dimethylformamide (DMF) solution at room temperature exhibited two characteristic main absorption peaks in the B or Soret band around 340 nm and the Q band around 670 nm, with a shoulder around 604, as shown in Figure 12. This agrees with literature (Ogunsipe *et al.*, 2003). The spectrum showed monomeric behaviour recognisable by a single (narrow) Q-band typical of metal-phthalocyanines (Ugur *et al.*, 2012). Two well-resolved peaks at 670 nm and 604 nm can be assigned to monomer π-π* transitions from the highest occupied molecular orbital (HOMO) to the lowest unoccupied molecular orbital (LUMO) of the phthalocyanine ring, while the band at 340 nm can be attributed to a lower π-level LUMO transition (Snow & Jarvis, 1984; Sasmaz, *et al.*, 1999).

The aggregation behaviour of Zinc phthalocyanine was also investigated at various concentrations in DMF using UV-vis spectrophotometry. Deviations from Beer-Lambert Law in concentration-dependent measurements are often used to check aggregation of phthalocyanines in DMF, DMSO solutions, etc. Therefore, the solubility of the zinc phthalocyanine dye in DMF was evaluated at various concentrations ranging from 0.26 to 55.5 μM to check for dimerization and aggregation. Absorbance of the Q-band at 670 nm was plotted against zinc phthalocyanine concentration in DMF to check if the Beer-Lambert law is obeyed. The results are presented in Figure 14.

72
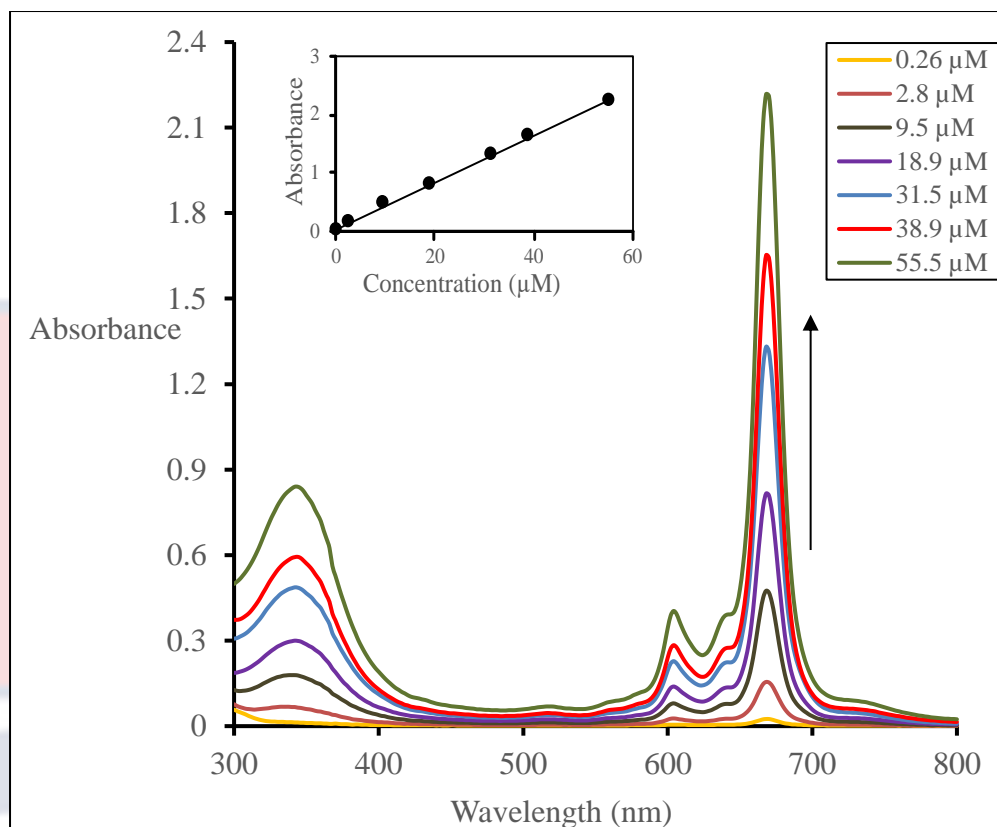
Figure 14: Absorption spectra of ZnPc displaying differences in absorbance with concentrations in DMF. Inserted: Beer- Lambert law.

The intensity of the Q band increased linearly with increasing concentration and aggregation did not result in the formation of new bands (usually blue-shifted). There is also a significant linear correlation between Q-band intensity and concentration (Figure 14), suggesting that the upper concentration range (55.5 µM) eliminates aggregation according to the Beer-Lambert law (inset).

Fluorescence Emission Spectral Analysis of Synthesised Zinc

Phthalocyanine in Solution

It has been reported that the molecule does not fluoresce in the aggregated state, but that fluorescent properties become apparent when aggregation is reduced (Kimura *et al.*, 1997). Therefore, the fluorescence emission spectra of the synthesised zinc phthalocyanines was studied to

73

determine their behaviour in both solid and solution forms (that is, DMF solvent). The emission spectrum is shown in Figure 15.
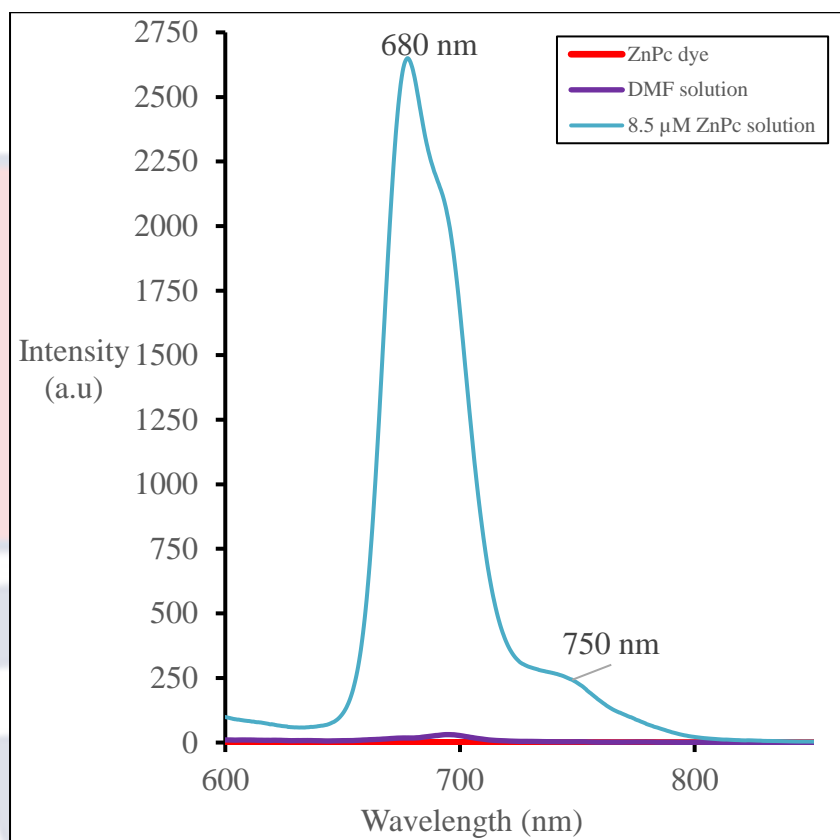
Figure 15: Emission spectra of zinc phthalocyanine dye (red), DMF solvent (purple) and zinc phthalocyanine solution (turquoise).

Fluorescence is usually quenched when the solution is concentrated or the compound is in the solid state. As seen in Figure 15, the Zinc phthalocyanine dye did not exhibit any fluorescence emission peaks, possibly because of the π-π stacking ascribed to the aggregation properties of the phthalocyanine complexes, whereas the zinc phthalocyanine solution (8.5 µM) exhibited two bands in the red spectral region, a strong Q-band emission maximum at ~680 nm and a corresponding minor peak at ~750 nm, similar to literature (Kahya *et al.*, 2019; Ogunsipe *et al.*, 2003; Scalise & Durantini, 2005). The DMF solution alone did not show any fluorescence emission peak

74

(Kahya *et al.*, 2019). Therefore, it is confirmed that the peak observed in solution is that of zinc phthalocyanine.

It is generally reported that, the fluorescence band $S_1 \rightarrow S_0$ of rigid molecules such as aromatic compounds is the mirror image of the absorption band ($S_0 \rightarrow S_1$). Also, emission is generally more red-shifted than absorption because, the vibrational energy levels involved are lower in fluorescence emission but higher in absorption (Michl & Bonacic-Kotechy, 1990). Therefore, the emission and absorption behaviours of the synthesised Zinc phthalocyanines were compared, as shown in Figure 16.
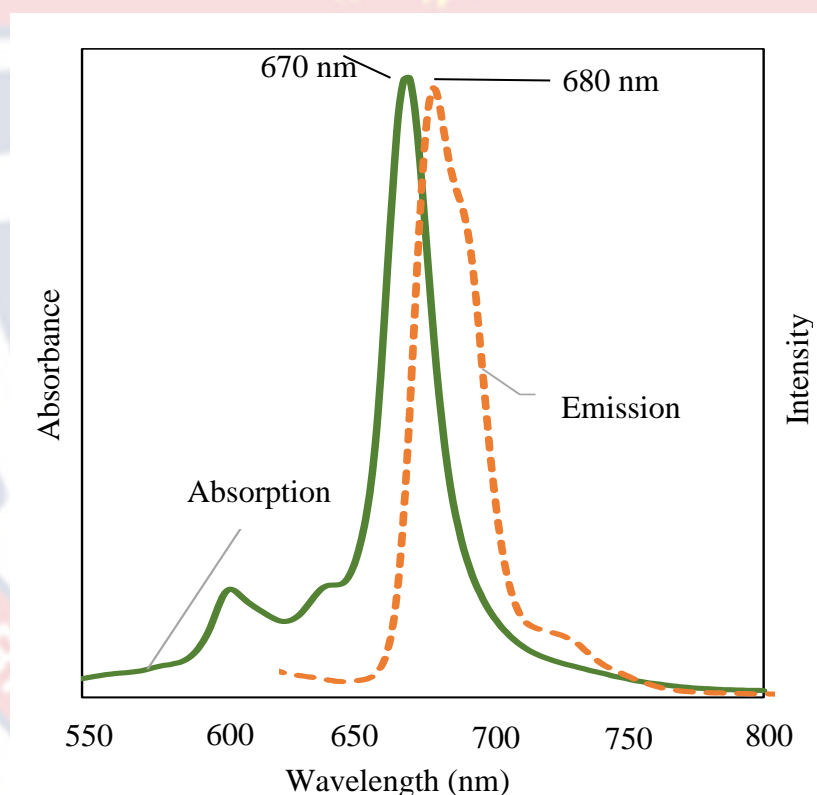
Figure 16: Absorption and emission spectra of the synthesised Zinc phthalocyanine in DMF.

The Q-band absorption maximum of zinc phthalocyanine was observed at λmax 670 nm (figure 13) and the emission peak was observed at λmax 680 nm (figure 15) and is slightly red-shifted with a Stokes shift of ~10 nm,

75

relative to the absorption spectrum. Furthermore, the emission band was observed to be a mirror image of the absorption band (Figure 16), consistent with the literature (Michl & Bonacic-Kotechy, 1990).

Effect of zinc phthalocyanine concentration on fluorescence

The usual phenomenon is that fluorescence intensity increases with substance concentration (at very low concentrations), but this was not the case in this study. This is believed to be due to aggregation (π-π stacking), normally associated with the concentrated solution and solid state of zinc phthalocyanine. As the amount of zinc phthalocyanine molecules in solution increases, the electrostatic interaction between them becomes stronger and aggregates are formed. The radiation emitted in solution is absorbed in the process (Kahya, 2012), quenching the fluorescence. The fluorescence emission spectrum of zinc phthalocyanine in DMF analysed, at various concentrations to evaluate its effect on emission intensity is shown in Figure 17. They showed typical shapes of phthalocyanines with a peak around 680 nm.
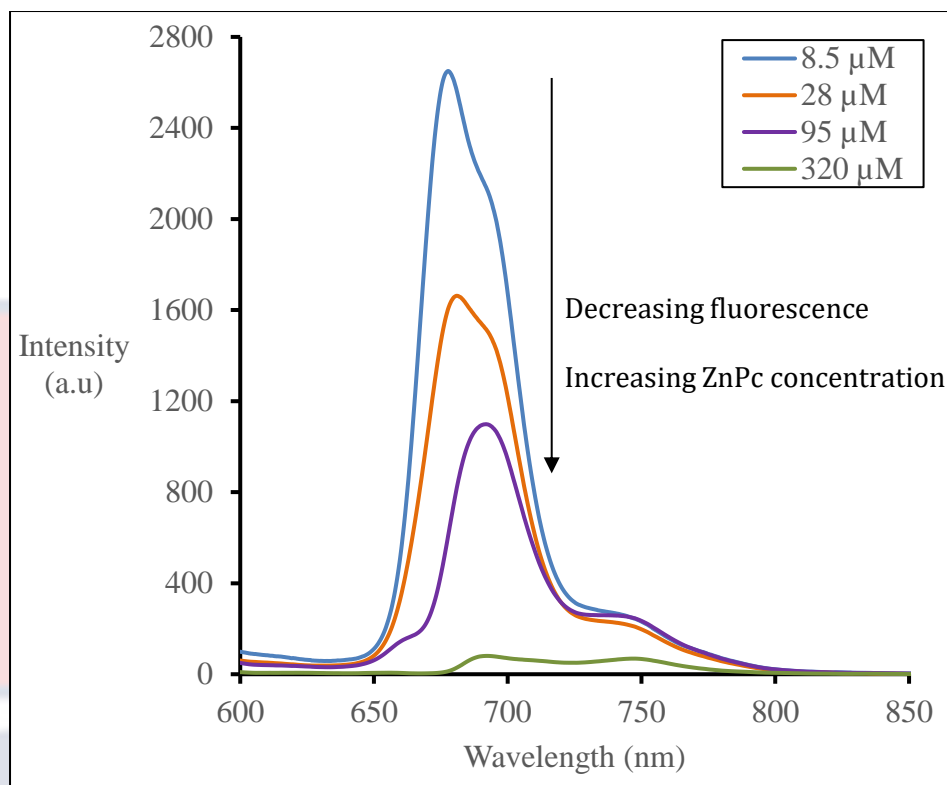
Figure 17: Emission spectra of the zinc phthalocyanine in DMF at various
concentrations.

The fluorescence intensity peaked at the Q-band is shown to decrease with increasing zinc phthalocyanine concentration from 8.5 μM to 320 μM. The decrease in intensity with concentration may be as a result of photon self-absorption in the Zinc phthalocyanine solution as previously described, which is consistent with the literature (Kahya *et al.*, 2019). Therefore, as the concentration increases, photon self-absorption in solution increases and fluorescence is quenched. It is also observed that, the more concentrated the solution (as shown in Figure 17), the more red-shifted the peaks appeared.

Infrared Spectroscopic Analysis of Synthesised Zinc Phthalocyanine

The infra-red spectra of the synthesised zinc phthalocyanine dye, was performed over the range of 4000–400 cm^{-1} to identify the types of functional groups present in the compound. The result is presented in Figure 18.

77
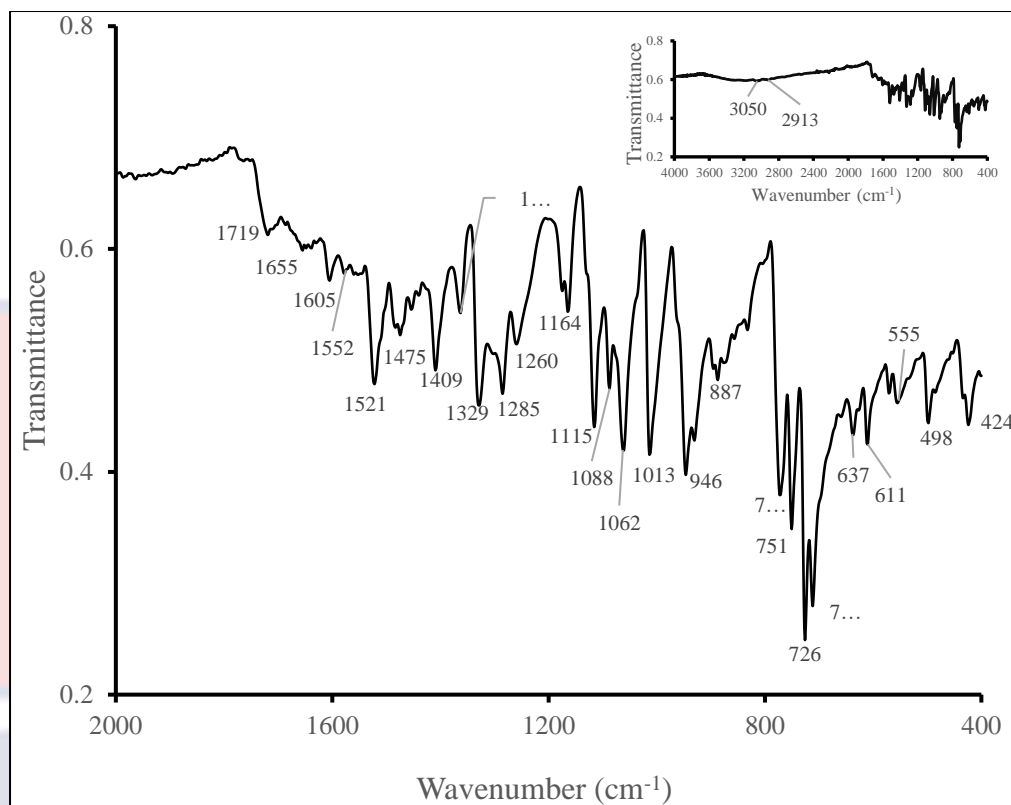
Figure 18: Infra-red spectrum of the synthesised zinc phthalocyanine. Insert: Full spectrum.

The peak at 3050 cm^{-1} is assigned to Ar-H stretching and the peak at 2913 to aliphatic C-H stretching (Kaya *et al.*, 2014; Sağlam, 2016). The peak at 1605 cm^{-1} is attributed to deformation of the C=C macrocyclic ring of pyrrole, and the peaks at 1521, 1475, and 1285 cm^{-1} are attributed to the aromatic phenyl ring and C=N stretching vibrations. The C–C stretching of isoindole occurred at 1409 and 1329 cm^{-1}. The peaks at 1285, 1164 and 1088 cm^{-1} are assigned to the isoindole C-N stretch, C-N in-plane bend and C-H in-plane bend respectively. The peak at 1062 cm^{-1} corresponds to C-H bending in planar deformation. C-H bending out of planar deformation is observed at 946, 887 and 726 cm^{-1}. The peaks at 1329, 1164, 1115, 1088, 1062, 1013, 946, 887, 772, 751, 726 and 712 cm^{-1} are attributed to phthalocyanine backbone vibrations (Li *et al.*, 2018; Kahya, 2019). The transmittance peaks of the

78

synthesised zinc phthalocyanine and it's functional group divisions are presented in Table 6.

Table 6: Transmittance Peaks of the Synthesised Zinc Phthalocyanine and it's Functional Group Divisions

Transmittance Peaks (cm^{-1})	Functional Group Division
3050	Ar-H stretching
2913	C-H Stretching
1605	C=C macrocyclic pyrrole ring deformation
1521, 1475, and 1285	C=N stretching vibrations
1409 and 1329	C–C stretching of isoindole
1285	C-N stretching of isoindole
1164	C-N in-plane bend
1088	C-H in-plane bend
1062	C-H bending in planar deformation
946, 887 and 726	C-H bending out of planar deformation
1329, 1164, 1115, 1088, 1062, 1013, 946, 887, 772, 751, 726 and 712	Phthalocyanine backbone vibrations

Source: Laboratory Analysis (2016-2021)

Scanning Electron Microscopic Analysis of Zinc Phthalocyanine

The zinc phthalocyanine was characterized to evaluate its morphology. The images are presented in Figure 19.
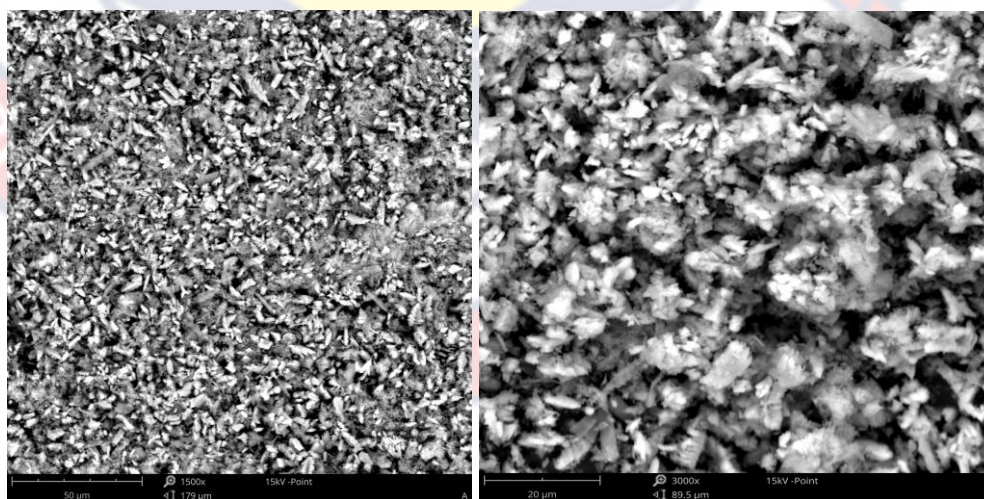
Figure 19: SEM images of the synthesised zinc phthalocyanine at different magnifications.

79

The particles of zinc phthalocyanine somehow appear as well-defined irregular shapes ranging from 2.4 to 14 μm in diameter.

Energy-Dispersive X-Ray Spectroscopic Analysis of Zinc Phthalocyanine

Energy-dispersive X-ray spectroscopy was performed to confirm the elemental composition of the synthesised zinc phthalocyanine. The result is presented in Figure 20.

Element Symbol	Atomic Conc.	Weight Conc.
C	65.09	53.34
N	31.11	29.73
Zn	3.80	16.93
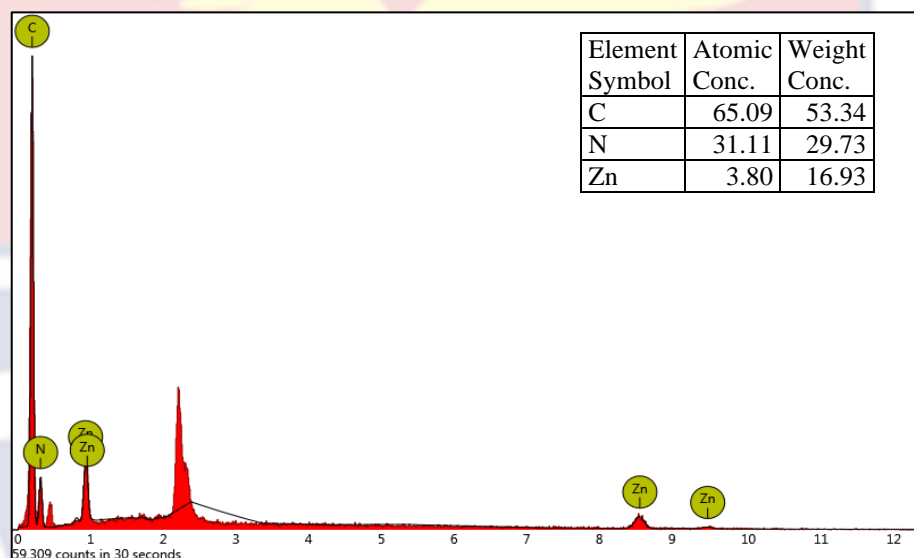
Figure 20: EDS spectra of the synthesised zinc phthalocyanine.

The dye exhibited C, N, and Zn peaks, characteristic of zinc phthalocyanine. This indicates the successful synthesis of the dye, as confirmed in the literature (Kahya *et al.*, 2019; Sindole *et al.*, 2022).

Powder X-Ray Diffraction Analysis of Synthesised Zinc Phthalocyanine

Powder X-ray diffraction (PXRD) technique was used to evaluate the crystallinity and the structure of the synthesised zinc phthalocyanine dye (Haq *et al.*, 2022; Zafar *et al.*, 2022).

Highscore peak search/match

Peak search/match was performed using HighScore software (Degen *et al.*, 2014) to identify possible phases of the synthesised zinc phthalocyanine

80

dye, using data from the Open Database of Crystals (Gražulis *et al.*, 2009). The four best proposed candidate phases (powder diffraction file [PDF] names and map numbers) and the percentage of each phase in each sample are shown in Table 7. Ranking was based on full width at half maximum (FWHM). The synthesised compound was identified as zinc phthalocyanine in all the four most likely compounds suggested by the search (Table 7).

Table 7: Best Plausible Phases in the Sample using the HighScore Peak Search

Ref.Code	Score	Compound Name	Scale Factor	Chem.Formula
00-039-1882	45	β-Zinc phthalocyanine	0.633	$C_{32}H_{16}N_8Zn$
00-021-1985	33	Zinc phthalocyanine	0.424	$C_{32}H_{16}N_8Zn$
00-011-0714	58	Zinc phthalocyanine	0.765	$C_{32}H_{16}N_8Zn$
02-063-7832	37	Phthalocyanato-zinc(ii)	0.641	$C_{32}H_{16}N_8Zn$

Source: Laboratory Analysis (2016-2021)

Quantitative analysis

Diffraction pattern screening, including profile fitting based on the Rietveld and Le Bail fitting method, was performed using Material Analysis Using Diffraction (MAUD) software (Lutterotti *et al.*, 1999). This was used for quantitative analysis of zinc phthalocyanine. The results are presented in Figure 21.
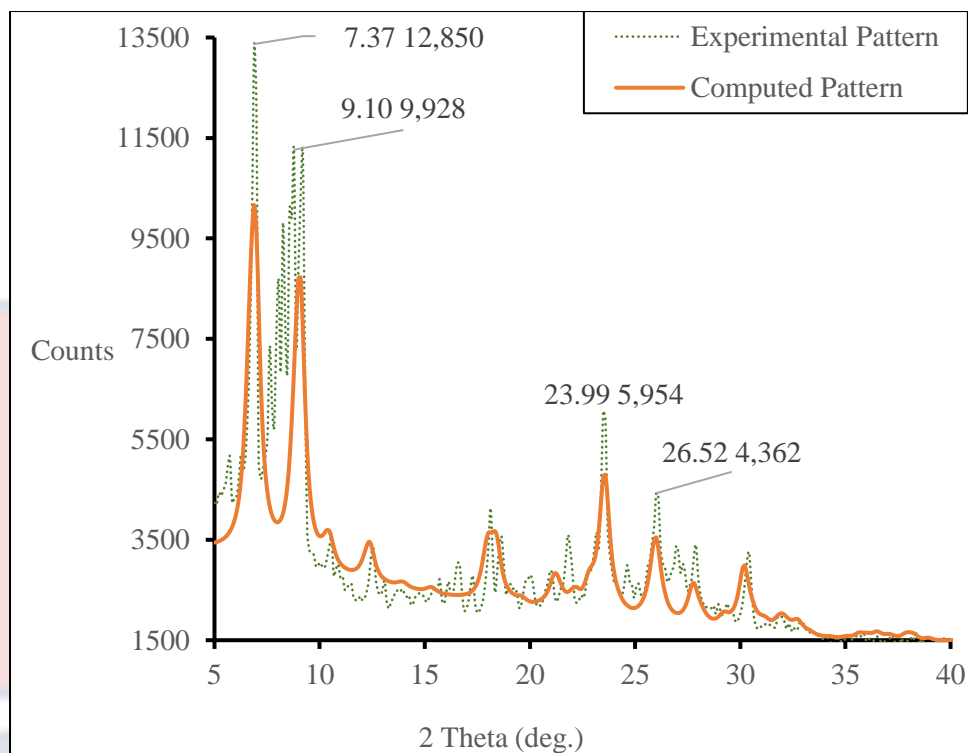
Figure 21: Powder X-ray diffraction patterns of zinc phthalocyanine
(Experimental and computed/refined patterns from the MAUD
analysis).

The angle (2θ) of the highest peak is around 7.37° and the d-spacing
[$d_{(1\,0\,0)}$] for this peak is 11.955 nm which, is the highest and it is from the Zinc
phthalocyanine phase (Table 8). Other major peaks from the Zinc
phthalocyanine phase are found at angles (2θ) 9.10°, 23.99° and 26.52° which,
are attributed to $d_{(-1\,0\,2)}$, 9.599 nm; $d_{(2\,1\,0)}$, 3.706 nm and $d_{(-2\,1\,1)}$, 3.359 nm
respectively. All these peaks are strong and sharp in the pattern (Figure 21)
which, implies that the crystallites are relatively large and/or low lattice strain
planes (Kari *et al.*, 2021) and are attributed to monoclinic Zinc
phthalocyanine, $C_{32}H_{16}N_8Zn$ (Li *et al.*, 2018).

Table 8 shows the four sharpest reflections, the angles (2θ) at which
they occur, and the quality indices (crystal size and lattice strain) of the zinc
phthalocyanine phase.

82

Table 8: Properties of Major Peaks of Zinc Phthalocyanine

2 θ (deg.)	Intensity (counts)	h k l	d-spacing (nm)	Phase
7.37	12,850	1 0 0	11.955	zinc phthalocyanine
9.10	9,928	-1 0 2	9.599	zinc phthalocyanine
23.99	5,954	2 1 0	3.706	zinc phthalocyanine
26.51	4,362	-2 1 1	3.359	zinc phthalocyanine

Source: Laboratory Analysis (2016-2021)

The predominantly intense diffraction peaks indicate the (100) dominant growth orientation, and all diffractions, including weak ones, are well assigned to the monoclinic $C_{32}H_{16}N_8Zn$ (Table 8) (JCPDS #11-714). According to the intensity ratio of the two peaks in the low angle range of 5–10 (Fig. 21), the synthesised zinc phthalocyanine may belong to the α-crystal form (Li *et al.*, 2018).

Composition of synthesised zinc phthalocyanine by MAUD analysis

The results of the screening test are shown in Table 9. Purification of the sample yielded nearly pure zinc phthalocyanine (97.28%) with a small amount of urea (2.72%).

Table 9: Percentage Weight Composition of Zinc phthalocyanine

Phase Name	Wt.(%)
Zinc Phthalocyanine	97.28
Urea	2.72

Source: Laboratory Analysis (2016-2021)

Thermogravimetric Analysis (TGA) of Synthesised Zinc Phthalocyanine

The thermal stability of the synthesised zinc phthalocyanine was measured by thermogravimetric analysis (TGA) to test its potential use in the catalytic reactions. Thermal stability of phthalocyanines is an important

83

requirement for many catalytic applications. The results are presented in Figure 22.
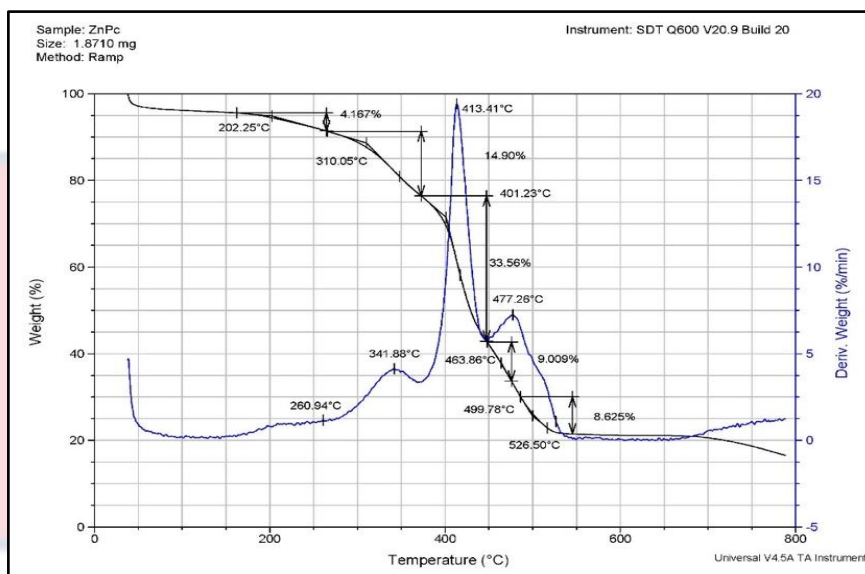
Figure 22: Thermal decomposition curve of zinc phthalocyanine showing
      weight losses

Phthalocyanines and their metal derivatives have been reported to be thermally stable up to 400 °C (Pirbazari, 2017; Zhao *et al.*, 2009). The initial temperature drop at 50 °C is caused by evaporation of the solvent and/or other volatile impurities used in the synthesis. This is also seen in the DSC curve (Figure 23) as an endothermic peak around 50 °C. Zinc phthalocyanine exhibited five distinct thermal events (decomposition) at approximately 200 °C, 300 °C, 400 °C, and 500 °C (Figure 22 and Table 10). A thermal event near 200°C with a weight loss of 4.167% may be the result of the decomposition of unstable chemical fragments within the sample. Maximum weight loss occurred at 413.41 °C, with a weight loss of 33.56% between 400 and 450 °C (Figure 22 and Table 10). This represents the main degradation step, due to the decomposition of the zinc phthalocyanine skeleton (Li *et al.*, 2018; Sharma *et al.*, 2012). This means that the synthesised zinc

84

phthalocyanine has high thermal stability above 400 °C and can be used in photocatalytic processes at high temperatures without affecting the compound. These mass losses are observed as three peaks at 341.88 °C, 413.41 °C and 477.26 °C in DTG. Table 10 shows the onset temperatures (T_{onset}), inflection points (T_{max}), and weight percent (%) losses of zinc phthalocyanine (ZnPc).

Table 10: Onset Temperatures (T_{onset}), Inflection Temperatures (T_{max}) and Weight Percent (%) Losses of Zinc phthalocyanine (ZnPc).

Sample	T_{onset} (^oC)	T_{max} (^oC)	Wt. loss percent (%)
ZnPc	202.25	260.94	4.167
	310.05	341.88	14.90
	401.23	413.41	33.56
	463.86	477.26	9.009
	499.78	526.78	8.625

Source: Laboratory Analysis (2016-2021)

Differential Scanning Calorimetry (DSC) Analysis of Synthesised Zinc Phthalocyanine

Differential scanning calorimetry (DSC) is a thermal analysis technique that measures the temperature difference between a sample and a reference material as a function of temperature, while applying a controlled temperature program to both sample and reference material. This technique is used to qualitatively and quantitatively determine temperature changes, especially in terms of exotherms, endotherms, and heat capacities (Akash & Rehman, 2020).

The DSC curve of the synthesised zinc phthalocyanine was measured to determine the melting point (Tm), glass transition temperature (Tg), and enthalpy of the thermal events (Cp). The results are shown in Figure 23.

85
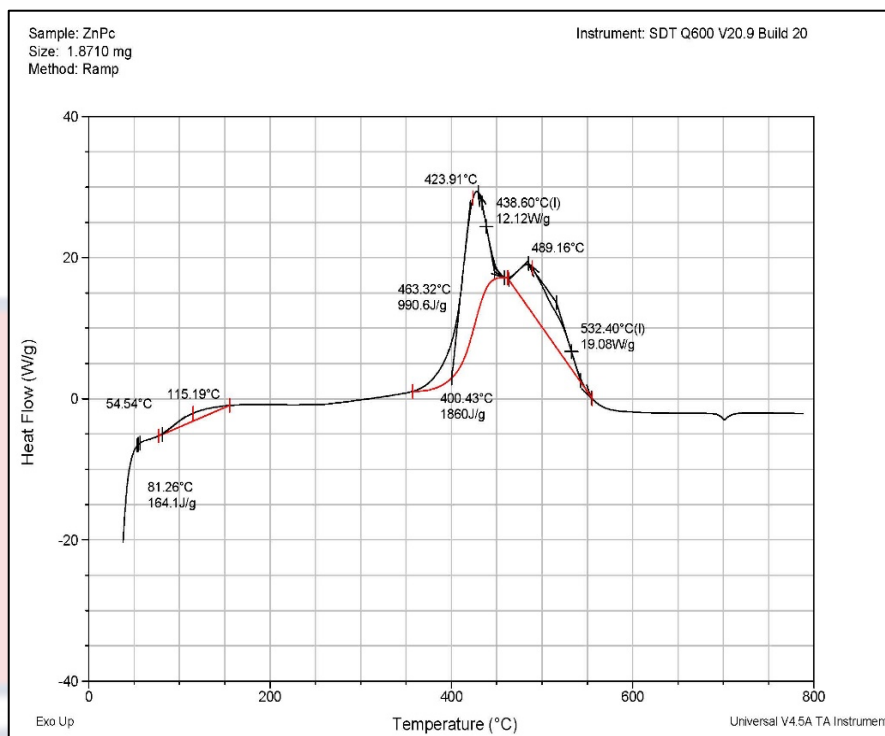
Figure 23: Glass transition temperature, (Tg) and decomposition enthalpies (Cp) of zinc phthalocyanine.

The differential scanning calorimetry curve of the synthesised zinc phthalocyanine shows a thermal event at approximately 700 °C (Figure 23). This phenomenon is endothermic and is probably due to the melting point of zinc phthalocyanine. The initial temperature is 695.37 °C and the peak temperature is 701.14 °C. The required energy is 24.52 J/g (Table 11). The endothermic phenomenon at ~50°C is likely due to the evaporation of the solvent and/or other volatile impurities used in the synthesis.

Table 11: The Melting Point (Tm) and Enthalpy Change (Cp) of the ZnPc

Sample	Tm (ºC)	Onset Temp. (ºC)	Enthalpy Change (J/g)
ZnPc	701.14	695.37	24.52

Source: Laboratory Analysis (2016-2021)

86

Photostability Capacity of the Synthesised Zinc Phthalocyanine

Degradation of photosensitisers under light is used to investigate the stability of applications such as photocatalysis (Awaji et al., 2019) and photodynamic therapy, among others. Photodegradation of the synthesised Zinc phthalocyanine was therefore, monitored in DMF and the decrease in the absorption peak, together with deformations in the shape, would confirm its' degradation to other kinds in the presence of light. The results are presented in Figure 24.
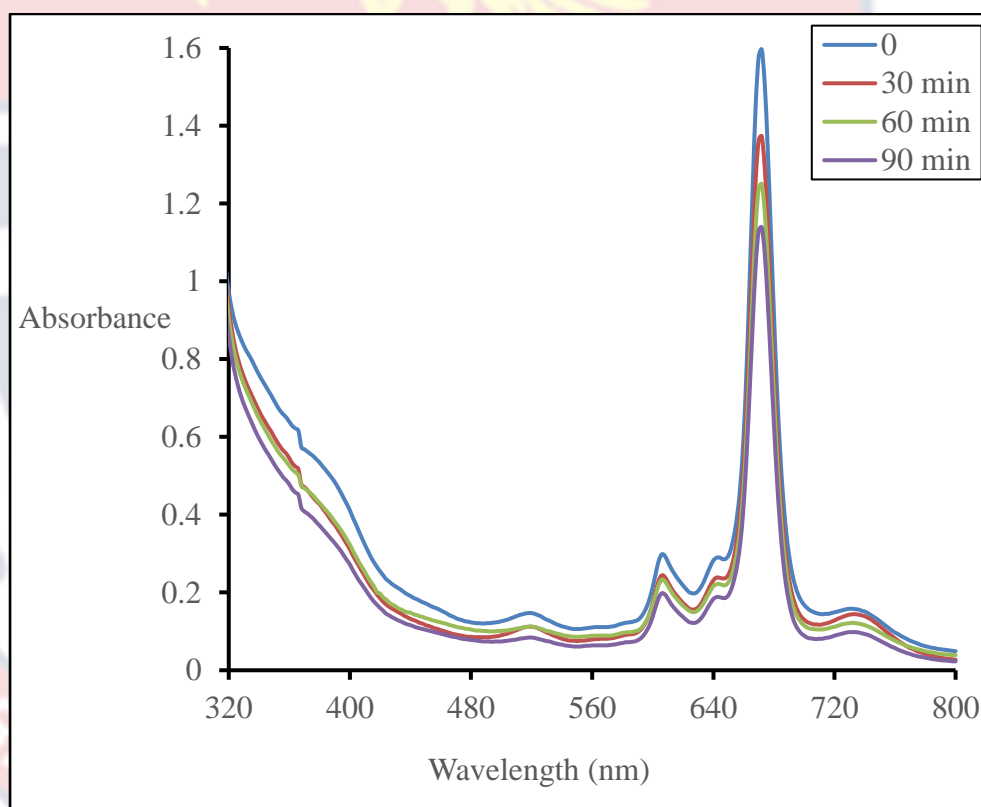
Figure 24: UV-Vis absorption spectra analysis of the degradation of zinc phthalocyanine in DMF under redlight radiation.

The reduction in Q-band absorbance of the zinc phthalocyanine solution upon irradiation with LED redlight (10000-14000 lx) was very small (8%) over the 90-minute irradiation period and 92% of the initial absorbance (photostability coefficient) was retained. This means that zinc phthalocyanine

87

dyes are very stable to light and can withstand long exposures without significant material loss. However, the photodegradation mechanisms of phthalocyanines are complex and depend on the solution and biological medium (Ochsner, 1997; Scalise & Durantini, 2005; Seven *et al.*, 2008). Also, there was no new band formation as evidenced by the absorption range from 300 to 800 nm. This suggests that, photodegradation of the zinc phthalocyanine dye in the presence of light is not accompanied by decomposition into other forms, but only by a decrease in absorbance or concentration, as evidenced by the decrease in the Q band as a result of long light exposure times.

Singlet Oxygen Production Capacity of Zinc Phthalocyanine Solution

Production of singlet oxygen is the most important property a sensitiser should have for use in antimicrobial photodynamic therapy and photooxidation applications. Therefore, the ability of zinc phthalocyanine dyes in solution (DMF) to generate singlet oxygen was evaluated using the 1,3-diphenylisobenzofuran (DPBF) method. DPBF (a known singlet oxygen quencher) is decomposed by singlet oxygen ($^1O_2$) to produce colourless o-dibenzoylbenzene (Ogilby, 2010). Figure 25 shows results of the photooxidation of DPBF, used as an indicator of singlet oxygen production, in the presence of zinc phthalocyanine under daylight and LED redlight illuminations.
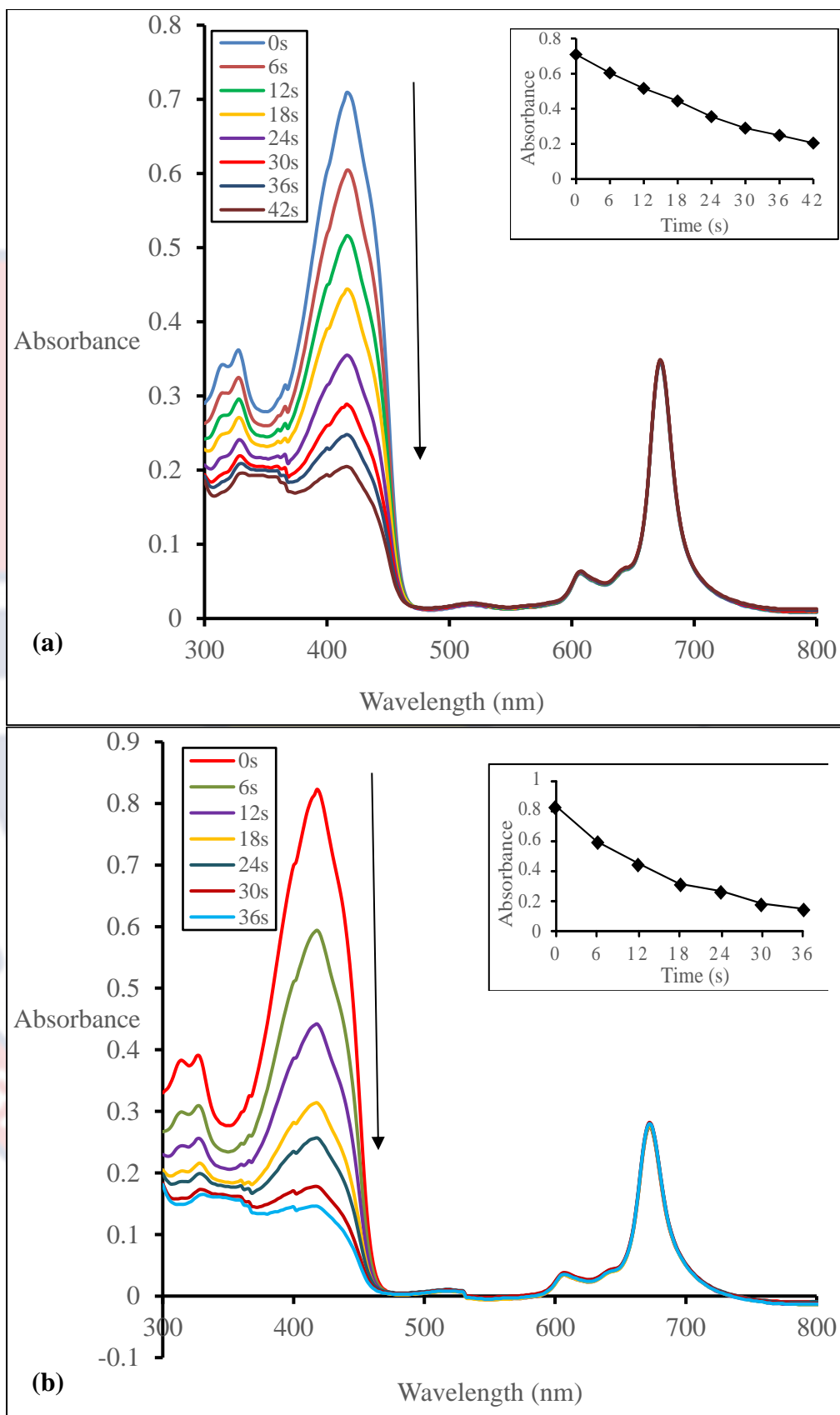
Figure 25: Spectral changes of the photodegradation of DPBF with zinc phthalocyanine solution under (a) daylight and (b) LED redlight irradiations. Inserts: absorbance versus time curve.

89

The DPBF absorption peaks at 416 nm and 418 nm under daylight (Figure 25a) and LED redlight (Figure 25b) illumination, respectively, continued to decrease with time, whereas the Q-band of the Zinc phthalocyanine dye remained unchanged over the illumination period, as observed in literature (Ramos et al., 2015). This suggests that, singlet oxygen ($^1O_2$) was being produced and is the agent responsible for the degradation of the 1,3-diphenylisobenzofuran (DPBF). It also, confirms the stability of the Zinc phthalocyanine dye, as it did not degrade with time as observed at the Q band regions of the spectra, which is an important property of a good photosensitiser

Extraction of Cellulose from Unrefined Fibres

Cellulose-based fibres were extracted from oil palm mesocarp and pineapple leaf wastes by treatment with alkaline hydrogen peroxide. Hydrogen peroxide (H_2O_2) bleaching treatment had a huge effect on fibre brightness, as shown in Figures 26c and 26f below. Using H_2O_2 as an oxidising bleach, discoloured the fibres. In theory, perhydroxyl ions (HOO-) are formed when hydrogen peroxide dissociate in alkaline media and are responsible for fibre discolouration. These ions attack the light-absorbing chromophore groups (carbonyl groups, conjugated carbonyl groups, quinones) of lignin and cellulose (Rayung *et al.*, 2014).
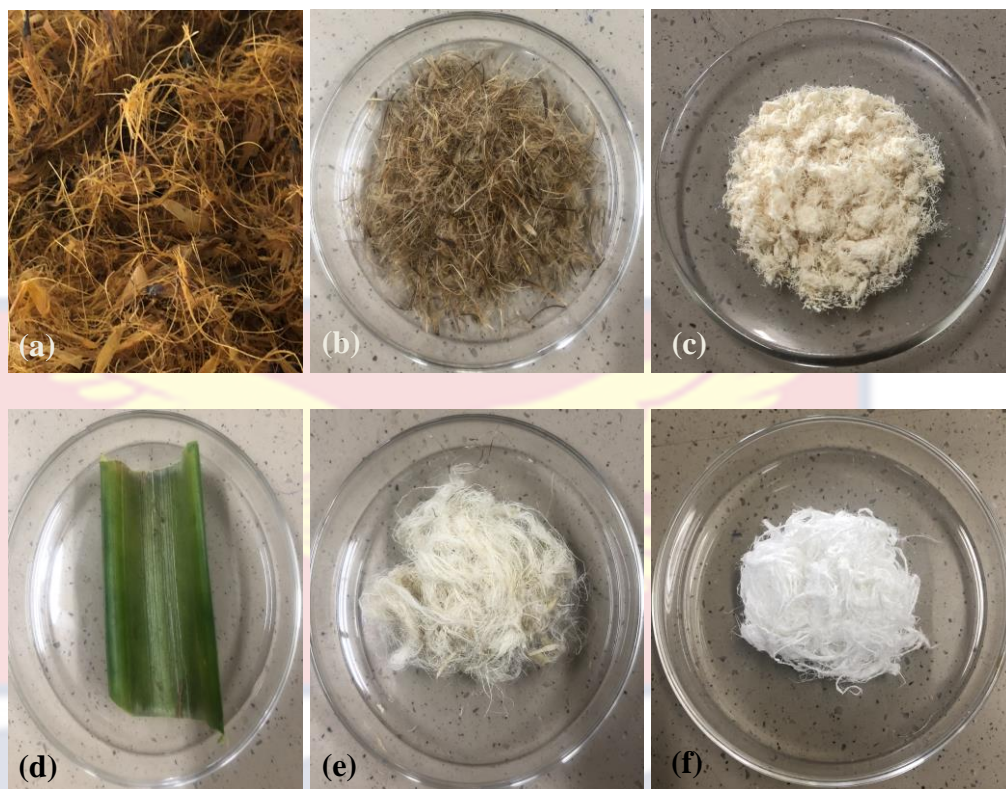
Figure 26: Images of the (a) unrefined oil palm mesocarp fibres (Ur-OPMF); (b) hot water treated oil palm mesocarp fibres; (c) bleached oil palm mesocarp fibres (B-OPMF); (d) unrefined pineapple leaf fibres (Ur-PLF); (e) extracted hot water treated pineapple leaf fibres and (f) bleached pineapple leaf fibres (B-PLF).

The extracted/bleached cellulose-based fibres from the oil palm mesocarps (B-OPMF) and the pineapple leaves (B-PLF) were whiter in appearance (Figures 26c & 26f) as compared to the unrefined (Ur-OPMF and Ur-PLF) fibres (Figures 26a & 26d). However, the B-PLF (Figure 26c) appeared to be whiter and softer in nature, as the commercial reference P-GB (Figure 27a) whereas, the B-OPMF (Figure 27b) was more fibrous in nature and harder.

91
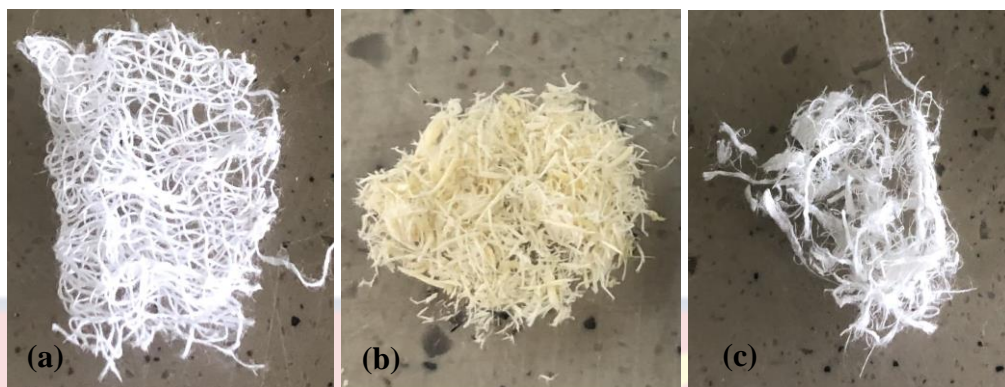
Figure 27: Images of the (a) plain gauze bandage (P-GB); (b) bleached oil palm mesocarp fibres (B-OPMF) and (c) bleached pineapple leaf fibres (B-PLF) used in this work.

Immobilisation Of Zinc Phthalocyanine on the Cellulose-Based Fibres

The zinc phthalocyanine dye was immobilised onto the cellulose-based fibres (P-GB, B-OPMF and B-PLF) by sorption forces to achieve, novel zinc phthalocyanine-functionalised fibres (ZnPc-GB, ZnPc-OPMF and ZnPc-PLF) Figure 28, for gas sensing, photocatalytic and photodynamic applications.
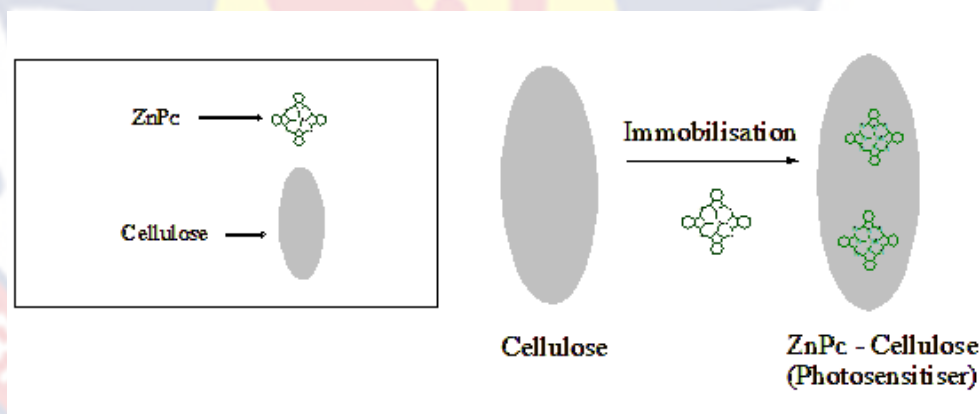
Figure 28: Schematic presentation of the immobilisation process

The cellulose-based and functionalised fibres were then observed under a UV lamp to see if the zinc phthalocyanine dye was successfully immobilised. The images in Figure 29 depicts that.

92
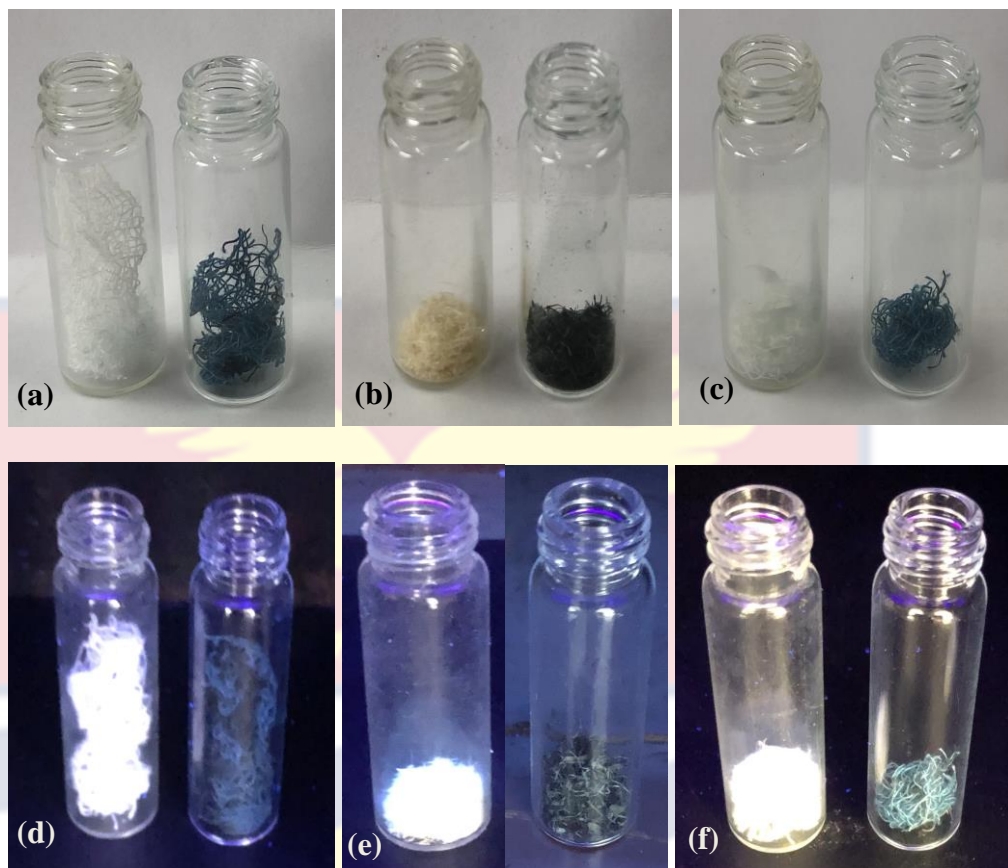
Figure 29: Images of (a) P-GB & ZnPc-GB, (b) B-OPMF & ZnPc-OPMF and
(c) B-PLF & ZnPc-PLF and their appearance under the UV lamp
(d), (e) and (f) respectively.

The functionalised fibres (ZnPc-GB, ZnPc-OPMF and ZnPc-PLF),
although appeared darker physically to the eye (Figure 29 a-c), exhibited the
characteristic green colour of zinc phthalocyanine when brought under the UV
lamp (Figure 29 d-f), whereas the plain fibres (P-GB, B-OPMF and B-PLF)
did not exhibit the green colour, Figure 29. This suggests the successful
immobilisation of the zinc phthalocyanine dye on the cellulosed-based fibres.

**Solid-State Fluorescence Emission Spectroscopy of the Functionalised
Fibres**

The molecule is reportedly non-fluorescent in the aggregated state, but
fluorescence properties become apparent when aggregation is reduced

93

(Kimura et al., 1997). Therefore, the fluorescence emission spectra of the zinc phthalocyanine embedded in the cellulose-based fibres was studied to investigate its' behaviour. The emission spectrum is shown in Figure 29.

As observed in Figure 30 a-c, the functionalised cellulose-based fibres (ZnPc-GB; ZnPc-OPMF & ZnPc-PLF) exhibited fluorescence as, evidenced in their enhanced emission intensities at the Q-bands whereas, the plain (bleached) cellulose-based fibres alone (P-GB; B-OPMF & B-PLF), did not fluoresce. This means that the fluorescence exhibited by the functionalised fibres, was as a result of the Zinc phthalocyanine within them and that the embedded zinc phthalocyanine is quite dispersed within the fibre matrices and therefore, functional. This also implies that the functionalised fibres retained all the properties of the free zinc phthalocyanine within them.
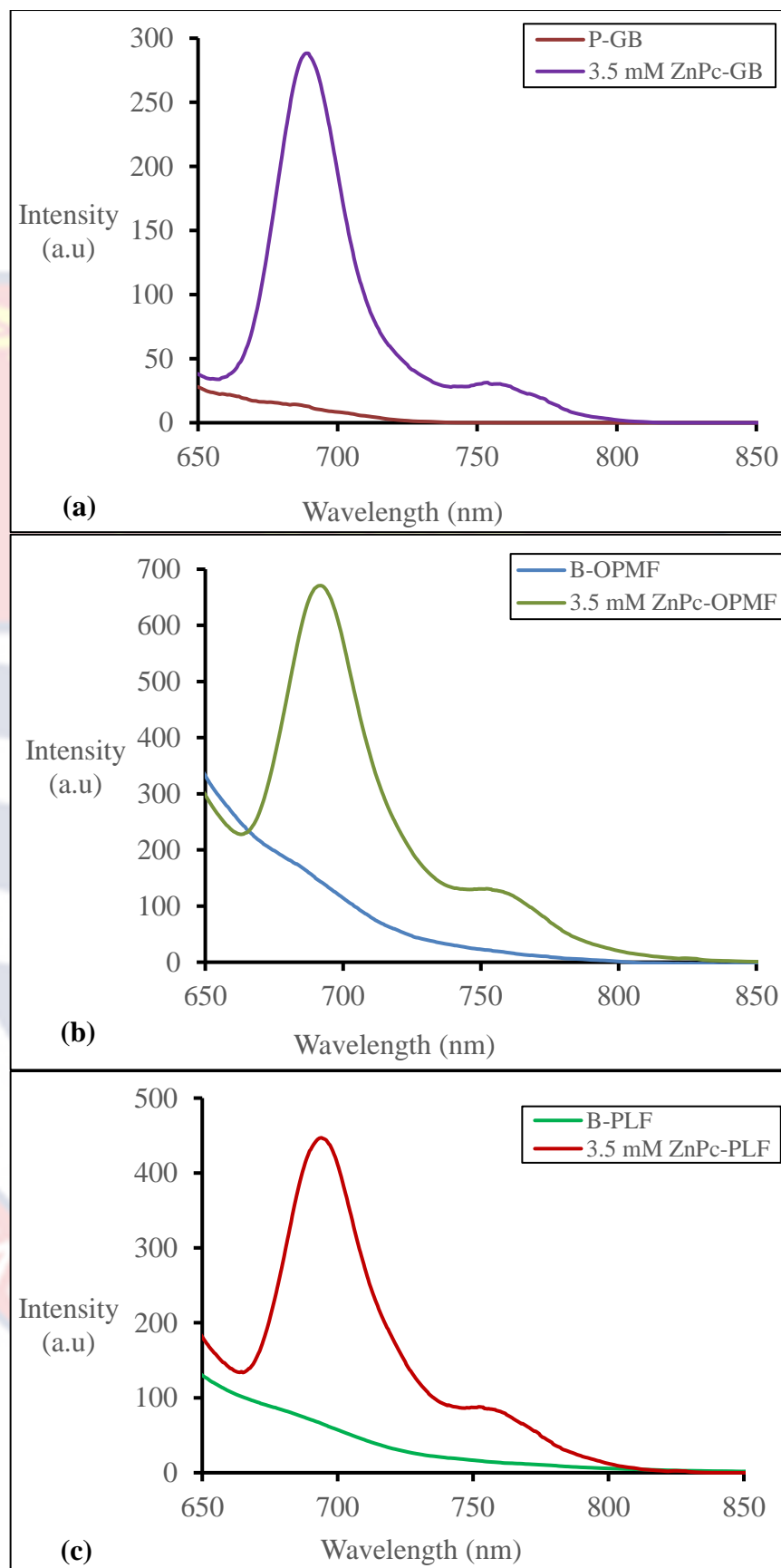
Figure 30: Emission spectra of (a) P-GB & ZnPc-GB; (b) B-OPMF & ZnPc-OPMF and (c) B-PLF & ZnPc-PLF.

95

The fluorescence behaviour of the zinc phthalocyanine within the functionalised fibre supports was also, compared with that in the DMF solution. They also exhibited the typical emission intensities of phthalocyanines at the Q-band, as with the free zinc phthalocyanine in solution. However, the peaks were much more red-shifted in the functionalised fibre supports (λ_{max} 690 nm) than the corresponding spectrum in the DMF solution (λ_{max} 680 nm) in Figure 15. This may give them enhanced photosensitising properties over the free zinc phthalocyanine.

Effect of the functionalised fibre concentration on fluorescence

The fluorescence emission spectra of the functionalised fibres was analysed at various concentrations, to evaluate their effects on the emission intensity. The results are shown in Figure 31.

As seen in Figure 31, they also exhibited the same concentration gradient as was observed by the free zinc phthalocyanine in solution (Figure 17). The fluorescence intensities decreased with increasing zinc phthalocyanine concentration at the Q-band within all the functionalised fibre matrices. Also, their emission intensities were much more red-shifted (λ_{max} 690 nm) as compared to the corresponding intensities of the free zinc phthalocyanine in DMF solution (λ_{max} 680 nm) in Figure 17. This may give them enhanced photosensitising properties over the free zinc phthalocyanine.

96
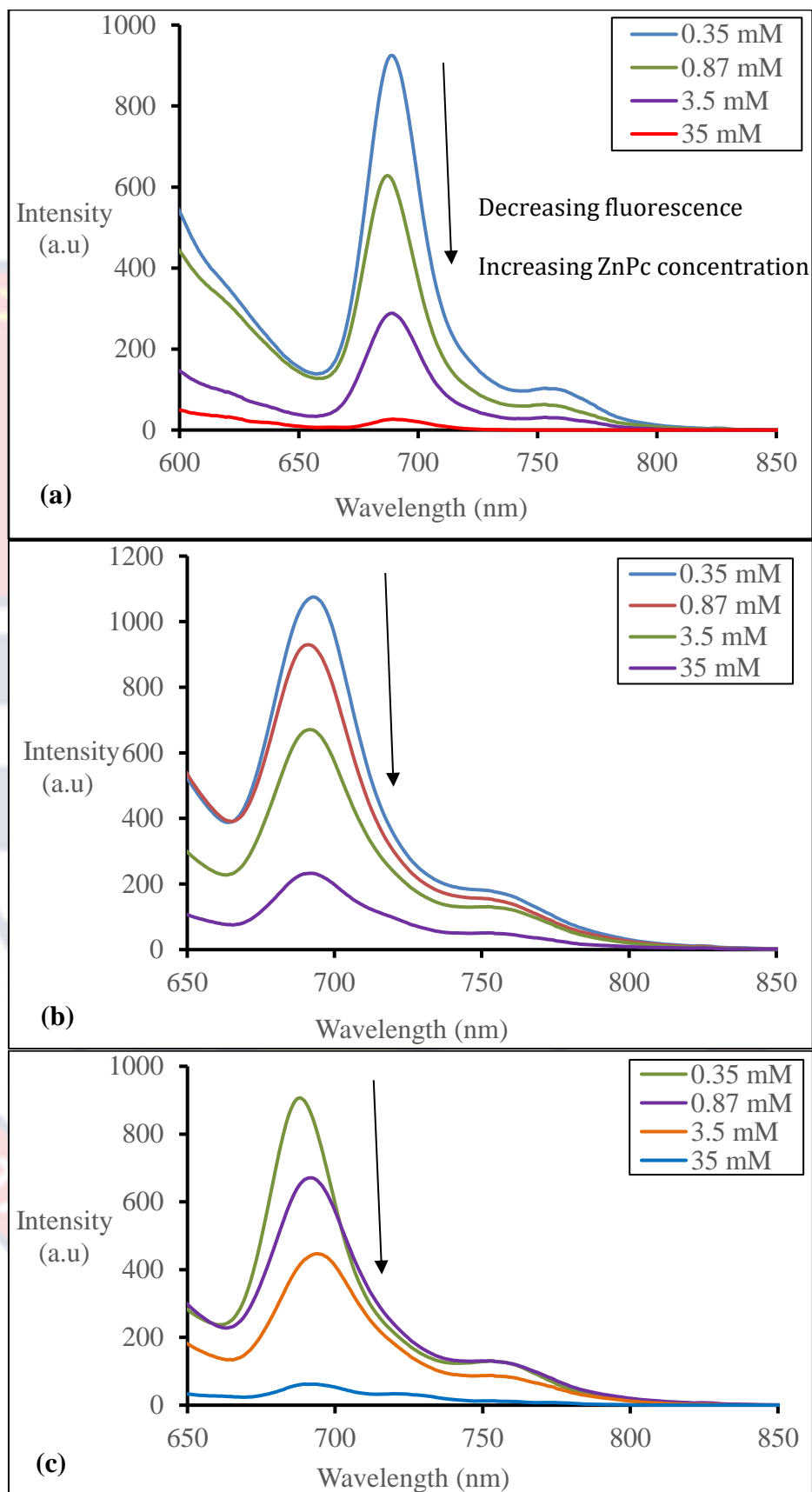
Figure 31: Emission spectra of the functionalised fibres (a) ZnPc-GB; (b) ZnPc-OPMF and (c) ZnPc-PLF at various concentrations (0.35–35 mM).

Infra-Red Spectral Analysis of the Unrefined and Bleached Cellulose-Based Fibres

The infra-red spectra of the unrefined and bleached/refined cellulose-based fibres were determined to identify the type of functional groups present in them. Also, to confirm whether pure cellulose was successfully extracted from the unrefined oil palm mesocarp fibres and the fresh pineapple leaves.

Figure 32 shows the FT-IR spectra of unrefined, bleached, and reference fibres. Bleaching unrefined fibres has been reported to produce high-quality cellulose fibres (Jabber *et al.*, 2017). The broad peaks between 3278 - 3336 cm^{-1} in all the fibres are attributed to the presence of hydroxyl groups (O-H). In figure 32a, the two peaks at 2919 cm^{-1} and 2851 cm^{-1} which, are attribute to the C–H stretching, present in the unrefined Ur-OPMF were reduced to only one peak in the refined B-OPMF at 2915 cm^{-1}, and those at 2917 cm^{-1} and 2849 cm^{-1} in the unrefined Ur-PLF (figure 32b) to only one at 2896 cm^{-1} in B-PLF. The extended peaks at 1740 cm^{-1} and 1631 cm^{-1} in Ur-OPMF and those in the Ur-PLF at 1733 cm^{-1} and 1626 cm^{-1} in (Figure 32a & 32b), attributed to the C=O stretching of the acetyl and ester groups in hemicellulose and aromatic lignin components (Megashah *et. al.*, 2018; Nazir *et al.*, 2013), were missing in the refined fibres (P-GB, B-OPMF & B-PLF*)* [Figure 32c and Table 12].

98
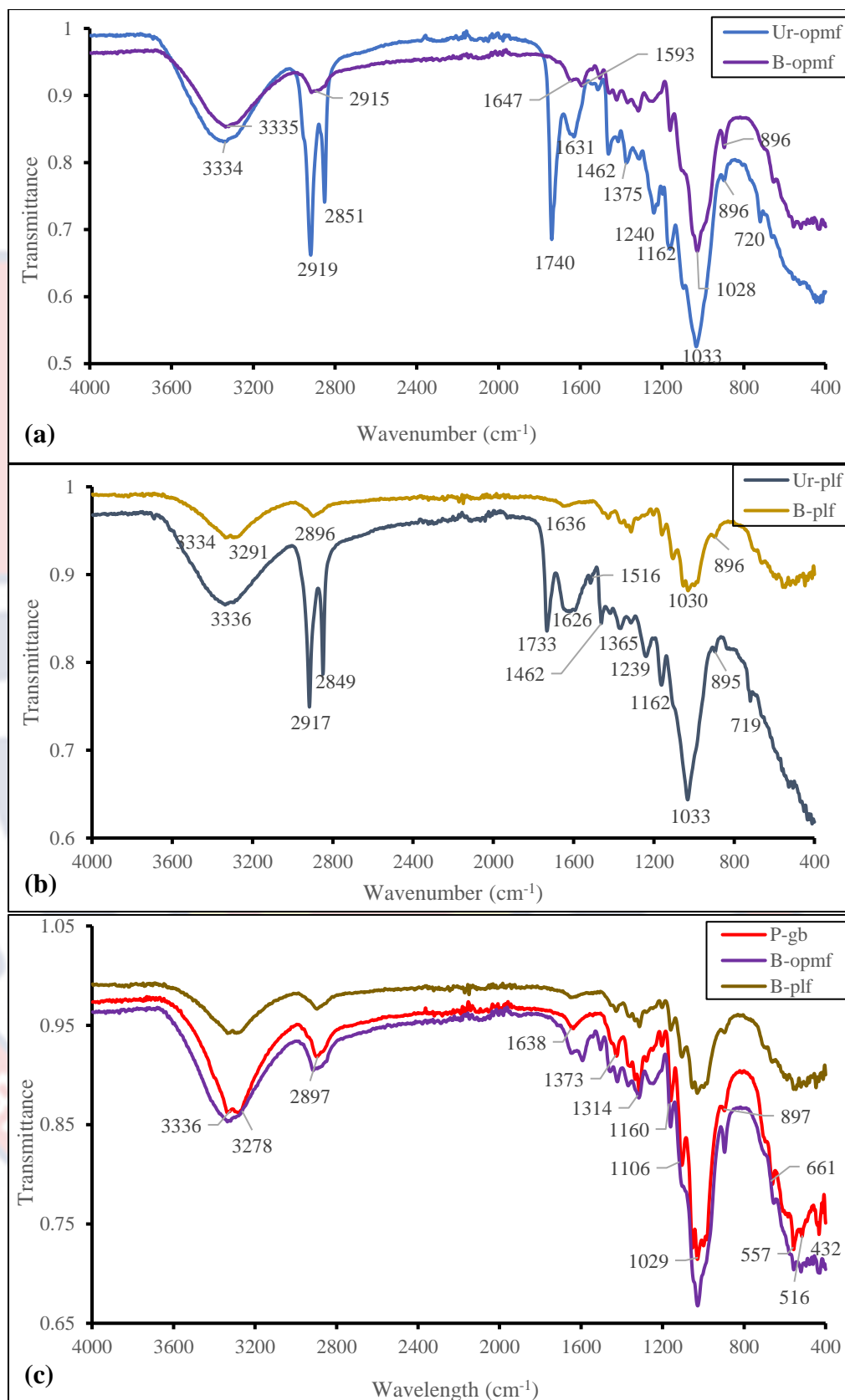
Figure 32: Infra-red spectra of the (a) Unrefined & Bleached oil palm mesocarp fibres (Ur-OPMF & B-OPMF); (b) Unrefined & Bleached pineapple leaf fibres (Ur-PLF & B-PLF) and (c) Bleached/Plain fibres (P-GB, B-OPMF & B-PLF).

99

This confirms the removal of most, if not all of the lignin and hemicellulose from the unrefined fibres, giving rise to pure cellulose fibres. Another evidence of the lignin and hemicellulose removal in the purification process is the decrease in the intensity of the peaks around 1240 cm^{-1} in the Ur-OPMF (Figure 32a) and 1239 cm^{-1} in the Ur-PLF (Figure 32b), attributed to the –COO vibration of acetyl groups in hemicellulose and/or the C–O stretching of the aryl group in lignin (Khenblouche *et al.*, 2019). The peaks around 1626-1647 cm^{-1} in all the fibres are attributed to the O–H bending of the absorbed water, present in the cellulose, hemicellulose and lignin structures (Ismail *et al.*, 2021). The peaks at 895-897 cm^{-1} in all the fibres are attributed to the ß-glycosidic linkage of cellulose and those at 1028-1033 cm^{-1} in all the fibres to the C-O groups of the cellulose. The B-PLF was closer in similarity to the commercial reference P-GB than the B-OPMF. This may be attributed to the fibrous nature of the Ur-OPMF hence, the hemicellulose/lignin may not be removed completely through the bleaching process. This was confirmed and validated by the TGA analysis which, indicated the purity in terms of their thermal stability.

Overall, the FTIR spectra showed that purified cellulose-based fibres (B-OPMF and B-PLF) were successfully isolated from the unrefined fibres (Ur-OPMF and Ur-PLF) and are similar in composition with respect to their functional groups to the commercial reference gauze bandage (P-GB) spectra.

Table 12 presents, transmittance peaks of the cellulose-based fibres and their functional group divisions.

Table 12: Transmittance Peaks of the Cellulose-Based Fibres and their Functional Group Divisions

Ur-OPMF	B-OPMF	Ur-PLF	B-PLF	P-GB	Division
3334	3335	3336	3291/3332	3278/3336	O-H Stretching
2919/2851	2915	2917/2849	2896	2897	C-H Stretching
1740	-	1733	-	-	C=O Bond vibrations of lignin
1631	1647	1626	1636	1638	O-H bending of absorbed water
1512	1593	1516	-	-	C=C Plane symmetric stretching of lignin
1248	-	1239	-	-	C-O-C pyranose ring stretching
1033	1028	1033	1030	1029	C-O group of Cellulose
896	896	895	896	897	C-H out of plane deformation

Source: Gopinathan *et al.,* 2017

*** Ur-OPMF: unrefined oil palm mesocarp fibres; B-OPMF: bleached oil palm mesocarp fibres; Ur-PLF: pineapple leaf fibres; B-PLF: bleached pineapple leaf fibres and P-GB: plain gauze bandage.

Infra-Red Spectral Analysis of the Bleached Cellulose-Based and Functionalised Fibres

The infra-red spectra of the bleached cellulose-based and functional fibre supports were determined to identify the type of functional groups present in them. Also, to confirm whether the zinc phthalocyanine dye was successfully immobilised on the fibre supports. The results are presented in Figure 33.
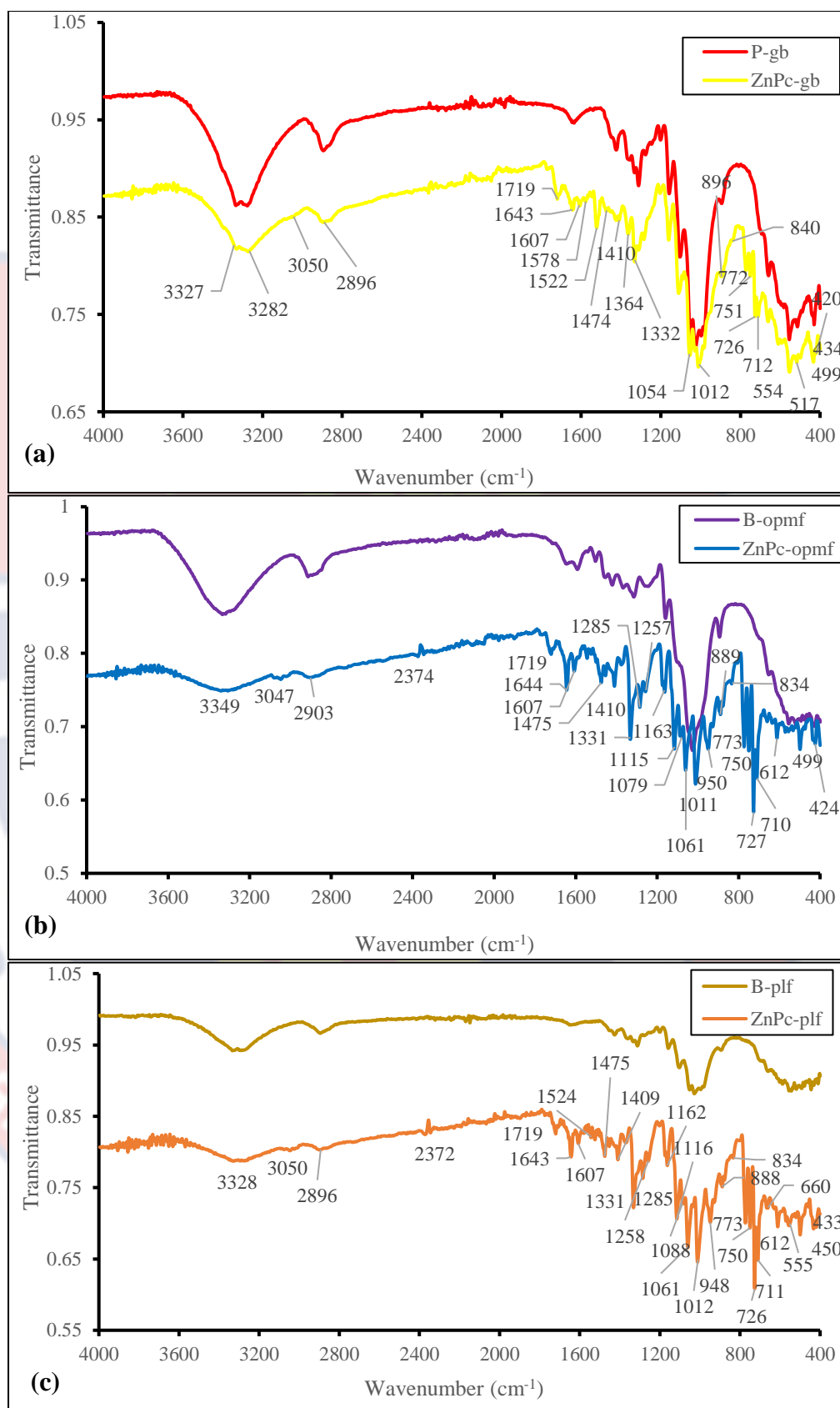
Figure 33: Infra-red spectra of the (a) plain & functionalised gauze bandage fibres (P-GB & ZnPc-GB); (b) bleached & functionalised oil palm mesocarp fibres (B-OPMF & ZnPc-OPMF) and (c) Bleached & functionalised pineapple leaf fibres (B-PLF & ZnPc-PLF).

102

The peaks at 1329, 1164, 1115, 1088, 1062, 1013, 946, 887, 772, 751, 726 and 712 cm^{-1} attributed to the phthalocyanine skeletal vibration (Li *et al.*, 2018) in Figure 34 below, are missing in all the bleached cellulose-based fibres (P-GB, B-OPMF and B-PLF) in Figure 32c but, are present in the functionalised fibres at 1332, 1054, 1012, 772, 751, 726 and 712 cm^{-1} in ZnPc-GB; 1331, 1163, 1115, 1079, 1061, 1011, 960, 889, 773, 750, 727 and 710 cm^{-1} in ZnPc-OPMF and 1331, 1162, 1116,1088, 1061, 1012, 948, 888, 773, 750, 726 and 711 cm^{-1} in ZnPc-PLF respectively (Figure 33 a-c). All these are suggestive that, the zinc phthalocyanine dye was successfully incorporated into the bleached cellulose-based fibre matrices. However, the functionalised fibres (ZnPc-GB, ZnPc-OPMF and ZnPc-PLF) maintained their cellulosic nature as evidenced in the peaks at 3282-3349 cm^{-1}, attributed to the presence of the hydroxyl (O–H) group, and those at 2896-2908 cm^{-1} to the C–H stretching.
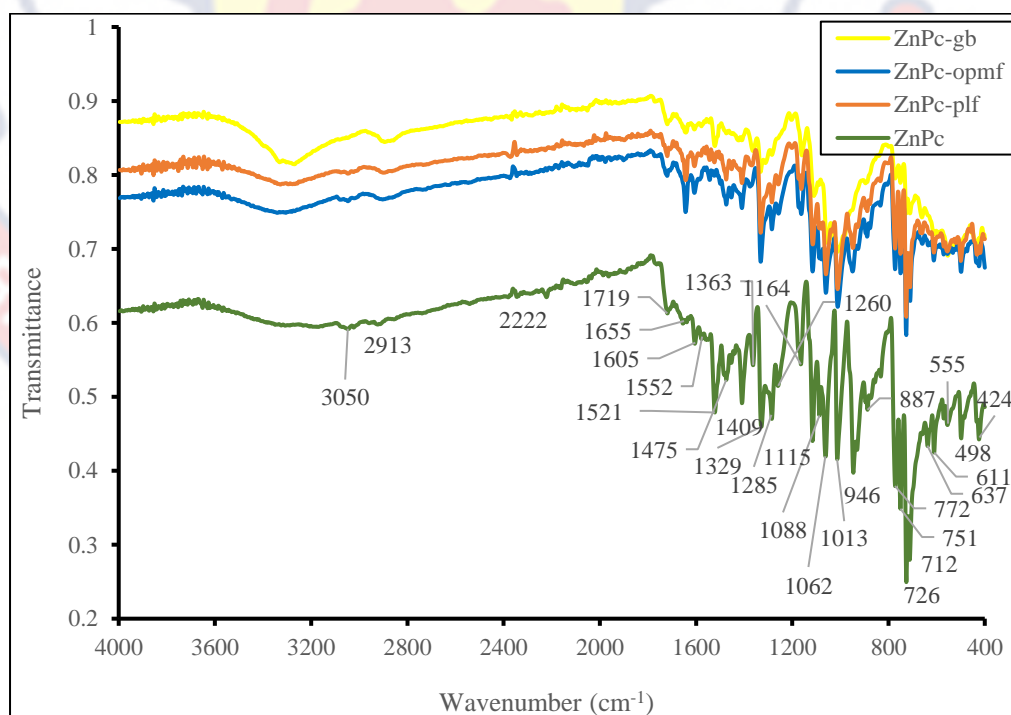
Figure 34: Infra-red spectra of the Synthesised ZnPc with the functionalised cellulose-based fibres (ZnPc-GB, ZnPc-OPMF and ZnPc-PLF).

103

Scanning Electron Microscopic Analysis of the Cellulose-Based and Functionalise Fibres

The fibres were coated with gold before they were observed under the Phenox ProX desktop Scanning Electron Microscope, because of their non-conducting nature. The fibre diameters and morphologies of the bleached cellulose-based fibres and those functionalised with Zinc phthalocyanine are presented in Figures 35 and 36 respectively.

104

(a)   (b)   (c)

(d)   (e)   (f)

(g)   (h)   (i)
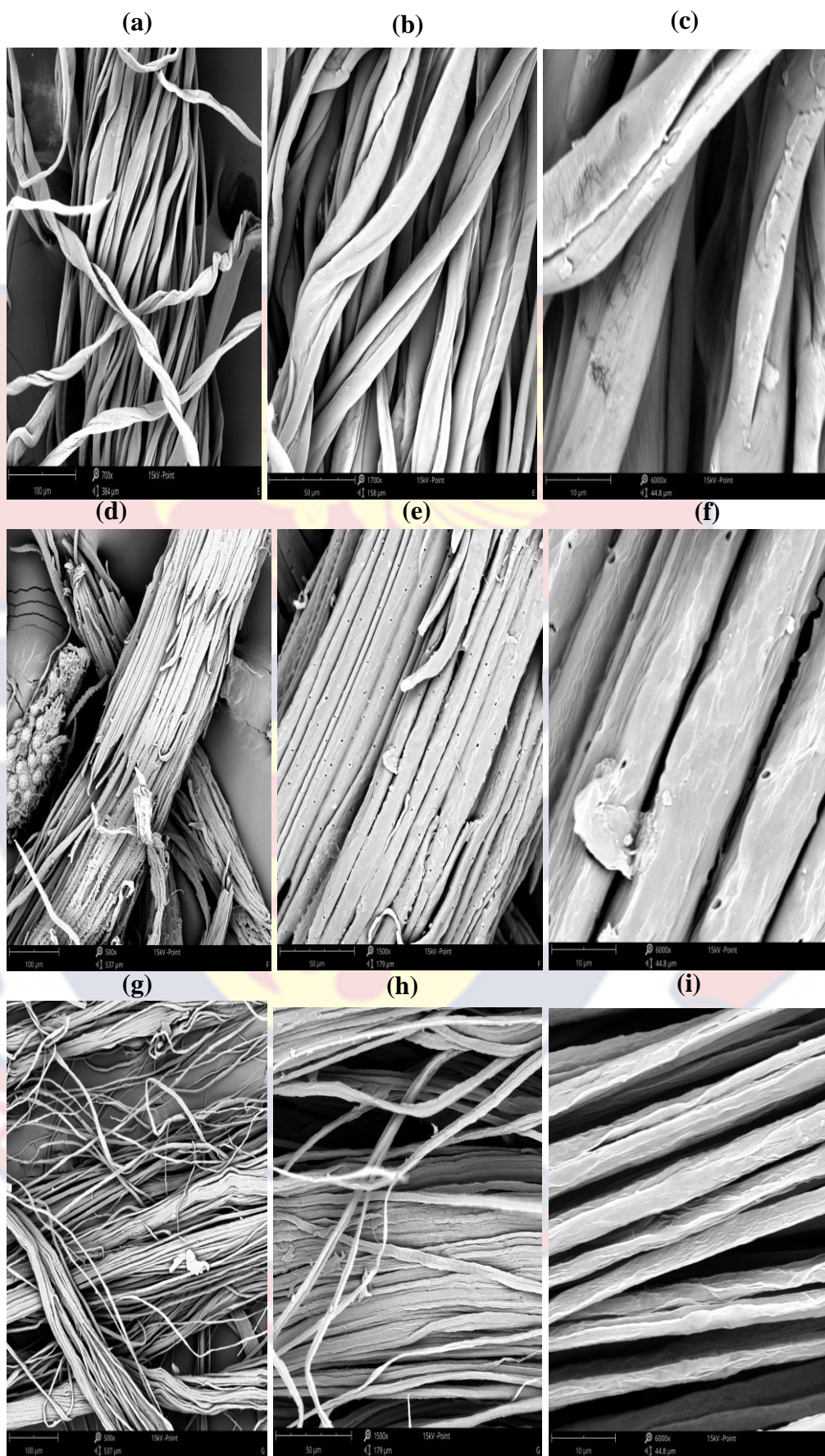
Figure 35: SEM images of the bleached cellulose-based fibres P-GB (a-c); B-OPMF (d-f) and B-PLF (g-i).

105

The SEM images of the bleached fibres at different magnifications clearly revealed the removal of pectin, lignin, and hemicellulose particles from the surfaces of the B-OPMF and B-PLF, giving out cleaner and smoother surfaces. The fibres were porous in nature. The P-GB and B-PLF fibres appeared similar in morphology and consist of mostly long cylindrical individual strands, which are separated from each other whilst, those of the B-OPMF are short and still stacked together (Figure 35). The surface of the B-OPMF consists of pores of similar shapes and sizes and some patches. The patches might be residues from some of the lignin and hemicelluloses, which may not be completely removed during the bleaching and purification processes, due to the fibrous nature of the oil palm mesocarp fibres (OPMF). This was corroborated by the FTIR and TGA results. The diameters of the individual strands (micro-sized) within the cellulose-based fibres when measured (not shown) ranged between 9.45-16.8 μm for P-GB; 3.31-11.5 μm for B-OPMF and 2.75-5.5 μm for B-PLF.

The surface morphologies of the cellulose-based fibres functionalised with the zinc phthalocyanine were also assessed to verify the success of the immobilisation process. The results are presented in Figure 36.
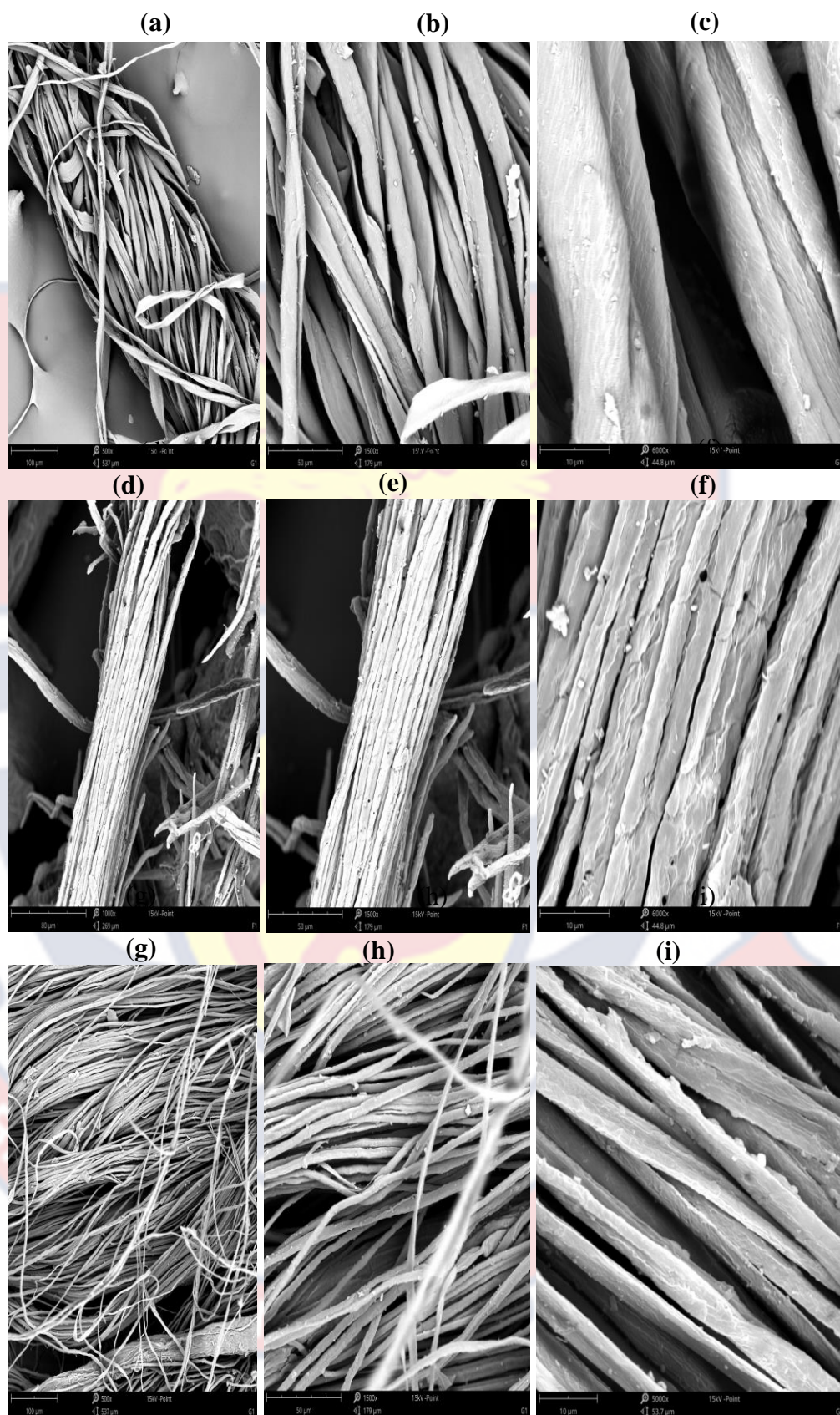
Figure 36: SEM images of the functionalised cellulose-based fibres ZnPc -GB (a-c); ZnPc-OPMF (d-f) and ZnPc -PLF (g-i).

107

The SEM images show the presence of zinc phthalocyanine particles dispersed over the surfaces of all the functionalised fibres (ZnPc-GB, ZnPc-OPMF and ZnPc-PLF). This visual evidence confirms the successful immobilisation of the Zinc phthalocyanine on the fibre surfaces. The diameters of the individual strands (micro-sized) within the functionalised cellulose-based fibres when measured (not shown) ranged between 9.72-18.3 µm for ZnPc-GB, 6.57-13.9 µm for ZnPc-OPMF and 3.08-6.41 µm for ZnPc-PLF. The increase in the diameters of the functionalised cellulose-based fibres compared to their bleached counterparts, may be due to the immobilised zinc phthalocyanine particles deposited within/on them.

Energy-Dispersive X-Ray Spectroscopy (EDS) Analysis of the Cellulose-Based and Functionalise Fibres

Energy-dispersive X-ray spectroscopy (EDS) analysis was conducted to verify the elemental composition of the cellulose-based fibres and to confirm the elemental identity of the particulates on the surfaces of the functionalised fibres, observed in the SEM micrographs. The results are presented in Figure 37.
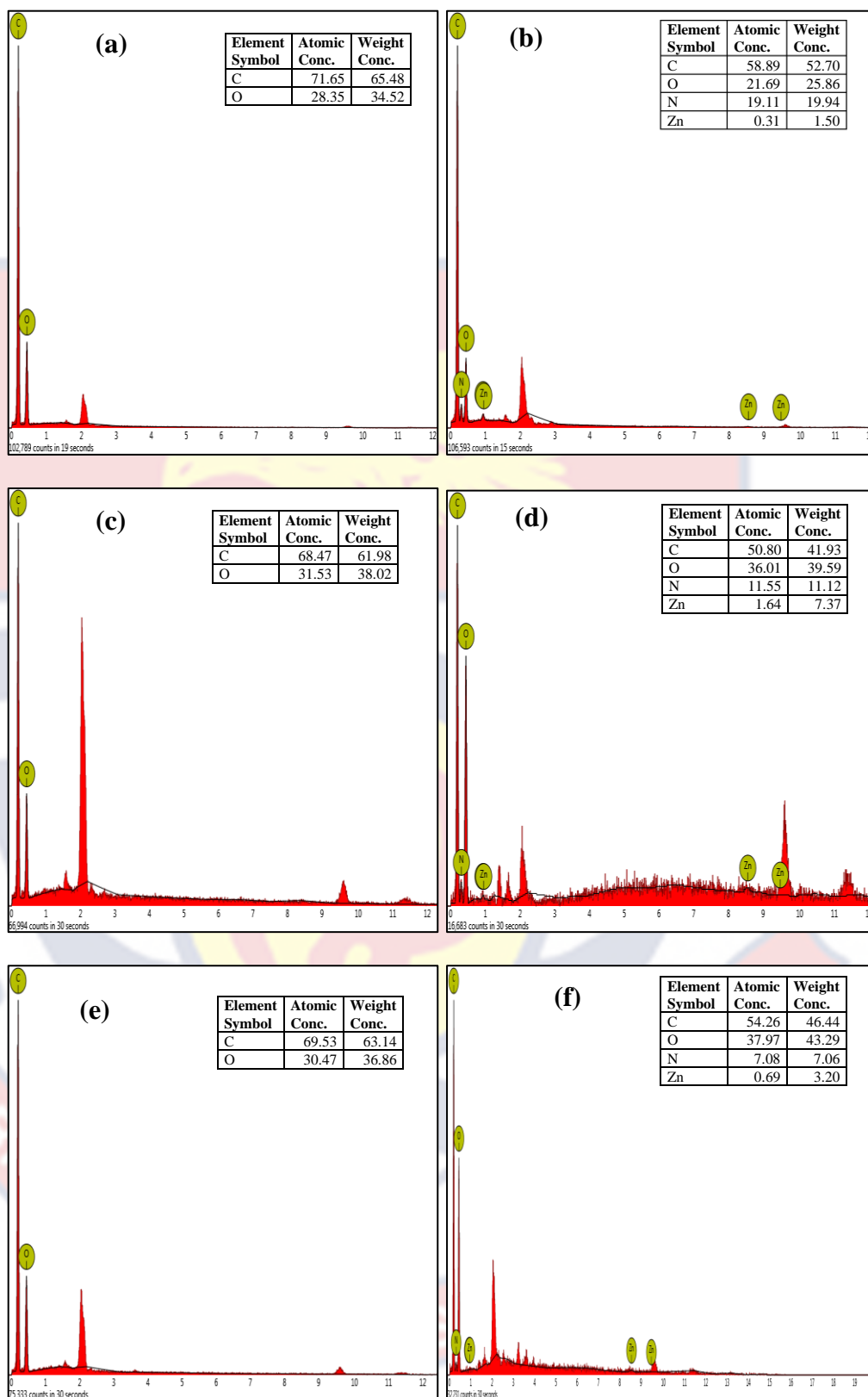
Figure 37: EDS spectra of (a) B-GB, (b) ZnPc-GB, (c) B-OPMF, (d) ZnPc-OPMF, (e) B-PLF and (f) ZnPc-PLF.

109

The reference commercial gauze bandage (P-GB) contains mainly of C and O. The B-OPMF and B-PLF also exhibited the characteristic peaks of C and O, which confirmed the success of the bleaching process and the cellulosic nature of the B-OPMF and B-PLF fibres as compared to the reference commercial gauze bandage (P-GB). However, in the functionalised fibres (ZnPc-GB, ZnPc-OPMF and ZnPc-PLF), two additional peaks of N and Zn were observed alongside the C and O peaks. This confirms that, the particles immobilised on the cellulose-based fibres, which were observed in the SEM images (Figure 36) are in-fact zinc phthalocyanine particles.

Thermogravimetric Analyses (TGA) of the Cellulose-Based Fibres

TGA curves of cellulose-based fibres (P-GB, B-OPMF and B-PLF) were measured to determine the thermal events that occurred. Multiple decomposition curves indicate multiple components within the sample structure. Weight loss is caused by non-oxidative degradation of the sample (Abdullah *et al.*, 2016). The temperature was between 0° C. and 800° C., the heating rate in nitrogen atmosphere was 20° C./min, and the purge rate was 100.0 ml/min. The results are presented in Figure 38.

110
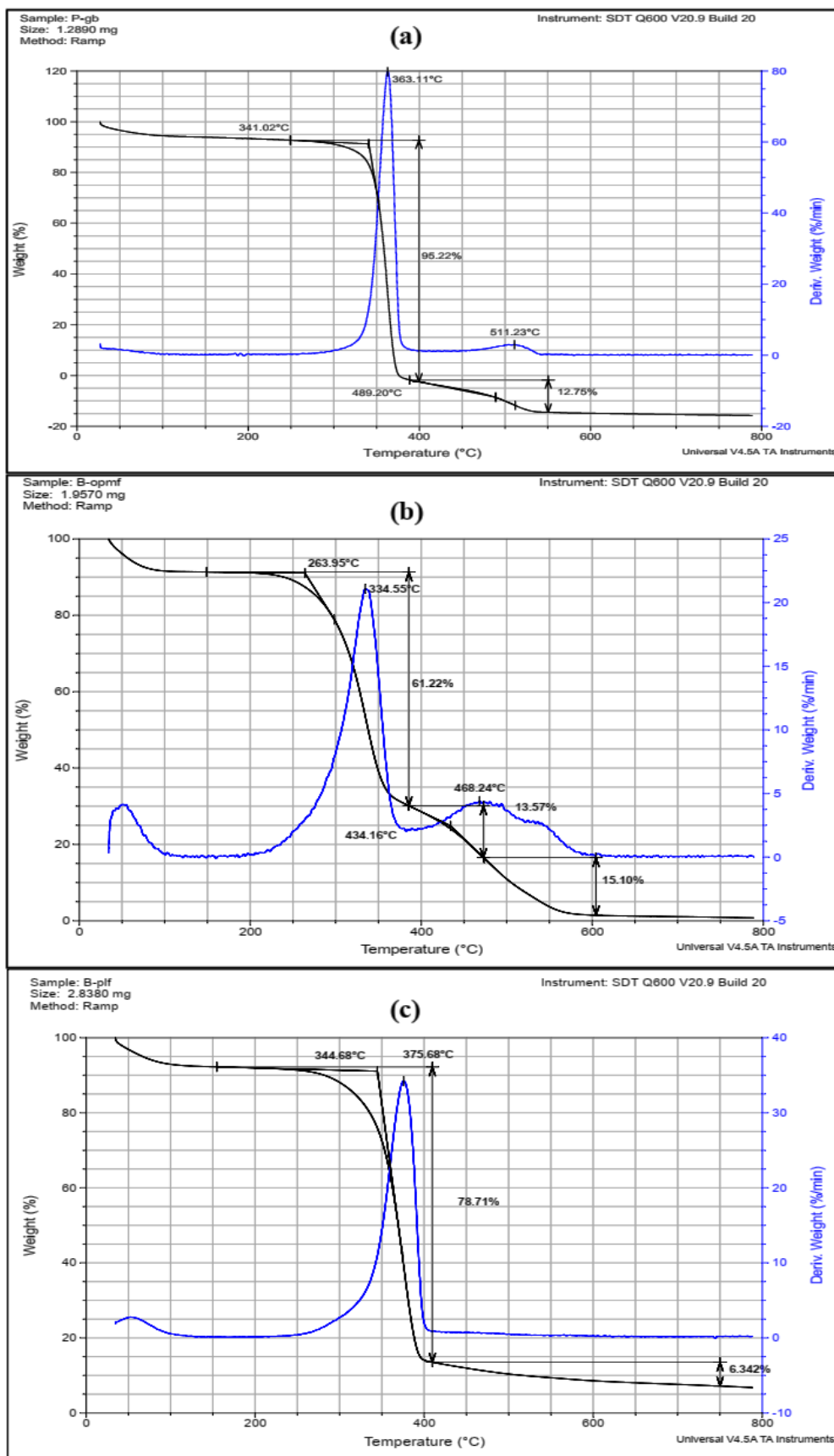
Figure 38: Thermal decomposition curves of the plain cellulose-based fibres (a) P-GB; (b) B-OPMF and (c) B-PLF showing weight losses.

111

All the plain cellulose-based fibres (P-GB, B-OPMF and B-PLF) showed degradation of their components upon heating (Figure 38). The initial reduction in weight in all the cellulose-based fibres from 50-100 ºC, may be as a result of the samples drying up due, to the evaporation of absorbed water and other volatile compounds within the cellulose-based fibres (Ismail *et al.*, 2021). The presence of the absorbed water was confirmed in the FT-IR results. P-GB and B-OPMF displayed two distinct thermal events, around 350-400 ºC and 400-600 ºC for P-GB and 350-400 ºC and 400-600 ºC for B-OPMF whereas, B-PLF displayed only one at around 300-400 ºC (Figure 38 and Table 13 below). This implies that the three thermal events displayed by the functionalised fibres (ZnPc-GB, ZnPc-OPMF and ZnPc-PLF) in Figure 39 below, may result from the Zinc phthalocyanine within their metrices. All three fibres experienced significant weight loss in the 250–400 C region because, the hemicellulose and glycosidic bonds of the cellulose were depolymerised and broken (Mahardika *et al.*, 2018). The maximum weight degradation in P-GB, occurred at 363.11 ºC, with a 95.22 % weight loss from 350-400 ºC; in B-OPMF at 334.55 ºC with a 61.22 % weight loss from 250-400 ºC and in B-PLF at 357.83 ºC with a 78.71 % weight loss from 250-400 ºC (Figure 38 and Table 13) which, corresponds to cellulose decomposition. This is consistent with literature (Said *et al.*, 2021). The residue remaining after heating the fibres to 800°C for all samples indicates the presence of carbon material in the fibres (Chieng *et al.*, 2017). The two intense peaks displayed by B-OPMF, one at 334.55 °C corresponds to the dehydration, decarboxylation, depolymerization and degradation of glycosyl units of cellulose (Ismail *et al.*, 2021) and the other at 468.24 °C corresponds to the

112

degradation of lignin, in addition to its simultaneous degradation with other degradation steps due to its complex structure (Khenblouche *et al.*, 2019). The lower starting temperature of B-OPMF may be a result of the presence of hemicellulose and lignin (He *et al.*, 2014) which, could not be completely removed in the extraction and bleaching processes, due to its fibrous nature. These results are in agreement with the results of the FTIR. B-PLF exhibited, only a single peak at 375.68 °C, which corresponds to dehydration, decarboxylation, depolymerization and degradation of cellulose glycosyl units (Ismail *et al.*, 2021). This indicates a high purity of the extracted B-PLF, which would have otherwise produced different phases if impurities were present. The degradation stages attributed to hemicelluloses (> 180 °C) and lignin (> 390 °C) [Nazir *et al.*, 2013] were absent in the B-PLF. The high weight loss with linearity of the thermal curve from 345-376 °C is comparable to that of the commercial P-GB (341-363 °C). The thermal stability of B-PLF (376 °C) was also superior to commercial P-GB (363 °C) and B-OPMF (335 °C). This may be due to the high crystallinity of the cellulose (Ismail *et al.*, 2021) in B-PLF, due to the complete removal of hemicellulose and lignin components during extraction, which results in better quality of cellulose as compared to the commercial P-GB. These findings, therefore, are in consolidation with the FTIR results.

Table 13, gives the onset temperatures (T_{onset}), lnflection temperatures (T_{max}) and weight percent (%) losses of the plain cellulose-based fibres.

Table 13: Onset Temperatures (T_{onset}), Inflection Temperatures (T_{max}) and Weight Percent (%) Losses of the Plain Cellulose-Based Fibres

Sample	T_{onset} (^oC)	T_{max} (^oC)	Wt. loss percent (%)
P-GB	341.02	363.11	95.22
	489.20	511.23	12.75
B-OPMF	263.95	334.55	61.22
	434.16	468.24	13.57
B-PLF	344.68	375.68	78.71

Source: Laboratory Analysis (2016-2021)

Thermogravimetric Analyses (TGA) of the Functionalised Fibres

The TGA curves of zinc phthalocyanine-functionalised cellulose-based fibres (ZnPc-GB, ZnPc-OPMF, and ZnPc-PLF) were measured to determine the thermal events generated and their suitability for use in photocatalysis and antimicrobial photodynamic therapy (APDT) applications. Multiple decomposition curves indicate multiple components within the sample structure. Weight loss is caused by non-oxidative degradation of the sample (Abdullah *et al.*, 2016). The temperature was between 0° C. and 800° C., the heating rate in nitrogen atmosphere was 20° C./min, and the purge rate was 100.0 ml/min. The results are presented in Figure 39.
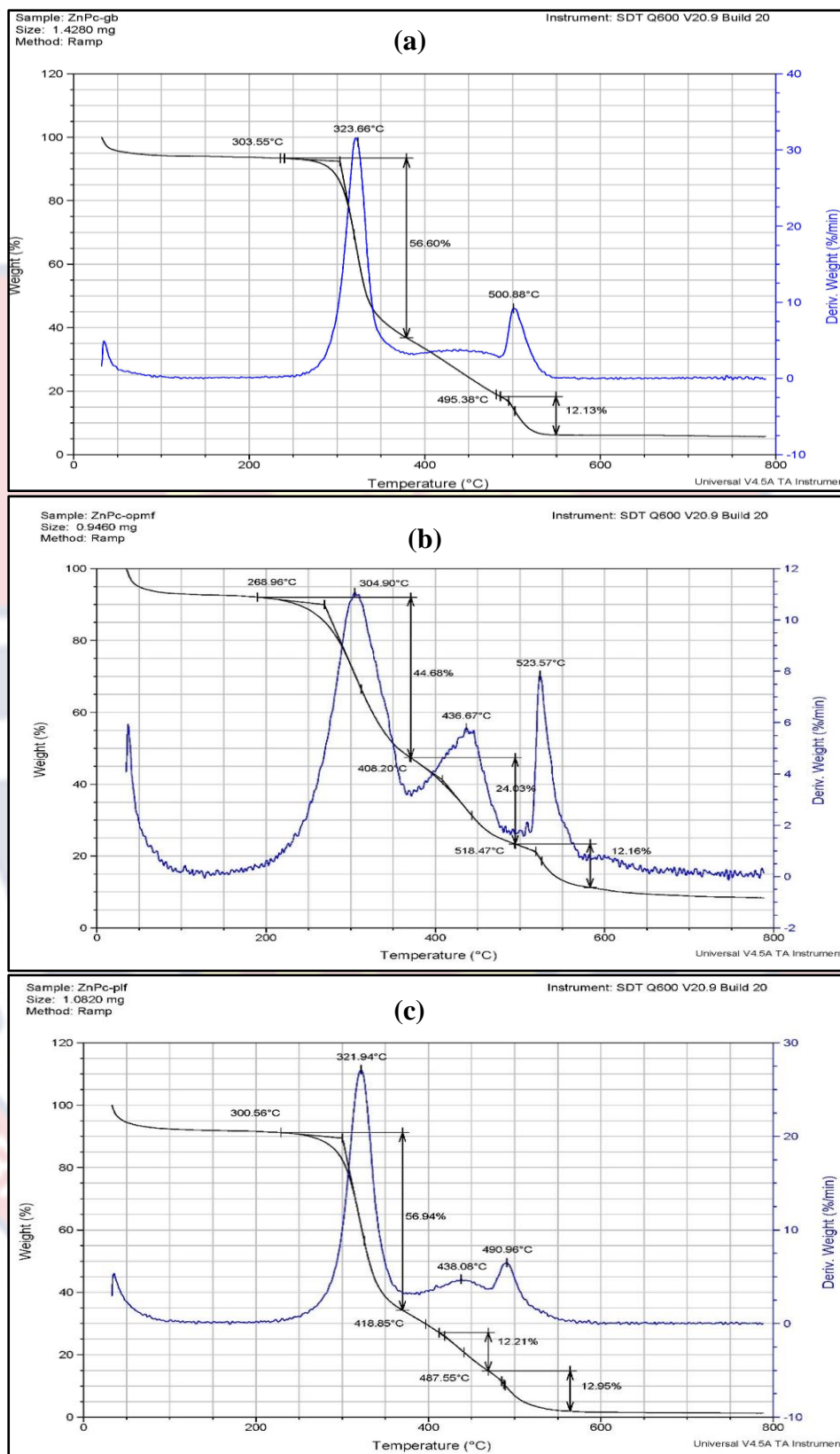
Figure 39: Thermal decomposition curves of the functionalised fibres (a) ZnPc-GB, (b) ZnPc-OPMF and (c) ZnPc-PLF showing weight loss changings.

115

All the functionalised fibres (ZnPc-GB, ZnPc-OPMF and ZnPc-PLF) exhibited various decomposition stages as they were heated. The initial temperature loss around 50-100 °C in all the functionalised fibres may be due to the evaporation of solvents used in the synthesis and/or other volatile impurities. Both (ZnPc-OPMF and ZnPc-PLF) displayed three distinct thermal decomposition events around 300 °C, 400 °C and 500 °C whilst, ZnPc-GB displayed only two around 300 °C and 400 °C. ZnPc-GB and ZnPc-PLF presented thermal stability up to 300 °C after which, they started decomposing whilst, ZnPc-OPMF was stable to about 268.96 °C after which, it started to decompose (Figure 39 and Table 14 below). As a result of the high thermal stability of the phthalocyanine core, cleavage of the substituent takes place first and then the main decomposition occurs above 400°C (Wöhrle & Schulte, 1985; Yurtseven *et al.*, 2014). For the first thermal event, the maximum weight degradation in ZnPc-GB occurred at 323.66 °C with a 56.60 % weight loss from 300-400 °C; in ZnPc-OPMF at 304.90 °C, with a 44.68 % weight loss from 268-400 °C and in ZnPc-PLF at 321.94 °C with a 56.94 % weight loss from 300-400 °C (Figure 39 and Table 14). These weight losses coincide with those of the pure cellulose-based fibres (Figure 38 and Table 13) hence, in light of the former information, it can be said that, for this stage, it is the cellulose-based fibres (and not the embedded zinc phthalocyanine) that are being decomposed. The second thermal event that occurred between 400-500 °C in all the functionalised fibres, coinciding with the main thermal event of the zinc phthalocyanine (Table 14), is that of the zinc phthalocyanine embedded in the fibres that are being decomposed. This implies that, the zinc phthalocyanine dye maintained its thermal property within the functionalised

116

fibres, it is more stable and decomposed at higher temperatures when immobilised on the cellulose-based fibre supports. Table 14 presents, the onset temperatures (T_{onset}), inflection temperatures ($_{max}$) and weight percent (%) losses of the functionalised fibres.

Table 14: Onset Temperatures (T_{onset}), Inflection Temperatures (T_{max}) and Weight Percent (%) Losses of the Functionalised Fibres

Sample	T_{onset} (^{o}C)	T_{max} (^{o}C)	Wt. loss (%)
ZnPc-GB	303.55	323.66	56.60
	495.38	500.88	12.13
ZnPc-OPMF	268.96	304.90	44.68
	408.20	436.67	24.03
	518.47	523.57	12.16
ZnPc-PLF	300.56	321.94	56.94
	418.85	438.08	12.21
	487.55	490.96	12.95
ZnPc	202.25	260.94	4.167
	310.05	341.88	14.90
	401.23	413.41	33.56
	463.86	477.26	9.009
	499.78	526.78	8.625

Source: Laboratory Analysis (2016-2021)

In summary, all the fibres (both plain and functionalised) and zinc phthalocyanine, showed degradation of their components upon heating. Areas of initial weight loss of about 50 °C may be due to evaporation of surface water in the samples, due to drying, while other regions of weight loss may be

due to breakdown of components in the fibres (plain and functionalised) and Zinc phthalocyanine (Morshed, 2021; Wei *et. al.*, 2017). Zinc phthalocyanine and the fibres experienced significant rapid weight losses at temperatures higher than 300 ºC, indicating their high thermal stability, an important requirement for many catalytic applications.

Differential Scanning Calorimetry Analysis of the Cellulose-Based Fibres

Differential scanning calorimetry (DSC) is a thermal analysis technique that measures the temperature difference between a sample and a reference material as a function of temperature while applying a controlled temperature program to both sample and reference material. This technique is used to qualitatively and quantitatively measure temperature changes in exothermic, endothermic and heat capacity reactions (Akash & Rehman, 2020). The differential scanning calorimetry (DSC) curves of the cellulose-based fibres (P-GB, B-OPMF and B-PLF) were measured to determine their melting points (Tm), glass transition temperatures (Tg) and the enthalpies (Cp) of the thermal events. The results are presented in Figure 40.
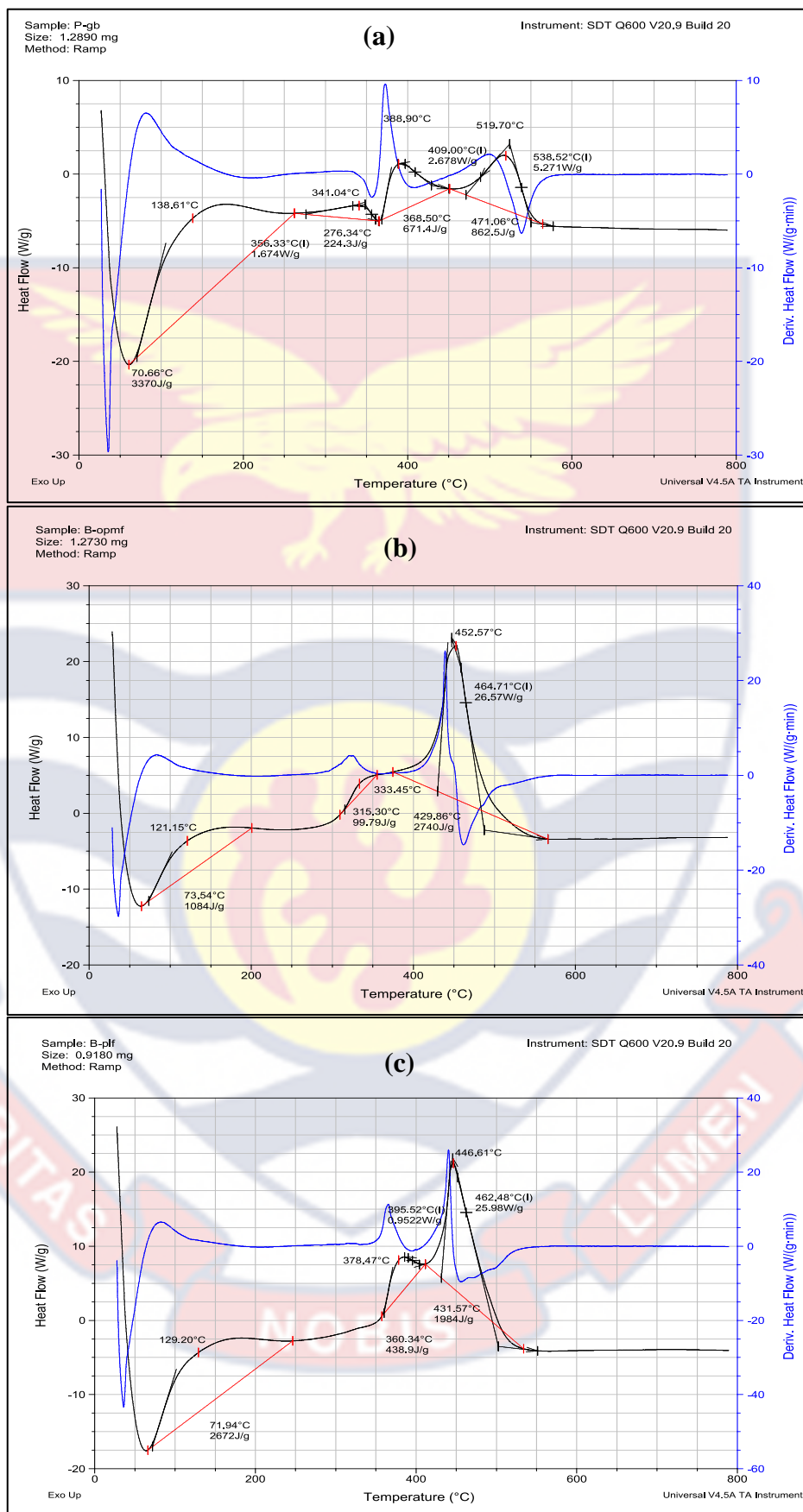
Figure 40: Glass transition temperatures, (Tg) and decomposition enthalpies (Cp) of (a) P-GB (b) B-OPMF and (c) B-PLF.

119

All the cellulose-based fibres were stable at lower temperatures, below 50 °C (Figure 40). A look at the curves shows, there are no melting points rather, they seem to decompose on heating. There were various regions for the increase in the heat given off (exothermic) by the fibres while they were heated. Table 15 shows, the glass transition temperatures, Tg, of P-GB, B-OPMF and B-PLF when heated. The table also gives the temperatures at which P-GB, B-OPMF and B-PLF decompose into different components, the maximum decomposition temperature and the heat absorbed during the thermal process.

Table 15: Glass Transition Temperatures (Tg), the Minimum and Maximum Temperatures (T₁ and T₂) of Decomposition, the Heat Flow (ΔH) and the Heat absorbed (Cₚ) during the Thermal Event of the Cellulose-Based Fibres

Sample	T_g (°C)	ΔH (W/g)	T_1 (°C)	T_2 (°C)	C_p (J/g)
P-GB			70.66	138.61	3,370
	356.33	1.674	276.34	341.54	224.3
	409.00	2.678	368.50	388.90	671.4
	538.52	5.271	471.06	519.70	862.5
B-OPMF			73.54	121.15	1,084
			315.30	333.45	99.8
	464.71	26.57	429.86	452.57	2,740
B-PLF			71.94	129.20	2,672
	395.52	0.9522	360.34	378.47	438.9
	462.48	25.98	431.57	446.61	1,984

Source: Laboratory Analysis (2016-2021)

Differential Scanning Calorimetry Analysis of the Functionalised Fibres

The differential scanning calorimetry (DSC) curves of the functionalised fibres (ZnPc-GB, ZnPc-OPMF and ZnPc-PLF), were measured to determine their melting points (Tm), glass transition temperatures (Tg) and the enthalpies (Cp) of the thermal events. The results are presented in Figure 41.
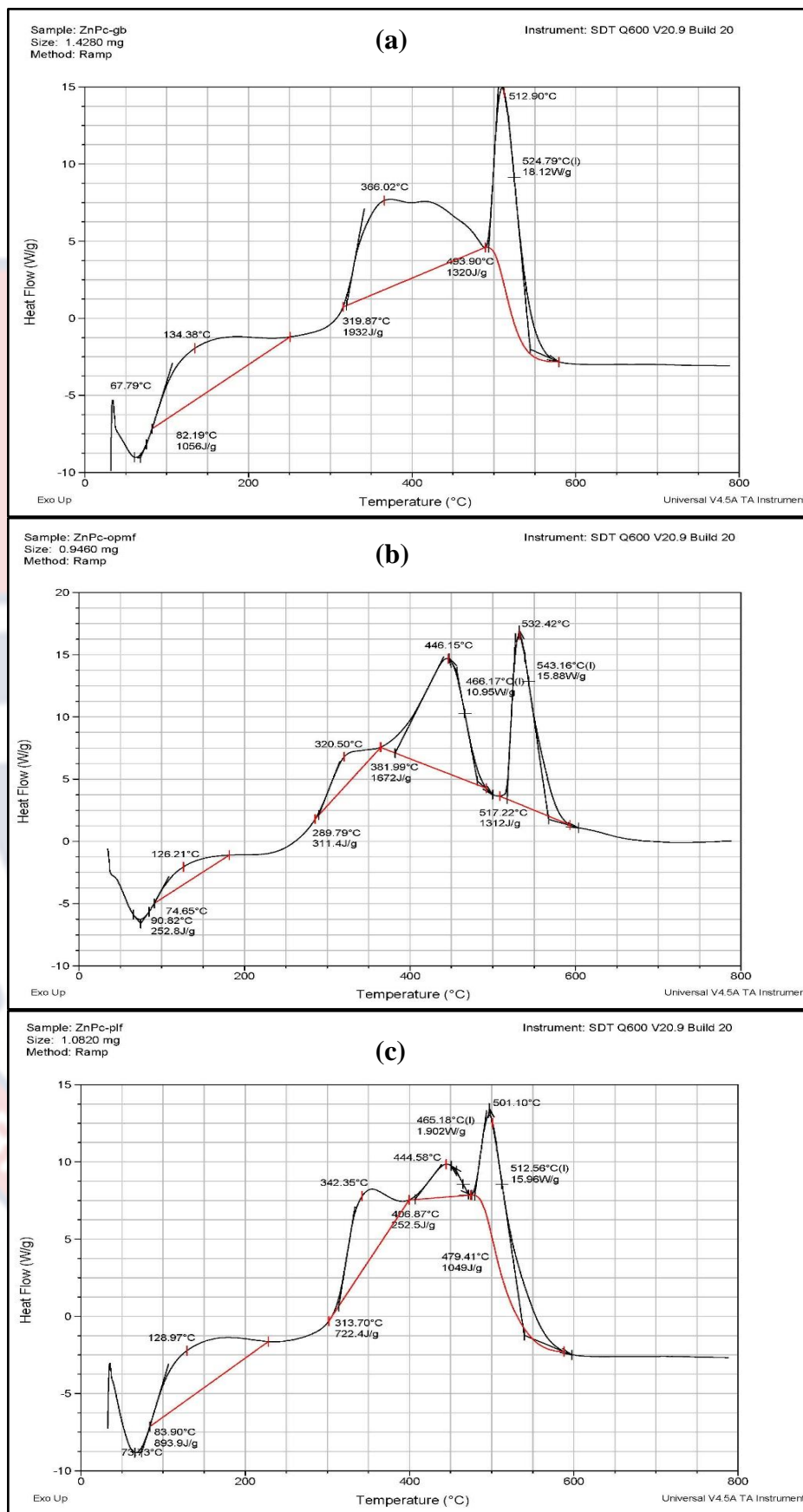
Figure 41: Glass transition temperatures (Tg) and decomposition enthalpies (Cp) of (a) ZnPc-GB, (b) ZnPc-OPMF and (c) ZnPc-PLF.

121

All the functionalised fibres were stable at lower temperatures, below 50 ℃. ZnPc-OPMF and ZnPc-PLF displayed two glass transition temperatures (Tg) at 466.17 ℃ & 543.16 ℃ and 465.18 ℃ & 512.56 ℃ respectively whilst, ZnPc-GB displayed only one at 524.79 ℃. The second glass transition of the zinc phthalocyanine at 532.40 ℃ which, may be the main thermal event is seen in all the functionalised fibres at close temperatures (Table 16). The ZnPc-GB displayed three different decomposition products/stages with a total energy of 4,308 J/g whilst, ZnPc-OPMF and ZnPc-PLF have four with a total energy of 3,548.2 J/g and 2,917.8 J/g respectively (Table 16).

Table 16: Glass Transition Temperatures (Tg), the Minimum and Maximum Temperatures (T$_1$ and T$_2$) of Decomposition, the Heat Flow (ΔH) and the Heat absorbed (C$_p$) during the Thermal Event of the Functionalized Fibres

Sample	Tg (℃)	ΔH (W/g)	T$_1$ (℃)	T$_2$ (℃)	C$_p$ (J/g)
ZnPc-GB	524.79	18.12	82.19	134.38	1056
			319.87	366.02	1932
			493.90	512.90	1320
ZnPc-OPMF	466.17	10.95	90.82	126.21	252.8
	543.16	15.88	289.79	320.50	311.4
			381.99	446.15	1672
			517.22	532.42	1312
ZnPc-PLF	465.18	1.902	83.90	128.97	893.9
	512.56	15.96	313.70	342.35	722.4
			406.87	444.58	252.5
			479.41	501.10	1049
ZnPc	438.60	12.12	81.26	115.19	164.1
	532.40	19.08	400.43	423.91	1860
			463.32	489.16	990.6

Source: Laboratory Analysis (2016-2021)

The lowest onset temperature for the decomposition occurred in the zinc phthalocyanine at 54.54 ℃ (Table 17). Since the functionalised fibres would be used at room temperature, they are suitable and could also, be stored at room temperature.

122

Table 17: Onset Temperature for Initial Decomposition of Material

Sample	Onset Temperature (^{o}C)
ZnPc-GB	67.79
ZnPc-OPMF	74.65
ZnPc-PLF	73.73
ZnPc	54.54

Source: Laboratory Analysis (2016-2021)

Singlet Oxygen Production Capacity of the Functionalised Fibres

The iodometric technique was used to evaluate the singlet oxygen production capacity of the functionalised fibres, since they are intended for use in aqueous media. It is a fast, sensitive, and straightforward spectrophotometric analysis of photosensitiser-generated singlet oxygen ($^{1}O_2$) in weakly acidic or neutral air-saturated aqueous solutions (Mosinger & Mosinger, 1995). This technique is based on the reaction of the generated singlet oxygen ($^{1}O_2$) with iodide ions (I^-). The reaction product, I_2 (Eqn. 4) is believed to be proportional to the amount of singlet oxygen produced in the reaction and is monitored spectrophotometrically around 355 nm (Zugle, 2014). The results are presented in Figures 42 and 43.

$$2I^-_{(aq)} \longrightarrow I_{2\,(aq)} + 2e^- \dots\dots\dots\dots\dots \text{Eqn. 4}$$

123
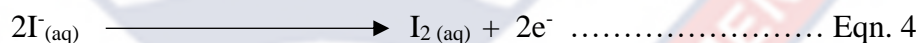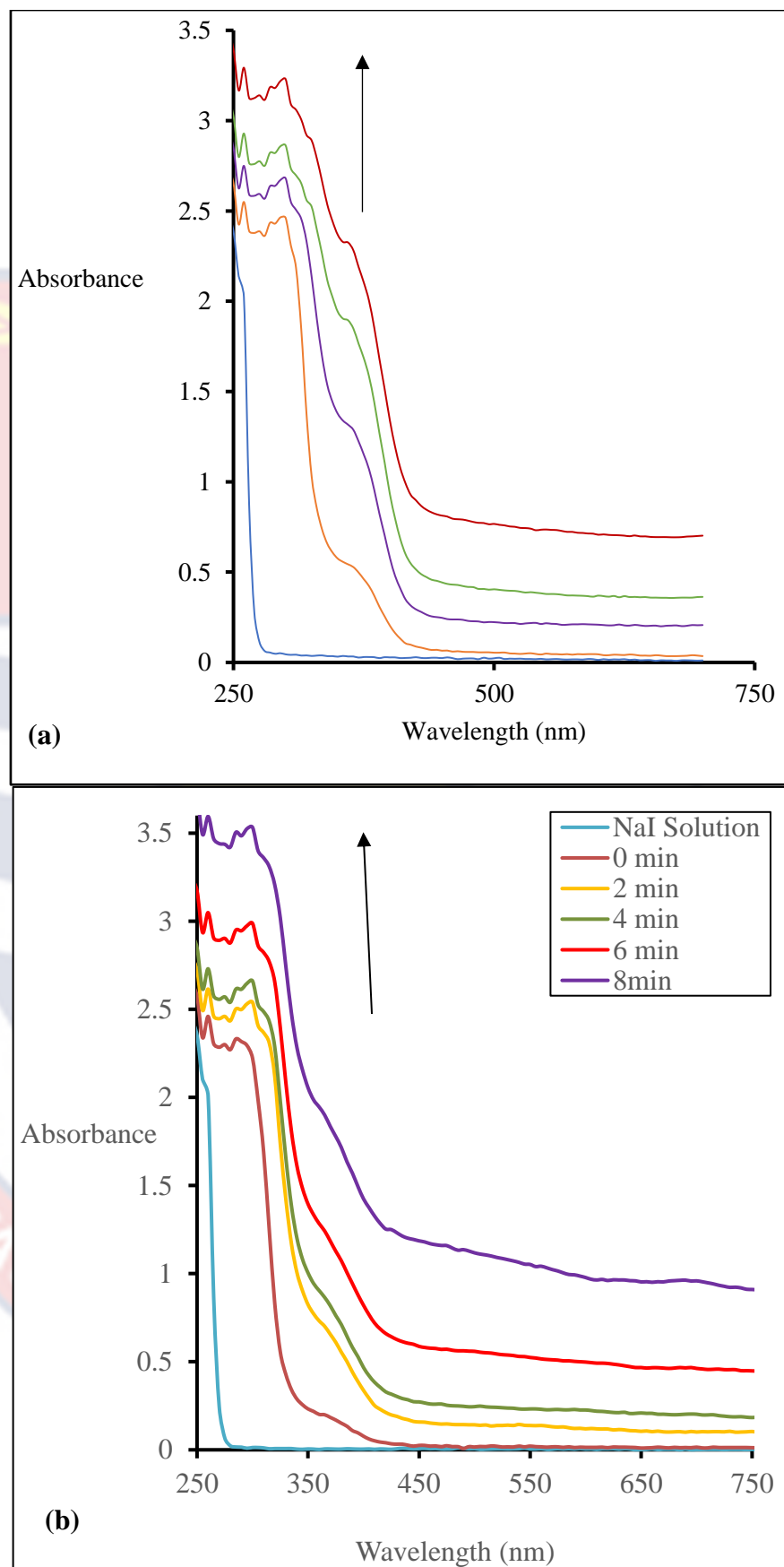
Figure 42: Absorption spectra of 0.1 M NaI solution containing (a) ZnPc-GB and (b) ZnPc-OPMF, upon irradiation with daylight

124
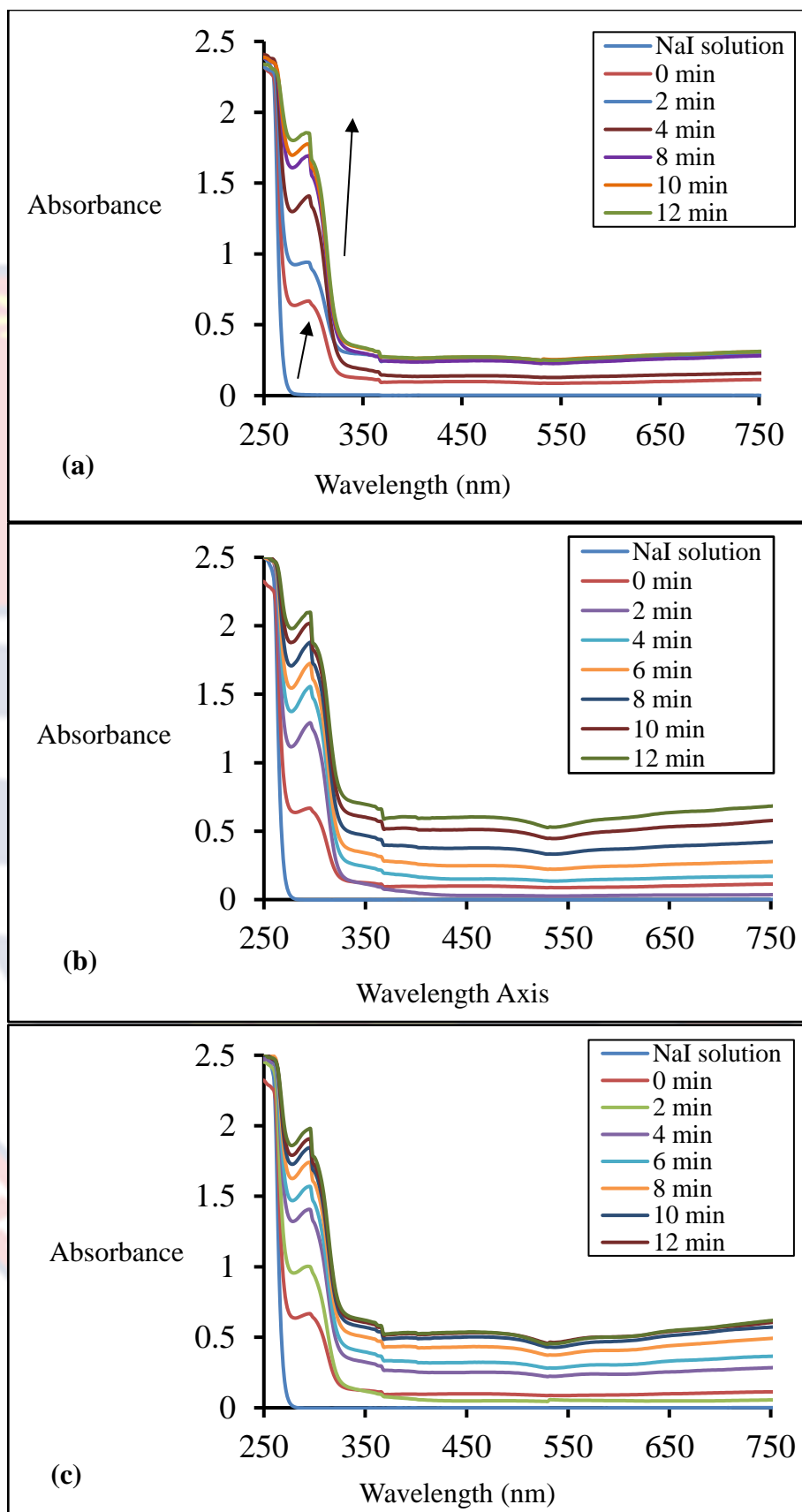
Figure 43: Absorption spectra of 0.1 M NaI solution containing (a) ZnPc-GB, (b) ZnPc-OPMF and (c) ZnPc-PLF upon irradiation with LED redlight

125

Molecular iodine (I_2) was generated from the iodide solution as indicated by the increase in the maximum absorption peak around 300-355 nm (arrow) under both daylight and LED redlight radiations which, parallels the molecular iodine (I_2) produced (Mosinger & Mosinger, 1995). However, no such increase in the absorption peak at 355 nm was observed when the plain gauze bandage (P-GB) was used (not shown).

This suggests that the zinc phthalocyanine dye in the functionalised fibres was, the agent involved in the production of the molecular iodine. This also means that the zinc phthalocyanine molecules are fairly distributed within the functionalised fibre matrices and thus can produce singlet oxygen. The zinc phthalocyanine also did not leach into the solution during the degradation process, as shown by the Q-band (670 nm) region of the sample solution (Figures 42 and 43). This confirmed the binding properties and stability of zinc phthalocyanine dye in the functionalised fibres. It has been reported that phthalocyanines are stacked in the solid state therefore, do not produce singlet oxygen (Zugle, 2014).

Singlet Oxygen Quenching Test

To further verify singlet oxygen production, a singlet oxygen quencher, sodium azide (NaN_3), was introduced into the sample solutions and the same experimental conditions were applied. Figure 44, shows the corresponding UV-visible spectral change.
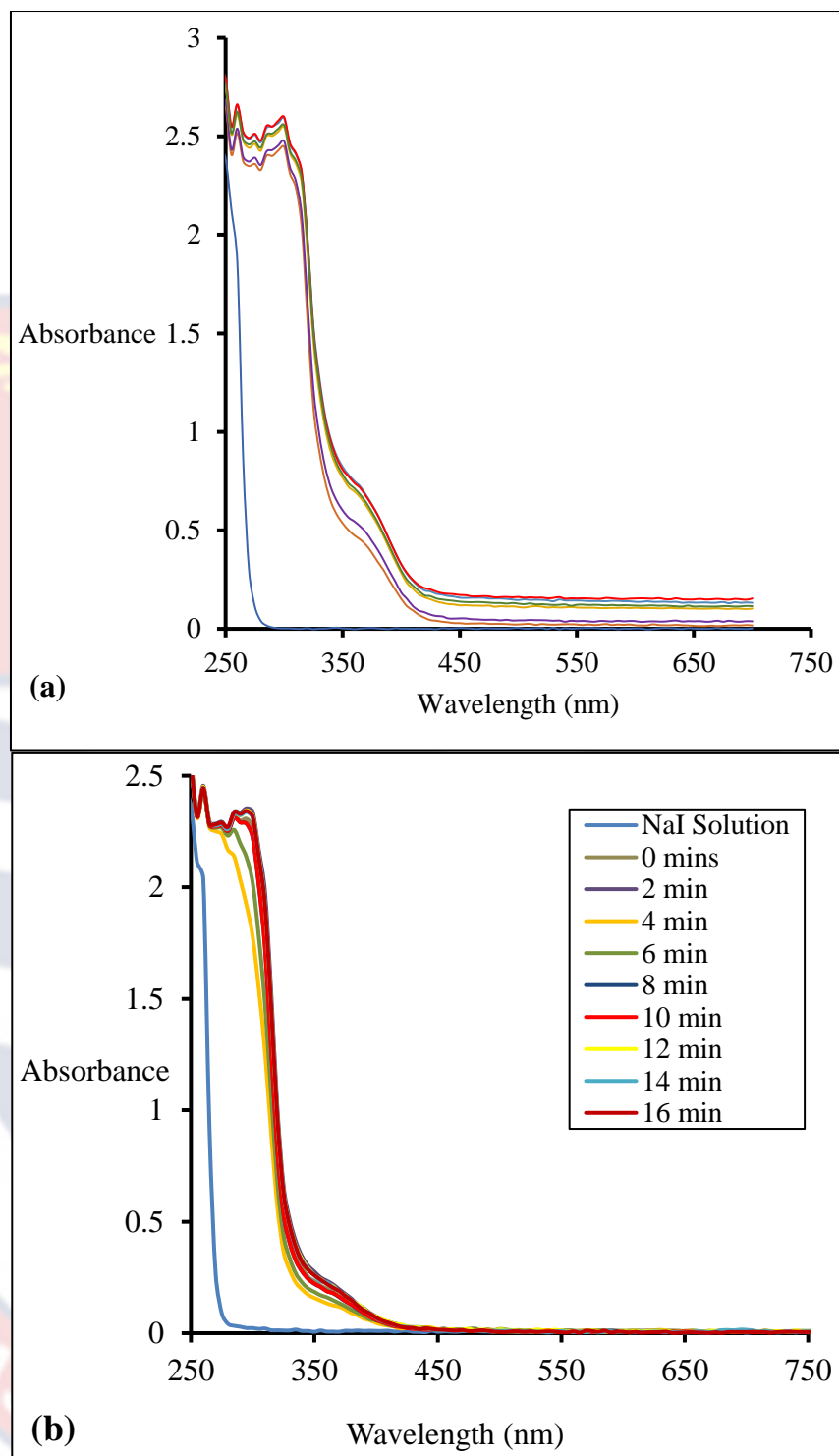
Figure 44: Absorption spectra of 0.1M NaI + 0.1M NaN$_3$ solution containing (a) ZnPc-GB and (b) ZnPc-OPMF upon irradiation with daylight.

There was no significant increase in the molecular iodine production in Figure 44 as compared to that of (Figures 42 and 43), as evidenced by the decrease in the absorption maximum around 300-350 nm (arrow). This

127

indicates that sodium azide (NaN_3) could quench the singlet oxygen generated in the sample solution, leading to its reduction. This confirms that singlet oxygen is the agent that converts the iodide to molecular iodine in the solution.
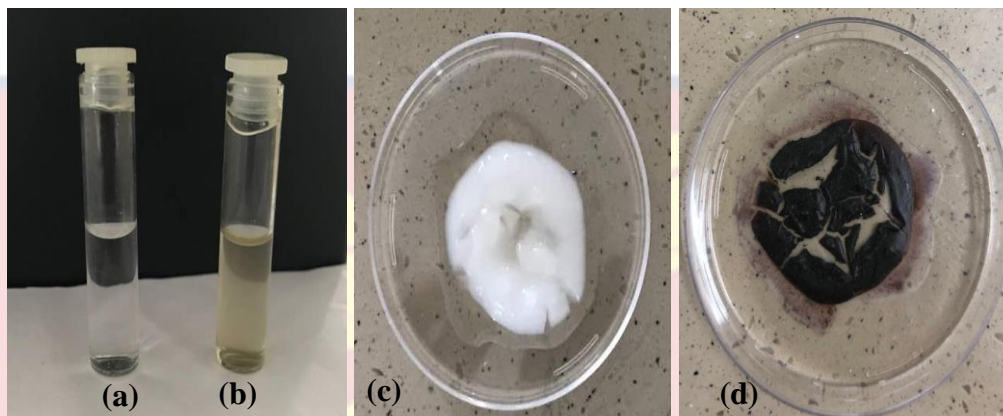
Figure 45: Digital images of (a) 0.1 M NaI aqueous solution, (b) aqueous solution containing iodine after irradiation in the presence of the functionalised fibres, (c) cooked starch and (d) cooked starch in contact with iodine generated.

The actual iodine molecule formation was also investigated by comparing the colour of the sodium iodide solution before and after irradiation. The clear, colourless sodium iodide solution (Figure 45a) turned into a yellow-brown solution (Figure 45b) after irradiation, confirming the formation of molecular iodine.

Molecular iodine production was further determined using the starch test. When the irradiated iodine solution (Figure 45b) was introduced into the cooked starch (Figure 45c), a blue-black colour was formed (Figure 45d), confirming the production of molecular iodine.

Leaching Studies of the Functionalised Fibres

The functionalised fibres are intended for use in real-life applications as topical bandages in PDT and as catalysts for photo-oxidation of contaminants in aqueous environments. Leaching studies were therefore,

128

conducted to find suitable solvents, in which the zinc phthalocyanine dye will not leach into. The functionalised fibres were immersed in various aqueous solutions separately for 24 hours and analysed by UV-Vis spectroscopy. The results are presented in Figure 46.
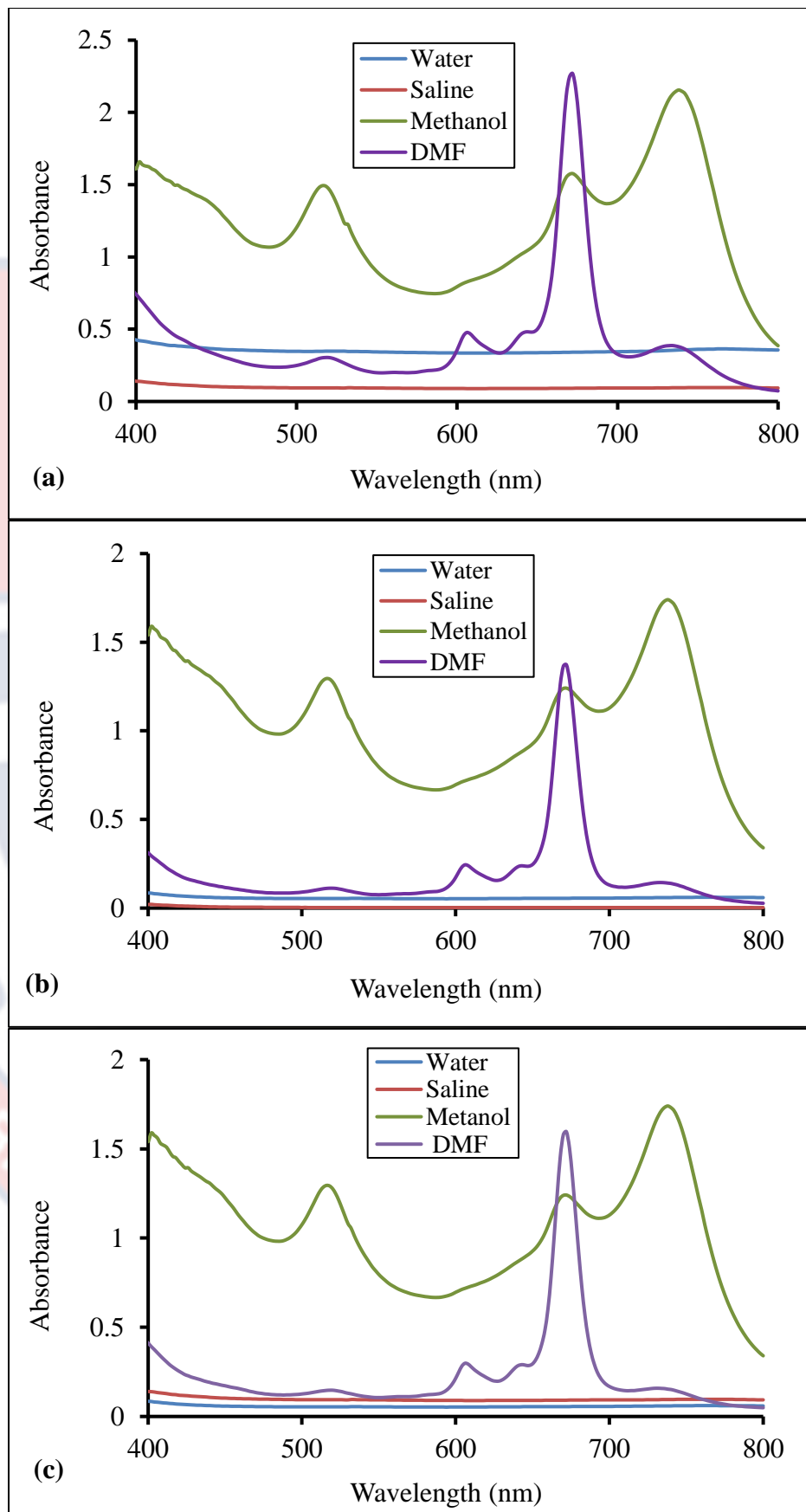
Figure 46: Absorption spectra of (a) ZnPc-GB, (b) ZnPc-OPMF and (c) ZnPc-PLF after 24 hours in water, saline, methanol and briefly in DMF.

There was no leaching of the zinc phthalocyanine dye from the functionalised fibres into the water, saline, and methanol, as the solution UV-vis spectra did not have a Q-band absorption peak corresponding to zinc phthalocyanine (Figure 46). This demonstrates their suitability in practical applications, especially aqueous solutions. However, the dye leached out of the fibres immediately after being introduced into the DMF solution.

Fluorometric Sensing of Nitrogen Dioxide by Zinc Phthalocyanine Solution

Nitrogen dioxide is projected to be a reactive radical hence, may be capable of quenching fluorescence because, it has an unpaired electron (Ishii *et al.*, 2011; Zugle & Nyokong, 2012). Therefore, the functionalised cellulose-based fibres may be promising for fluorescence sensing of $NO_{2(g)}$. Therefore, initial studies were performed by measuring the fluorescence emission of zinc phthalocyanine solution in the presence of $NO_{2(g)}$. NO_2 gas was produced by the reaction of copper metal and dilute nitric acid solution. The zinc phthalocyanine solution was then exposed to the generated NO_2 gas and the fluorescence emission spectra was recorded. The results are presented in Figure 46.
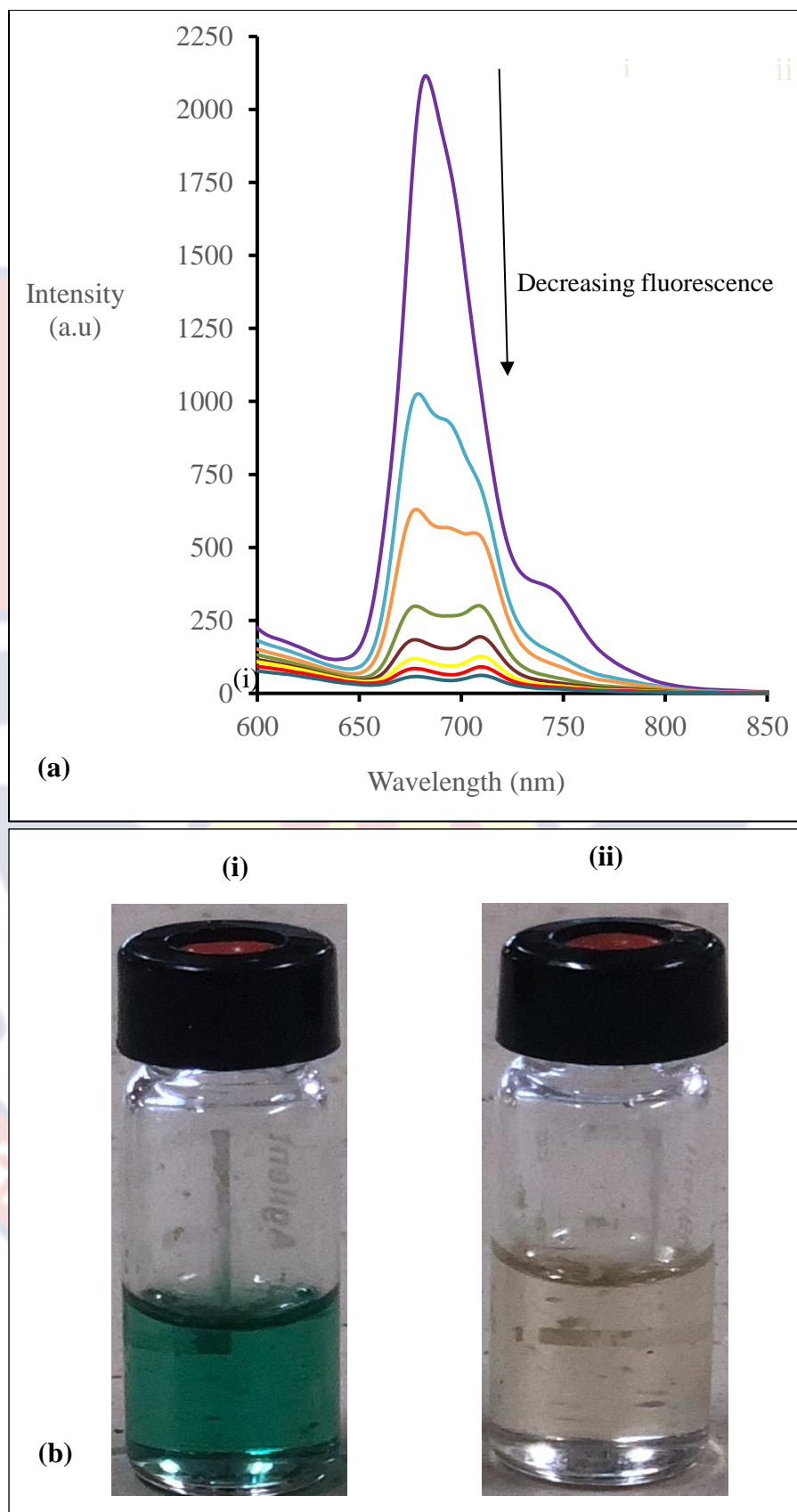
Figure 47: (a)Emission spectra of 95 μM zinc phthalocyanine solution in the presence of $NO_{2(g)}$ and (b) zinc phthalocyanine solution before (i) and after (ii) exposure to $NO_{2(g)}$.

A decrease in zinc phthalocyanine fluorescence emission intensity was observed when the solution was exposed to NO_2 gas for each exposure cycle, which is consistent with literature (Zugle and Nyokong, 2012). A colour change from the characteristic green zinc phthalocyanine solution (Figure 47 bi) to brown solution (Figure 47 bii), after exposure to $NO_2(g)$ confirms the quenching of the fluorescence in the zinc phthalocyanine solution by the NO_2 gas. Although it was impossible to measure the exact amount of NO_2 gas in each exposure, variations in the emission spectra of the solution indicate that, zinc phthalocyanine would be promising for fluorometric sensing of Nitrogen dioxide gas in the environment. Therefore, the cellulose-based fibres, functionalised with the zinc phthalocyanine dye, were used to sense for the gas.

Fluorometric Sensing of Nitrogen Dioxide Gas by the Functionalised Fibres

The functionalised fibres were then exposed to NO_2 gas and their emission spectra, recorded. The results are presented in Figure 48.

133
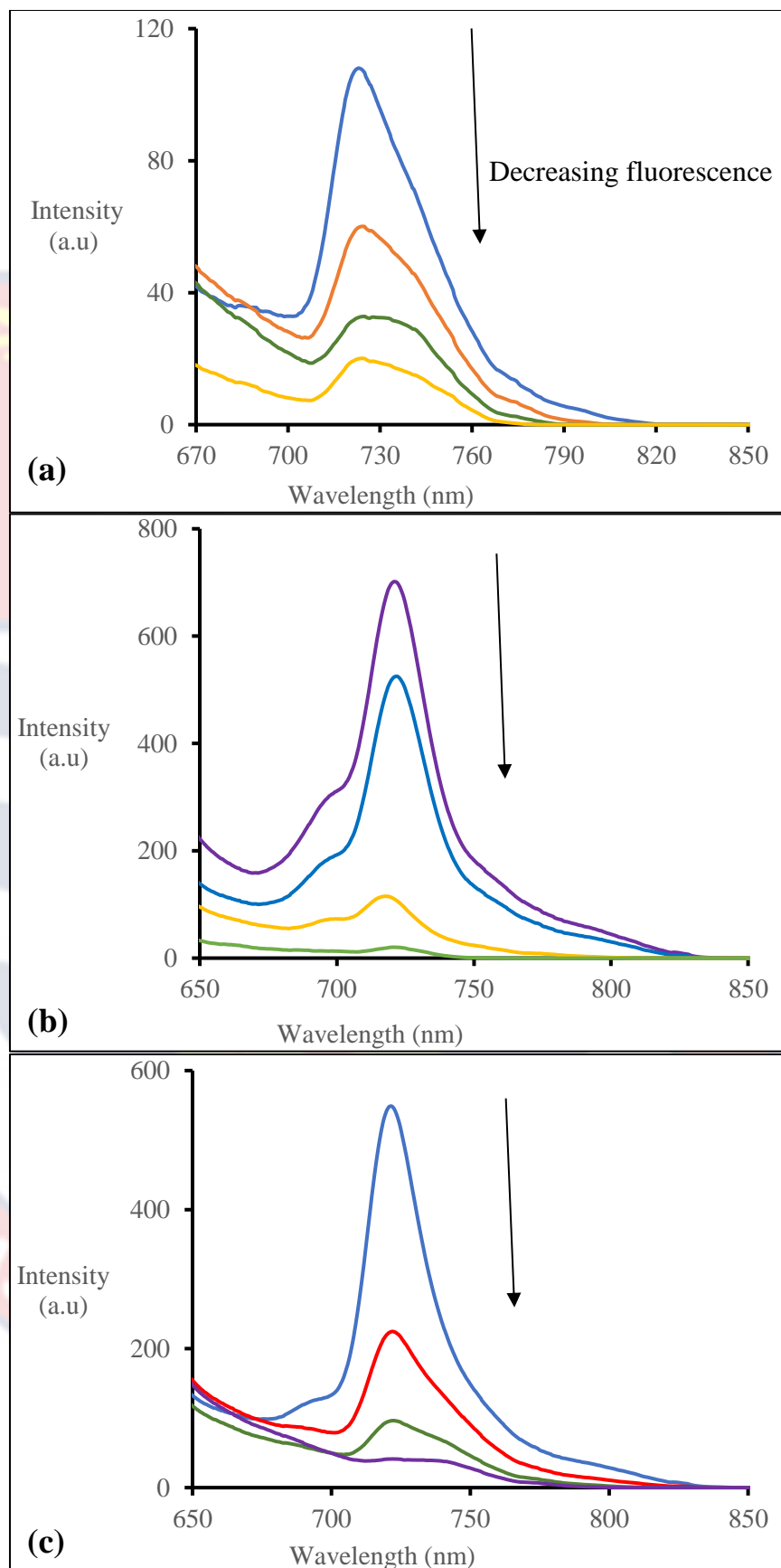
Figure 48: Emission spectral changes of (a) ZnPc-GB, (b) ZnPc-OPMF and (c) ZnPc-PLF in the presence of $NO_{2(g)}$.

134

The fluorescence emission intensity was observed to decrease after, every cycle of exposure to NO_2 gas until it diminished. Though again, the exact amount of NO_2 gas at each exposure could not be measured, the variations in the emission spectra imply that, the zinc phthalocyanine-functionalised fibres are permeable to gas and could be used for fluorometric detection of NO_2 gas in the environment. It also suggests that, the functionality of the zinc phthalocyanine dye are maintained within the functionalised fibre matrices. The fluorescence emission spectra also, became more red-shifted in the fibres after exposure to $NO_{2(g)}$ (~725 nm), as compared to that of the original functionalised fibres (~ 690 nm) in Figure 22 above.
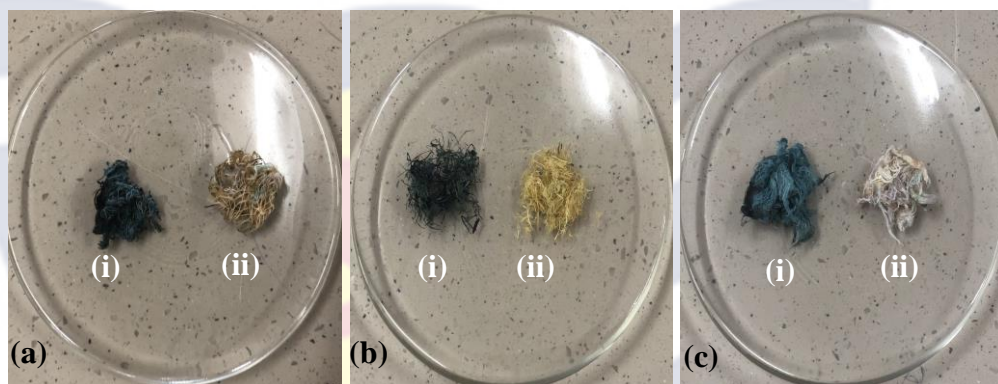
Figure 49: Images of the Functionalised Fibres (a) ZnPc-GB, (b) ZnPc-OPMF and (c) ZnPc-PLF before (i) and after (ii) exposure to $NO_{2(g)}$.

As seen in Figure 49, a colour change from the characteristic dark green zinc phthalocyanine-functionalised fibres (Figure 49 (ai), (bi) and (ci)) to brown fibres (Figure 49 (aii), (bii) and (cii)), after exposure to $NO_{2(g)}$ confirmed the complete depletion of the zinc phthalocyanine in the fibres as, evidenced in the decreased fluorescence emission intensities in Figure 47 above. Other polymer supports for zinc phthalocyanine such as thin films (Inagaki *et al*., 1996) and electrospun nanofabric materials (Zugle & Nyokong, 2012), have been used to detect NO_2 gas. But, the application of natural

135

cellulose-based fibre supports (extracted from oil palm mesocarp and pineapple leave wastes) is reported for the first time, and the ease of production, recovery, disposal and eco-friendly nature of these fibres may make them a better choice for large-scale applications.

Heterogeneous Photocatalytic Application of the Functionalised Cellulose-Based Fibres

The cellulose-based fibres, functionalised with zinc phthalocyanine were applied as photocatalyst for crystal violet dye (a model organic pollutant) mineralisation, in a heterogeneous photodegradation process. The effects of initial crystal violet concentration (30, 40, 50 and 60 mgL^{-1}), catalysts concentration (27, 35 and 50 mM), and light intensities and the mechanism of the photodegradation process were studied. Catalyst loads of 200 mg and crystal violet volume of 50 mL were used for all analysis. Photodegradation of the crystal violet dye was measured with the UV-Vis spectrophotometer. The final and the initial absorbance peak ratio of crystal violet in the solution (A_t/A_0) was measured at different time intervals. The percentage degradation was calculated as a function of the concentration at different time intervals using Eqn. 5 (Deb *et al.*, 2018).

Degradation % = $\frac{(C_0 - C_t)}{C_0} \times 100$ ……….…………..……………….. Eqn. 5

where C_0 is the initial concentration, and C_t is the concentration of the dye at time 't'. For low concentration solutions, the photodegradation reactions follow an apparent first-order kinetics, described by equation (6):

Ln $\frac{C_0}{C_t}$ = $k_{obs} \cdot t$ ……….…………………………………………….. Eqn. 6

where C_t is the dye concentration at specific time, C_0 is the initial concentration and k_{obs} is the rate constant. By plotting Ln (C_0/C_t) vs. time, the

136

k_{obs} values can be determined. The UV-vis absorption spectra of the crystal violet in deionised water at its' physiological pH of 5.8 is presented in Figure 50.
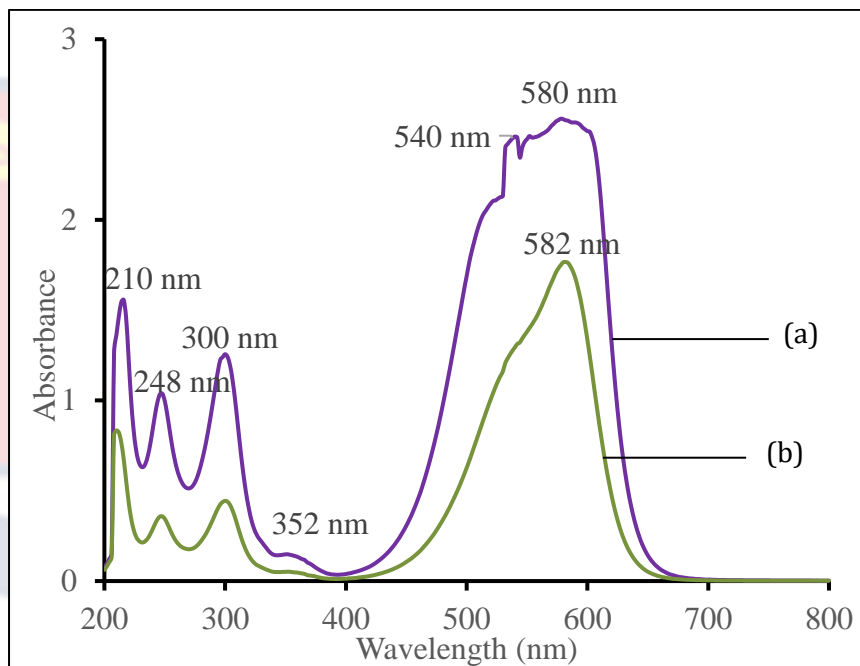
Figure 50: UV-Vis absorption spectra of crystal violet in (a) 40 and (b) 20 mgL^{-1} solutions.

The absorption spectrum of the crystal violet in deionised water (Figure 50) showed three bands at the ultra-violet region around 210, 248, and 300 nm with a shoulder around 352 nm relating to the aromatic rings (Abbas *et al.*, 2020; Mapukata *et al.*, 2019; Sindelo *et al.*, 2022) and two main bands in the visible region around 540 and 580 nm relating to the chromophore (Abbas *et al.*, 2020; Palma-Goyes *et al.*, 2010). These are the characteristic absorption bands of crystal violet dye.

Heterogeneous photodegradation of crystal violet dye

The photodegradation reaction was carried out, using the zinc phthalocyanine-functionalised cellulose-based fibres (ZnPc-GB, ZnPc-OPMF & ZnPc-PLF) as the photocatalysts, and the plain/bleached cellulose-based

137

fibres (P-GB, B-OPMG & B-PLF) as control. The photocatalysts are not soluble in water, hence they were suspended in the crystal violet solution as solids (threadlike fibres). The studies were conducted using crystal violet solution at its' physiological pH of 5.8 and sunlight and LED redlight, as light sources. The absorbance of the sample solutions was measured at various time intervals during the degradation process.

Changes in the absorption spectra, when the aqueous solutions of crystal violet dye was irradiated with sunlight in the presence of (a) ZnPc-GB, (b) ZnPc-OPMF, (c) ZnPc-PLF and (d) P-GB (as example of the plain non-functionalised fibre supports) at varying time intervals are presented in Figures 51 and 52.
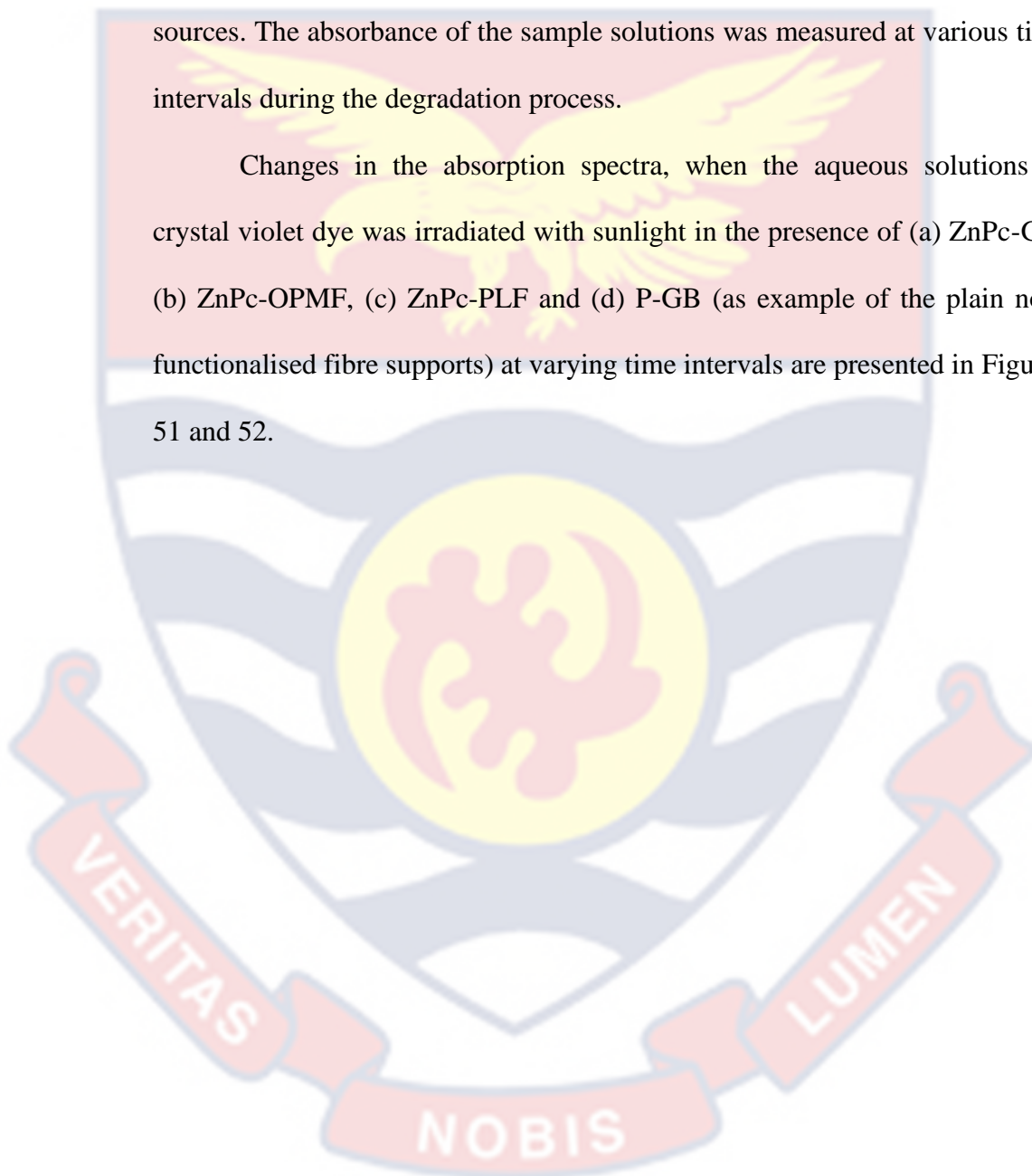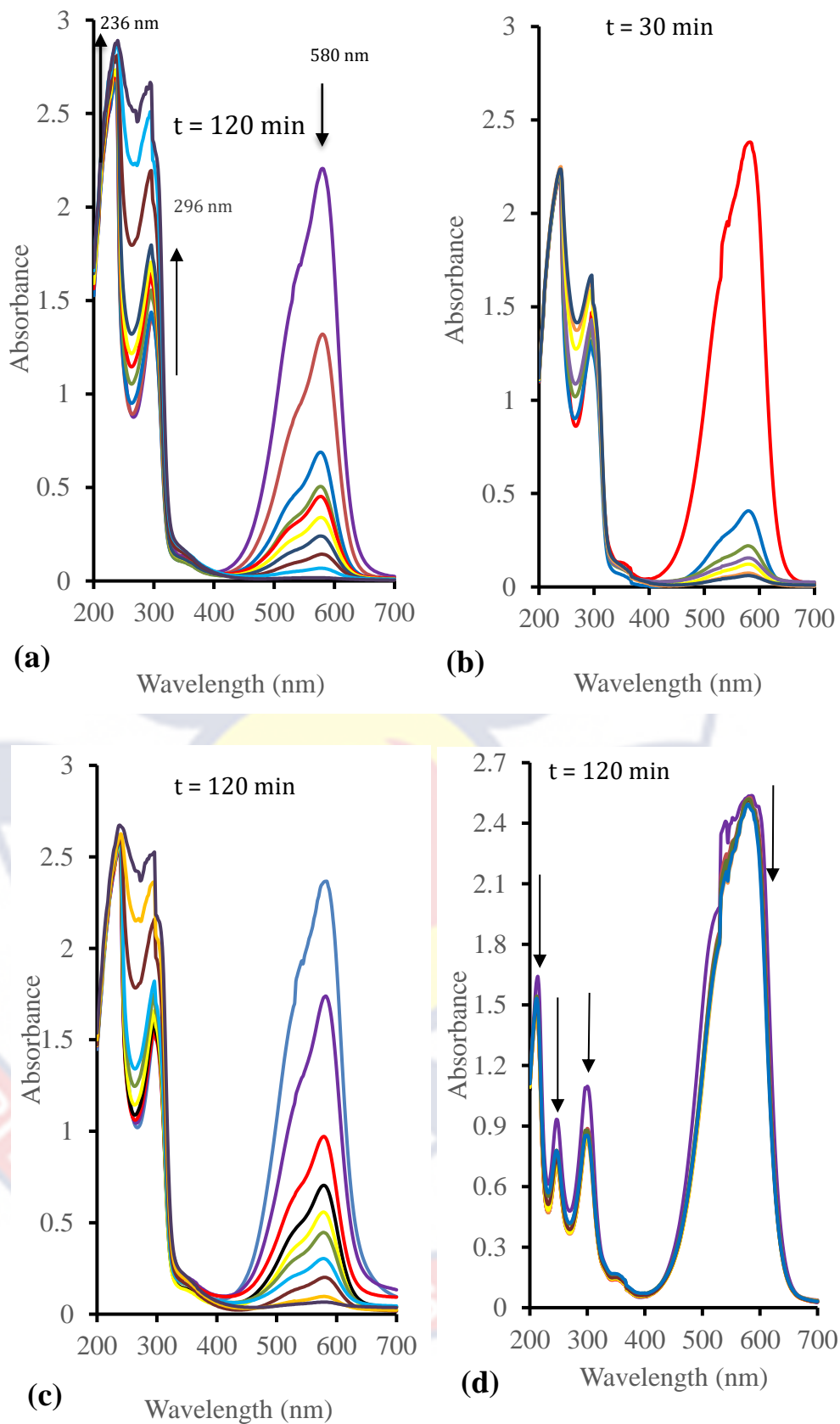
Figure 51: Absorption profiles of the degradation of crystal violet in the presence of (a) ZnPc-GB, (b) ZnPc-OPMF (c) ZnPc-PLF and (d) P-GB under sunlight radiation (irradiance = 20000-50000 lx (lm/m^2).

139

Upon illumination of the crystal violet solution with both sunlight (Figure 51) and LED redlight (Figure 52 below), both the visible and the ultra violet (UV) bands underwent a hypsochromic shift (in reference to Figure 50). As shown in Figures 51 and 52, there was a rapid decrease in intensity of the crystal violet visible band at 580 nm in the presence of the functionalised fibres (ZnPc-GB, ZnPc-OPMF and ZnPc-PLF), suggesting the depletion of the chromophore (i.e conversion to colourless products) in the solution. The decrease in intensity with time of the visible band, may be due to the cleavage of the aromatic rings by oxidation (Abbas *et al.*, 2020*)*. There was also, a steady blue shift of the ultra violet (UV) bands from 300 nm to ~ 296 nm and that from 248 nm to ~ 236 nm which, increased with time, whilst the 210 nm band, disappeared. The increase in the bands at the UV region suggests that, the benzene rings remain intact and are not degraded during the photodegradation process (Mapukata *et al.*, 2020). Consequently, rather than crystal violet dye superficial adsorption, a photochemically induced process is proposed as the cause of the spectra changes (Sindelo *et al.*, 2022). There was also, no leaching of the zinc phthalocyanine from the fibres into the aqueous solutions of the crystal violet dye, as there was no appearance of the Q absorption band of ZnPc (λ670 nm) in the visible region. Similar observations took place under LED redlight radiation (Figures 52 (a), (b), (c) below). Thus, suggesting the functionalised fibres (b) ZnPc-GB, (c) ZnPc-OPMF and (d) ZnPc-PLF, can serve as good photocatalysts for the conversion of organic dyes in water.

When the plain fibres were used as control under similar conditions, there was only a slight decrease in the bands at both the visible regions at 580

nm and the UV regions at 210, 248, and 300 nm (Figure 51d). This may be attributed to the fibre surface adsorption of the crystal violet dye. Thus, suggesting that, the zinc phthalocyanine in the functionalised fibres is the agent involved in the degradation of the crystal violet because, it is able to produce singlet oxygen.

Likewise, when crystal violet solution alone was irradiated with both sources (sunlight and redlight) at higher light intensities (sunlight, 80,000-85,000 lx), there were no changes in the absorbance (Figure 52d). The understanding is that, both light and the photocatalysts (ZnPc-GB, ZnPc-OPMF and ZnPc-PLF) are needed for the degradation of crystal violet dye and that, light alone cannot carry out the photodegradation reaction.
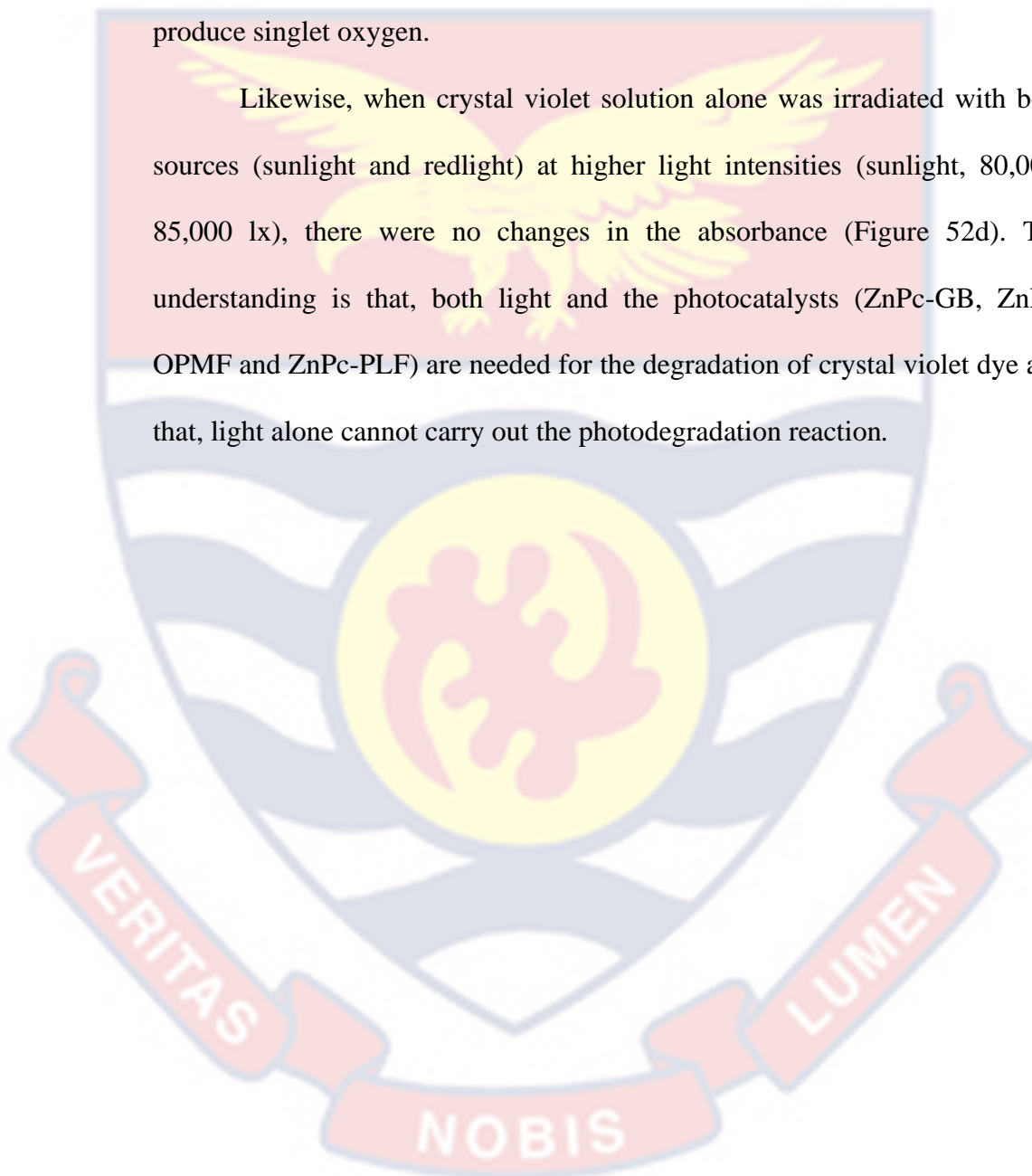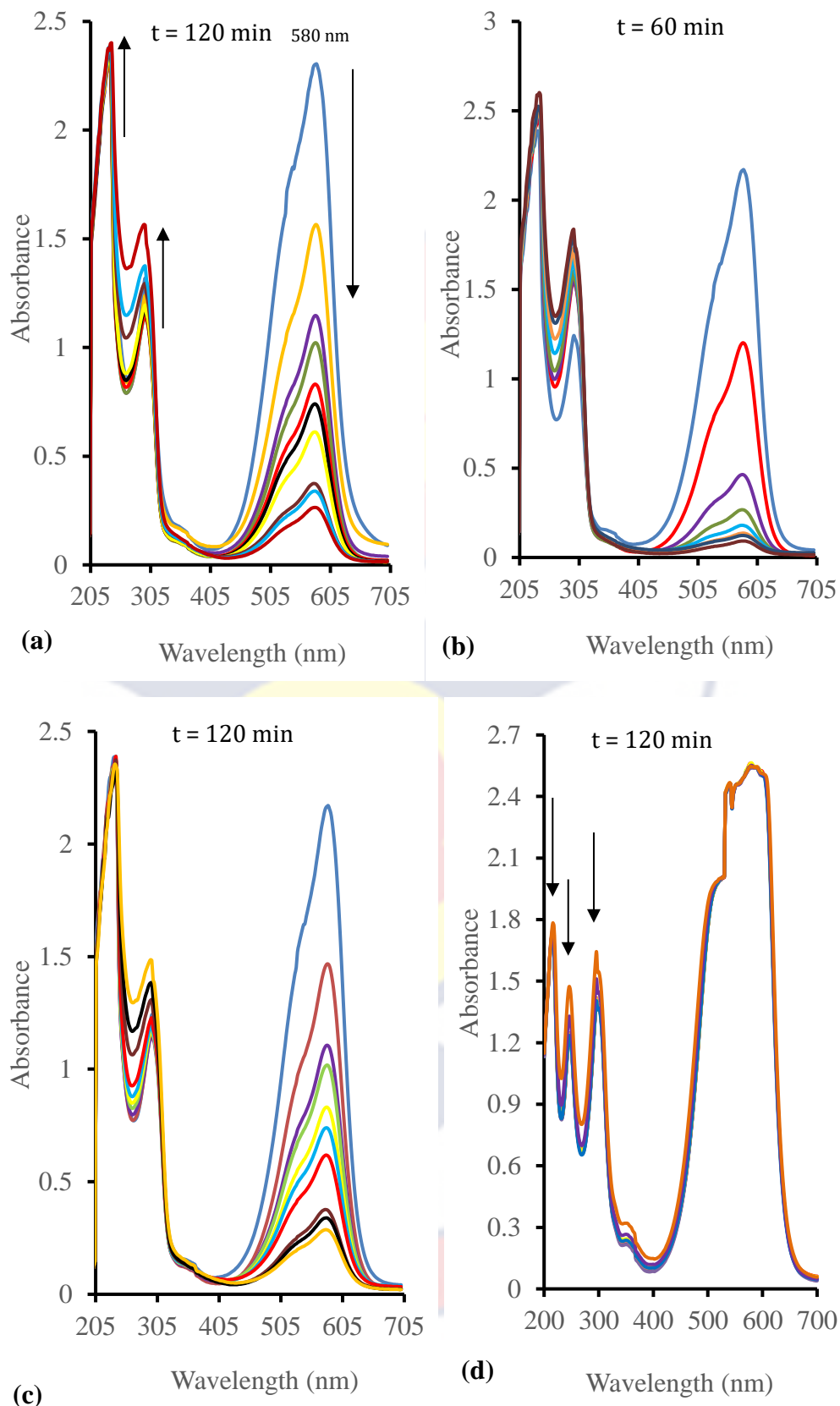
Figure 52: Absorption profiles of the degradation of crystal violet dye in the presence of (a) ZnPc-GB, (b) ZnPc-OPMF and (c) ZnPc-PLF under LED redlight radiation and (d) Light-only [irradiance = 8000-10000 lx (lm/m^2)].

142

Photocatalyst degradation efficiency as a function of time

The degradation efficiency of the photocatalysts (ZnPc-GB, ZnPc-OPMF and ZnPc-PLF) was determined from the graph of degradation percentage versus irradiation time in Figure 53. All the functionalised cellulose-based fibres were found to be effective towards the removal of crystal violet dye in a heterogeneous photodegradation environment, providing complete degradation within 30-120 min. The high degradation efficiency of the photocatalysts (ZnPc-GB, ZnPc-OPMF and ZnPc-PLF), can be attributed to the robust static interactions concerning the zinc phthalocyanine in the fibres and crystal violet dye molecules (Chen *et al.*, 2011). The degradation efficiency was observed to increase with increasing concentration of dissolved oxygen suggesting that, photooxidation is the major pathway of the photodegradation reaction (Zakharian, 2000).
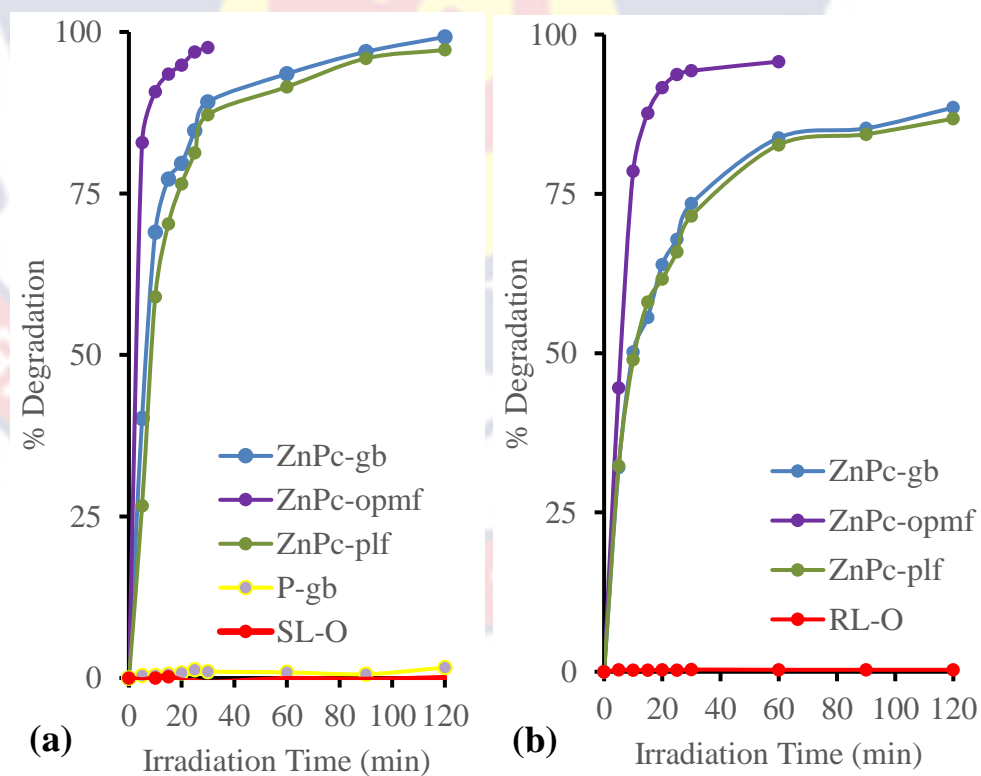
Figure 53: Degradation efficiency of photocatalysts (ZnPc-GB, ZnPc-OPMF, ZnPc-PLF, and P-GB) vs time under (a) sunlight and (b) redlight radiations.

143

ZnPc-OPMF photocatalyst achieved the most removal performance of 97.56% within 30 mins, compared to ZnPc-GB at 99.23% in 120 min and ZnPc-PLF at 97.56% in 120 min under sunlight radiation (Figure 53a). Similar observations were made under LED redlight radiation, where ZnPc-OPMF achieved rapid removal of crystal violet at 95.75% within 60 min, followed by ZnPc-GB at 88.54% in 120 min and ZnPc-PLF at 86.80% in 120 min (Figure 55a below). Such high percentages of colour removal by the cellulose-based fibres may be due to the highly stable immobilised zinc phthalocyanine in them, yielding high production of reactive oxygen species especially, the singlet oxygen for the degradation process (Morshed *et al.*, 2020). The slightly lower degradation rates observed under LED redlight radiation as compared with sunlight radiation, may be due to the differences in their intensities. Redlight irradiation experiments were done at lower intensities ranged between [8000-10000 lx (lm/m^2)] as compared with the sunlight irradiation [20000-50000 lx (lm/m^2)]. Figure 54 shows a digital presentation of the complete crystal violet (CV) removal by the functionalised fibres.

Photodegradation

ZnPc-fibres, light, O$_2$, 25-30 °C

CV solution   CV-free solution
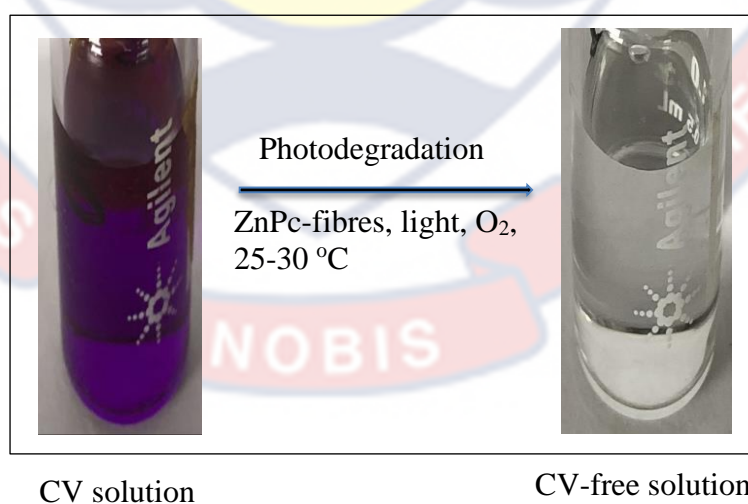
Figure 54: Digital image presentation of complete photodegradation of crystal violet dye in aqueous solution.

A control removal reaction was carried out with plain fibres + light (P-GB as an example), sunlight-only (SL-O) and redlight-only (RL-O), where no decrease in colour intensity was observed (Figures 52a and 52b above).

Kinetic studies of crystal violet dye removal

Degradation kinetics is one of the most important characteristics that represent the catalytic efficiency of the fibre support and, therefore, largely illustrate its' potential applications (Morshed *et al.*, 2020). Thus, kinetic experiments were performed in which, the rate of decomposition as a function of irradiation time was studied. The results are presented in Figure 55.
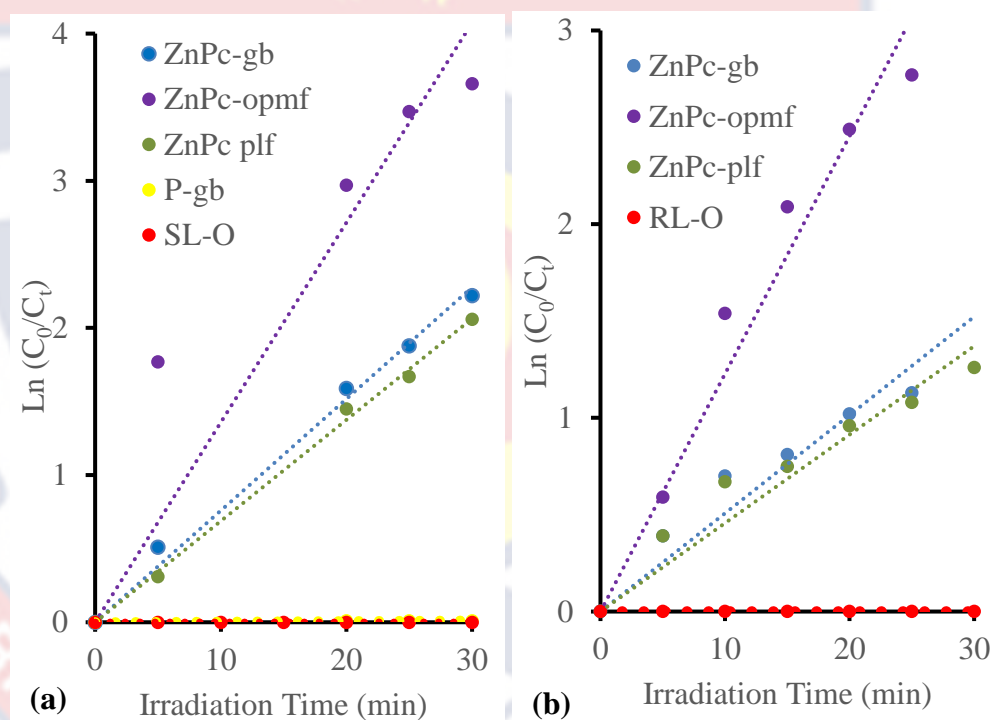
Figure 55: Plots of Ln (C_0/C_t) vs time for (ZnPc-GB, ZnPc-OPMF, P-gb and SL-O/RL-O with (a) sunlight and (b) redlight irradiations. (SL-O = sunlight-only and RL-O = redlight-only).

Plots of the photocatalysts (ZnPc-GB, ZnPc-OPMF and ZnPc-PLF), exhibited good linear relationships of Ln (C_0/C_t) versus reaction time, following first-order kinetics with respect to crystal violet dye degradation for

145

both sunlight and LED redlight sources (Figures 55a and 55b). Zinc phthalocyanine conjugated to glass wool has been reportedly used to photodegrade methyl orange with similar kinetics (Sindole *et al.*, 2022).

The rate constants were inferred from Figures 55a and 55b and equations 7 and 8 were used to calculate the initial rates and half-lives.

Initial Rate (R) = k_{obs} [CV]$_0$ …………………………………………….. Eqn. 7

where [CV]$_0$ = initial concentration of crystal violet dye

$$t_{1/2} = \frac{\ln 2}{k_{obs}}$$

Ln 2 = 0.6931 …………………………………………………………... Eqn. 8

Table 18: Kinetic Data of the Crystal Violet Photodegradation at the Starting Concentration of 40 mgL^{-1} with (ZnPc-GB, ZnPc-OPMF and ZnPc-PLF)

Catalyst	$K_{obs} \times 10^{-2}$ (min^{-1})		Initial Rate (mgL^{-1}min^1)		Half-life (min)		$R^2 \times 10^2$	
	SL	RL	SL	RL	SL	RL	SL	RL
ZnPc-GB	7.59	5.07	3.04	2.03	9.13	13.67	99.77	97.86
ZnPc-OPMF	13.58	12.27	5.43	4.91	5.10	5.65	96.17	98.80
ZnPc-PLF	6.88	4.57	2.75	1.83	10.07	15.16	99.90	98.06
P-GB	0.04					0		97.40

Source: Laboratory Analysis (2016-2021)

It is evident from the summary in Table 18 that, among all the photocatalysts studied, ZnPc-OPMF exhibited the swiftest degradation efficiency of crystal violet at 97.56% within, 30 min of irradiation, at a rate of 0.1358 min^{-1}, with $R^2 \sim 0.9617$, followed by ZnPc-GB at 99.23% in 120 min of irradiation, at a rate of 0.0759 min^{-1} with $R^2 \sim 0.9977$ and then ZnPc-PLF at 97.56% within 120 min of irradiation, at a rate of 0.0688 min^{-1} with $R^2 \sim 0.999$

146

under sunlight (SL) radiation. Similar observation was made under LED redlight (RL) radiation, with ZnPc-OPMF achieving the fastest colour removal of 95.75% in 60 min of irradiation, at a rate of 0.1227 min^{-1}, with R^2 ~ 0.988, followed by ZnPc-GB at 88.54% in 120 min of irradiation, at a rate of 0.0507 min^{-1}, with R^2 ~ 0.9786 and ZnPc-PLF at 86.80% in 120 min of irradiation, at a constant rate of 0.0457 min^{-1}, with R^2 ~ 0.9806. The rate constant (k_{obs}) values of the photocatalysts (ZnPc-GB, ZnPc-OPMF and ZnPc-PLF) under sunlight (SL) radiation, were observed to be higher than those observed under LED redlight (RL) radiation (Table 18), resulting in corresponding higher half-lives of the photocatalysts under redlight radiation as compared to sunlight radiation. This may be due to the differences in their intensities for the photodegradation process. LED redlight intensities ranged between [8000-10000 lx (lm/m^2)] compared to sunlight [20000-50000 lx (lm/m^2)].

The half-lives of the photodegradation of crystal violet by the functionalised fibres within the experimental concentrations as seen in Table 18, have smaller values than other organic dyes (methyl orange for example) in literature (Sindelo *et al.*, 2022). An encouraging aspect is that these half-lives for the photocatalysts (ZnPc-GB, ZnPc-OPMF and ZnPc-PLF) are within 10 and 15 minutes of exposure to both sunlight and red LED light respectively. Implying that, about 50 % of the contaminant (crystal violet) has been removed within 10 and 15 minutes of exposure to both sunlight and red LED light respectively. This suggests that the functionalised fibres can be practically used to treat organic dyes in water, due to the short photodegradation time.

147

Effect of concentration of crystal violet dye

The initial concentration of a dye is an important factor that affects the photodegradation efficiency. Therefore, the effects of the initial concentration of crystal violet dye on the photocatalytic activity of the functionalised fibres were also investigated. Initial concentration of 30, 40, 50, and 60 mgL^{-1} solutions were used in the photodegradation experiments under similar experimental conditions. The results are presented in Figures 56-58.

148
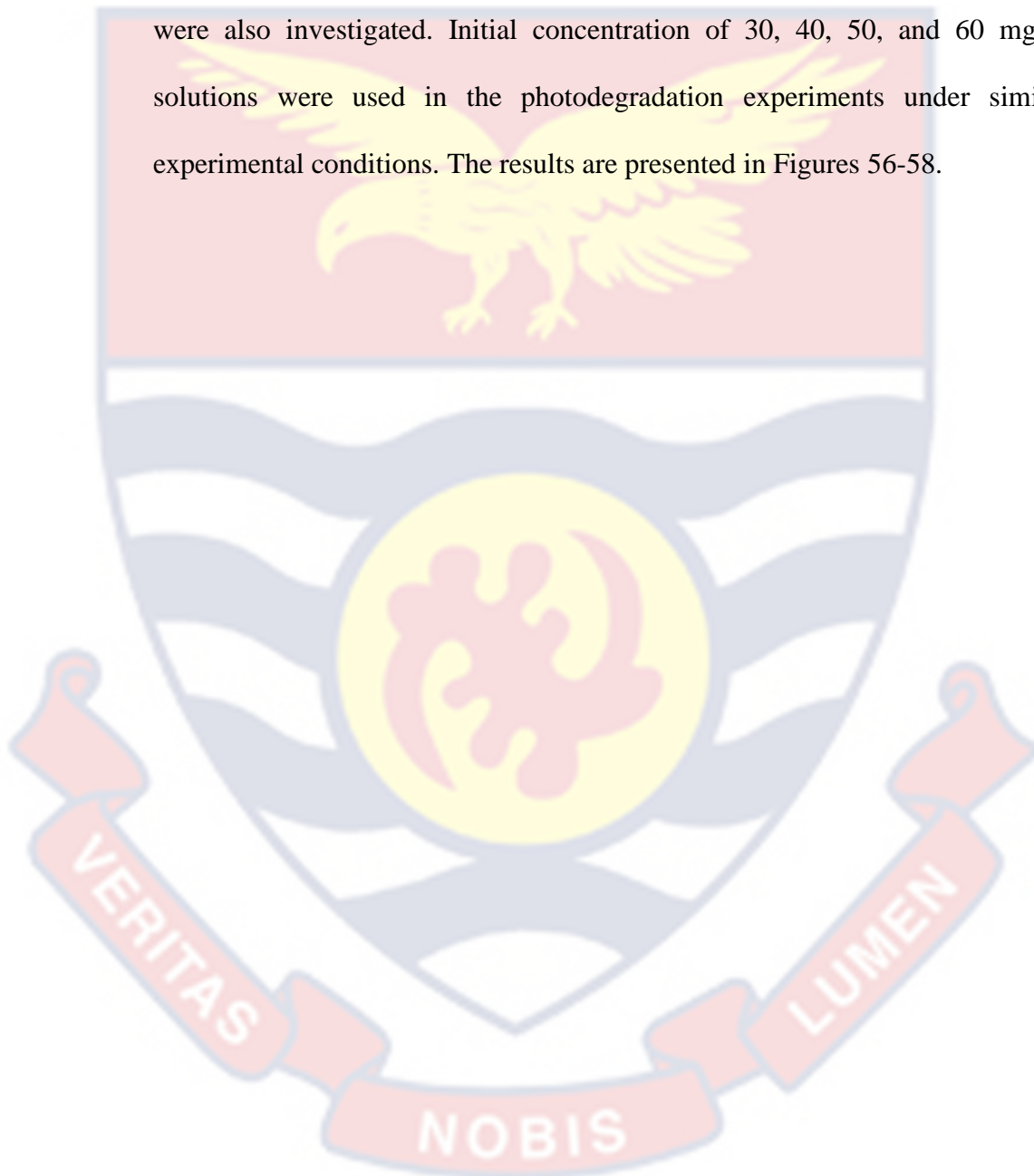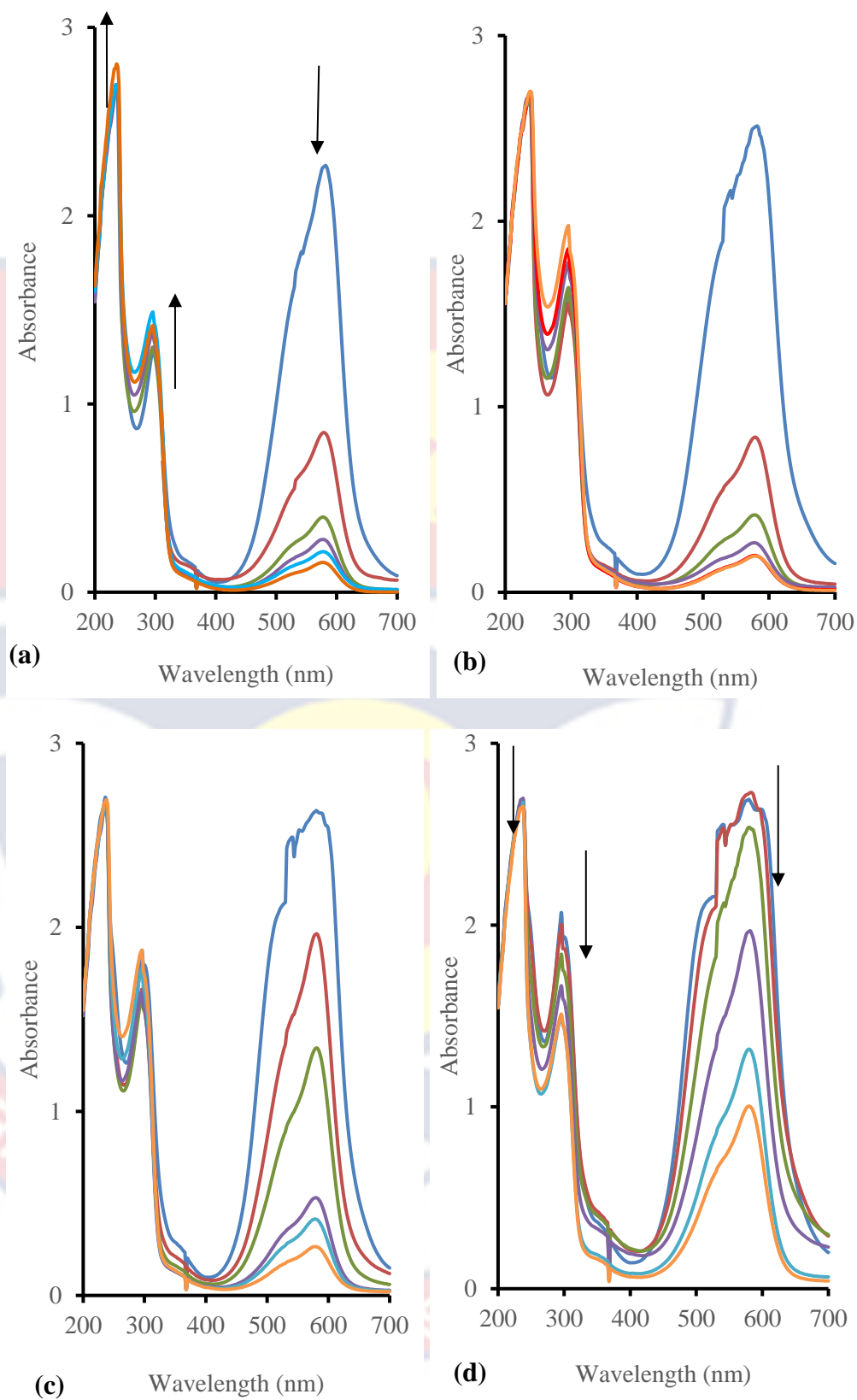
Figure 56: Absorption profiles of the degradation of crystal violet at (a) 30 mgL^{-1}, (b) 40 mgL^{-1}, (c) 50 mgL^{-1} and (d) 60 mgL^{-1} initial concentrations in the presence of ZnPc-GB under sunlight radiation.
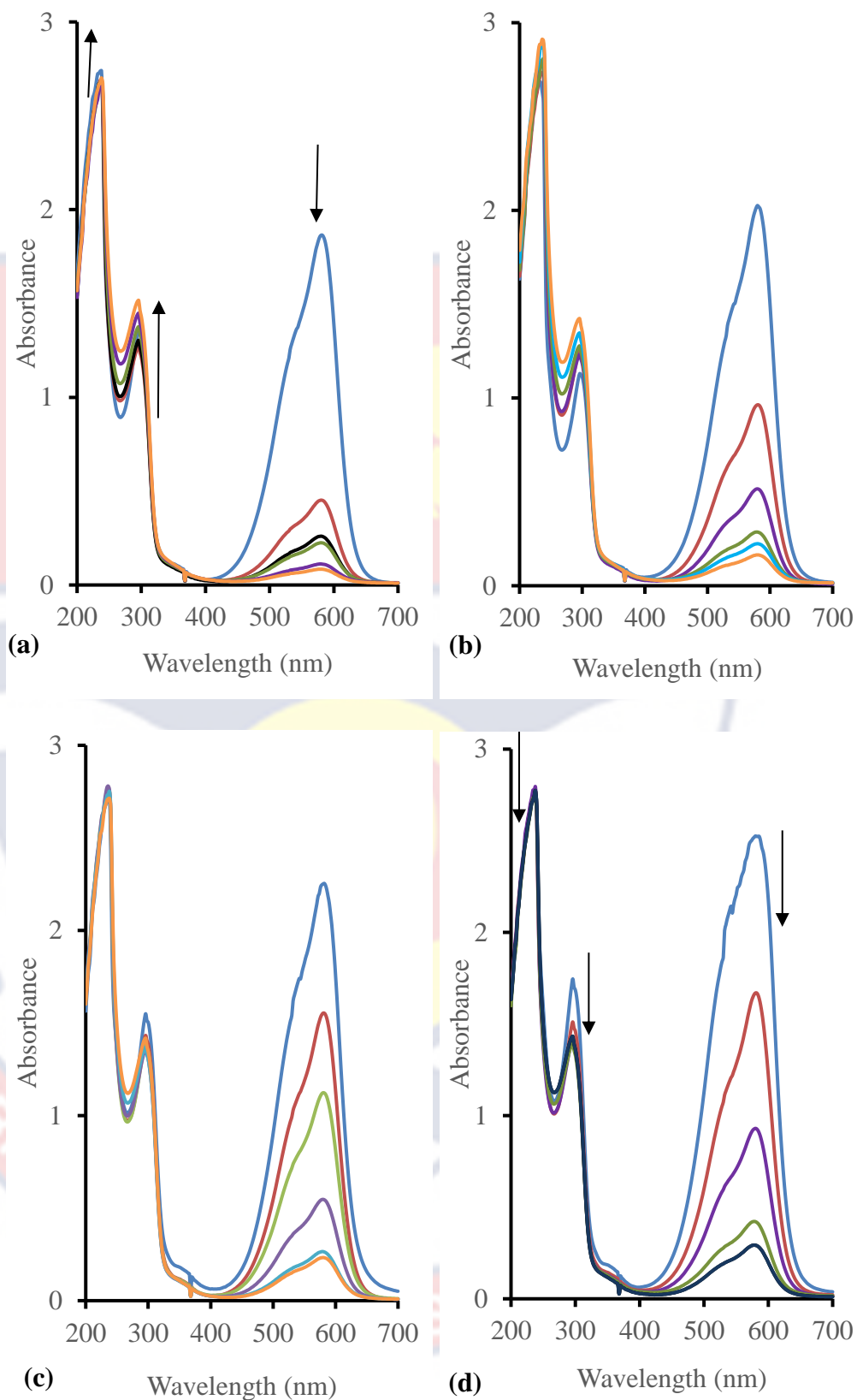
Figure 57: Absorption profiles of the degradation of crystal violet at (a) 30 mgL^{-1}, (b) 40 mgL^{-1}, (c) 50 mgL^{-1} and (d) 60 mgL^{-1} initial concentrations in the presence of ZnPc-OPMF under sunlight radiation.

150
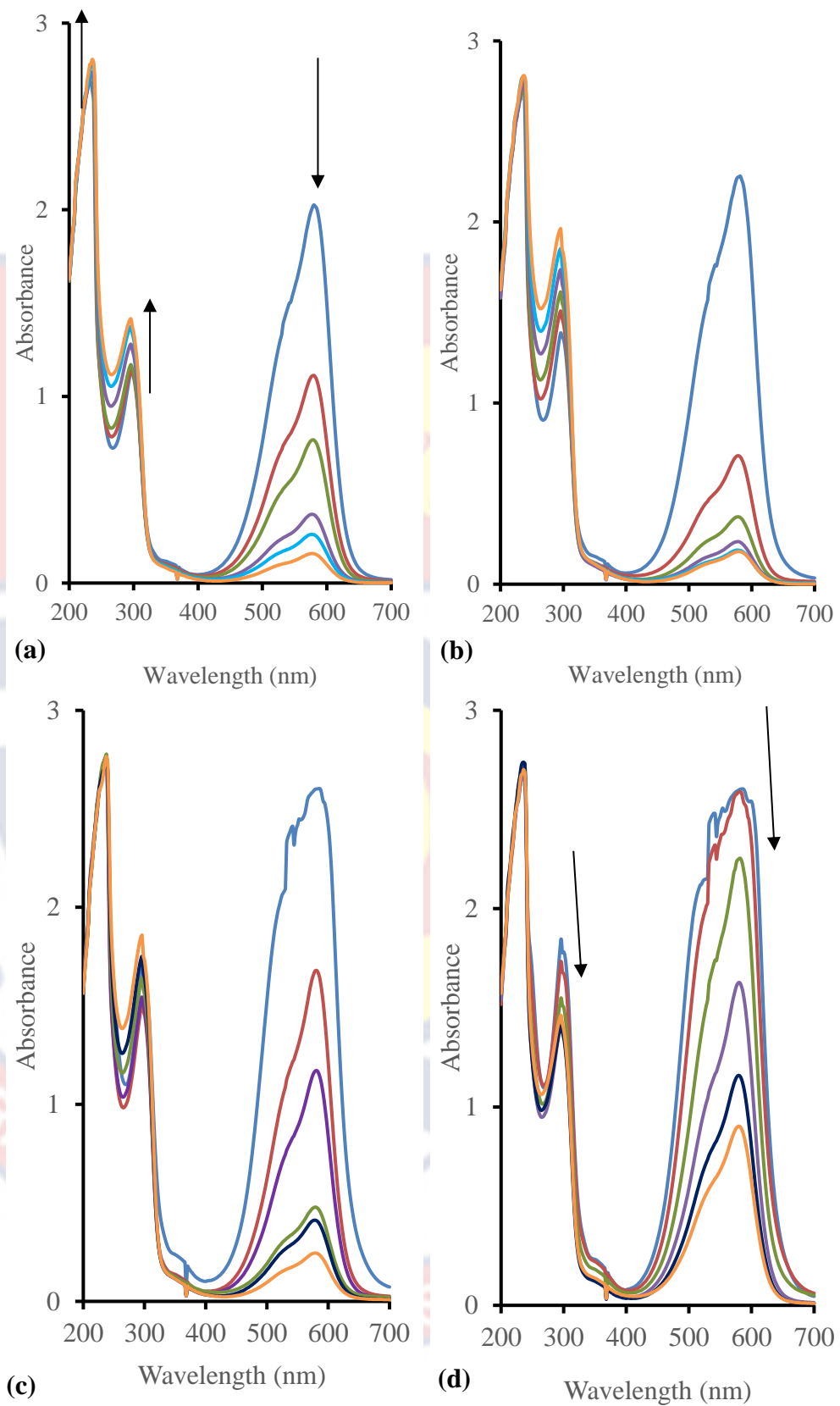
Figure 58: Absorption profiles of the degradation of crystal violet at (a) 30 mgL^{-1}, (b) 40 mgL^{-1}, (c) 50 mgL^{-1} and (d) 60 mgL^{-1} initial concentrations in the presence of ZnPc-PLF under sunlight radiation.

151

The results in Figures 56-58 showed that, photodegradation efficiencies of the three catalysts decreased with increasing concentration of the crystal violet. The highest photodegradation efficiency was observed in the crystal violet solution with initial concentration of 30 mgL^{-1}, for all the photocatalysts followed by 40 mgL^{-1}, 50 mgL^{-1} and 60 mgL^{-1} initial concentrations (Figure 59 d).
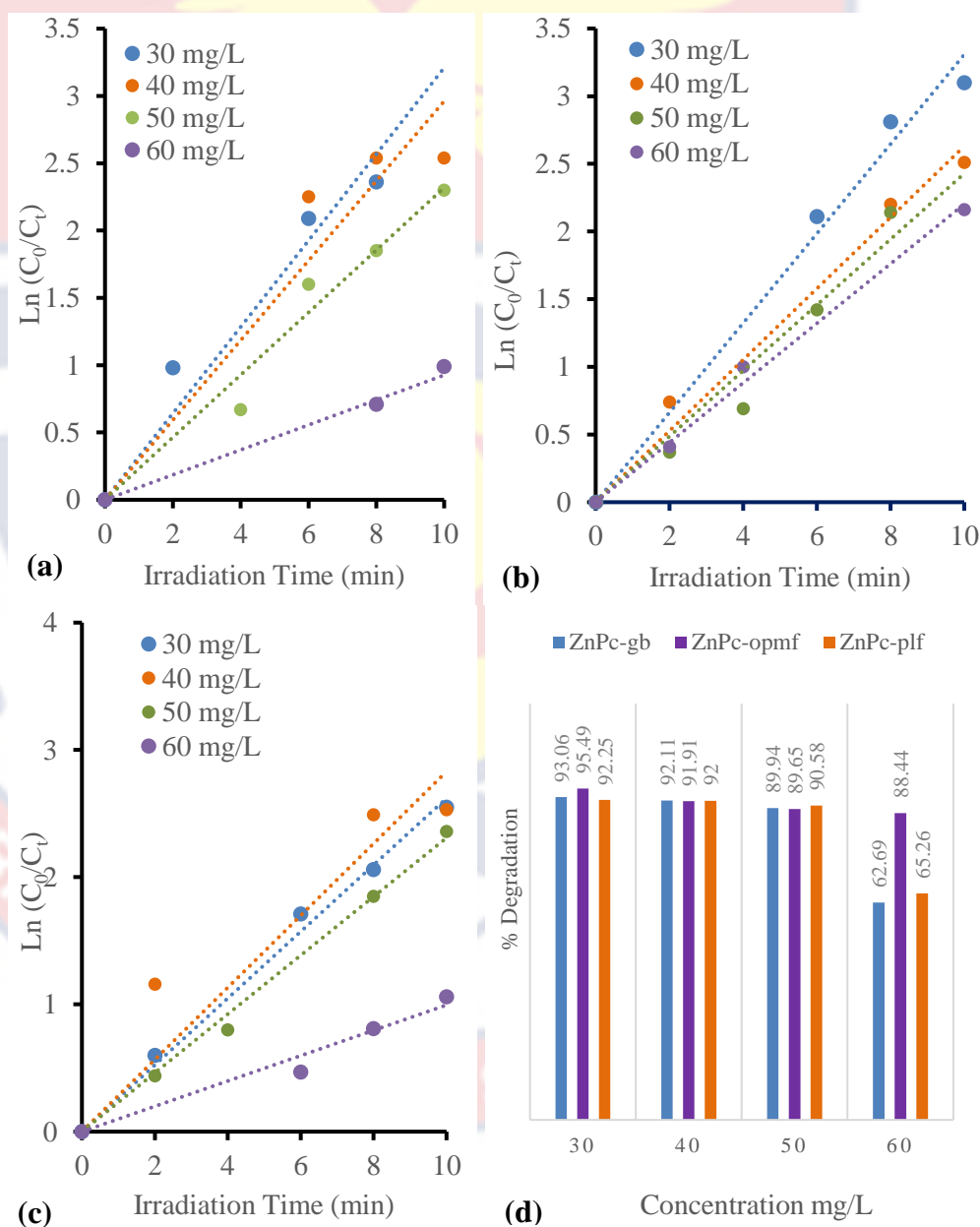
Figure 59: Plots of Ln (C$_0$/C$_t$) vs time for different crystal violet concentration degradation by (a) ZnPc-GB, (b) ZnPc-OPMF (c) ZnPc-PLF under Sunlight irradiation and (d) Degradation % of ZnPc-GB, ZnPc-OPMF and ZnPc-PLF.

152

The kinetic plots in Figure 59 (a-c), are linear and follow first order kinetics as usual. The degradation rate constant (k_{obs}) decreased (whilst the half-lives increased) with the increase in crystal violet concentration for (ZnPc-GB, ZnPc-OPMF and ZnPc-PLF) Table 19. However, the slight differences in the values of the ZnPc-PLF photocatalyst at the crystal violet initial concentration of 40 mgL^{-1} (Table 19), may be due to mass transfer and diffusion challenges, normally encountered in the immobilisation processes involving fibrous materials (Boyacı, 2005; Morshed *et al.*, 2020).

Table 19: Kinetic Data for Photodegradation of Crystal Violet Dye at Various Initial Concentrations with ZnPc-GB, ZnPc-OPMF, ZnPc-PLF

CV Concentration (mg/L)	$K_{obs} \times 10^{-2}$ (min^{-1})			Initial Rate (mgL^{-1} min^{-1})			Half-life (min)		
	ZnPc-GB	ZnPc-OPMF	ZnPc-PLF	ZnPc-GB	ZnPc-OPMF	ZnPc-PLF	ZnPc-GB	ZnPc-OPMF	ZnPc-PLF
30	32.10	33.07	26.20	9.63	9.92	7.86	2.16	2.10	2.65
40	29.61	26.30	28.30	11.84	10.52	11.32	2.34	2.63	2.45
50	23.19	24.28	23.09	11.60	12.14	11.55	2.99	2.85	3.00
60	9.26	22.02	9.95	5.56	13.21	5.97	7.48	3.15	6.97

Source: Laboratory Analysis (2016-2021)

***CV: crystal violet, ZnPc-GB: Zinc phthalocyanine-gauze bandage, ZnPc-OPMF: Zinc phthalocyanine-oil palm mesocarp fibres and ZnPc-PLF: Zinc phthalocyanine-pineapple leaves fibres.

Effect of catalyst concentration

The use of the right concentration/amount of catalyst in any catalytic degradation process is paramount, since higher concentration dose may result in light scattering thereby, decreasing the reaction rate. Lesser amount of

153

catalyst may also, result in the generation of lower rate of reactive oxygen species upon light irradiation thereby, decreasing the reaction rate (Mousali & Zanjanchi, 2020). Three different concentrations of 27mM, 35mM and 50mM of Zinc phthalocyanine immobilised on the fibre supports were used in similar experimental conditions, to establish the right amount that will achieve the best efficiency for the degradation process. The results are presented in Figure 60.

154
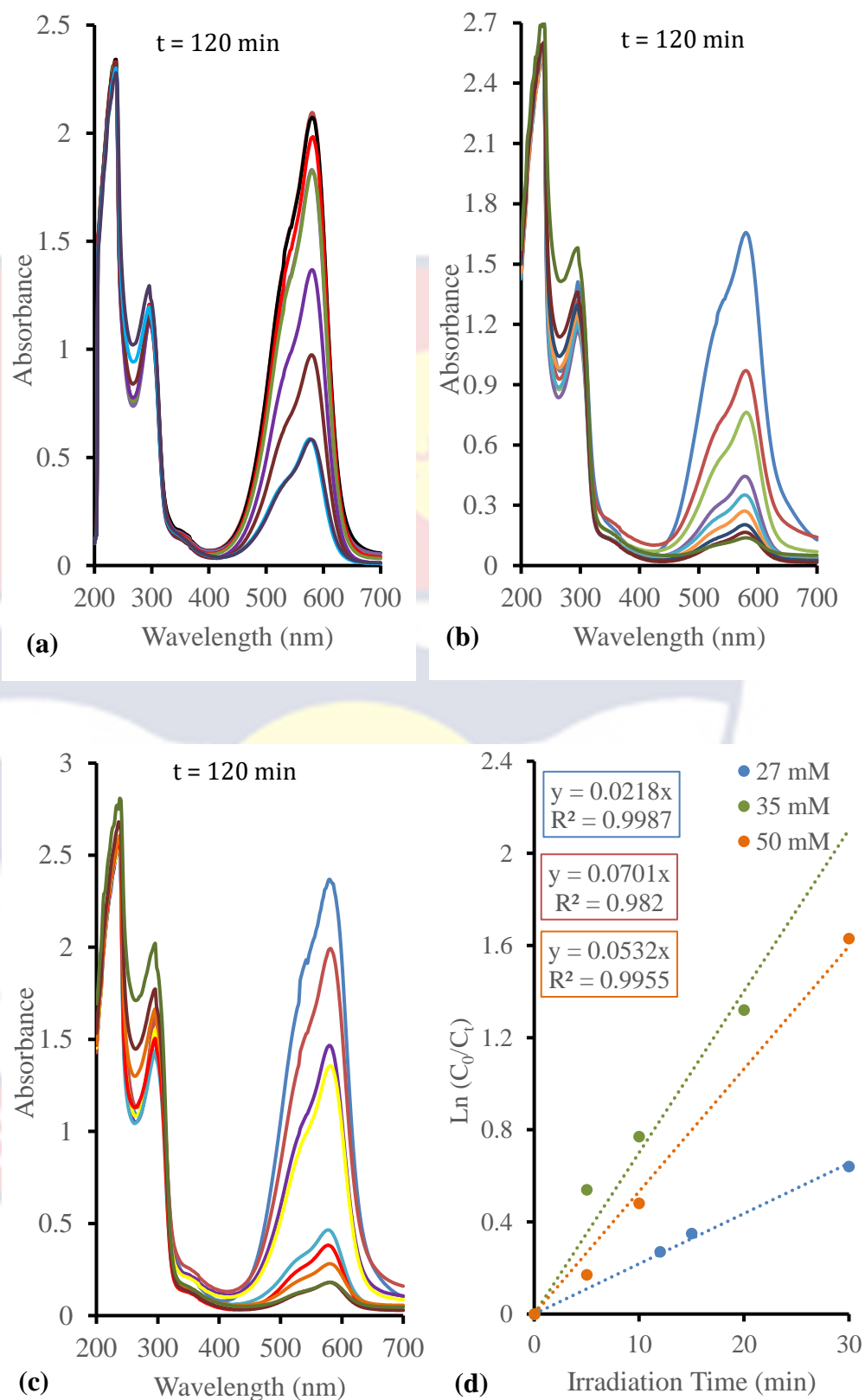
Figure 60: Absorption profiles of the degradation of crystal violet in the presence of ZnPc-GB (as example) at different concentrations of (a) 27 mM, (b) 35 mM & (c) 50 mM, and (d) Plots of Ln (C$_0$/C$_t$) vs time for (a) 27 mM, (b) 35 mM and (c) 50 mM ZnPc-GB under daylight radiation (9000-12000 lx).

155

As shown in Figure 60 (a)-(c), increase in zinc phthalocyanine concentration (from 27-35 mM) on the surface of the fibre supports resulted in an increase in the rate of degradation (from 0.0218 min^{-1} to 0.0701 min^{-1}) until the highest concentration that was effective in complete removal of the crystal violet dye was reached (0.0701 min^{-1}) [Figure 59 (d)] beyond which, further increase in the concentration of Zinc phthalocyanine (about 50 mM) on the surface of the support resulted in a decrease in the rate of degradation (0.0532 min^{-1}). This may be attributed to aggregation (usually with phthalocyanine complexes), which causes mass transfer and diffusion limitations, as a result of the excess amount of zinc phthalocyanine on the fibres. After all the zinc phthalocyanine is linked to the substrate, additional amount does not have any positive impact on the reaction since, the available sites on the surface of the supports are concentrated and working at their maximum (Boyacı, 2005; Morshed *et al.*, 2020).

Similar observations were made with ZnPc-OPMF and ZnPc-PLF photocatalysts under similar conditions (Table 20 below). Overall, the highest concentration/amount of zinc phthalocyanine immobilised on the cellulose fibre support to achieved the best degradation efficiency is 35 mM for all the three fibre supports (Table 20).

Table 20: Kinetic Data of the Crystal Violet Photodegradation with Various (ZnPc-GB, ZnPc-OPMF & ZnPc-PLF) Concentrations

Catalyst	Concentration (mgL^{-1})	$K_{obs} \times 10^{-2}$ (min^{-1})		Initial Rate (mgL^{-1}min^1)		Half-life (min)		$R^2 \times 10^2$	
		DL	RL	DL	RL	DL	RL	DL	RL
ZnPc-GB	35	23.12	28.69	8.09	10.04	3.00	2.42	99.39	98.21
	50	7.59	5.07	3.80	2.53	9.13	13.67	99.77	97.86
ZnPc-OPMF	35	24.23	33.71	8.48	11.80	2.86	2.06	99.01	95.33
	50	13.59	12.27	6.80	6.14	5.10	5.65	96.17	98.80
ZnPc-PLF	35	18.62	15.75	6.52	5.51	3.72	4.40	97.31	99.83
	50	6.88	4.57	3.44	2.29	10.07	15.16	99.90	98.06

Source: Laboratory Analysis (2016-2021)

***DL: Daylight, RL: Redlight, ZnPc-GB: zinc phthalocyanine-gauze bandage, ZnPc-OPMF: zinc phthalocyanine-oil palm mesocarp fibres and ZnPc-PLF: zinc phthalocyanine-pineapple leaves fibres.

Effect of light intensities

The intensities of the light sources were also assessed, to ascertain their effects on the photodegradation process under similar experimental conditions. The results are presented in Figures 61 and 62.
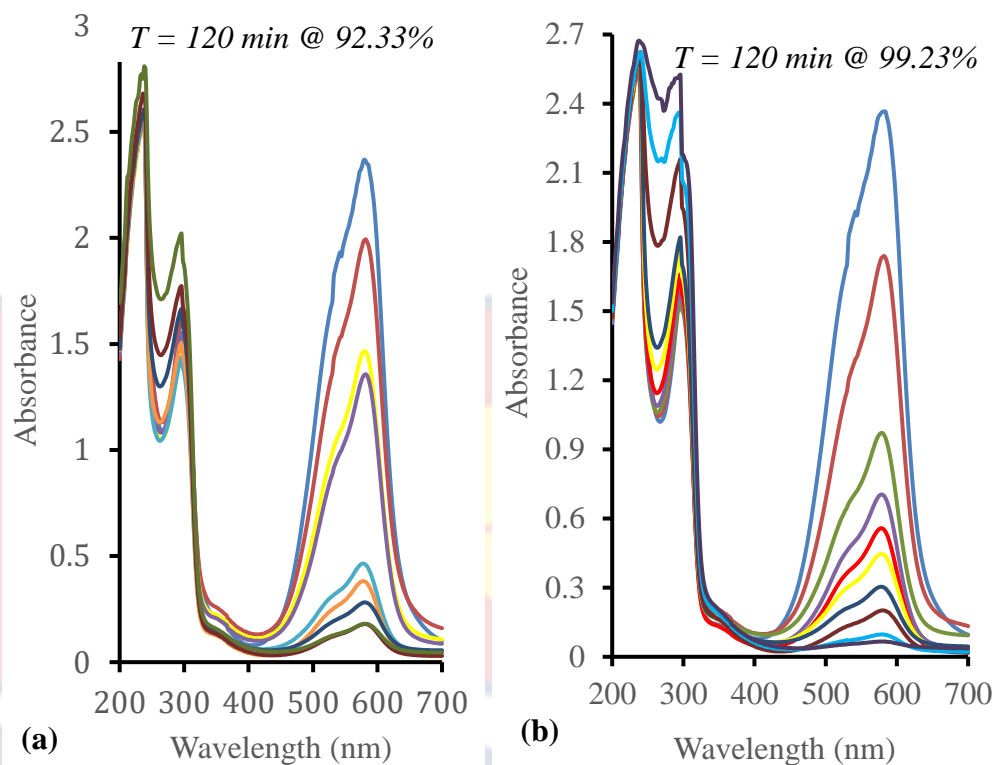
Figure 61: Absorption profiles of the degradation of crystal violet in the presence of ZnPc-GB under (a) daylight (12000 lx) and (b) sunlight (30000 lx) radiations.
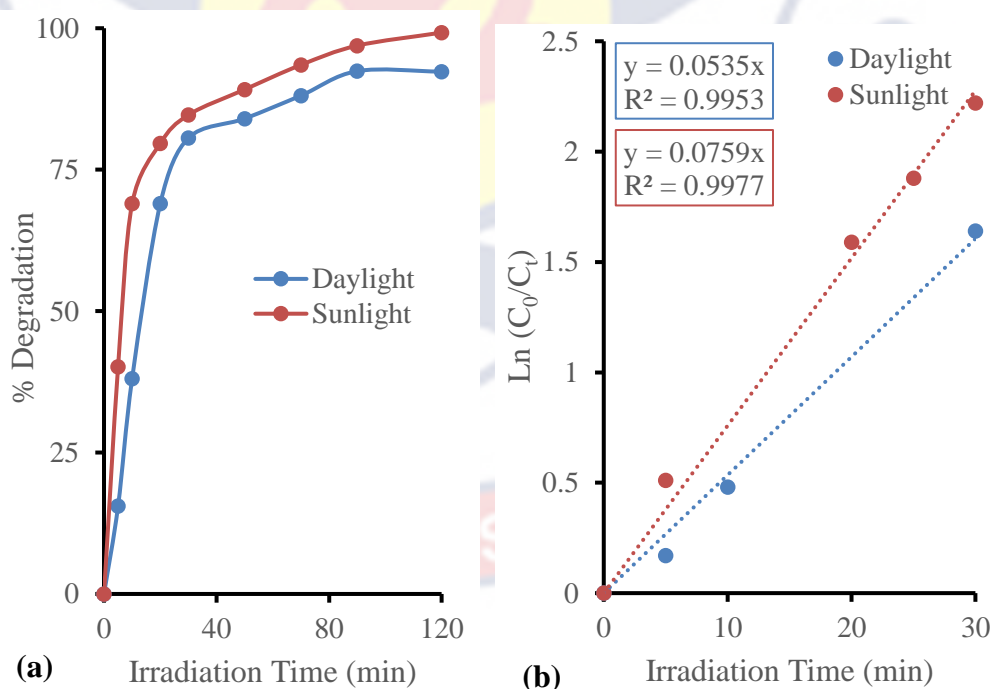
Figure 62: (a) Degradation efficiency of photocatalyst ZnPc-GB vs time under daylight [12000 lx (lm/m^2)] and sunlight [30000 lx (lm/m^2)] radiations and (b) Plots of Ln (C_0/C_t) vs time.

158

The results in Figures 61-62 showed that, photodegradation efficiencies increased with increasing light intensities. Sunlight (high) intensity [30000 lx (lm/m^2)] resulted in a higher photodegradation efficiency of 99.23% in 120 min of irradiation (Figures 61b and 62a), at a rate of 0.0759 min^{-1}, with R^2 of 0.9977 (Figure 62b above) compared with daylight intensity [12000 lx (lm/m^2)] with photodegradation efficiency of 92.33% in 120 min of irradiation (Figures 61a and 62a), at a rate of 0.0535 min^{-1}, with R^2 of 0.9953 (Figure 62b).

Photocatalysts recyclability studies

One of the great advantages of porous heterogeneous catalysts is their potential to be recycled and reused in continuous cycles. Recyclability studies demonstrates, the effectiveness of the ZnPc immobilisation process, which is comparable to the stability of the ZnPc dye. To investigate the durability and stability of functionalised cellulose-based fibre catalysts (ZnPc-GB, ZnPc-OPMF, and ZnPc-PLF), they were subjected to at least 3 cycles of crystal violet dye removal under the same experimental conditions. The results are presented in Figure 63.
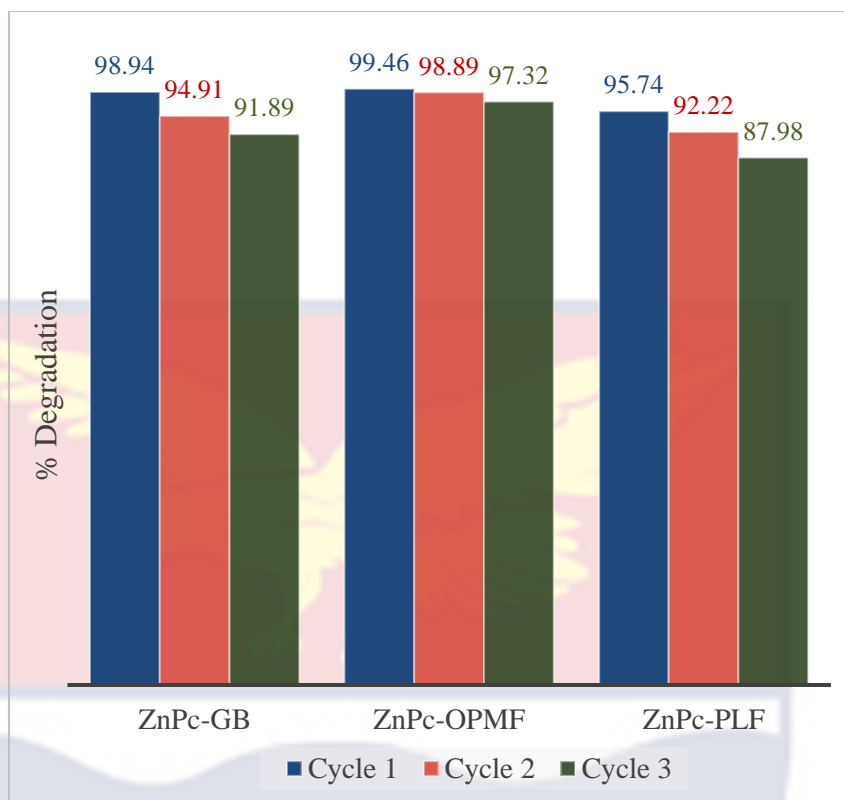
Figure 63: Degradation efficiency of the photocatalyst (ZnPc-GB, ZnPc-OPMF, and ZnPc-PLF) for three successive cycles of crystal violet removal.

In response to the basic motive of immobilising zinc phthalocyanine on the cellulose-based fibres, all the photocatalysts (ZnPc-GB, ZnPc-OPMF, and ZnPc-PLF) showed the ability to be reused for at least three consecutive cycles, without significant loss of the removal efficiency. This shows, the high photostability of the catalysts.

Mechanism of the photodegradation process

The alleged involvement of singlet oxygen in the photodegradation of the crystal violet dye, was evaluated by running photolysis in aqueous solutions and adding sodium azide (NaN$_3$), which is known to quench singlet oxygen to the solutions. The results are presented in Figure 64.
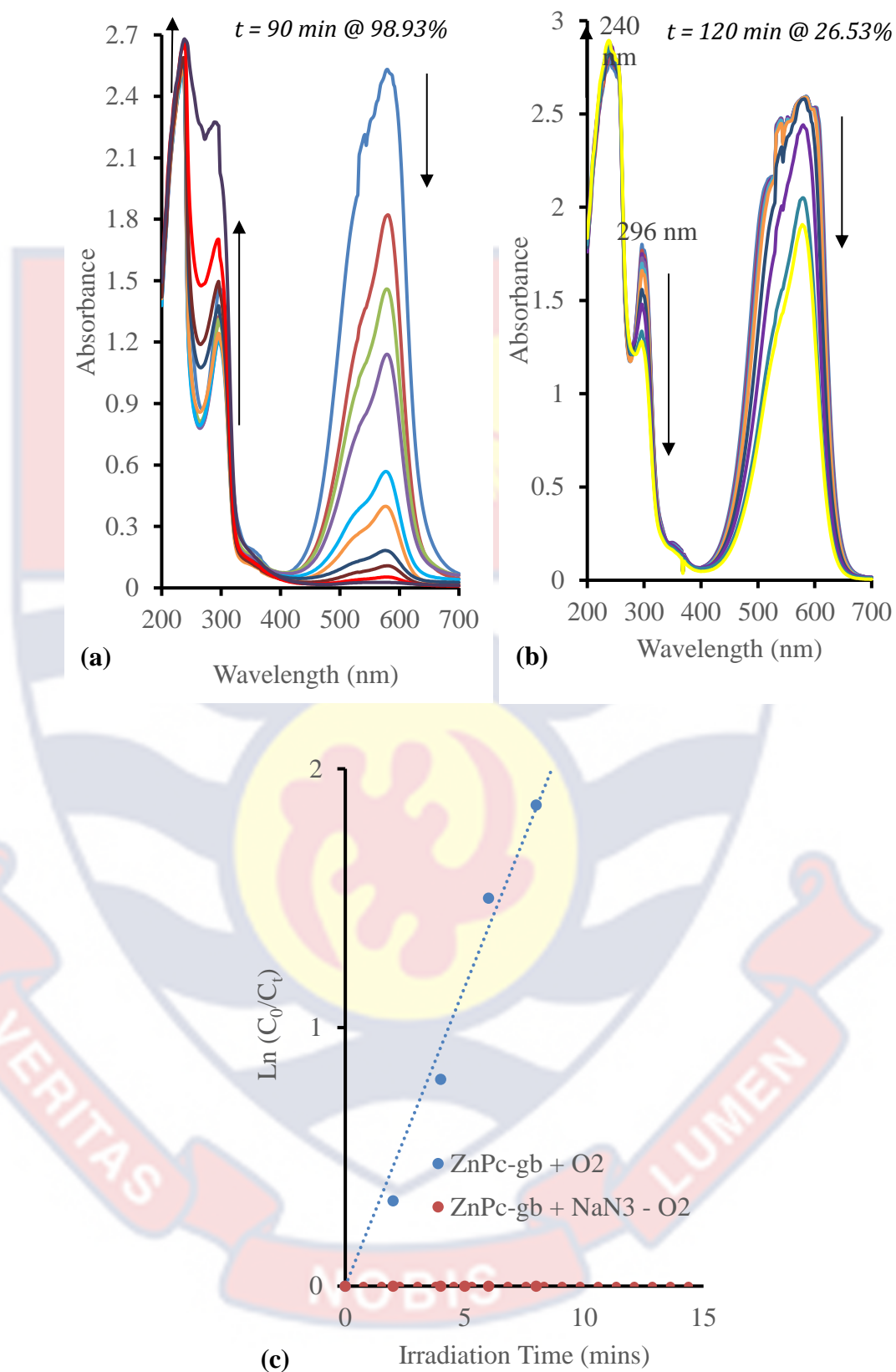
Figure 64: Absorption profiles of the degradation of crystal violet in the presence of (a) 35 mM ZnPc-GB, (b) 35 mM ZnPc-GB + 0.1 M NaN$_3$ - O$_2$, under sunlight radiation and (c) the Plots of Ln (C$_0$/C$_t$) vs time.

161

Figure 64a shows the complete degradation of the crystal violet dye in the presence of ZnPc-GB and oxygen, with degradation efficiency of 98.93% after 90 mins of irradiation. When sodium azide (a singlet oxygen quencher) was added to the crystal violet solution in the presence of ZnPc-GB minus oxygen (in an air-tight reaction vessel), only slight spectral changes were observed after 120 mins of irradiation, with degradation efficiency of 26.52% (Fig. 64b). This is an indication that, singlet oxygen is the key agent involved in the photodegradation process, favouring Type II mechanism.

Linear plots of Ln (C_0/C_t) vs. time of the inhibition process which, follow the first order reaction kinetics (Fig. 61c) are presented in Table 21.

Table 21: Kinetic Data of the Crystal Violet Photodegradation with Quencher (NaN$_3$) and Catalyst (ZnPc-GB, as an example)

Catalysts + quencher	$K_{obs} \times 10^{-2}$ (min^{-1})	Initial Rate (mgL^{-1} min^{-1})	Half-life (min)	$R^2 \times 10^2$
ZnPc-GB + O$_2$	23.12	9.25	3.0	99.29
ZnPc-GB + NaN$_3$ - O$_2$	0	0	0	-

Source: Laboratory Analysis (2016-2021)

The photocatalytic properties of phthalocyanines are due to their ability to produce highly reactive singlet oxygen ($^1O_2$). These highly reactive species are formed in the presence of light and the excited photocatalyst upon exposure to molecular oxygen. Zinc phthalocyanines with the help of light, then convert the triplet-oxygen ($^3O_2$) to singlet oxygen ($^1O_2$), which causes non-radical oxidation of the crystal violet dye (Gao *et al.*, 2014).

The mechanism of the degradation of crystal violet dye (a model organic pollutant) by the photocatalysts (ZnPc-GB, ZnPc-OPMF and ZnPc-PLF) may be described as below:

162

ZnPc-GB (ZnPc-OPMF, ZnPc-PLF) $\xrightarrow{h\nu}$ ^{1}ZnPc*-gb ……………... Eqn. 9

^{1}ZnPc*-GB $\xrightarrow{ISC}$ ^{3}ZnPc*-GB ……….………...………………. Eqn. 10

^{3}ZnPc*-GB + ^{3}O$_2$ → ZnPc-GB + ^{1}O$_2$ ……..…….……………… Eqn. 11

^{1}O$_2$ + CV → Oxidation products ………………………………… Eqn. 12
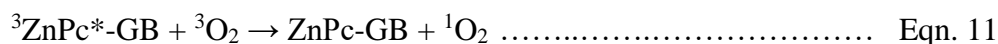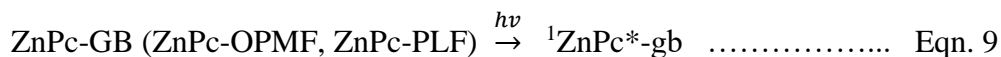
In this process, the zinc phthalocyanine immobilised on the cellulose-based fibre supports (i.e., ZnPc-GB) is excited by sunlight/redlight irradiation to form the singlet excitation state (^{1}ZnPc*-GB), Eqn. 9, and then (^{1}ZnPc*-GB) turn through intersystem crossing into the excited triplet states (^{3}ZnPc*-GB), Eqn. 10. The ^{3}ZnPc*-GB then interact with the ground state triplet oxygen (^{3}O$_2$) to generate the highly active singlet oxygen (^{1}O$_2$) Eqn. 11, which then, leads to the degradation of crystal violet Eqn. 12, (Mousali & Zanjanchi, 2020; Wan *et al.*, 2015).

In summary, when the crystal violet solution was irradiated with light (sunlight/redlight), a hypsochromic shift and decrease in intensity occurred in the visible and ultraviolet peaks. New species were formed with absorbances near 240 nm and 296 nm, which increased with irradiation time (Figures 51 and 52, above). An increase in photodegradation efficiency occurred with increased dissolved oxygen (Figure 52), suggesting that photooxidation is the predominant pathway. The blue shift of the irradiated absorption spectra is attributed to the demethylation of crystal violet to form methyl violet and other methylated pararoanilines (Zakharian, 2000). The general decrease in absorbance in the visible range indicates that decomposition to colourless products occurred in addition to demethylation. The increase in absorbance near 240 nm and 296 nm can be explained by the formation of intermediates in

163

the conversion to colourless products (CO_2 and H_2O). This aligned with the proposed degradation mechanism by Kuramoto & Kitao, (1982) in Figure 65.
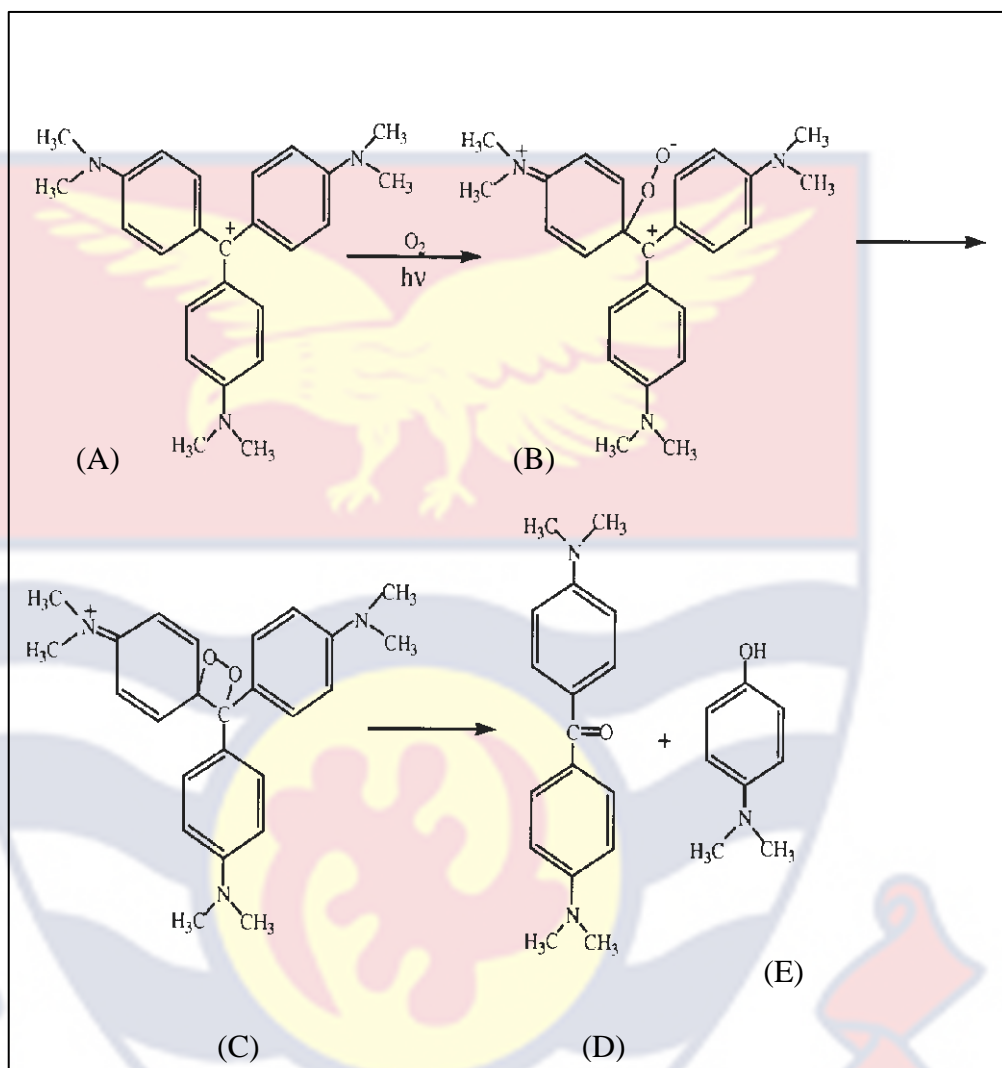
Figure 65: Modified photodegradation mechanism of crystal violet (Kuramoto & Kitao, 1982).

******(A): Crystal Voilet; (B/C): dioxeran intermediates; (D): 4,4-bis(dimethylamino)-benzophenone and (E): p-(dimethylamino)phenol.

Antibacterial Photodynamic Application of the Functionalised Cellulose-Based Fibres In-Vitro

The bacteria samples on the Müeller-Hinton agar plates, were irradiated with both daylight and LED redlight (670 ± 5 nm) sources with irradiances of 400-1500 lx (lm/m^2) and 2000-2500 lx (lm/m^2) respectively, for

164

30 min at ambient temperature. The daylight source was not stable due to inconsistent changes in weather conditions. Nonetheless, the daylight irradiance as low as 400 lx (lm/m^2), was very effective.

The study bacteria strains were subjected to the following treatment regiments: the effect of the functionalised fibre (photosensitiser) alone and the effect of light alone (daylight or LED redlight) as the negative control with 10 µg gentamicin discs as the positive control, the effect of APDT (photosensitiser + light + O$_2$) and the effect of the photosensitiser concentration on the strains in-vitro.

Effect of light alone and the functionalised fibres alone

The bacteria strains were individually given, light-only and photosensitiser-only treatment doses as control treatments.
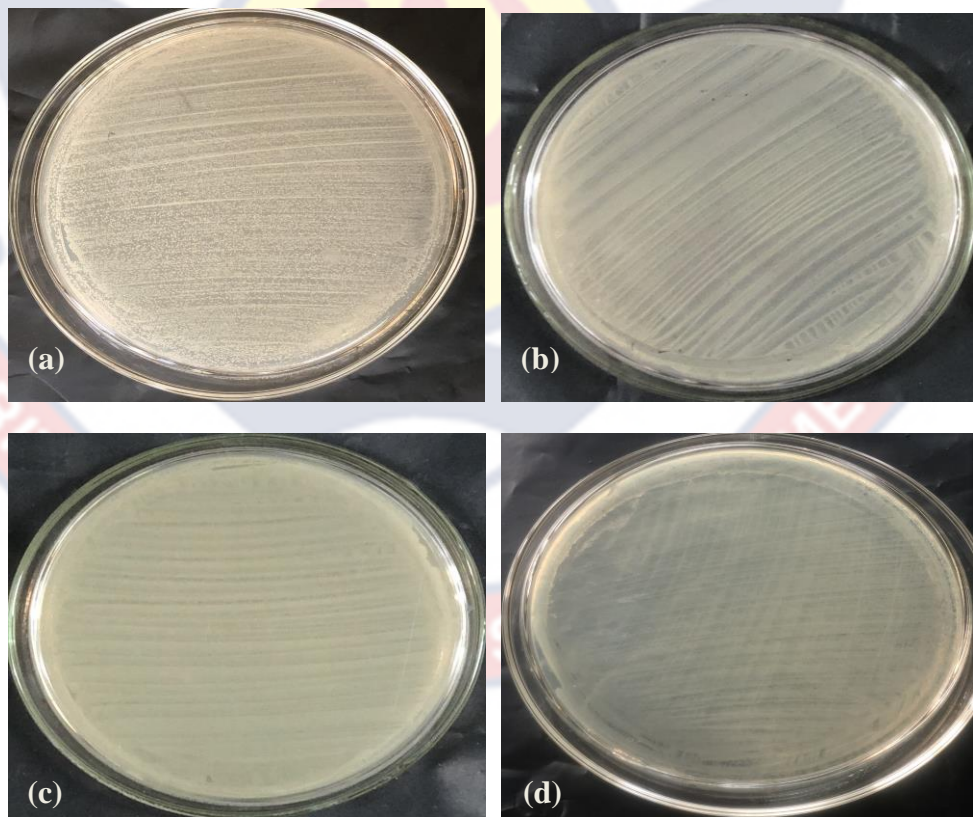
Figure 66: Images of (a) *S. aureus* ATCC 25923, (b) MRSA ATCC 43300, (c) *P. aeruginosa* and (d) *P. aeruginosa* ATCC 27312 after 16-24 hr incubation, under Light-only treatment.

165

Light treatment alone (both daylight and red light) had no effect on the bacteria, as shown in figure 66, corroborating the literature (Catão & Batista 2020). However, *Pseudomonas aeruginosa* ATCC 27312 lost its characteristic blue colour due to high dose of LED redlight source (5000 lx).
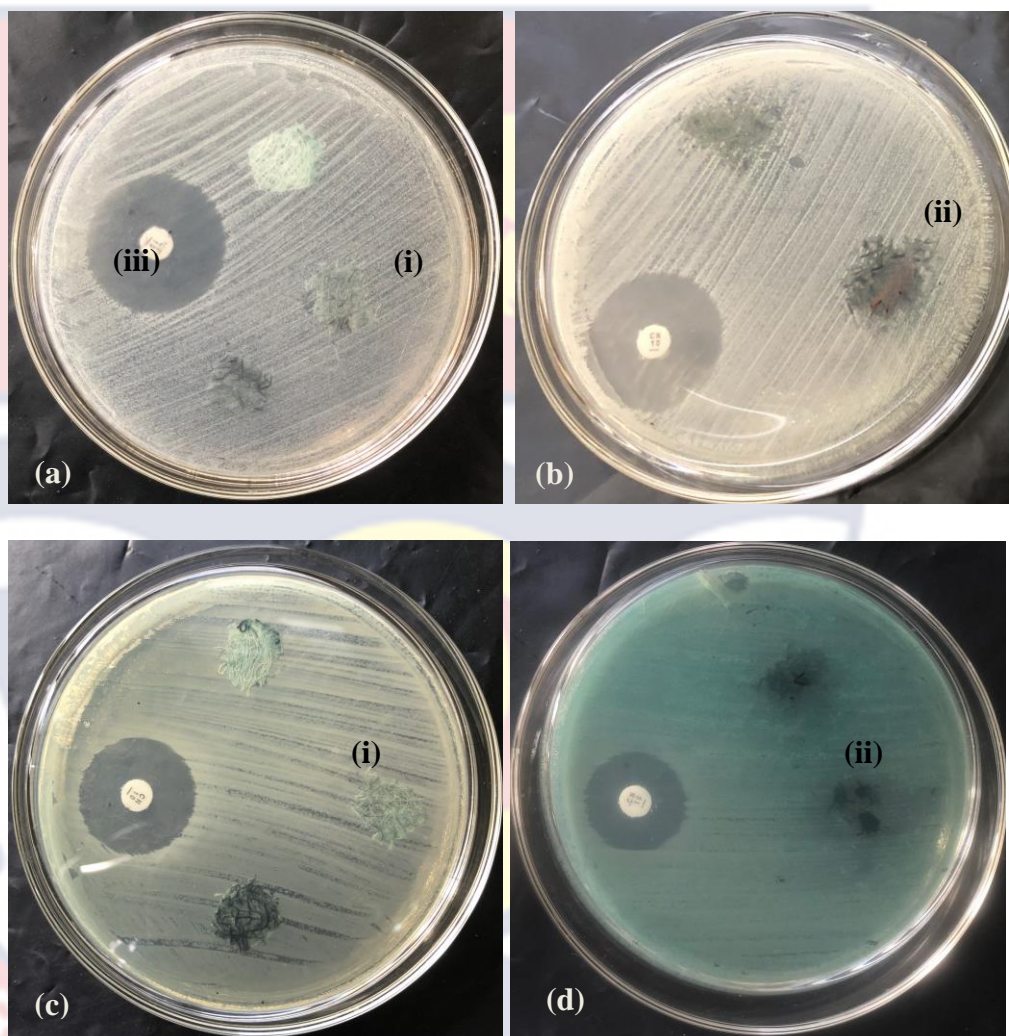
Figure 67: Images of S. aureus ATCC 25923 (a & b) and P. aeruginosa ATCC 27312 (c & d) plates with the functionalised fibre discs (ZnPc-GB (i), ZnPc-OPMF (ii) & Gentamicin (iii)) after 16-24 hr incubation, under dark conditions.

As depicted in figure 67, there was no effect on the bacteria and no zone of inhibition was exhibited, when the functionalised fibres (photosensitizers) alone were used, with 10 µg gentamicin discs as the positive control. Studies have revealed that an important aspect of the antibacterial

166

photodynamic therapy (APDT) is that, the two components (i.e. light and photosensitisers) in combination must work together in order to effectively inactivate bacteria. When used individually, does not affect bacteria in anyway (Burns *et al.*, 1993, Williams *et al.*, 2003, 2004) as observed in this study.

Effect of APDT on bacteria strains in-vitro under daylight irradiation

For photodynamic therapy (PDT) to be successful for antibacterial purposes, it is critical to select a suitable, effective and non-toxic photosensitiser with high absorption capacity, over the period of time the light is used (Meisel & Kocher, 2005). Hence the two components, daylight and the functionalised fibres (photosensitisers) were used in combination to assess their effect on bacteria.

167
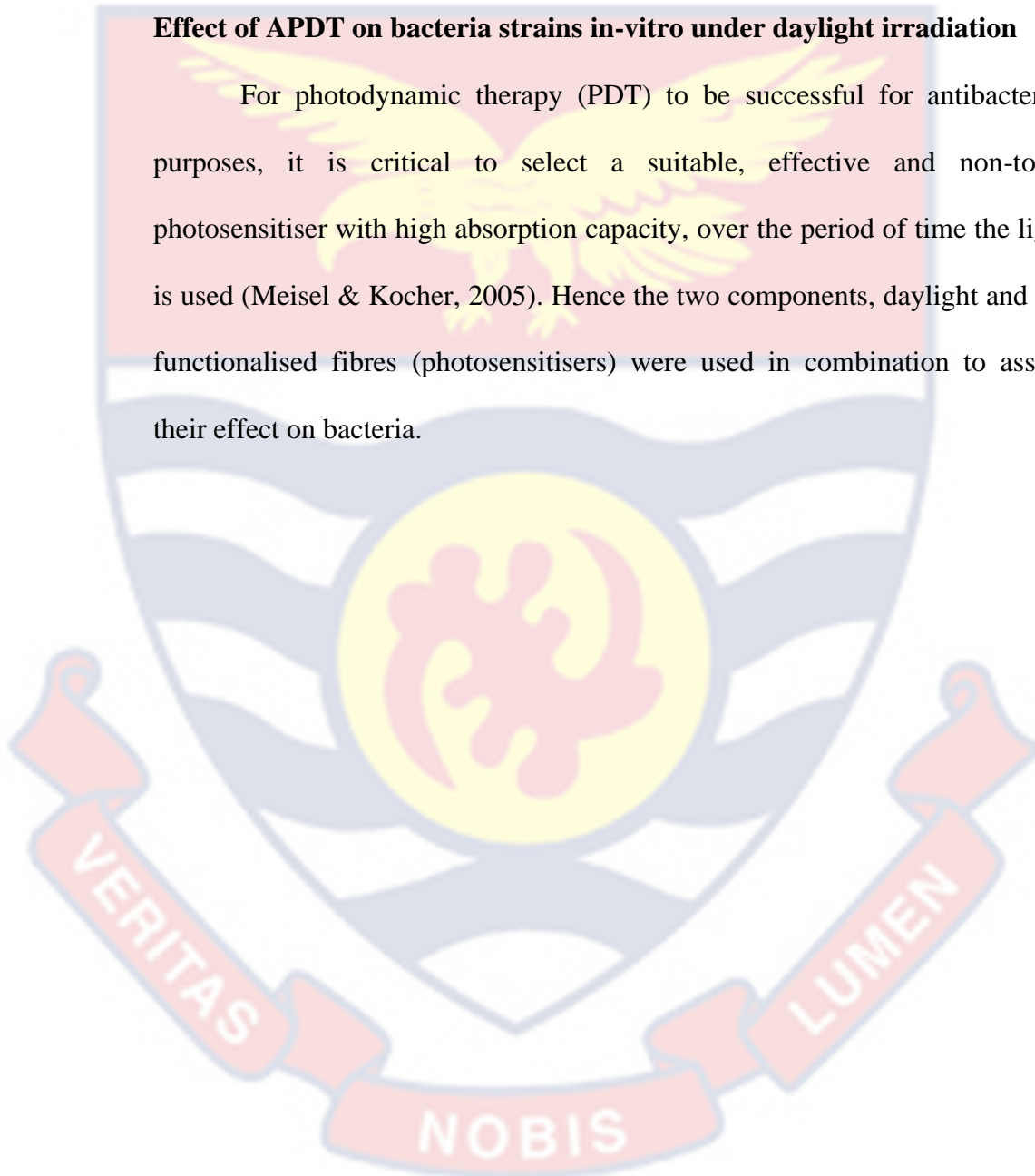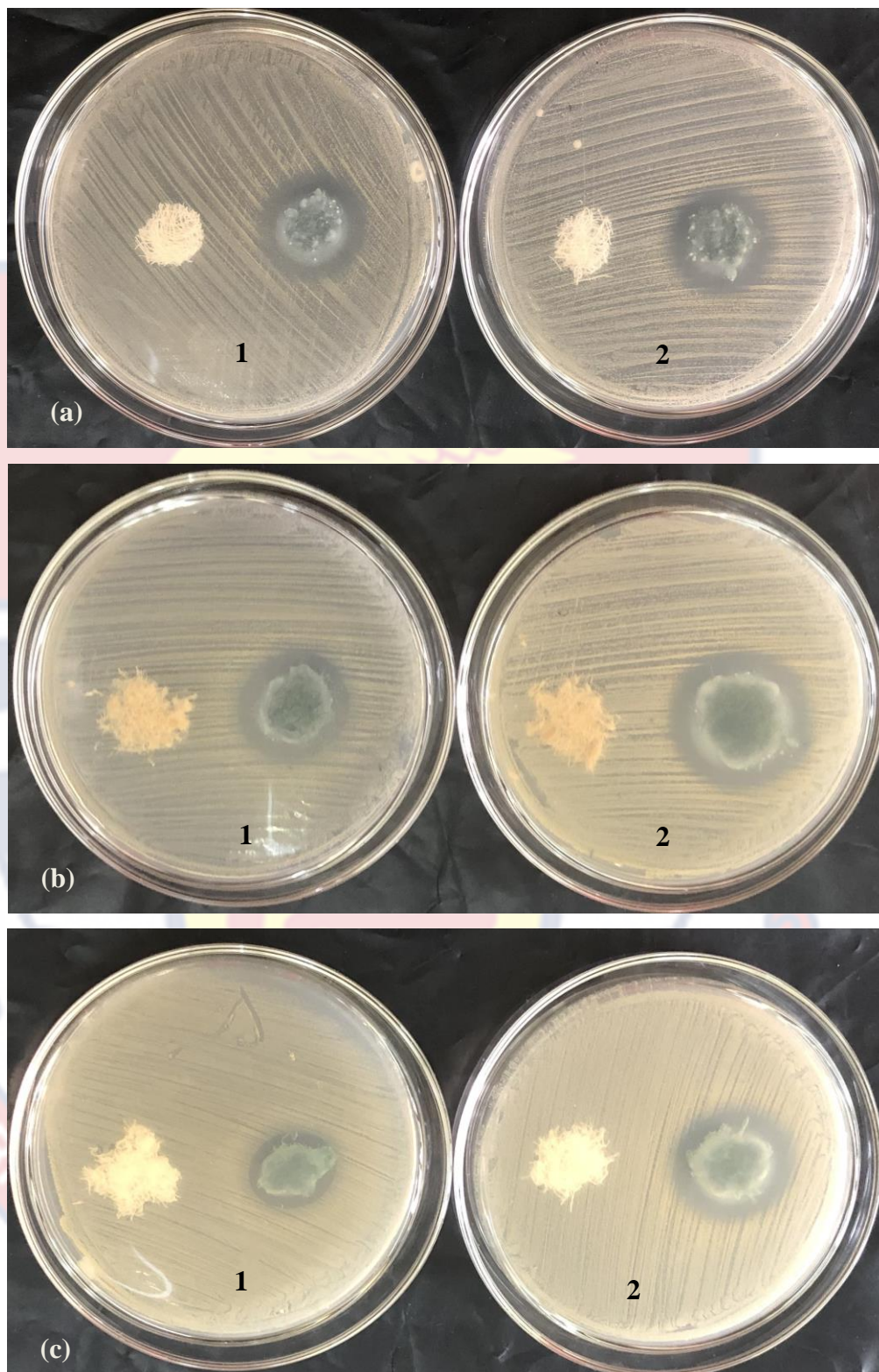
Figure 68: Images of (1) MRSA 3646 and (2) MRSA ATCC 43300 plates with (a) P-GB & ZnPc-GB, (b) B-OPMF & ZnPc-OPMF and (c) B-PLF & ZnPc-PLF discs after 16-24 hr incubation, under daylight irradiation.

For the gram-positive bacteria (*Staph aureus* ATCC 25923, MRSA 3646 and MRSA ATCC 43300) under daylight irradiation, as seen in figures 68 above and 69 below, the plain cellulose-based fibres (P-GB, B-OPMF and B-PLF) did not exhibit any zone of inhibition, meaning that, they do not possess any antibacterial property whilst, the functionalised fibres (ZnPc-GB, ZnPc-OPMF and ZnPc-PLF) effectively, inhibited the bacteria growth with zones of inhibition ranging from 24-35 mm under daylight irradiance as low as 500 – 600 lx (lm/m^2). This confirms the effective immobilisation of zinc phthalocyanine on the plain cellulose-based fibres and their superior antibacterial properties, especially on the resistant strains (MRSA 3646 and MRSA ATCC 43300).
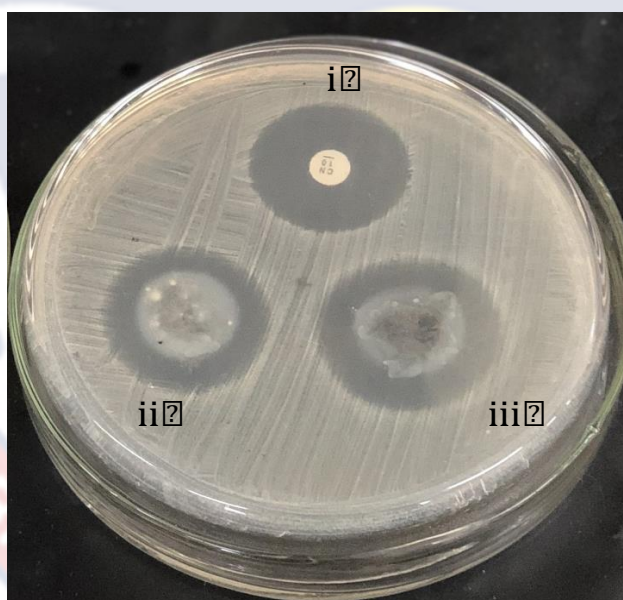
Figure 69: S aureus ATCC 25923 plates with (i) Gentamicin, (ii) ZnPc-OPMF and (iii) ZnPc-GB discs after 16-24 h incubation, under daylight irradiation.

169
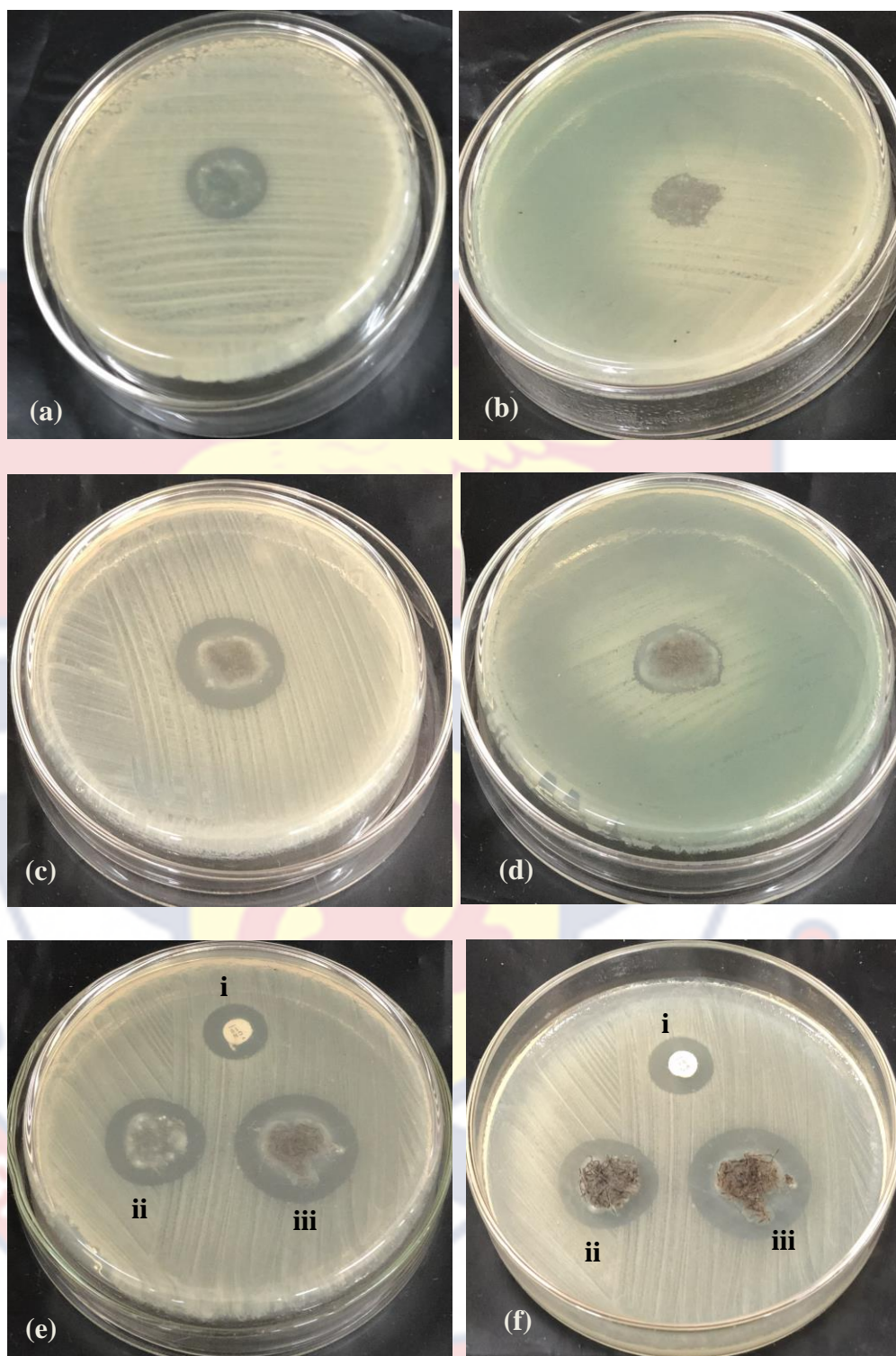
Figure 70: (a & c) *P. aeruginosa* and (b & d) *P. aeruginosa* ATCC 27312 plates with ZnPc-GB (a & b) and ZnPc-OPMF (c & d) discs and *P. aeruginosa* plates (e & f) with (i) GN, (ii) ZnPc-GB & (iii) ZnPc-OPMF discs after 24 h incubation, under daylight irradiation.

For the gram-negative bacteria (*P. aeruginosa* and *P. aeruginosa* ATCC 27312) under daylight irradiation, all the functionalised fibres (ZnPc-

170

GB, ZnPc-OPMF as example) effectively inhibited *P. aeruginosa* (clinical isolate) with zones of inhibition ranging from 21-26 mm, but the *P. aeruginosa* ATCC 27312 was not inhibited, as depicted in Figure 70, above. Perhaps because, the concentration of the photosensitiser needed to cause bactericidal effects were too small or because of its complex structure (Awad *et al.*, 2016). This corroborates other reports (Catão & Batista, 2020; Huang *et al.*, 2010; Tseng *et al.*, 2009) in the literature that, may be justified by the difficulty of obtaining inhibitory or bactericidal effects in gram-negative bacterial species, especially P. aeruginosa. The binding and uptake of photosensitisers into bacterial cells varies by bacterial species. The special structure of the cell envelope makes Gram-positive pathogens much more sensitive to anionic and neutral photosensitisers due to the thick and porous layer of peptidoglycan on their outer surface (Tim, 2015). Gram-negative bacteria on the other hand, are known to be relatively resistant to neutral or anionic drugs (Malik *et al.*, 1990; Minnock *et al.*, 1996), and require a disturbance of the cytoplasmic membrane to render them sensitive to anionic or neutral photosensitisers (Nitzan *et al.*, 1992) and zinc phthalocyanine is a neutral photosensitiser. However, the reduced susceptibility of gram-negative bacteria *P. aeruginosa* was overcome in this study, by the use of the functionalised cellulose-based fibres (immobilised zinc phthalocyanine) which, may be attributed to their porous and hydrophilic nature.

Effect of APDT on bacteria strains in-vitro under redlight irradiation

The two components i.e. LED redlight and the functionalised fibres (photosensitisers) were also, applied in combination to assess their effect on bacteria.

171
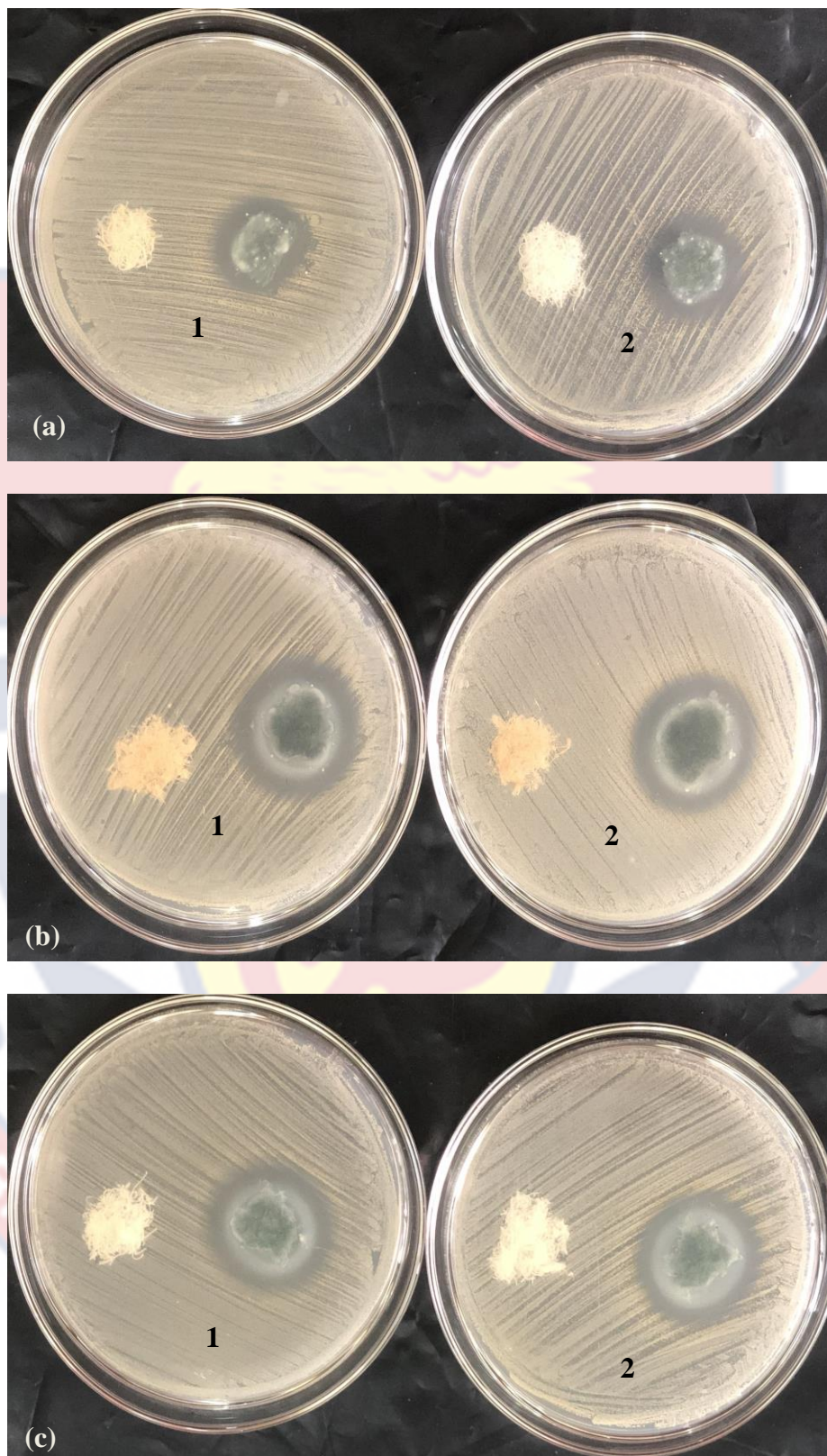
Figure 71: Images of (1) MRSA 3646 and (2) MRSA ATCC 43300 plates with (a) P-GB & ZnPc-GB, (b) B-OPMF & ZnPc-OPMF and (c) B-PLF & ZnPc-PLF discs after 16-24 hr incubation, under redlight irradiation.

172

For the gram-positive bacteria (*Staph aureus* ATCC 25923, MRSA 3646 and MRSA ATCC 43300) under redlight irradiation, as seen in Figure 71 above, the plain cellulose-based fibres (P-GB, B-OPMF and B-PLF) did not exhibit any zone of inhibition, meaning that they do not possess any antibacterial property whilst, the functionalised fibres (ZnPc-GB, ZnPc-OPMF and ZnPc-PLF) effectively inhibited the bacteria growth with zones of inhibition ranging from 24-35 mm under redlight irradiance ranging between 1500-2500 lx (lm/m^2). This confirms the effective immobilisation of Zinc phthalocyanine on the plain cellulose fibres and their superior antibacterial properties especially, on the resistant strains (MRSA 3646 and MRSA ATCC 43300).
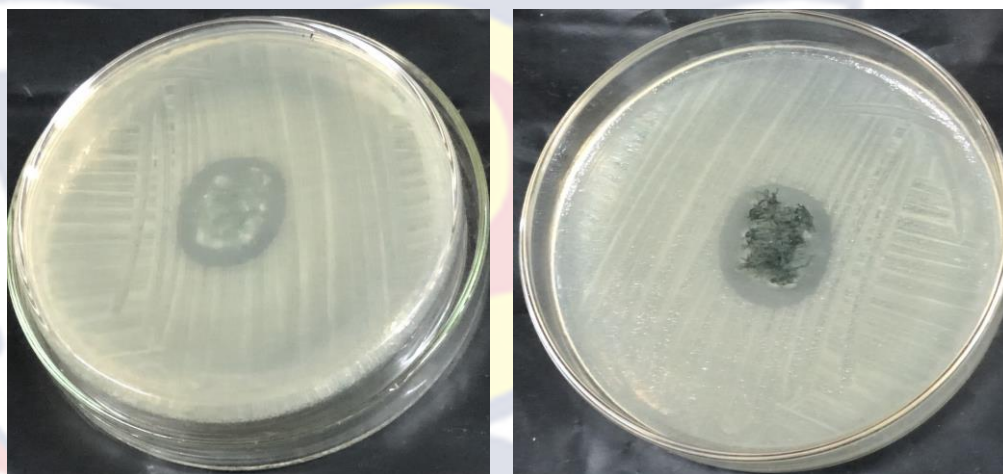
Figure 72: *P. aeruginosa* plate with ZnPc-GB disc after 24 hr incubation, under redlight irradiation.

For the gram-negative bacteria (*P. aeruginosa* and *P. aeruginosa* ATCC 27312) under redlight irradiation, all the functionalised fibres (ZnPc-GB as example, Figure 72) effectively inhibited *P. aeruginosa* (clinical isolate) with zone of inhibition around 22 mm, but the P. aeruginosa ATCC 27312 was not inhibited. Perhaps because, the concentration of the

173

photosensitiser needed to cause a bactericidal effect was too small or because of its' complex structure (Awad *et al.*, 2016). This supports other reports (Catão & Batista, 2020; Huang *et al.*, 2010; Tseng *et al.*, 2009) in the literature that, may be justified by the difficulty of obtaining inhibitory or bactericidal effects in gram-negative bacterial species, especially *P. aeruginosa.*

Several studies have shown that Gram-negative organisms such as *Pseudomonas aeruginosa* are less susceptible to APDT and much more difficult to treat (Sperandio *et al.*, 2013). The difference in susceptibility of Gram-negative and Gram-positive bacteria to APDT may be due to their physiology. The cell wall of Gram-negative bacteria consists of an inner and outer cytoplasmic membrane of a multi-layered complex consisting of a glycocalyx, an outer membrane lipid bilayer, a lipopolysaccharide, a periplasm, a peptidoglycan cell wall, and a cell membrane lipid bilayer. In particular, lipopolysaccharide (LPS) acts as an effective permeability barrier between cells and their environment, tending to restrict attachment and penetration of most photosensitiser structures (Hancock, 1997; Jori, 2006; Maisch *et al.*, 2004; Minnock *et al.*, 2000). Gram-positive bacteria, on the other hand, have a cytoplasmic membrane composed of a porous cell wall made of peptidoglycan and lipoteichoic acid which, are less effective permeation barriers for photosensitiser structures (Jori & Brown, 2004; Minnock *et al.*, 2000) and are therefore more sensitive to APDT.

Effect of photosensitiser concentration on bacteria

Four different photosensitiser (functionalised cellulose-based fibre) concentrations ranging from 8.5 µM-14 mM were applied to assess their effect on the bacteria using ZnPc-GB as an example.
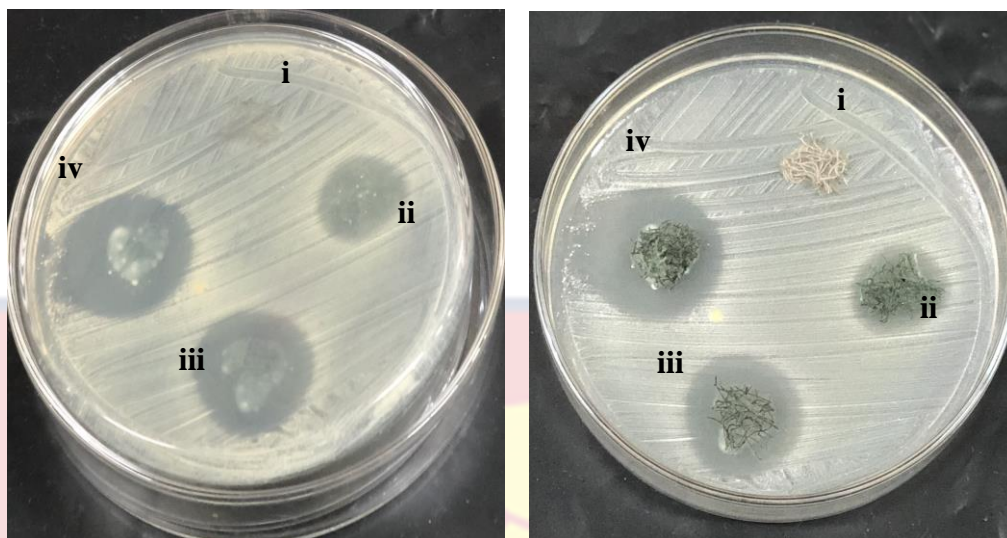
Figure 73. *S. aureus* ATCC 25923 plate with (i) 8.5 µM ZnPc-GB, (ii) 3.5 mM ZnPc-GB, (iii) 7 mM ZnPc-GB and (iv) 14 mM ZnPc-GB discs after 16-24 hr incubation, under both Light Conditions.

A concentration-dependent response was observed with all the functionalised fibres in all the bacteria strains except for the *P. aeruginosa* ATCC 27312 strain (which, did not exhibit antibacterial effect), and the APDT activity was found to increase with increasing concentration of the amount of zinc phthalocyanine on the functionalised cellulose-based fibres, under both light conditions as depicts in Figure 73 and Table 21 below, using daylight irradiance at 1000-1400 lx (lm/m^2), ZnPc-GB and *S. aureus* ATCC 25923 as examples. Unfortunately, the exact amount of photosensitiser that was adsorbed/immobilised on the cellulose-based fibre discs could not be quantified.

Table 22 presents, the zone of inhibition (ZOI) of MRSA ATCC 43300, *S. aureus* ATCC 25923 and *P. aeruginosa* with ZnPc-GB discs at various concentrations.

175

Table 22: Zone of Inhibition (ZOI) of MRSA ATCC 43300, S. aureus ATCC 25923 and P. aeruginosa with ZnPc-GB Discs at Various Concentrations

Bacteria Strain	ZnPc-GB Discs	ZOI (mm)
MRSA ATCC 43300	8.5 µM	0
	3.5 mM	15
	7.0 mM	25
	14.0 mM	30
S. aureus ATCC 25923	8.5 µM	0
	3.5 mM	17
	7.0 mM	22
	14.0 mM	23
P. aeruginosa	8.5 µM	0
	3.5 mM	15
	7.0 mM	23
	14.0 mM	25

Source: Laboratory Analysis (2016-2021)

Comparison of light sources

The effect of both daylight and LED redlight sources on the bacteria activity were also compared to ascertain, which of the two light sources was more efficient. The results are presented in Table 23.

176

Table 23: APDT Activities under Daylight and Redlight Irradiances

Bacteria Strain	ZnPc-fibre Discs	Zone of Inhibition (mm)	
		Daylight	Redlight
MRSA 3646	ZnPc-GB	24	24
	ZnPc-OPMF	25	30
	ZnPc-PLF	28	29
	10 µg GN	23	23
MRSA ATCC 43300	ZnPc-GB	23	25
	ZnPc-OPMF	31	30
	ZnPc-PLF	28	29
	10 µg GN	20	20
S. aureus ATCC 25923	ZnPc-GB	18	20
	ZnPc-OPMF	35	33
	ZnPc-PLF	35	35
	10 µg GN	27	27
P. aeruginosa	ZnPc-GB	21	22
	ZnPc-OPMF	26	-
	10 µg GN	18	18
P. aeru ATCC 27312	ZnPc-GB	0	0
	ZnPc-OPMF	0	0
	ZnPc-PLF	0	0

Source: Laboratory Analysis (2016-2021)

The daylight and LED redlight sources (670 ± 5 nm) combined with the photosensitiser, showed similar inhibitory effects on the bacterial strains (except P. aeruginosa ATCC 27312) regardless of the intensities at ambient temperature (Table 23 above). Although, the daylight source was unstable throughout the research, due to inconsistent weather conditions, it was just as effective as the LED redlight source (670 ± 5 nm) even, at intensities as low as 500-600 lx (lm/m^2). Perhaps because, daylight is part of the visible section of

177

the electromagnetic spectrum, that emits electromagnetic radiation at broad wavelengths between 380 and 750 nm (Starr *et al.*, 2005) and therefore, could emit light that matches the exact light absorption wavelength of the Zinc phthalocyanine (photosensitiser). The photosensitiser is usually activated upon exposure to light of a specific wavelength corresponding to its own peak absorption wavelength (Tedesco *et al.*, 2003). The LED redlight used for this study has a light emission at λ_{max} 670 nm which, equals the light absorption (λ_{max}670nm) of the photosensitiser (zinc phthalocyanine). Therefore, good energy transfer from the electrical phase to the photosensitiser was ensured. LEDs convert electrical energy with high efficiency in the photon domain at suitable wavelengths (Ye *et al.*, 2017). The stronger the light absorbed by the photosensitiser at the right wavelength, the higher the efficiency of the quantum excited state and the ROS (Rak *et al.*, 2019), thereby improving the bacterial inhibition rate.

In summary, APDT with daylight and LED redlight sources (670 ± 5 nm) along with the functionalised fibres showed similar antibacterial effects against the methicillin/multidrug resistant strains, *Staphylococcus aureus* ATCC 25923, MRSA 3646, MRSA ATCC 43300 and *Pseudomonas aeruginosa* except *P. aeruginosa* ATCC 27312. Daylight and redlight sources alone did not show antibacterial effects against any of the strains used. Both daylight and LED redlight sources (670 ± 5 nm) combined with the photosensitiser exhibited similar inhibitory effects on the bacterial strains (except P. aeruginosa ATCC 27312) regardless of the intensities at ambient temperature.

The whitish film seen around the functionalised fibre discs in all the results, may be due to aggregation, which results in quenching, as a result of stacking up of the fibres on the bacterial samples in the agar plate instead of spreading them out (Jia *et al.*, 2019). Nevertheless, all the functionalised cellulose-based fibres (ZnPc-GB, ZnPc-OPMF and ZnPc-PLF) showed effective photodynamic antibacterial activity against methicillin/multidrug resistant strains, Staph aureus ATCC 25923, MRSA 3646, MRSA ATCC 43300 and the clinical isolate Pseudomonas aeruginosa.

Activated photosensitisers can induce photosensitisation near bacterial cells. When the photosensitiser is absorbed by the bacterial cell, the site of damage to the light depends on its subcellular location (Minnock *et al.*, 1996). Various cellular components can be attacked, including amino acids (mainly cysteine, histidine, tryptophan, tyrosine and methionine), nucleosides (mainly guanine) and unsaturated lipids, that can react with $^1O_2$ (Girotti, 2001). The diffusion distance of $^1O_2$ is up to 75 nm (Moan, 1990; Ouedraogo & Redmond, 2003) hence, the use of immobilised support may lead to more efficient photosensitisation.

In life, countless skin injuries occur due to accidents, illnesses, post-surgery, etc. In many cases, many progress to a chronic stage (may not heal within 6 weeks) and are often complicated by infections (Bowler *et al.*, 2001). Chronic injuries are very common, painful for patients and expensive to treat, antimicrobial photodynamic therapy (APDT) therefore, may come as a cheaper alternative.

Chapter Summary

A zinc phthalocyanine complex was synthesised using microwave irradiation and characterised using various techniques. The dye is photoactive, fluorescent, and can generate singlet oxygen, a key agent in photosensitisation processes. Natural cellulose-based fibres (B-OPMF and B-PLF) were extracted from oil palm mesocarp fibers and pineapple leaves wastes. The synthesised zinc phthalocyanine was incorporated into these fibres to make them functional, exhibiting the fluorescence behavior, photoactivity and singlet oxygen producing capacity characteristic of the zinc phthalocyanine. These functionalised cellulose-based fibres were used for gas detection, photodegradation, and photodynamic inactivation of bacteria.

CHAPTER FIVE

SUMMARY, CONCLUSIONS AND RECOMMENDATIONS

Overview

Zinc phthalocyanine dye is fluorescent, photoactive and can produce singlet oxygen, an essential component of most photosensitisation processes. Nonetheless, its solubility is restricted in physiological, aqueous, and certain organic solvents, due to its hydrophobic and insoluble nature. Consequently, immobilisation on suitable solid supports that can display their photosensitising qualities as in solution will aid in resolving the problems associated with aqueous solution aggregation, recovery, and disposal. Thus, using microwave irradiation, the monomeric unsubstituted zinc phthalocyanine complex was synthesised and characterised using a variety of methods. Next, oil palm mesocarp fibres and pineapple leaves wastes were processed to create environmentally friendly natural cellulose-based fibres which, were then utilised as supports to help the zinc phthalocyanine dye become immobile. The now-functionalised cellulose-based were found to exhibit all the dye's characteristic features as in solution, due to their porous nature therefore, were used for qualitative gas detection, photodegradation of crystal violet dye in solutions, and photodynamic inactivation of bacteria in vitro.

Summary

Zinc phthalocyanine dye was synthesised and incorporated into porous natural cellulose-based fibres and applied for optical detection of nitrogen dioxide, photodegradation of crystal violet dye in aqueous media and invitro photodynamic antibacterial tests. The zinc phthalocyanine-functionalised

181

fibres were able to qualitatively sense nitrogen dioxide gas through fluorescence quenching; able to degrade crystal violet dye, an organic pollutant, in aqueous media under both sunlight and LED redlight irradiations, without using extra oxidizing agent and proved to be effective antibacterial agents against methicillin/multidrug resistant strains, *Staph aureus* ATCC 25923, MRSA 3646, MRSA ATCC 43300 and a clinical isolate *Pseudomonas aeruginosa* under both daylight and LED redlight irradiations.

Conclusions

In this study, zinc (II) phthalocyanine complex was synthesised using microwave irradiation and characterised by various spectroscopic, microscopic and thermal techniques. The results confirmed the synthesis of the monomeric unsubstituted zinc phthalocyanine dye. The photophysical and photochemical analysis showed tha, it is photoactive, has fluorescence and can also generate singlet oxygen, the principal agent, involved in most photosensitisation processes.

Natural cellulose-based fibres (B-OPMF and B-PLF), which were intended for use as supports for the immobilisation of zinc phthalocyanine, were extracted from oil palm mesocarp fibres and pineapple leaves wastes and purified. The extracted fibres were taken through spectroscopic, microscopic and thermal characterisation to establish their cellulosic nature. The results confirmed that, pure cellulose was successfully extracted from the raw fibre wastes, when compared with the commercial cotton gauze bandage as the reference cellulose.

The synthesised zinc phthalocyanine was incorporated into the extracted natural cellulose-based fibres and characterised as before. The

results showed that the zinc phthalocyanine was successfully embedded and well distributed within the cellulose-based fibres.

The photophysical and photochemical properties of the cellulose-based fibres, functionalised with zinc phthalocyanine (ZnPc-GB, ZnPc-OPMF and ZnPc-PLF) were also assessed. They were found to exhibit the same fluorescence behaviour, that is characteristic of the zinc phthalocyanine in solution. Thus, making them promising fibres for qualitative detection of gases through fluorescence quenching. Also, the photoactivity and the singlet oxygen producing capacity of the zinc phthalocyanine was sustained within their matrices. Therefore, making them promising fibre materials for most photosensitisation applications.

The zinc phthalocyanine-functionalised cellulose-based fibres (ZnPc-GB, ZnPc-OPMF and ZnPc-PLF) could qualitatively sense nitrogen dioxide gas through fluorescence quenching.

The zinc phthalocyanine-functionalised cellulose-based fibres (ZnPc-GB, ZnPc-OPMF and ZnPc-PLF) were found to be promising fibres for the photodegradation of crystal violet dye, an organic pollutant under both sunlight and LED redlight irradiations in aqueous media without the aid of extra oxidising agent.

The zinc phthalocyanine-functionalised cellulose-based fibres (ZnPc-GB, ZnPc-OPMF and ZnPc-PLF) showed effective photodynamic antibacterial activity against methicillin/multidrug resistant strains, *Staphylococcus aureus* ATCC 25923, MRSA 3646, MRSA ATCC 43300 and a clinical isolate *Pseudomonas aeruginosa* under both daylight and LED

183

redlight irradiations and could therefore, be applied as topical antibacterial fibres for wound healing using daylight irradiation as a cheaper alternative.

Normal daylight source was as effective as the LED redlight source (670 ± 5 nm) in the photodegradation and photodynamic applications. Therefore, normal daylight source can be used in place of redlight as a cost-effective alternative.

Recommendations

The findings of this study led to the identification of some areas that required additional research. These recommendations include:

1. Cellulose is abundant and related to green chemistry. However, cellulosic phthalocyanines that can increase the effective surface area of the catalyst by reducing various accumulation states are rare. Thus, the porosity and catalyst loading of these cellulose fibres can be studied, along with the efficiency of the photocatalytic reaction (moles of contaminant substrate converted by moles of catalyst), and other conditions that affect fibre quality.

2. Pre-treatment of the Gram (-) bacterial with membrane-disrupting agents such as ethylenediaminetetraacetic acid (EDTA) or Polymyxin Nonapeptide PMNP together with the neutral ZnPc-cellulose fibres or the use of cationic conjugated ZnPc-cellulose fibres for the APDT, will help with the complete inactivation of the Gram-negative bacteria.

184

REFERENCES

Abate, S., Barbera, K., Centi, G., Lanzafame, P., & Perathoner, S. (2016). Disruptive catalysis by zeolites. *Catalysis Science & Technology*, *6*(8), 2485-2501.

Abbas, H. A., Nasr, R. A., Abu-Zurayk, R., Al Bawab, A., & Jamil, T. S. (2020). Decolourization of crystal violet using nano-sized novel fluorite structure Ga2Zr2− x W x O7 photocatalyst under visible light irradiation. *Royal Society open science*, *7*(3), 191632.

Abbasi, M., Amiri, R., Bordbar, A. K., Ranjbakhsh, E., & Khosropour, A. R. (2016). Improvement of the stability and activity of immobilized glucose oxidase on modified iron oxide magnetic nanoparticles. *Applied Surface Science*, *364*, 752-757.

Abdullah, M. A., Nazir, M. S., Raza, M. R., Wahjoedi, B. A., & Yussof, A. W. (2016). Autoclave and ultra-sonication treatments of oil palm empty fruit bunch fibers for cellulose extraction and its polypropylene composite properties. *Journal of Cleaner Production*, *126*, 686-697.

Ackroyd, R., Kelty, C., Brown, N., & Reed, M. (2001). The history of photodetection and photodynamic therapy. *Photochemistry and photobiology*, *74*(5), 656-669.

Agboola, B. O. (2007). Catalytic activities of Metallophthalocyanines towards detection and transformation of pollutants. Unpublished doctoral dissertation, Faculty of Science, Rhodes University, South Africa.

Agboola, B., Ozoemena, K. I., & Nyokong, T. (2006). Comparative efficiency of immobilized non-transition metal phthalocyanine photosensitizers for the visible light transformation of chlorophenols. *Journal of Molecular Catalysis A: Chemical*, *248*(1-2), 84-92.

Ahsen, A. Ş., Segade, A., Velasco, D., & Öztürk, Z. Z. (2009). Liquid crystal porphyrins as chemically sensitive coating materials for chemical sensors. *Journal of Porphyrins and Phthalocyanines*, *13*(11), 1188-1195.

Akash, M. S. H., & Rehman, K. (2020). Differential scanning calorimetry. *Essentials of pharmaceutical analysis*, 199-206.

Alam, K. M., Kumar, P., Gusarov, S., Kobryn, A. E., Kalra, A. P., Zeng, S., ... & Shankar, K. (2020). Synthesis and characterization of zinc phthalocyanine-cellulose nanocrystal (CNC) conjugates: toward highly functional CNCs. *ACS Applied Materials & Interfaces*, *12*(39), 43992-44006.

Altomare, A., Corriero, N., Cuocci, C., Falcicchio, A., Moliterni, A., & Rizzi, R. (2015). QUALX2. 0: a qualitative phase analysis software using the freely available database POW_COD. *Journal of Applied Crystallography*, *48*(2), 598-603.

Alzeer, J., Roth, P. J., & Luedtke, N. W. (2009). An efficient two-step synthesis of metal-free phthalocyanines using a Zn (II) template. *Chemical communications*, (15), 1970-1971.

Amissah, N. A., van Dam, L., Ablordey, A., Ampomah, O. W., Prah, I., Tetteh, C. S., ... & Stienstra, Y. (2017). Epidemiology of Staphylococcus aureus in a burn unit of a tertiary care center in Ghana. *PloS one*, *12*(7), e0181072.

Anaya-Plaza, E., van de Winckel, E., Mikkilä, J., Malho, J. M., Ikkala, O., Gulías, O., ... & de la Escosura, A. (2017). Photoantimicrobial biohybrids by supramolecular immobilization of cationic phthalocyanines onto cellulose nanocrystals. *Chemistry–A European Journal*, *23*(18), 4320-4326.

Angel, D. E., Lloyd, P., Carville, K., & Santamaria, N. (2011). The clinical efficacy of two semi-quantitative wound-swabbing techniques in identifying the causative organism (s) in infected cutaneous wounds. *International wound journal*, *8*(2), 176-185.

Arnold, D. R., Baird, N. C., Bolton, J. R., Brand, J. C. D., Jacobs, P. W. M., de Mayo, P., Ware, W. R. (1974). *Photochemistry – an Introduction (Photochemie-Eine Einführung)*. 283 S., 44 Abb., 14 Tab. Academic Press, Inc., New York, London.

Artarsky, S., Dimitrova, S., Bonnett, R., & Krysteva, M. (2006). Immobilization of zinc phthalocyanines in silicate matrices and investigation of their photobactericidal effect on E. coli. *The Scientific World Journal*, *6*, 374-382.

Awad, M. M., Tovmasyan, A., Craik, J. D., Batinic-Haberle, I., & Benov, L. T. (2016). Important cellular targets for antimicrobial photodynamic therapy. *Applied microbiology and biotechnology*, *100*, 7679-7688.

187

Awaji, A. I., Köksoy, B., Durmuş, M., Aljuhani, A., & Alraqa, S. Y. (2018). Novel hexadeca-substituted metal free and zinc (II) phthalocyanines; design, synthesis and photophysicochemical properties. *Molecules*, *24*(1), 77.

Bannwarth, W. (2004). *Immobilized Catalysts: Solid Phases, Immobilization and Applications* (Vol. 242). Springer Science & Business Media.

Barthel, M., & Hanack, M. (2000). Axially substituted titanium (IV) phthalocyanines. *Journal of Porphyrins and Phthalocyanines*, *4*(07), 635-638.

Bartók, M. (2015). Advances in immobilized organocatalysts for the heterogeneous asymmetric direct aldol reactions. *Catalysis Reviews*, *57*(2), 192-255.

Bauer, A. W., Kirby, W. M. M., Sherris, J. C., & Turck, M. (1966). Antibiotic susceptibility testing by a standardized single disk method. *American journal of clinical pathology*, *45*(4_ts), 493-496.

Benbow, M. (2010). Wound swabs and chronic wounds. *Practice nurse*, *39*(9), 27-30.

Benvindo, R. G., Braun, G., Carvalho, A. R. D., & Bertolini, G. R. F. (2008). Effects of photodynamic therapy and of a sole low-power laser irradiation on bacteria in vitro. *Fisioterapia e pesquisa*, *15*, 53-57.

Bertolini, G., Rossi, F., Valduga, G., Jori, G., & Van Lier, J. (1990). Photosensitizing activity of water-and lipid-soluble phthalocyanines on Escherichia coli. *FEMS microbiology letters*, *71*(1-2), 149-155.

Bhaduri, S., & Mukesh, D. (2014). *Homogeneous catalysis: mechanisms and industrial applications*. John Wiley & Sons.

Bone, S., Alum, A., Markovski, J., Hristovski, K., Bar-Zeev, E., Kaufman, Y., ... & Perreault, F. (2018). Physisorption and chemisorption of T4 bacteriophages on amino functionalized silica particles. *Journal of colloid and interface science*, *532*, 68-76.

Bonnett, R., Krysteva, M. A., Lalov, I. G., Artarsky, S. V. (2006). Water disinfection using photosensitizers immobilized on chitosan. Water Res. 40(6)1269-1275.

Bowler, P. G. (2002). Wound pathophysiology, infection and therapeutic options. *Annals of medicine*, *34*(6), 419-427.

Bowler, P. G., Duerden, B. I., & Armstrong, D. G. (2001). Wound microbiology and associated approaches to wound management. *Clinical microbiology reviews*, *14*(2), 244-269.

Boyacı, I. H. (2005). A new approach for determination of enzyme kinetic constants using response surface methodology. *Biochemical Engineering Journal*, *25*(1), 55-62.

Brasseur, N. (2003). Sensitizers for PDT: phthalocyanines. In *Photodynamic therapy*. The Royal Society of Chemistry, 105-118.

Braun & Tcherniac, J. Ber. (1907). Deut. Chem. Ges. 40, 2709.

Braun, A. M., Maurette, M. T., & Oliveros, E. (1986). *Technologie photochimique*. Lausanne: Presses polytechniques romandes, 444-447

Bumah, V. V., Masson-Meyers, D. S., Cashin, S., & Enwemeka, C. S. (2015). Optimization of the antimicrobial effect of blue light on methicillin-resistant Staphylococcus aureus (MRSA) in vitro. *Lasers in surgery and medicine*, *47*(3), 266-272.

Burns T, Wilson M, Pearson GJ (1993). Sensitisation of cariogenic bacteria to killing by light from a helium-neon laser. *Journal of Medical Microbiology* 38, 401-405.

Byrne, G. T., Linstead, R. P., Lowe, A. R. (1934). Phthalocyanines. Part II. The preparation of phthalocyanine and some metallic derivatives from o-cyanobenzamide and phthalimide. *Journal of the Chemical Society (Resumed)*. 1017-1022.

Carra, I., Pérez, J. A. S., Malato, S., Autin, O., Jefferson, B., & Jarvis, P. (2015). Application of high intensity UVC-LED for the removal of acetamiprid with the photo-Fenton process. *Chemical Engineering Journal*, *264*, 690-696.

Castano, A. P., Demidova, T. N., & Hamblin, M. R. (2004). Mechanisms in photodynamic therapy: part one—photosensitizers, photochemistry and cellular localization. *Photodiagnosis and photodynamic therapy*, *1*(4), 279-293.

Catão, M. H. C. D. V., & Batista, A. L. A. (2020). In vitro evaluation of the antibacterial effect of photodynamic therapy with methylene blue. *Pesquisa Brasileira em Odontopediatria e Clínica Integrada*, *20*.

Cavaleiro, J .A. S., Tomé, A. C., Neves, M. G. P. M. S (2010). In: Kadish KM, Smith KM, Guillard R (Ed.) Handbook of porphyrin, vol 2. *Meso-tetraarylporphyrin derivatives: new synthetic methodologies.* World Scientific, Singapore.

Chakane, S., Gokarna, A., & Bhoraskar, S. V. (2003). Metallophthalocyanine coated porous silicon gas sensor selective to NO_2. *Sensors and Actuators B: Chemical*, *92*(1-2), 1-5.

Chambers, H. F., & DeLeo, F. R. (2009). Waves of resistance: Staphylococcus aureus in the antibiotic era. *Nature Reviews Microbiology*, *7*(9), 629-641.

Chao, C., Liu, J., Wang, J., Zhang, Y., Zhang, B., Zhang, Y., ... & Chen, R. (2013). Surface modification of halloysite nanotubes with dopamine for enzyme immobilization. *ACS applied materials & interfaces*, *5*(21), 10559-10564.

Chauhan, S. M., Srinivas, K. A., Srivastava, P. K., & Sahoo, B. (2003). Solvent-free synthesis of phthalocyanines. *Journal of Porphyrins and Phthalocyanines*, *7*(08), 548-550.

Chen, B., Pogue, B. W., Hoopes, P. J., & Hasan, T. (2006). Vascular and cellular targeting for photodynamic therapy. *Critical Reviews™ in Eukaryotic Gene Expression*, *16*(4).

Chen, J., Chen, Z., Zheng, Y., Zhou, S., Wang, J., Chen, N., ... & Huang, M. (2011). Substituted zinc phthalocyanine as an antimicrobial photosensitizer for periodontitis treatment. *Journal of Porphyrins and Phthalocyanines*, *15*(04), 293-299.

191

Chen, S. L., Huang, X. J., & Xu, Z. K. (2011). Functionalization of cellulose nanofiber mats with phthalocyanine for decoloration of reactive dye wastewater. *Cellulose*, *18*, 1295-1303.

Chen, S. L., Huang, X. J., & Xu, Z. K. (2011). Functionalization of cellulose nanofiber mats with phthalocyanine for decoloration of reactive dye wastewater. *Cellulose*, *18*, 1295-1303.

Chen, S. L., Huang, X. J., & Xu, Z. K. (2012). Effect of a spacer on phthalocyanine functionalized cellulose nanofiber mats for decolorizing reactive dye wastewater. *Cellulose*, *19*, 1351-1359.

Chen, S., & Teng, Q. (2017). Quantitative immobilization of phthalocyanine onto bacterial cellulose for construction of a high-performance catalytic membrane reactor. *Materials*, *10*(7), 846.

Chen, W., Lu, W., Yao, Y., & Xu, M. (2007). Highly efficient decomposition of organic dyes by aqueous-fibre phase transfer and in situ catalytic oxidation using fibre-supported cobalt phthalocyanine. *Environmental science & technology*, *41*(17), 6240-6245.

Chen, X., Lu, W., Xu, T., Li, N., Qin, D., Zhu, Z., ... & Chen, W. (2017). A bio-inspired strategy to enhance the photocatalytic performance of g-C3N4 under solar irradiation by axial coordination with hemin. *Applied Catalysis B: Environmental*, *201*, 518-526.

Chen, Z., Zhou, S., Chen, J., Deng, Y., Luo, Z., Chen, H., ... & Huang, M. (2010). Pentalysine β-Carbonylphthalocyanine Zinc: An Effective Tumor-Targeting Photosensitizer for Photodynamic Therapy. *ChemMedChem: Chemistry Enabling Drug Discovery*, *5*(6), 890-898.

Chen, Z., Zhou, S., Chen, J., Li, L., Hu, P., Chen, S., & Huang, M. (2014). An effective zinc phthalocyanine derivative for photodynamic antimicrobial chemotherapy. *Journal of Luminescence*, *152*, 103-107.

Chieng, B. W., Lee, S. H., Ibrahim, N. A., Then, Y. Y., & Loo, Y. Y. (2017). Isolation and characterization of cellulose nanocrystals from oil palm mesocarp fiber. *Polymers*, *9*(8), 355.

Chu, Y. (2021). *Heterogeneous catalysis in photo-RDRP: towards green polymer manufacturing* (Doctoral dissertation, UNSW Sydney).

Claessens, C. G., Hahn, U. W. E., & Torres, T. (2008). Phthalocyanines: From outstanding electronic properties to emerging applications. *The Chemical Record*, *8*(2), 75-97.

Clinical and Laboratory Standards Institute (2021). Performance Standards for Antimicrobial Susceptibility Testing. 31st ed. CLSI supplement M100. Clinical and Laboratory Standards Institute, USA. ISBN 978-168440-105-5 (Electronic).

Copéret, C., Chabanas, M., Petroff Saint-Arroman, R., & Basset, J. M. (2003). Homogeneous and heterogeneous catalysis: bridging the gap through surface organometallic chemistry. *Angewandte Chemie International Edition*, *42*(2), 156-181.

Dahl, T., RobertMiddenand, W., & Hartman, P. (1987). Pure singlet oxygen cytotoxicity for bacteria. *Photochemistry and photobiology*, *46*(3), 345-352.

Daneshvar, N., Ashassi-Sorkhabi, H., & Tizpar, A. (2003). Decolorization of orange II by electrocoagulation method. *Separation and purification Technology*, *31*(2), 153-162.

193

Dasgupta, P. K., Genfa, Z., Poruthoor, S. K., Caldwell, S., Dong, S., & Liu, S. Y. (1998). High-sensitivity gas sensors based on gas-permeable liquid core waveguides and long-path absorbance detection. *Analytical Chemistry*, *70*(22), 4661-4669.

Davies, J., & Davies, D. (2010). Origins and evolution of antibiotic resistance. *Microbiology and molecular biology reviews*, *74*(3), 417-433.

De Filippis, M. P., Dei, D., Fantetti, L., & Roncucci, G. (2000). Synthesis of a new water-soluble octa-cationic phthalocyanine derivative for PDT. *Tetrahedron Letters*, *41*(47), 9143-9147.

De Lencastre, H., Sa Figueiredo, A. M., Urban, C., Rahal, J., & Tomasz, A. (1991). Multiple mechanisms of methicillin resistance and improved methods for detection in clinical isolates of Staphylococcus aureus. *Antimicrobial Agents and Chemotherapy*, *35*(4), 632-639.

De Rosa, F. S., & Bentley, M. V. L. (2000). Photodynamic therapy of skin cancers: sensitizers, clinical studies and future directives. *Pharmaceutical research*, *17*, 1447-1455.

De Saja, J. A., & Rodriguez-Mendez, M. L. (2005). Sensors based on double-decker rare earth phthalocyanines. *Advances in colloid and interface science*, *116*(1-3), 1-11.

de Sousa, N. T. A., Santos, M. F., Gomes, R. C., Brandino, H. E., Martinez, R., & de Jesus Guirro, R. R. (2015). Blue laser inhibits bacterial growth of Staphylococcus aureus, Escherichia coli, and Pseudomonas aeruginosa. *Photomedicine and laser surgery*, *33*(5), 278-282.

Deb, H., Xiao, S., Morshed, M. N., & Al Azad, S. (2018). Immobilization of cationic titanium dioxide (TiO_2^+) on electrospun nanofibrous mat: synthesis, characterization, and potential environmental application. *Fibres and Polymers*, *19*, 1715-1725.

Degen, T., Sadki, M., Bron, E., König, U., & Nénert, G. (2014). The highscore suite. *Powder diffraction*, *29*(S2), S13-S18.

Dekker, D., Wolters, M., Mertens, E., Boahen, K. G., Krumkamp, R., Eibach, D., ... & May, J. (2016). Antibiotic resistance and clonal diversity of invasive Staphylococcus aureus in the rural Ashanti Region, Ghana. *BMC Infectious Diseases*, *16*(1), 1-6.

Denis, T. G. S., & Hamblin, M. R. (2011). An introduction to photoantimicrobials: photodynamic therapy as a novel method of microbial pathogen eradication. *Science against microbial pathogens: communicating current research and technological advances, A. Méndez-Vilas (Ed.)*, 675-683.

Dent, C. E., & Linstead, R. P. (1934b). Copper Phthalocyanines. Part IV. *J. Chem. Soc*, 1027-1031.

Dent, C. E., Linstead, R. P., & Lowe, A. R. (1934a). Phthalocyanines. Part VI. The structure of the phthalocyanines. *J. Chem. Soc*, *1033*, 184.

Dhami, S., & Phillips, D. (1996). Comparison of the photophysics of an aggregating and non-aggregating aluminium phthalocyanine system incorporated into unilamellar vesicles. *Journal of Photochemistry and Photobiology A: Chemistry*, *100*(1-3), 77-84.

Ding, M., Jiang, X., Zhang, L., Cheng, Z., & Zhu, X. (2015). Recent progress on transition metal catalyst separation and recycling in ATRP. *Macromolecular Rapid Communications*, *36*(19), 1702-1721.

Ding, S., Xing, Y., Radosz, M., & Shen, Y. (2006). Magnetic nanoparticle supported catalyst for atom transfer radical polymerization. *Macromolecules*, *39*(19), 6399-6405.

Dogo, S., Germain, J. P., Maleysson, C., & Pauly, A. (1992). Interaction of NO2 with copper phthalocyanine thin films II: application to gas sensing. *Thin solid films*, *219*(1-2), 251-256.

Dolmans, D. E., Fukumura, D., & Jain, R. K. (2003). Photodynamic therapy for cancer. *Nature reviews cancer*, *3*(5), 380-387.

Doppagne, B., Chong, M. C., Bulou, H., Boeglin, A., Scheurer, F., & Schull, G. (2018). Electrofluorochromism at the single-molecule level. *Science*, *361*(6399), 251-255.

Dougherty, T. J. (1992). Photochemistry in the treatment of cancer. *Adv. Photochem*, *17*, 275-311.

Dougherty, T. J., Kaufman, J. E., Goldfarb, A., Weishaupt, K. R., Boyle, D., & Mittleman, A. (1978). Photoradiation therapy for the treatment of malignant tumors. *Cancer research*, *38*(8), 2628-2635.

Dumoulin, F. (2011). Design and conception of photosensitisers. In *Photosensitizers in medicine, environment, and security* (pp. 1-46). Dordrecht: Springer Netherlands.

Duquesne, E., Degée, P., Habimana, J., & Dubois, P. (2004). Supported nickel bromide catalyst for Atom Transfer Radical Polymerization (ATRP) of methyl methacrylate. *Chemical communications*, (6), 640-641.

Durmuş, M., & Nyokong, T. (2007). Synthesis and solvent effects on the electronic absorption and fluorescence spectral properties of substituted zinc phthalocyanines. *Polyhedron*, *26*(12), 2767-2776.

Duruk, E. G., Yenilmez, H. Y., Altındal, A., & Bayır, Z. A. (2015). Microwave-assisted synthesis of novel non-peripherally substituted metal-phthalocyanines and their sensing behaviour for a broad range of Lewis bases. *Dalton Transactions*, *44*(21), 10060-10068.

End, N., & Schöning, K. U. (2004). Immobilized catalysts in industrial research and application. *Immobilized Catalysts: Solid Phases, Immobilization and Applications*, 241-271.

Esquivel-Peña, V., Bastos-Arrieta, J., Muñoz, M., Mora-Tamez, L., Munguía-Acevedo, N. M., Ocampo, A. L., & de Gyves, J. (2019). Metal nanoparticle–carbon nanotubes hybrid catalysts immobilized in a polymeric membrane for the reduction of 4-nitrophenol. *SN Applied Sciences*, *1*(4), 347.

Fan, K., Li, F., Wang, L., Daniel, Q., Chen, H., Gabrielsson, E., ... & Sun, L. (2015). Immobilization of a molecular ruthenium catalyst on hematite nanorod arrays for water oxidation with stable photocurrent. *ChemSusChem*, *8*(19), 3242-3247.

Fernández-Sánchez, J. F., Nezel, T., Steiger, R., & Spichiger-Keller, U. E. (2006). Novel optical NO_2-selective sensor based on phthalocyaninato-iron (II) incorporated into a nanostructured matrix. *Sensors and Actuators B: Chemical*, *113*(2), 630-638.

Ferré, M., Pleixats, R., Man, M. W. C., & Cattoën, X. J. G. C. (2016). Recyclable organocatalysts based on hybrid silicas. *Green chemistry*, *18*(4), 881-922.

Ferreira, J., Menezes, P. F. C., Kurachi, C., Sibata, C. H., Allison, R. R., & Bagnato, V. S. (2007). Comparative study of photodegradation of three hematoporphyrin derivative: Photofrin®, Photogem®, and Photosan®. *Laser Physics Letters*, *4*(10), 743.

Filatov, M. A., Baluschev, S., & Landfester, K. (2016). Protection of densely populated excited triplet state ensembles against deactivation by molecular oxygen. *Chemical Society Reviews*, *45*(17), 4668-4689.

Fonda-Pascual, P., Moreno-Arrones, O. M., Alegre-Sanchez, A., Saceda-Corralo, D., Buendia-Castaño, D., Pindado-Ortega, C., ... & Jaen-Olasolo, P. (2016). In situ production of ROS in the skin by photodynamic therapy as a powerful tool in clinical dermatology. *Methods*, *109*, 190-202.

Gaigneaux, E. M., Maggi, R., Ruiz, P., & Delmon, B. (1996). Epoxidation of cyclohexene by iron and cobalt phthalocyanines, study of the side reactions. *Journal of Molecular Catalysis A: Chemical*, *109*(1), 67-74.

Gao, M., Li, N., Lu, W., & Chen, W. (2014). Role of cellulose fibers in enhancing photosensitized oxidation of basic green 1 with massive dyeing auxiliaries. *Applied Catalysis B: Environmental*, *147*, 805-812.

Ghani, F., Kristen, J., & Riegler, H. (2012). Solubility properties of unsubstituted metal phthalocyanines in different types of solvents. *Journal of Chemical & Engineering Data*, *57*(2), 439-449.

Gill, P., Moghadam, T. T., & Ranjbar, B. (2010). Differential scanning calorimetry techniques: applications in biology and nanoscience. *Journal of biomolecular techniques: JBT*, *21*(4), 167.

Giuliani, F., Martinelli, M., Cocchi, A., Arbia, D., Fantetti, L., & Roncucci, G. (2010). In vitro resistance selection studies of RLP068/Cl, a new Zn (II) phthalocyanine suitable for antimicrobial photodynamic therapy. *Antimicrobial agents and chemotherapy*, *54*(2), 637-642.

Goldberg, D. J. (2008). Photodynamic therapy in skin rejuvenation. *Clinics in Dermatology*, *26*(6), 608-613.

Gopinathan, P., Subramanian, K. S., Paliyath, G., & Subramanian, J. (2017). Genotypic variations in characteristics of nano-fibrillated cellulose derived from banana pseudostem. *BioResources*, *12*(4), 6984-7001.

Gounden, D., Nombona, N., & Van Zyl, W. E. (2020). Recent advances in phthalocyanines for chemical sensor, non-linear optics (NLO) and energy storage applications. *Coordination Chemistry Reviews*, *420*, 213359.

Gouterman, M., Wagnière, G. H., & Snyder, L. C. (1963). Spectra of porphyrins. *Journal of Molecular Spectroscopy*, *11*(1-6), 108-127.

Grammatikova, N. E., George, L., Ahmed, Z., Candeias, N. R., Durandin, N. A., & Efimov, A. (2019). Zinc phthalocyanine activated by conventional indoor light makes a highly efficient antimicrobial material from regular cellulose. *Journal of Materials Chemistry B*, *7*(28), 4379-4384.

Gražulis, S., Chateigner, D., Downs, R. T., Yokochi, A. F. T., Quirós, M., Lutterotti, L., ... & Le Bail, A. (2009). Crystallography Open Database–an open-access collection of crystal structures. *Journal of applied crystallography*, *42*(4), 726-729.

Grishkewich, N., Mohammed, N., Tang, J., & Tam, K. C. (2017). Recent advances in the application of cellulose nanocrystals. *Current Opinion in Colloid & Interface Science*, *29*, 32-45.

Gu, D., Chen, Q., Tang, X., Gan, F., Shen, S., Liu, K., & Xu, H. (1995). Application of phthalocyanine thin films in optical recording. *Optics communications*, *121*(4-6), 125-129.

Gursoy, H., Ozcakir-Tomruk, C., Tanalp, J., & Yılmaz, S. (2013). Photodynamic therapy in dentistry: a literature review. *Clinical oral investigations*, *17*, 1113-1125.

Güzel, E., Günsel, A., Bilgiçli, A. T., Atmaca, G. Y., Erdoğmuş, A., & Yarasir, M. N. (2017). Synthesis and photophysicochemical properties of novel thiadiazole-substituted zinc (II), gallium (III) and silicon (IV) phthalocyanines for photodynamic therapy. *Inorganica Chimica Acta*, *467*, 169-176.

Haisch, P., Winter, G., Hanack, M., Lüer, L., Egelhaai, H. J., & Oelkrug, D. (1997). Soluble alkyl-and alkoxy-substituted titaniumoxo phthalocyanines: Synthesis and photoconductivity. *Advanced Materials*, *9*(4), 316-321.

Hancock, R. E. (1997). The bacterial outer membrane as a drug barrier. *Trends in microbiology*, *5*(1), 37-42.

Haq, S., Ehsan, R., Menaa, F., Shahzad, N., Din, S. U., Shahzad, M. I., ... & Alsharef, S. A. (2022). A Novel Shift in the Absorbance Maxima of Methyl Orange with Calcination Temperature of Green Tin Dioxide Nanoparticle-Induced Photocatalytic Activity. *Catalysts*, *12*(11), 1397.

Hassan, G., Forsman, N., Wan, X., Keurulainen, L., Bimbo, L. M., Stehl, S., ... & Moreira, V. M. (2020). Non-leaching, highly biocompatible nanocellulose surfaces that efficiently resist fouling by bacteria in an artificial dermis model. *ACS Applied Bio Materials*, *3*(7), 4095-4108.

He, W., Jiang, X., Sun, F., & Xu, X. (2014). Extraction and characterization of cellulose nanofibers from Phyllostachys nidularia Munro via a combination of acid treatment and ultrasonication. *BioResources*, *9*(4), 6876-6887.

Hesse, M., Meier, H., Zeeh, B., & Belzner, J. (1997). Spektroskopische Methoden in der organischen Chemie. *Angewandte Chemie-German Edition*,*1 09*(5), 547.

Homaei, A. A., Sariri, R., Vianello, F., & Stevanato, R. (2013). Enzyme immobilization: an update. *Journal of chemical biology*, *6*, 185-205.

Hornung, R., Walt, H., Crompton, N. E., Keefe, K. A., Jentsch, B., Perewusnyk, G., ... & Köchli, O. R. (1998). m-THPC-mediated photodynamic therapy (PDT) does not induce resistance to chemotherapy, radiotherapy or PDT on human breast cancer cells in vitro. *Photochemistry and photobiology*, *68*(4), 569-574.

Howe, L., & Zhang, J. Z. (1998). The effect of biological substrates on the ultrafast excited-state dynamics of zinc phthalocyanine tetrasulfonate in solution. *Photochemistry and photobiology*, *67*(1), 90-96.

201

Hsieh, J. C., Liu, C. J., & Ju, Y. H. (1998). Response characteristics of lead phthalocyanine gas sensor: effects of film thickness and crystal morphology. *Thin Solid Films*, *322*(1-2), 98-103.

Huang, L., Dai, T., & Hamblin, M. R. (2010). Antimicrobial photodynamic inactivation and photodynamic therapy for infections. *Photodynamic Therapy: Methods and Protocols*, 155-173.

Huang, L., Xuan, Y., Koide, Y., Zhiyentayev, T., Tanaka, M., & Hamblin, M. R. (2012). Type I and Type II mechanisms of antimicrobial photodynamic therapy: an in vitro study on gram-negative and gram-positive bacteria. *Lasers in surgery and medicine*, *44*(6), 490-499.

Huang, Z. M., Zhang, Y. Z., Kotaki, M., & Ramakrishna, S. (2003). A review on polymer nanofibers by electrospinning and their applications in nanocomposites. *Composites science and technology*, *63*(15), 2223-2253.

Hush, N. S., & Woolsey, I. S. (1971). The electronic absorption spectra of phthalocyanine monomers and dimers. *Molecular physics*, *21*(3), 465-474.

Iliev, V., Alexiev, V., & Bilyarska, L. (1999). Effect of metal phthalocyanine complex aggregation on the catalytic and photocatalytic oxidation of sulfur containing compounds. *Journal of Molecular Catalysis A: Chemical*, *137*(1-3), 15-22.

Imada, H., Miwa, K., Imai-Imada, M., Kawahara, S., Kimura, K., & Kim, Y. (2016). Real-space investigation of energy transfer in heterogeneous molecular dimers. *Nature*, *538*(7625), 364-367.

International Organization for Standardization. (2004). BS EN ISO 20645: *Textile fabrics: determination of antibacterial activity: agar diffusion plate test*. ISO.

İşci, Ü., Beyreis, M., Tortik, N., Topal, S. Z., Glueck, M., Ahsen, V., ... & Plaetzer, K. (2016). Methylsulfonyl Zn phthalocyanine: a polyvalent and powerful hydrophobic photosensitizer with a wide spectrum of photodynamic applications. *Photodiagnosis and photodynamic therapy*, *13*, 40-47.

Ishii, K., Kubo, K., Sakurada, T., Komori, K., & Sakai, Y. (2011). Phthalocyanine-based fluorescence probes for detecting ascorbic acid: phthalocyaninatosilicon covalently linked to TEMPO radicals. *Chemical Communications*, *47*(17), 4932-4934.

Ismail, F., Othman, N. E. A., Wahab, N. A., Hamid, F. A., & Aziz, A. A. (2021). Preparation of microcrystalline cellulose from oil palm empty fruit bunch fibre using steam-assisted acid hydrolysis. *Journal of Advanced Research in Fluid Mechanics and Thermal Sciences*, *81*(1), 88-98.

Jabber, L. J., Grumo, J., Patricio, J., Magdadaro, M. R., Alguno, A., & Lubguban, A. (2017). Effect of cellulose-based fibers extracted from pineapple (Ananas comosus) leaf in the formation of polyurethane foam. *Journal of Fundamental and Applied Sciences*, *9*(7S), 134-143.

Jabłoński, A. (1935). Über den mechanismus der photolumineszenz von farbstoffphosphoren. *Zeitschrift für Physik*, *94*(1-2), 38-46.

Janssen, H., Janssen, I., Cooper, P., Kainyah, C., Pellio, T., Quintel, M., ... & Schulze, M. H. (2018). Antimicrobial-resistant bacteria in infected wounds, Ghana, 2014. *Emerging infectious diseases*, *24*(5), 916.

Jha, P., Sharma, M., Chouksey, A., Chaturvedi, P., Kumar, D., Upadhyaya, G., ... & Chaudhury, P. K. (2014). Functionalization of carbon nanotubes with metal phthalocyanine for selective gas sensing application. *Synthesis and Reactivity in Inorganic, Metal-Organic, and Nano-Metal Chemistry*, *44*(10), 1551-1557.

Jia, R., Tian, W., Bai, H., Zhang, J., Wang, S., & Zhang, J. (2019). Sunlight-driven wearable and robust antibacterial coatings with water-soluble cellulose-based photosensitizers. *Advanced Healthcare Materials*, *8*(5), 1801591.

Jiang, W., Wang, X., Chen, J., Liu, Y., Han, H., Ding, Y., ... & Tang, J. (2017). Deuterohemin-peptide enzyme mimic-embedded metal-organic frameworks through biomimetic mineralization with efficient ATRP catalytic activity. *ACS Applied Materials & Interfaces*, *9*(32), 26948-26957.

Jonoobi, M., Harun, J., Mathew, A. P., Hussein, M. Z. B., & Oksman, K. (2010). Preparation of cellulose nanofibers with hydrophobic surface characteristics. *Cellulose*, *17*, 299-307.

Jori, G. (2006). Photodynamic therapy of microbial infections: state of the art and perspectives. *Journal of Environmental Pathology, Toxicology and Oncology*, *25*(1-2) 505-519.

Jori, G., & Brown, S. B. (2004). Photosensitized inactivation of microorganisms. *Photochemical & Photobiological Sciences*, *3*(5), 403-405.

Jori, G., Fabris, C., Soncin, M., Ferro, S., Coppellotti, O., Dei, D., ... & Roncucci, G. (2006). Photodynamic therapy in the treatment of microbial infections: basic principles and perspective applications. *Lasers in Surgery and Medicine: The Official Journal of the American Society for Laser Medicine and Surgery*, *38*(5), 468-481.

Juzeniene, A., & Moan, J. (2007). The history of PDT in Norway: Part II. Recent advances in general PDT and ALA-PDT. *Photodiagnosis and Photodynamic Therapy*, *4*(2), 80-87.

Kadish, K., Guilard, R., & Smith, K. M. (Eds.). (2012). *The porphyrin handbook: applications of phthalocyanines*. Academic Press.

Kadish, K., Smith, K. M., & Guilard, R. (Eds.). (1999). *The Porphyrin Handbook, Volume 2*. Academic Press.

Kaestner, L., Cesson, M., Kassab, K., Christensen, T., Edminson, P. D., Cook, M. J., ... & Jori, G. (2003). Zinc octa-n-alkyl phthalocyanines in photodynamic therapy: photophysical properties, accumulation and apoptosis in cell cultures, studies in erythrocytes and topical application to Balb/c mice skin. *Photochemical & Photobiological Sciences*, *2*, 660-667.

Kahya, S. S. (2012). *Synthesis and characterization of fluorescent zinc phthalocyanine pigments and its combination pigment with mica titania pigment* (Master's thesis, Middle East Technical University).

Kahya, S. S., Sönmez, Y., Gündüz, G., & Mavis, B. (2019). Combination effect pigments with enhanced fluorescence. *Pigment & Resin Technology*, *48*(4), 277-292.

Kalia, S., Dufresne, A., Cherian, B. M., Kaith, B. S., Avérous, L., Njuguna, J., & Nassiopoulos, E. (2011). Cellulose-based bio-and nanocomposites: a review. *International journal of polymer science*, *2011*.

Kari, N., Zannotti, M., Giovannetti, R., Maimaiti, P., Nizamidin, P., Abliz, S., & Yimit, A. (2021). Sensing behavior of metal-free porphyrin and Zinc phthalocyanine thin film towards Xylene-Styrene and HCl vapors in planar optical waveguide. *Nanomaterials*, *11*(7), 1634.

Kauffmann, C., Shoseyov, O., Shpigel, E., Bayer, E. A., Lamed, R., Shoham, Y., & Mandelbaum, R. T. (2000). Novel methodology for enzymatic removal of atrazine from water by CBD-fusion protein immobilized on cellulose. *Environmental science & technology*, *34*(7), 1292-1296.

Kaya, E. C., Durmuş, M., Yanmaz, E., & Kantekin, H. (2014). Synthesis and spectral and thermal characterization of new metal-free and metallophthalocyanines: investigation of their photophysical, photochemical, and thin film properties. *Turkish Journal of Chemistry*, *38*(6), 1118-1134.

Khenblouche, A., Bechki, D., Gouamid, M., Charradi, K., Segni, L., Hadjadj, M., & Boughali, S. (2019). Extraction and characterization of cellulose microfibers from Retama raetam stems. *Polímeros*, *29*.

Kimura, M., Nakada, K., Yamaguchi, Y., Shirai, K. H. H., & Kobayashi, N. (1997). Dendritic metallophthalocyanines: synthesis and characterization of a zinc (II) phthalocyanine [8] 3-arborol. *Chemical Communications*, (13), 1215-1216.

Kirschning, A. (Ed.). (2004). *Immobilized catalysts: solid phases, immobilization and applications* (Vol. 242, pp. 241-271). Berlin: Springer.

Klemm, D., Heublein, B., Fink, H. P., & Bohn, A. (2005). Cellulose: fascinating biopolymer and sustainable raw material. *Angewandte chemie international edition*, *44*(22), 3358-3393.

Klibanov, A. M. (1979). Enzyme stabilization by immobilization. *Analytical biochemistry*, *93*, 1-25.

Klotz, L. O., Pellieux, C., Briviba, K., Pierlot, C., Aubry, J. M., & Sies, H. (1999). Mitogen-activated protein kinase (p38-, JNK-, ERK-) activation pattern induced by extracellular and intracellular singlet oxygen and UVA. *European journal of biochemistry*, *260*(3), 917-922.

Kluson, P., Drobek, M., Krejcikova, S., Krysa, J., Kalaji, A., Cajthaml, T., & Rakusan, J. (2008). Molecular structure effects in photodegradation of phenol and its chlorinated derivatives with phthalocyanines. *Applied Catalysis B: Environmental*, *80*(3-4), 321-326.

Kobak, R. Z. U., Arı, M. U., Tekin, A., & Gül, A. (2015). Aggregation behaviour in unsymmetrically substituted metal-free phthalocyanines. *Chemical Physics*, *448*, 91-97.

Kobayashi, N. (2002). Dimers, trimers and oligomers of phthalocyanines and related compounds. *Coordination Chemistry Reviews*, *227*(2), 129-152.

Kobayashi, N., Mack, J., Ishii, K., & Stillman, M. J. (2002). Electronic structure of reduced symmetry peripheral fused-ring-substituted phthalocyanines. *Inorganic chemistry*, *41*(21), 5350-5363.

Kong, T., Chen, Y., Ye, Y., Zhang, K., Wang, Z., & Wang, X. (2009). An amperometric glucose biosensor based on the immobilization of glucose oxidase on the ZnO nanotubes. *Sensors and Actuators B: Chemical*, *138*(1), 344-350.

Konopka, K. R. Y. S. T. Y. N. A., & Goslinski, T. O. M. A. S. Z. (2007). Photodynamic therapy in dentistry. *Journal of dental research*, *86*(8), 694-707.

Konovalova, N. V., Evstigneeva, R. P., & Luzgina, V. N. (2001). Synthetic molecular systems based on porphyrins as models for the study of energy transfer in photosynthesis. *Russian chemical reviews*, *70*(11), 939-969.

Kratochvılová, I., Nešprek, S., Šebera, J., Záliš, S., Pavelka, M., Wang, G., & Sworakowski, J. (2008). New organic FET-like photoactive device, experiments and DFT modeling. *The European Physical Journal E*, *25*, 299-307.

Krier, A., Abass, A. K., & Collins, R. A. (1993). The influence of chlorine on the optical properties of monoclinic lead phthalocyanine thin films. *Advanced Materials for Optics and Electronics*, *2*(6), 289-293.

Kuipers, J. (2014). *Distributed light sources for photocatalytic water treatment*. Wageningen University and Research.

Kuipers, J., Bruning, H., Yntema, D., & Rijnaarts, H. (2015). Wirelessly powered ultraviolet light emitting diodes for photocatalytic oxidation. *Journal of Photochemistry and Photobiology A: Chemistry*, *299*, 25-30.

Kumar, A., Park, G. D., Patel, S. K., Kondaveeti, S., Otari, S., Anwar, M. Z., ... & Lee, J. K. (2019). SiO_2 microparticles with carbon nanotube-derived mesopores as an efficient support for enzyme immobilization. *Chemical Engineering Journal*, *359*, 1252-1264.

Kumar, A., Samanta, S., Ramgir, N., Singh, A., Debnath, A. K., Muthe, K. P., & Barshilia, H. C. (2017). Improved H2S Sensitivity of Cobalt Phthalocyanine Film Fabricated on Plasma Treated Flexible Polyethylene Terephthalate Substrate. *Sensor Letters*, *15*(2), 104-110.

Kumawat, L. K., Mergu, N., Singh, A. K., & Gupta, V. K. (2015). A novel optical sensor for copper ions based on phthalocyanine tetrasulfonic acid. *Sensors and Actuators B: Chemical*, *212*, 389-394.

Kuramoto, N., & Kitao, T. (1982). The contribution of singlet oxygen to the photofading of triphenylmethane and related dyes. *Dyes and Pigments*, *3*(1), 49-58.

Lakowicz, J. R. (Ed.). (2006). Principles of fluorescence spectroscopy. Boston, MA: springer US.

Laptev, R., Nisnevitch, M., Siboni, G., Malik, Z., & Firer, M. A. (2006). Intracellular chemiluminescence activates targeted photodynamic destruction of leukaemic cells. *British Journal of Cancer* 95(2), 189-196.

209

Law, K. Y; Chem. Rev. 93, 449 (1993); M. J. Stillman and T. Nyokomg, "Phthalcyanines, Properties and Applications" (C. C. Leznoff and A. B. P. Lever, Eds.), Ch. 3. VCH, New York, 1989.

Law, W.; Liu, R. C. W.; Jinag, J.; Dennis, K. P. Ng; (1997). *Inorg. Chim. Acta*, *256*, 147-150.

Lbova, A. K., & Vasil'ev, M. P. (2008). Prospects for development of phthalocyanine-containing polymeric materials. *Fibre chemistry*, *40*(3), 217-225.

Leung, B., Dharmaratne, P., Yan, W., Chan, B. C., Lau, C. B., Fung, K. P., ... & Leung, S. S. (2020). Development of thermosensitive hydrogel containing methylene blue for topical antimicrobial photodynamic therapy. *Journal of Photochemistry and Photobiology B: Biology*, *203*, 111776.

Lever, A. P. (1965). The phthalocyanines. *Advances in Inorganic Chemistry and Radiochemistry*, *7*, 27-114.

Levin, E., Ivry, E., Diesendruck, C. E., & Lemcoff, N. G. (2015). Water in N-heterocyclic carbene-assisted catalysis. *Chemical reviews*, *115*(11), 4607-4692.

Li, B., Sun, L., Bian, J., Sun, N., Sun, J., Chen, L., ... & Jing, L. (2020). Controlled synthesis of novel Z-scheme iron phthalocyanine/porous WO_3 nanocomposites as efficient photocatalysts for CO_2 reduction. *Applied Catalysis B: Environmental*, *270*, 118849.

Li, D., & Xia, Y. (2004). Electrospinning of nanofibers: reinventing the wheel? *Advanced materials*, *16*(14), 1151-1170.

Li, D., Ge, S., Yuan, T., Gong, J., Huang, B., Tie, W., & He, W. (2018). Green synthesis and characterization of crystalline zinc phthalocyanine and cobalt phthalocyanine prisms by a simple solvothermal route. *CrystEngComm*, *20*(19), 2749-2758.

Li, T. T., Qian, J., Zhou, Q., Lin, J. L., & Zheng, Y. Q. (2017). A pyrene-modified cobalt salophen complex immobilized on multiwalled carbon nanotubes acting as a precursor for efficient electrocatalytic water oxidation. *Dalton Transactions*, *46*(38), 13020-13026.

Linstead, R. P. (1934). 212. Phthalocyanines. Part I. A new type of synthetic colouring matters. *Journal of the Chemical Society (Resumed)*, 1016-1017.

Linstead, R. P., & Lowe, A. R. (1934a). 'Phthalocyanines. Preliminary Experiments on the Preparation of Phthalocyanines from Phthalonitril', Part III. *J. Chem. Soc*, 1017-1022.

Linstead, R. P., & Lowe, A. R. (1934b). 216. Phthalocyanines. Part V. The molecular weight of magnesium phthalocyanine. *Journal of the Chemical Society (Resumed)*, 1031-1033.

Liu, D., Li, L., Chen, J., Chen, Z., Jiang, L., Yuan, C., & Huang, M. (2018). Dissociation of zinc phthalocyanine aggregation on bacterial surface is key for photodynamic antimicrobial effect. *Journal of Porphyrins and Phthalocyanines*, *22*(09n10), 925-934.

Liu, Q., Gao, L., Su, X., Zhou, F., & Duan, G. (2019). Interfacial self-assembly of CoPc thin films with their high sensing use as NO_2 sensors. *Materials Chemistry and Physics*, *234*, 94-101.

Liu, Y., & McCrory, C. C. (2019). Modulating the mechanism of electrocatalytic CO2 reduction by cobalt phthalocyanine through polymer coordination and encapsulation. *Nature communications*, *10*(1), 1683.

Lokesh, K. S., Uma, N., & Achar, B. N. (2009). The Microwave-assisted syntheses and a conductivity study of a platinum phthalocyanine and its derivatives. *Polyhedron*, *28*(5), 1022-1028.

Louati, A., El Meray, M., Andre, J. J., Simon, J., Kadish, K. M., Gross, M., & Giraudeau, A. (1985). Electrochemical reduction of new, good electron acceptors: the metallooctacyanophthalocyanines. *Inorganic Chemistry*, *24*(8), 1175-1179.

Lutterotti, L., Wenk, H., & Matthies, S. (1999). MAUD (material analysis using diffraction): a user-friendly Java program for Rietveld texture analysis and more. In *Proceeding of the twelfth international conference on textures of materials (ICOTOM-12)* (Vol. 2, pp. 1599-1604). NRC Research Press.

Mack, J., & Kobayashi, N. (2011). Low symmetry phthalocyanines and their analogues. *Chemical reviews*, *111*(2), 281-321.

Mahardika, M., Abral, H., Kasim, A., Arief, S., & Asrofi, M. (2018). Production of nanocellulose from pineapple leaf fibers via high-shear homogenization and ultrasonication. *Fibers*, *6*(2), 28.

Maisch, T., Bosl, C., Szeimies, R. M., Love, B., & Abels, C. (2007). Determination of the antibacterial efficacy of a new porphyrin-based photosensitizer against MRSA ex vivo. *Photochemical & Photobiological Sciences*, *6*, 545-551.

212

Maisch, T., Szeimies, R. M., Jori, G., & Abels, C. (2004). Antibacterial photodynamic therapy in dermatology. *Photochemical & Photobiological Sciences*, *3*(10), 907-917.

Makarov, S. G., Ketkov, S. Y., & Wöhrle, D. (2020). A planar binuclear cobalt (ii) phthalocyanine as a highly efficient catalyst for the oxidation of a mercaptan. *Chemical Communications*, *56*(42), 5653-5656.

Maleysson, C., Bouche-Pillon, D., Tomas, O., Blanc, J. P., Dogo, S., Germain, J. P., ... & Pauly, A. (1994). Conductivity and gas species content of (AlPcF) n thin films exposed to O_2 or NO_2. *Thin solid films*, *239*(1), 161-165.

Managa, M., Idowu, M. A., Antunes, E., & Nyokong, T. (2014). Photophysicochemical behavior and antimicrobial activity of dihydroxosilicon tris (diaquaplatinum) octacarboxyphthalocyanine. *Spectrochimica Acta Part A: Molecular and Biomolecular Spectroscopy*, *125*, 147-153.

Mantareva, V., Kussovski, V., Angelov, I., Borisova, E., Avramov, L., Schnurpfeil, G., & Wöhrle, D. (2007). Photodynamic activity of water-soluble phthalocyanine zinc (II) complexes against pathogenic microorganisms. *Bioorganic & Medicinal Chemistry*, *15*(14), 4829-4835.

Mapukata, S., Osifeko, O. L., & Nyokong, T. (2019). Dual phototransformation of the pollutants methyl orange and Cr (VI) using phthalocyanine-cobalt ferrite based magnetic nanocomposites. *Heliyon*, *5*(4).

213

Mårtensson, J., Arwin, H., & Lundström, I. (1990). Thin films of phthalocyanines studied with spectroscopic ellipsometry: an optical gas sensor? *Sensors and Actuators B: Chemical*, *1*(1-6), 134-137.

Masilela, N., Kleyi, P., Tshentu, Z., Priniotakis, G., Westbroek, P., & Nyokong, T. (2013). Photodynamic inactivation of Staphylococcus aureus using low symmetrically substituted phthalocyanines supported on a polystyrene polymer fiber. *Dyes and Pigments*, *96*(2), 500-508.

Mayhew, S., Vernon, D. I., Schofield, J., Griffiths, J., & Brown, S. B. (2001). Investigation of Cross-resistance to a Range of Photosensitizers, Hyperthermia and UV Light in Two Radiation-induced Fibrosarcoma Cell Strains Resistant to Photodynamic Therapy In Vitro¶. *Photochemistry and Photobiology*, *73*(1), 39-46.

McKeown, N. B. (1998). *Phthalocyanine materials: synthesis, structure and function* (No. 6). Cambridge university press.

Megashah, L. N., Ariffin, H., Zakaria, M. R., & Ando, Y. (2018, June). Characteristics of cellulose from oil palm mesocarp fibres extracted by multi-step pretreatment methods. In *IOP Conference Series: Materials Science and Engineering* (Vol. 368, No. 1, p. 012001). IOP Publishing.

Meisel, P., & Kocher, T. (2005). Photodynamic therapy for periodontal diseases: state of the art. *Journal of Photochemistry and Photobiology B: Biology*, *79*(2), 159-170.

Mejlholm, O., & Dalgaard, P. (2015). Modelling and predicting the simultaneous growth of Listeria monocytogenes and psychrotolerant lactic acid bacteria in processed seafood and mayonnaise-based seafood salads. *Food Microbiology*, *46*, 1-14.

Meyer-Betz, F. (1913). Untersuchungen über die biologische (photodynamische) Wirkung des Hämatoporphyrins und anderer Derivate des Blut-und Gallenfarbstoffs. *Dtsch. Arch. Klin. Med*, *112*(476-503), 0366-8576.

Michl, J., & Bonacic-Koutechy, V (1990). *Electronic Aspects of Organic Photochemistry*. Wiley Inter-science, New York.

Minnock, A., Vernon, D. I., Schofield, J., Griffiths, J., Parish, J. H., & Brown, S. B. (1996). Photoinactivation of bacteria. Use of a cationic water-soluble zinc phthalocyanine to photoinactivate both gram-negative and gram-positive bacteria. *Journal of Photochemistry and Photobiology B: Biology*, *32*(3), 159-164.

Minnock, A., Vernon, D. I., Schofield, J., Griffiths, J., Parish, J. H., & Brown, S. B. (2000). Mechanism of uptake of a cationic water-soluble pyridinium zinc phthalocyanine across the outer membrane of Escherichia coli. *Antimicrobial agents and chemotherapy*, *44*(3), 522-527.

Modica-Napolitano, J. S., Joyal, J. L., Ara, G., Oseroff, A. R., & Aprille, J. R. (1990). Mitochondrial toxicity of cationic photosensitisers for photochemotherapy. *Cancer research*, *50*(24), 7876-7881.

Mody, T. D. (2000). Pharmaceutical development and medical applications of porphyrin-type macrocycles. *Journal of Porphyrins and Phthalocyanines*, *4*(4), 362-367.

Molnár, Á., & Papp, A. (2017). Catalyst recycling-A survey of recent progress and current status. *Coordination Chemistry Reviews*, *349*, 1-65.

Moohan, J., Stewart, S. A., Espinosa, E., Rosal, A., Rodríguez, A., Larrañeta, E., ... & Domínguez-Robles, J. (2019). Cellulose nanofibers and other biopolymers for biomedical applications. A review. *Applied sciences*, *10*(1), 65.

Morshed, j M. N. (2021). *Immobilizing catalysts on textiles-case of zerovalent iron and glucose oxidase enzyme* (Doctoral dissertation, Université de Lille; Högskolan i Borås (Suède); Soochow university (Suzhou, China).

Morshed, M. N., Behary, N., Bouazizi, N., Vieillard, J., Guan, J., Le Derf, F., & Nierstrasz, V. (2020). Modification of fibrous membrane for organic and pathogenic contaminants removal: from design to application. *RSC advances*, *10*(22), 13155-13173.

Moses Phiri, M., Wingrove Mulder, D., Mason, S., & Christiaan Vorster, B. (2019). Facile immobilization of glucose oxidase onto gold nanostars with enhanced binding affinity and optimal function. *Royal Society open science*, *6*(5), 190205.

Mosinger, J., & Mosinger, B. (1995). Photodynamic sensitizers assay: rapid and sensitive iodometric measurement. *Experientia*, *51*, 106-109.

Mosinger, J., Lang, K., Kubát, P., Sýkora, J., Hof, M., Plíštil, L., & Mosinger, B. (2009). Photofunctional polyurethane nanofabrics doped by zinc tetraphenylporphyrin and zinc phthalocyanine photosensitizers. *Journal of fluorescence*, *19*, 705-713.

216

Mousali, E., & Zanjanchi, M. A. (2020). Loading of nickel phthalocyanine onto functionalized mesoporous KIT-6 solid support: an efficient visible photocatalyst for the degradation of 2, 4-dichlorophenol. *Reaction Kinetics, Mechanisms and Catalysis*, *130*(1), 547-566.

Nakai, K., Ishii, K., Kobayashi, N., Yonehara, H., & Pac, C. (2003). Theoretical calculations of the electronic absorption spectra of oxotitanium (IV) phthalocyanine in the solid State. *The Journal of Physical Chemistry B*, *107*(36), 9749-9755.

Nakano, A., Tamada, Y., Watanabe, D., Ishida, N., Yamashita, N., Kuhara, T., ... & Matsumoto, Y. (2009). A pilot study to assess the efficacy of photodynamic therapy for Japanese patients with actinic keratosis in relation to lesion size and histological severity. *Photodermatology, Photoimmunology & Photomedicine*, *25*(1), 37-40.

Nakonechny, F., Nisnevitch, M., Nitzan, Y., & Nisnevitch, M. (2013). Sonodynamic excitation of Rose Bengal for eradication of gram-positive and gram-negative bacteria. *BioMed Research International*, *2013*.

Nazir, M. S., Wahjoedi, B. A., Yussof, A. W., & Abdullah, M. A. (2013). Eco-friendly extraction and characterization of cellulose from oil palm empty fruit bunches. *BioResources*, *8*(2), 2161-2172.

Neves, P. R., Mamizuka, E. M., Levy, C. E., & Lincopan, N. (2011). Multidrug-resistant Pseudomonas aeruginosa: an endemic problem in Brazil. *Jornal Brasileiro de Patologia e Medicina Laboratorial*, *47*, 409-420.

Nguyen, J. V., & Jones, C. W. (2004). Design, behavior, and recycling of silica-supported CuBr- bipyridine ATRP catalysts. *Macromolecules*, *37*(4), 1190-1203.

Nguyen, K. A., & Pachter, R. (2001). Ground state electronic structures and spectra of zinc complexes of porphyrin, tetraazaporphyrin, tetrabenzoporphyrin, and phthalocyanine: A density functional theory study. *The Journal of Chemical Physics*, *114*(24), 10757-10767.

Nguyen, K. A., & Pachter, R. (2003). Jahn–Teller triplet excited state structures and spectra of zinc complexes of porphyrin and phthalocyanine: A density functional theory study. *The Journal of chemical physics*, *118*(13), 5802-5810.

Nikolaeva, O. I., Usacheva, T. S., Ageeva, T. A., & Koifman, O. I. (2006). Research of solutions of polystyrene and styrene copolymers with allyl alcohol. *Izv. Vyssh. Uchebn. Zaved. Khim. Khim. Tekhnol*, *49*(6), 46-48.

Nitzan, Y., Gutterman, M., Malik, Z., & Ehrenberg, B. (1992). Inactivation of gram-negative bacteria by photosensitized porphyrins. *Photochemistry and photobiology*, *55*(1), 89-96.

Nyokong, T., & Ahsen, V. (Eds.). (2012). *Photosensitizers in medicine, environment, and security*. Springer Science & Business Media.

O'Riordan, K., Akilov, O. E., & Hasan, T. (2005). The potential for photodynamic therapy in the treatment of localized infections. *Photodiagnosis and Photodynamic Therapy*, *2*(4), 247-262.

Ochsner, M. (1996). Light scattering of human skin: A comparison between zinc (II)—phthalocyanine and photofrin II®. *Journal of Photochemistry and Photobiology B: Biology*, *32*(1-2), 3-9.

Ochsner, M. (1997). Photophysical and photobiological processes in the photodynamic therapy of tumours. *Journal of Photochemistry and Photobiology B: Biology*, *39*(1), 1-18.

Ogilby, P. R. (2010). Singlet oxygen: there is indeed something new under the sun. *Chemical Society Reviews*, *39*(8), 3181-3209.

Ogunsipe, A., & Opeolu, S. (2020). Synthesis, Characterization and Photostability Studies on Aluminium Phthalocyanine Chloride. *Chem. Res. J*, *5*, 136-143.

Ogunsipe, A., Maree, D., & Nyokong, T. (2003). Solvent effects on the photochemical and fluorescence properties of zinc phthalocyanine derivatives. *Journal of Molecular Structure*, *650*(1-3), 131-140.

Önal, E., Dumoulin, F., & Hirel, C. (2009). Tetraimidazophthalocyanines: influence of protonation and aggregation on spectroscopic observations. *Journal of Porphyrins and Phthalocyanines*, *13*(06), 702-711.

Orhan, M., Kut, D., & Gunesoglu, C. (2009). Improving the antibacterial activity of cotton fabrics finished with triclosan by the use of 1, 2, 3, 4-butanetetracarboxylic acid and citric acid. *Journal of Applied Polymer Science*, *111*(3), 1344-1352.

Öztürk, Z. Z., Kılınç, N., Atilla, D., Gürek, A. G., & Ahsen, V. (2009). Recent studies chemical sensors based on phthalocyanines. *Journal of Porphyrins and Phthalocyanines*, *13*(11), 1179-1187.

Paczkowski, J., & Neckers, D. C. (1985). Polymer-based sensitizers for the formation of singlet oxygen: new studies of polymeric derivatives of rose bengal. *Macromolecules*, *18*(6), 1245-1253.

Pakapongpan, S., & Poo-Arporn, R. P. (2017). Self-assembly of glucose oxidase on reduced graphene oxide-magnetic nanoparticles nanocomposite-based direct electrochemistry for reagentless glucose biosensor. *Materials Science and Engineering: C*, *76*, 398-405.

Palma-Goyes, R. E., Guzmán-Duque, F. L., Peñuela, G., González, I., Nava, J. L., & Torres-Palma, R. A. (2010). Electrochemical degradation of crystal violet with BDD electrodes: Effect of electrochemical parameters and identification of organic by-products. *Chemosphere*, *81*(1), 26-32.

Pan, G.T; Huang, C.M.; Chen, L.C and Shiu, W.T. (2006). Immobilization of TiO_2 onto Nonwoven Fibre Textile by Silica Sol: Photocatalytic Activity and Duradibility Studies, Journal of Environmental Engineering and Management, Vol. 16, No. 6, pp. 413-420.

Pasiuk-Bronikowska, W., Krajewska, M., & Flis-Kabulska, I. (1998). Transformations of manganese tetrasulphophthalocyanine in oxidative conditions. *Polyhedron*, *18*(3-4), 561-570.

Paul, S., Islam, M. M., & Islam, S. M. (2015). Suzuki–Miyaura reaction by heterogeneously supported Pd in water: Recent studies. *RSC advances*, *5*(53), 42193-42221.

Pergrale, C., & Sorokin, A. B. (2000). Designing a dimeric phthalocyanine-supported catalyst for the selective oxidation of aromatic compounds. *Comptes Rendus de l'Académie des Sciences-Series IIC-Chemistry*, *3*(10), 803-810.

Piermatti, O., Abu-Reziq, R., & Vaccaro, L. (2020). Strategies to Immobilized Catalysts: A Key Tool for Modern Chemistry. *Catalyst Immobilization: Methods and Applications*, 1-22.

Pinho, E., Magalhães, L., Henriques, M., & Oliveira, R. (2011). Antimicrobial activity assessment of textiles: standard methods comparison. *Annals of microbiology*, *61*, 493-498.

Pirbazari, A. E. (2017). Photocatalytical treatment of synthetic wastewater containing chlorophenols by TiO_2 nanoparticles sensitized with cobalt phthalocyanine under visible light. *J. Chem. Eng. Process. Technol*, *8*.

Raab, O. (1900). Uber die wirkung fluoreszierender stoffe auf infusorien. *Zeitschr Biol*, *39*, 524-546.

Raghuwanshi, V. S., Su, J., Garvey, C. J., Holt, S. A., Holden, P. J., Batchelor, W. J., & Garnier, G. (2017). Visualization and Quantification of IgG Antibody Adsorbed at the Cellulose–Liquid Interface. *Biomacromolecules*, *18*(8), 2439-2445.

Rahman, M. M., Saleh Ahammad, A. J., Jin, J. H., Ahn, S. J., & Lee, J. J. (2010). A comprehensive review of glucose biosensors based on nanostructured metal-oxides. *Sensors*, *10*(5), 4855-4886.

Rak, J., Pouckova, P., Benes, J., & Vetvicka, D. (2019). Drug delivery systems for phthalocyanines for photodynamic therapy. *Anticancer research*, *39*(7), 3323-3339.

Ramos, A. A., Nascimento, F. B., De Souza, T. F., Omori, A. T., Manieri, T. M., Cerchiaro, G., & Ribeiro, A. O. (2015). Photochemical and photophysical properties of phthalocyanines modified with optically active alcohols. *Molecules*, *20*(8), 13575-13590.

Rashki, S., Shakour, N., Yousefi, Z., Rezaei, M., Homayoonfal, M., Khabazian, E., ... & Mirzaei, H. (2021). Cellulose-based nanofibril composite materials as a new approach to fight bacterial infections. *Frontiers in Bioengineering and Biotechnology*, *9*, 732461.

Rayung, M., Ibrahim, N. A., Zainuddin, N., Saad, W. Z., Razak, N. I. A., & Chieng, B. W. (2014). The effect of fiber bleaching treatment on the properties of poly (lactic acid)/oil palm empty fruit bunch fiber composites. *International journal of molecular sciences*, *15*(8), 14728-14742.

Ren, S., Joulié, D., Salvatore, D., Torbensen, K., Wang, M., Robert, M., & Berlinguette, C. P. (2019). Molecular electrocatalysts can mediate fast, selective CO_2 reduction in a flow cell. *Science*, *365*(6451), 367-369.

Renge, I. (1993). Solvent effects on the visible absorption maxima of tetrapyrrolic pigments. *The Journal of Physical Chemistry*, *97*(25), 6582-6589.

Roberts, D. J., & Cairnduff, F. (1995). Photodynamic therapy of primary skin cancer: a review. *British journal of plastic surgery*, *48*(6), 360-370.

Robertson, J. M. (1935). 136. An X-ray study of the structure of the phthalocyanines. Part I. The metal-free, nickel, copper, and platinum compounds. *Journal of the Chemical Society (Resumed)*, 615-621.

Rocha, D. M., Venkatramaiah, N., Gomes, M. C., Almeida, A., Faustino, M. A., Almeida Paz, F. A., ... & Tome, J. P. (2015). Photodynamic inactivation of Escherichia coli with cationic ammonium Zn (II) phthalocyanines. *Photochemical & Photobiological Sciences*, *14*, 1872-1879.

Roeder, K. D. (1998). *Nerve cells and insect behavior* (Vol. 4). Harvard University Press.

Ryter, S. W., & Tyrrell, R. M. (1998). Singlet molecular oxygen ($^1O_2$): a possible effector of eukaryotic gene expression. *Free radical biology and medicine*, *24*(9), 1520-1534.

Sağlam, M. B. (2016). Microwave-assisted synthesis and characterization of a new metal-free phthalocyanine and four metallophthalocyanines bearing 9-flourene methanol moities. *Anadolu University Journal of Science and Technology A-Applied Sciences and Engineering*, *17*(2), 327-336.

Said, M. M., Rehan, M., El-Sheikh, S. M., Zahran, M. K., Abdel-Aziz, M. S., Bechelany, M., & Barhoum, A. (2021). Multifunctional hydroxyapatite/silver nanoparticles/cotton gauze for antimicrobial and biomedical applications. *Nanomaterials*, *11*(2), 429.

Sanchez, M., Chap, N., Cazaux, J. B., & Meunier, B. (2001). Metallophthalocyanines linked to organic copolymers as efficient oxidative supported catalysts. *European Journal of Inorganic Chemistry*, *2001*(7), 1775-1783.

Santos, A. L. D., Santos, D. O., Freitas, C. C. D., Ferreira, B. L. A., Afonso, I. F., Rodrigues, C. R., & Castro, H. C. (2007). Staphylococcus aureus: visiting a strain of clinical importance. *Jornal Brasileiro de Patologia e Medicina Laboratorial*, *43*, 413-423.

Scalise, I., & Durantini, E. N. (2005). Synthesis, properties, and photodynamic inactivation of Escherichia coli using a cationic and a noncharged Zn (II) pyridyloxyphthalocyanine derivatives. *Bioorganic & medicinal chemistry*, *13*(8), 3037-3045.

Schaap, A. P., Thayer, A. L., Blossey, E. C., & Neckers, D. C. (1975). Polymer-based sensitizers for photooxidations. II. *Journal of the American Chemical Society*, *97*(13), 3741-3745.

Schieweck, K., Capraro, H. G., Isele, U., van Hoogevest, P., Ochsner, M., Maurer, T., & Batt, E. (1994, March). CGP 55 847, liposome-delivered zinc (II)-phthalocyanine as a phototherapeutic agent for tumours. In *Photodynamic Therapy of Cancer* (Vol. 2078, pp. 107-118). SPIE.

Šebera, J., Nešpůrek, S., Kratochvílová, I., Záliš, S., Chaidogiannos, G., & Glezos, N. (2009). Charge carrier mobility in sulphonated and non-sulphonated Ni phthalocyanines: experiment and quantum chemical calculations. *The European Physical Journal B*, *72*, 385-395.

Seven, O., Dindar, B., Aydemir, S., & Cilli, F. (2008). Synthesis, properties and photodynamic activities of some zinc (II) phthalocyanines against Escherichia coli and Staphylococcus aureus. *Journal of Porphyrins and Phthalocyanines*, *12*(08), 953-963.

Shaabani, A., Maleki-Moghaddam, R., Maleki, A., & Rezayan, A. H. (2007). Microwave assisted synthesis of metal-free phthalocyanine and metal-phthalocyanines. *Dyes and pigments*, *74*(2), 279-282.

Shaabani, A., Safari, N., Bazgir, A., Bahadoran, F., Sharifi, N., & Rajabali Jamaat, P. (2003). Synthesis of the tetrasulfo-and tetranitrophthalocyanine complexes under solvent-free and reflux conditions using microwave irradiation. *Synthetic communications*, *33*(10), 1717-1725.

Shaabani, Ahmad. "Synthesis of metallophthalocyanines under solvent-free conditions using microwave irradiation." *Journal of Chemical Research, Synopses* 10 (1998): 672-673.

Sharma, R. K., Gulati, S., & Sachdeva, S. (2012). One pot and solvent-free synthesis of 2, 9, 16, 23-tetrachlorometal (II) phthalocyanines. *Green Chemistry Letters and Reviews*, *5*(1), 83-87.

Sharman, W. M., Allen, C. M., & Van Lier, J. E. (1999). Photodynamic therapeutics: basic principles and clinical applications. *Drug discovery today*, *4*(11), 507-517.

Shen, T., Yuan, Z. L., & Xu, H. J. (1989). Fluorescent properties of phthalocyanines. *Dyes and pigments*, *11*(1), 77-80.

Shimomura, T., Itoh, T., Sumiya, T., Mizukami, F., & Ono, M. (2008). Electrochemical biosensor for the detection of formaldehyde based on enzyme immobilization in mesoporous silica materials. *Sensors and Actuators B: Chemical*, *135*(1), 268-275.

Shinohara, H., Tsaryova, O., Schnurpfeil, G., & Wöhrle, D. (2006). Differently substituted phthalocyanines: Comparison of calculated energy levels, singlet oxygen quantum yields, photo-oxidative stabilities, photocatalytic and catalytic activities. *Journal of Photochemistry and Photobiology A: Chemistry*, *184*(1-2), 50-57.

Silva, E., Pereira, M. M., Burrows, H. D., Azenha, M. E., Sarakha, M., & Bolte, M. (2004). Photooxidation of 4-chlorophenol sensitised by iron meso-tetrakis (2, 6-dichloro-3-sulfophenyl) porphyrin in aqueous solution. *Photochemical & Photobiological Sciences*, *3*, 200-204.

Sindelo, A., Britton, J., Lanterna, A. E., Scaiano, J. C., & Nyokong, T. (2022). Decoration of glass wool with zinc (II) phthalocyanine for the photocatalytic transformation of methyl orange. *Journal of Photochemistry and Photobiology A: Chemistry*, *432*, 114127.

Slokar, Y. M., & Le Marechal, A. M. (1998). Methods of decoloration of textile wastewaters. *Dyes and pigments*, *37*(4), 335-356.

Sobbi, A. K., Wöhrle, D., & Schlettwein, D. (1993). Photochemical stability of various porphyrins in solution and as thin film electrodes. *Journal of the Chemical Society, Perkin Transactions 2*, (3), 481-488.

Soncin, M., Fabris, C., Busetti, A., Dei, D., Nistri, D., Roncucci, G., & Jori, G. (2002). Approaches to selectivity in the Zn (II)–phthalocyanine-photosensitized inactivation of wild-type and antibiotic-resistant Staphylococcus aureus. *Photochemical & Photobiological Sciences*, *1*, 815-819.

Sönmez, Y. (2014). *Synthesis and characterization of tetranitro and tetraamino zinc phthalocyanines and their combinations with mica-titania pigment* (Master's thesis, Middle East Technical University).

Sorokin, A. B. (2013). Phthalocyanine metal complexes in catalysis. *Chemical reviews*, *113*(10), 8152-8191.

Spagnul, C., Turner, L. C., & Boyle, R. W. (2015). Immobilized photosensitizers for antimicrobial applications. *Journal of photochemistry and photobiology B: biology*, *150*, 11-30.

Sperandio, F. F., Huang, Y. Y., & R Hamblin, M. (2013). Antimicrobial photodynamic therapy to kill Gram-negative bacteria. *Recent patents on anti-infective drug discovery*, *8*(2), 108-120.

Spesia, M. B., & Durantini, E. N. (2013). Photodynamic inactivation mechanism of Streptococcus mitis sensitized by zinc (II) 2, 9, 16, 23-tetrakis [2-(N, N, N-trimethylamino) ethoxy] phthalocyanine. *Journal of Photochemistry and Photobiology B: Biology*, *125*, 179-187.

Starr, C., Evers, C. A., & Starr, L. (2005). *Basic concepts in biology*. Thomson Brooks/Cole.

Stillman, M. J., & Thomson, A. J. (1974). Assignment of the charge-transfer bands in some metal phthalocyanines. Evidence for the S= 1 state of iron (II) phthalocyanine in solution. *Journal of the Chemical Society, Faraday Transactions 2: Molecular and Chemical Physics*, *70*, 790-804.

Stillman, M. J., Nyokong, T., Leznoff, C. C., & Lever, A. B. P. (1989). Phthalocyanines: properties and applications. *by CC Leznoff and ABP Lever, VCH, New York*, *1*, 133.

Sudakar, P., Gunasekar, G. H., Baek, I. H., & Yoon, S. (2016). Recyclable and efficient heterogenized Rh and Ir catalysts for the transfer hydrogenation of carbonyl compounds in aqueous medium. *Green Chemistry*, *18*(24), 6456-6461.

Sun, Q., Feng, W., Yang, P., You, G., & Chen, Y. (2018). Highly selective room-temperature NO 2 sensors based on a fluoroalkoxy-substituted phthalocyanine. *New Journal of Chemistry*, *42*(9), 6713-6718.

Suppan, P. (1994). *Chemistry and light*. Royal Society of Chemistry.

Suri, R. P., Liu, J., Hand, D. W., Crittenden, J. C., Perram, D. L., & Mullins, M. E. (1993). Heterogeneous photocatalytic oxidation of hazardous organic contaminants in water. *Water Environment Research*, *65*(5), 665-673.

Tan, D. S. W., Gerlinger, M., Teh, B. T., & Swanton, C. (2010). Anti-cancer drug resistance: understanding the mechanisms through the use of integrative genomics and functional RNA interference. *European Journal of Cancer*, *46*(12), 2166-2177**.**

Tao, X., Ma, W., Li, J., Huang, Y., Zhao, J., & Jimmy, C. Y. (2003). Efficient degradation of organic pollutants mediated by immobilized iron tetrasulfo-phthalocyanine under visible light irradiation. *Chemical communications*, (1), 80-81.

Tao, X., Ma, W., Zhang, T., & Zhao, J. (2002). A novel approach for the oxidative degradation of organic pollutants in aqueous solutions mediated by iron tetrasulfo-phthalocyanine under visible light radiation. *Chemistry–A European Journal*, *8*(6), 1321-1326.

228

Tau, P., & Nyokong, T. (2007). Comparative photocatalytic efficiency of oxotitanium (IV) phthalocyanines for the oxidation of 1-hexene. *Journal of Molecular Catalysis A: Chemical*, *273*(1-2), 149-155.

Tedesco, A. C., Rotta, J. C., & Lunardi, C. N. (2003). Synthesis, photophysical and photochemical aspects of phthalocyanines for photodynamic therapy. *Current Organic Chemistry*, *7*(2), 187-196.

Teng, Q., Chen, S., & Xie, W. (2018). Preparation of phthalocyanine immobilized bacterial cellulose nanocomposites for decoloration of dye wastewater: Key role of spacers. *Applied Sciences*, *8*(7), 1021.

Terekhov, D. S., Nolan, K. J., McArthur, C. R., & Leznoff, C. C. (1996). Synthesis of 2, 3, 9, 10, 16, 17, 23, 24-octaalkynylphthalocyanines and the effects of concentration and temperature on their 1H NMR spectra. *The Journal of organic chemistry*, *61*(9), 3034-3040.

Thangaraj, B., & Solomon, P. R. (2019). Immobilization of lipases−A review. Part I: Enzyme immobilization. *ChemBioEng Reviews*, *6*(5), 157-166.

Tian, H., Li, X., Zeng, L., & Gong, J. (2015). Recent advances on the design of group VIII base-metal catalysts with encapsulated structures. *ACS Catalysis*, *5*(8), 4959-4977.

Tim, M. (2015). Strategies to optimize photosensitizers for photodynamic inactivation of bacteria. *Journal of Photochemistry and Photobiology B: Biology*, *150*, 2-10.

Tomé, J. P., Neves, M. G., Tomé, A. C., Cavaleiro, J. A., Soncin, M., Magaraggia, M., ... & Jori, G. (2004). Synthesis and antibacterial activity of new poly-S-lysine− porphyrin conjugates. *Journal of medicinal chemistry*, *47*(26), 6649-6652.

Tseng, S. P., Teng, L. J., Chen, C. T., Lo, T. H., Hung, W. C., Chen, H. J., ... & Tsai, J. C. (2009). Toluidine blue O photodynamic inactivation on multidrug-resistant pseudomonas aeruginosa. *Lasers in Surgery and Medicine: The Official Journal of the American Society for Laser Medicine and Surgery*, *41*(5), 391-397.

Uğur, A. L., Dinçer, H. A., & Erdoğmuş, A. (2012). Synthesis, photophysical and thermal studies of symmetrical and unsymmetrical zinc phthalocyanines. *Polyhedron*, *31*(1), 431-437.

Van Rie, Jonas and Wim, Thielemans (2017). "Cellulose–gold nanoparticle hybrid materials." *Nanoscale* 9, no. 25: 8525-8554.

Varghese, O. K., & Grimes, C. A. (2003). Metal oxide nanoarchitectures for environmental sensing. *Journal of nanoscience and nanotechnology*, *3*(4), 277-293.

Vecchio, D., Dai, T., Huang, L., Fantetti, L., Roncucci, G., & Hamblin, M. R. (2013). Antimicrobial photodynamic therapy with RLP068 kills methicillin-resistant Staphylococcus aureus and improves wound healing in a mouse model of infected skin abrasion PDT with RLP068/Cl in infected mouse skin abrasion. *Journal of biophotonics*, *6*(9), 733-742.

Veerakumar, P., Thanasekaran, P., Lu, K. L., Liu, S. B., & Rajagopal, S. (2017). Functionalized silica matrices and palladium: A versatile heterogeneous catalyst for Suzuki, Heck, and Sonogashira reactions. *ACS Sustainable Chemistry & Engineering*, *5*(8), 6357-6376.

Verma, S., & Sillanpää, M. (2015). Degradation of anatoxin-a by UV-C LED and UV-C LED/H2O2 advanced oxidation processes. *Chemical Engineering Journal*, *274*, 274-281.

Villemin, D., Hammadi, M., Hachemi, M., & Bar, N. (2001). Applications of microwave in organic synthesis: an improved one-step synthesis of metallophthalocyanines and a new modified microwave oven for dry reactions. *Molecules*, *6*(10), 831-844.

Wainwright, M. (1998). Photodynamic antimicrobial chemotherapy (PACT). *The Journal of antimicrobial chemotherapy*, *42*(1), 13-28.

Wainwright, M. (2009). *Photosensitisers in biomedicine*. John Wiley & Sons.

Wainwright, M., & Crossley, K. B. (2002). Methylene blue-a therapeutic dye for all seasons? *Journal of chemotherapy*, *14*(5), 431-443.

Wainwright, M., & Crossley, K. B. (2004). Photosensitising agents—circumventing resistance and breaking down biofilms: a review. *International biodeterioration & biodegradation*, *53*(2), 119-126.

Wan, Y., Liang, Q., Cong, T., Wang, X., Tao, Y., Sun, M., ... & Xu, S. (2015). Novel catalyst of zinc tetraamino-phthalocyanine supported by multi-walled carbon nanotubes with enhanced visible-light photocatalytic activity. *RSC advances*, *5*(81), 66286-66293.

Wang, D., Zhang, Y., Yan, S., Chen, Z., Deng, Y., Xu, P., ... & Chen, Z. (2017). An effective zinc phthalocyanine derivative against multidrug-resistant bacterial infection. *Journal of Porphyrins and Phthalocyanines*, *21*(03), 205-210.

Williams, J. A., Pearson, G. J., Colles, M. J., & Wilson, M. (2003). The effect of variable energy input from a novel light source on the photoactivated bactericidal action of toluidine blue O on Streptococcus mutans. *Caries research*, *37*(3), 190-193.

Williams, J. A., Pearson, G. J., Colles, M. J., & Wilson, M. (2004). The photo-activated antibacterial action of toluidine blue O in a collagen matrix and in carious dentine. *Caries research*, *38*(6), 530-536.

Wisniak, J. (2010). The history of catalysis. From the beginning to Nobel Prizes. *Educación química*, *21*(1), 60-69.

Wöhrle, D., & Schulte, B. (1985). Polymeric phthalocyanines and their precursors, 10. Thermal stability of polymeric phthalocyanines and their low molecular analogues. *Die Makromolekulare Chemie: Macromolecular Chemistry and Physics*, *186*(11), 2229-2245.

Wöhrle, D., Suvorova, O., Gerdes, R., Bartels, O., Lapok, L., Baziakina, N., ... & Slodek, A. (2004). Efficient oxidations and photooxidations with molecular oxygen using metal phthalocyanines as catalysts and photocatalysts. *Journal of Porphyrins and Phthalocyanines*, *8*(08), 1020-1041.

Wright, J. D., Roisin, P., Rigby, G. P., Nolte, R. J., Cook, M. J., & Thorpe, S. C. (1993). Crowned and liquid-crystalline phthalocyanines as gas-sensor materials. *Sensors and Actuators B: Chemical*, *13*(1-3), 276-280.

Wu, H., Chen, Z., Zhang, J., Wu, F., He, C., Wang, B., ... & Ren, Z. (2016a). Stably dispersed carbon nanotubes covalently bonded to phthalocyanine cobalt (II) for ppb-level H_2S sensing at room temperature. *Journal of Materials Chemistry A*, *4*(3), 1096-1104.

Wu, X., Shi, Z., Fu, S., Chen, J., Berry, R. M., & Tam, K. C. (2016b). Strategy for synthesizing porous cellulose nanocrystal supported metal nanocatalysts. *ACS Sustainable Chemistry & Engineering*, *4*(11), 5929-5935.

Wu, Y., Jiang, Z., Lu, X., Liang, Y., & Wang, H. (2019). Domino electroreduction of CO2 to methanol on a molecular catalyst. *Nature*, *575*(7784), 639-642.

Ye, Y., Bruning, H., Yntema, D., Mayer, M., & Rijnaarts, H. (2017). Homogeneous photosensitized degradation of pharmaceuticals by using red light LED as light source and methylene blue as photosensitizer. *Chemical Engineering Journal*, *316*, 872-881.

Yuan, S. F., & Chen, Z. R. (2005). Study on the prediction of visible absorption maximum of phthalocyanine compounds by semiempirical quantum methods. *The Journal of Physical Chemistry A*, *109*(11), 2582-2585.

Yuliarto, B., Zhou, H., Yamada, T., Honma, I., Katsumura, Y., & Ichihara, M. (2004). Effect of tin addition on mesoporous silica thin film and its application for surface photovoltage NO2 gas sensor. *Analytical Chemistry*, *76*(22), 6719-6726.

233

Yurtseven, H., Kaya, M. A., Altındal, A., & Şener, M. K. (2014). Synthesis, thermal, and electrical properties of stilbene-bridged polymeric zinc phthalocyanine. *Designed Monomers and Polymers*, *17*(1), 58-68.

Zafar, N., Uzair, B., Menaa, F., Khan, B. A., Niazi, M. B. K., Alaryani, F. S., ... & Sajjad, S. (2022). Moringa concanensis-Mediated Synthesis and Characterizations of Ciprofloxacin Encapsulated into Ag/TiO2/Fe2O3/CS Nanocomposite: A Therapeutic Solution against Multidrug Resistant E. *coli* Strains of Livestock Infectious Diseases. *Pharmaceutics*, *14*(8), 1719.

Zakharian, T.Y (2000). *Photodecomposition of crystal violet dye in water solution and suspensions of metal oxides*. Dissertations and Theses @ UNI. 649.

Zdarta, J., Meyer, A. S., Jesionowski, T., & Pinelo, M. (2018). A general overview of support materials for enzyme immobilization: characteristics, properties, practical utility. *Catalysts*, *8*(2), 92.

Zeng, J., Zeng, Z., Cheng, Z., Wang, Y., Wang, X., Wang, B., & Gao, W. (2021). Cellulose nanofibrils manufactured by various methods with application as paper strength additives. *Scientific Reports*, *11*(1), 11918.

Zhang, J., Wang, L., Zhang, B., Zhao, H., Kolb, U., Zhu, Y., ... & Xiao, F. S. (2018). Sinter-resistant metal nanoparticle catalysts achieved by immobilization within zeolite crystals via seed-directed growth. *Nature Catalysis*, *1*(7), 540-546.

Zhang, J., Zhang, F., Yang, H., Huang, X., Liu, H., Zhang, J., & Guo, S. (2010). Graphene oxide as a matrix for enzyme immobilization. *Langmuir*, *26*(9), 6083-6085.

Zhang, Y., & Rojas, O. J. (2017). Immunosensors for C-reactive protein based on ultrathin films of carboxylated cellulose nanofibrils. *Biomacromolecules*, *18*(2), 526-534.

Zhao, X. S., Bao, X. Y., Guo, W., & Lee, F. Y. (2006). Immobilizing catalysts on porous materials. *Materials Today*, *9*(3), 32-39.

Zhao, Z., Fan, J., Xie, M., & Wang, Z. (2009). Photo-catalytic reduction of carbon dioxide with in-situ synthesized CoPc/TiO2 under visible light irradiation. *Journal of Cleaner Production*, *17*(11), 1025-1029.

Zhong, R., Lindhorst, A. C., Groche, F. J., & Kühn, F. E. (2017). Immobilization of N-heterocyclic carbene compounds: a synthetic perspective. *Chemical Reviews*, *117*(3), 1970-2058.

Zhu, Y., Xie, Q., Sun, Y., Wang, L., Sun, Q., & Wang, L. (2020). High-performance NO_2 sensors based on ultrathin heterogeneous interface layers. *Advanced Materials Interfaces*, *7*(1), 1901579.

Ziolo, R. F., & Extine, M. (1981). New alkali metal phthalocyanine (Pc) complexes. Structure of the quasi-multimacrocycle K2Pc (DMF) 4 and the KPcK template. *Inorganic Chemistry*, *20*(8), 2709-2711.

Ziolo, R. F., Guenther, W., & Troup, J. M. (1981). Planar, pleated, and saddle-shaped structures of the phthalocyanine dianion in two novel multidentate oxygen-donor complexes of dipotassium phthalocyanine. *Journal of the American Chemical Society*, *103*(15), 4629-4630.

Zugle, R. (2012). *Phototransformation of Pollutants Using Lutetium and Zinc Phthalocyanines Anchored on Electrospun Polymer Fibers* (Doctoral dissertation, Rhodes University).

Zugle, R., & Nyokong, T. (2012). Electrospun polyacrylic acid polymer fibers functionalized with metallophthalocyanines for photosensitizing and gas sensing applications. *Journal of Macromolecular Science, Part A*, *49*(4), 279-287.

APPENDIX

Identification/ Confirmation Tests

Before using the obtained Staphylococcus aureus strains for APDT, identification and confirmation tests were performed using mannitol salt agar (MGA) medium. A positive result, resulted in a yellow colour change on pink mannitol salt agar plates after 18-48 hours of incubation.
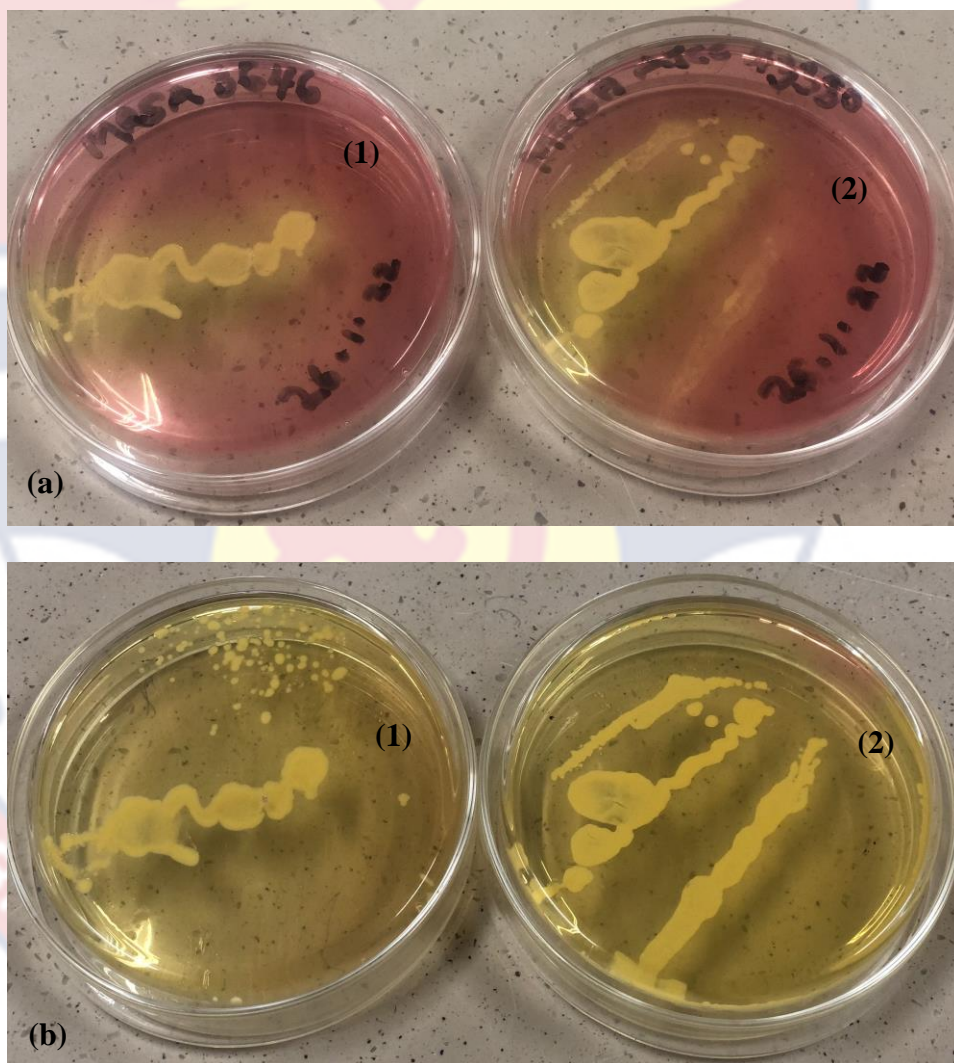
Images of (1) MRSA 3646 and (2) MRSA ATCC 43300 on mannitol salt agar plates after (a) 18-24 and (b) 24-48 hrs of incubation.

237